Hydrogen Bonding:

A Tool for Synthesis and Control of Motion in Rotaxane and Catenane Architectures

By

Jenny Ka Yan Wong

Degree of Doctor of Philosophy

Department of Chemistry

University of Edinburgh

October 2002

Table of Contents

Abstract

Although mechanical interlocking at the molecular level can be achieved through statistical or covalently-directed methods, the most effective and efficient routes to rotaxane architectures invoke supramolecular assistance – the use of attractive noncovalent interactions between the macrocycle and thread (or their precursors) – to preorganise the components prior to interlocking. Hydrogen bonding offers a particularly powerful method for preorganising precursors in such a way that efficient interlocking of the components to form rotaxanes and catenanes can occur in high yields. The restricted degrees of freedom inherent in rotaxane and catenane architectures also make them attractive candidates as components for molecular level devices. This Thesis outlines the investigation of the role of hydrogen bonding in the assembly of rotaxane architectures; how it can be used as a directing tool for synthesis and in the control of submolecular motion, including (i) controlled translational motion of the components of two-station rotaxanes and (ii) unidirectional rotation in a catenane system incorporating three different stations. The submolecular movements are mediated using heat and light.

List of Attended Lectures, Meetings and Conferences

1. Chromatography course, October 1999, University of Warwick, UK.
2. *X*-ray crystallography course, October 1999, University of Warwick, UK.
3. NMR spectroscopy course, March 2000, University of Warwick, UK.
4. Royal Society of Chemistry lectures, University of Warwick, UK.
5. Organic research seminars, University of Edinburgh, UK.
6. Modern Trends in Colour Chemistry – conference organised by SCI, 24th November 1999, UMIST, Manchester, UK.
7. Second COST D11 Workshop on Supramolecular Chemistry, 10–12th December 1999, Strasbourg, France.
8. European Network on Benzylic Amide Catenanes (ENBAC) TMR network meeting, 31st August–3rd September 2000, La Londe, France [talk: "Elucidating the Mechanism of Rotaxane Formation"].
9. 25th International Symposium on Macrocyclic Chemistry, 2–7th July 2000, University of St Andrews, UK.
10. 34th International Conference on Coordination Chemistry, 9–14th July 2000, University of Edinburgh, UK.
11. European Network on Benzylic Amide Catenanes (ENBAC) TMR network meeting, 5–8th April 2001, Riezlern, Austria [talk: "Structural Requirements for Rotaxanes Assembly"].
12. Mechanically Interlocked Polymer Architectures (MIPA) RTN network meeting, 7–10th June 2001, Sardinia, Italy. [talk: "Templates Used for Rotaxane Formation"].
13. 26th International Symposium on Macrocyclic Chemistry, 15–21st July 2001, Fukuoka, Japan [talk: "Large Amplitude Unidirectional Motion in Catenanes"].
14. 13th (Scottish) Graduate Symposium on Novel Organic Chemistry, 11th April 2002, University of St Andrews, UK.
15. 16th IUPAC conference on Physical-Organic Chemistry, 4–9th August 2002, University of California, San Diego, USA.

Acknowledgements

I would first like to take this opportunity to give my biggest thanks to my Supervisor Prof. David Leigh who, after my MChem project amazingly thought I didn't already cause enough trouble (ref. Lipari!) and took me on to do a PhD. My gratitude goes to Dave for all of his support and guidance during the last three years, not forgetting all the wonderful places that I was so gratefully sent to (Holland, Spain, Italy, France, Austria, Germany, Japan, San Diego…to name a few!) to attend meetings and conferences to present my work. Thanks!

My first two years of study was at Warwick University and from there, I would like to thank the following people who have made my life and work there so memorable and enjoyable. A special thank you goes to go to Laura, for knocking on my door back in 1995 (!) but also to have put up with my madness for six years – that's a mean feat! Thanks also to Matt! I would also like to thank Helen and Gianni who provided endless entertainment in Claycroft and have been such cool friends! And also to Matt (Bee)! To Mandy, Freida, Eugenia and Jenny for endurance training of a 40-hour trip from England-to-Calais-to-Brussels-to-Germany and back…eventually, in a car! A big thank you goes to Alex Slawin, Simon Teat and Stephen Lacy for introducing me to the wonderful world of crystallography and teaching me some real cool stuff and especially to the wonders of the Synchrotron (I will never forget!)! Thanks also to Francesco (lemon tree!) for teaching some NMR experiments, to Paul and Guy "wee-man" Clarkson for some helpful discussion and to all the Leigh group of the old.

Up in Edinburgh, I would like to give a special thank you to Frédéric (Freddie!), Delphine and Camille Coutrot. They have given me endless support as well as great entertainment for life in Edinburgh! And especially to Fred for being such great help at times of need and even to listen to my madness in the lab! To Gianni and Emilio for keeping the 400 MHz NMR running and all of the Leigh group of the new! A thank you

goes to Dr. Ian Sadler for allowing me as much time as I wanted on the 600 MHz NMR machine thus gaining some invaluable experience. Also thanks to Alan Taylor for being so amazingly quick on all mass specs at such short notice! At this point, I would also like to give a special thank you to Tracy all the way down in London, those phone calls and visits (with the snow!) have meant a lot! And to Jo for being a good friend since we met back in 1988!

I would like to thank my parents for supporting me in all my years of study and just generally being really cool! I have to thank my sister, Liza for dropping me down the stairs when I was just two months old, which apparently knocked my brain into place (still not too sure about that!)! And my brother, Simon for all the mad things we do together, anywhere in the world where we happen to meet up! A big thanks goes to my dear Grandma and Granddad who have taught me so much. I would also like to give a very special thank you to Henry for being so understanding and supportive throughout, especially for always being there for me, no matter what time it is!

"Size matters not! Judge me by my size, do you?"

Yoda

Layout of this Thesis

The work presented in this Thesis describes the use of hydrogen bonding in (i) the synthesis of rotaxane and catenane architectures and (ii) the control of motion of their submolecular components. A brief review of the literature is given in Chapter One describing the background to controlled motion at the molecular level, from rotational motion in triptycene groups to the translational motion in molecular shuttles.

The remainder of the Thesis discusses my own experiments in this area – sometimes in collaboration with colleagues – and is presented in the form of five Chapters that are actually articles that have either already been published, are in press or have been prepared for submission to a peer-reviewed journal. No attempt has been made to rewrite the work out of context, instead the contributions of others are gratefully acknowledged at the start of each Chapter. For the benefit of the reader – and the flow of the story – a brief synopsis is included before each chapter to set the scene, outline the ideas behind the work and the approach that was taken. I hope that the reader will forgive me for the small amount of repetition that stems from this approach!

JKYW October 2002

謹以此論文獻給我摯愛的父母

CHAPTER ONE

In Search of Molecular and Supramolecular Devices...

"It would be possible to describe everything scientifically, but it would make no sense; it would be without meaning, as if you described a Beethoven symphony as a variation of wave pressure."

Albert Einstein

1.1 In search of molecular and supramolecular devices

Supramolecular structures are assemblies of molecules held together by favourable noncovalent interactions. Whilst the development of synthetic methods in covalent chemistry has led to new and more efficient reactions, and the preparation of natural products of ever-increasing complexity, recent advances in the utility of noncovalent interactions in synthesis[1,2] has opened the gateway to whole new classes of complexes and mechanically interlocked molecules[3] that were previously unobtainable using conventional organic synthesis.

Until recently, mechanically interlocked molecules such as catenanes, knots, and rotaxanes[4] were regarded somewhat as curiosities – intriguing molecules in the world of nanoscale architectures. The rapid advances in self-assembly methodology in the last decade has not only resulted in an increase in the diversity of types of mechanically interlocked structures available, but has also dramatically improved synthetic routes and yields. The challenge is no longer to obtain structures merely to satisfy the imagination of chemists, but has moved towards the development of molecular 'machines'.[5,6]

The idea of utilising molecules as mechanical parts in molecular level machines was famously raised nearly fifty years ago. Richard P. Feynman, Nobel Laureate in Physics, said of such an idea in his 1959 lecture "There's Plenty of Room at the Bottom":

> *"What would be the utility of such machines? Who knows? I cannot see exactly what would happen, but I can hardly doubt that when we have some control of the arrangement of things on a molecular scale we will get an enormously greater range of possible properties that substances can have, and of the different things we can do."*

However, in the intervening decades it has been the so-called 'top-down' approach to miniaturisation that has revolutionised science and society. It is only in the last few years that chemists have begun to attempt to gain control over the motion of molecular and submolecular fragments, the first step in the quest for molecular machines.

1.2 Molecules with covalently-connected moving parts

1.2.1 From propellers to gears

Diphenylmethylene and triphenylmethylene compounds were probably the first synthetic structures which chemists realised featured structure-dependent rotational motion of submolecular fragments. The *correlated rotation* of two or more aryl rings attached to a central carbon atom was likened to a molecular propeller where the aryl rings can be considered as "blades" in a fully rotating system, **1** and **2**.[7] A combination of NMR spectroscopy and *X*-ray crystallography provided evidence that the aryl rings were twisted in the same sense to a reference plane (defined by the three carbon atoms attached to Z in **2**). The energetically disfavoured *independent* rotation of each ring meant that even though no restrictions are imposed on the individual torsion angles of the bonds connected to the central atom, the molecular propellers worked by correlated rotation of the rings due to the constraints imposed upon the three torsion angles *in combination.*

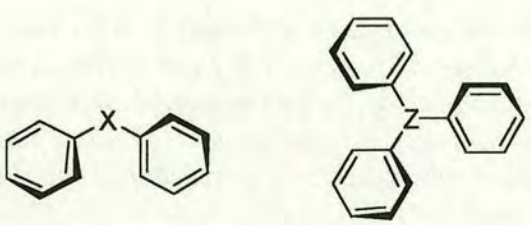

1 **2**

Out of the concept of molecular propellers was born the idea of molecular "bevel gears" where the concerted rotation of tightly intermeshed rotors could be exploited like mechanical gears in motion through the constriction in the torsion angles of the two rotors. Molecular rotors that could form parts of a molecular gear was realised through the studies by Ōki showing that hindered rotation occurs in bridgehead-substituted triptycenes.[8] Molecular bevel gears independently designed by the groups of Iwamura[9] and Mislow[10] harnessed the correlated rotation through the locking of two 9-triptycyl units joined to a central carbon atom in a fashion likened to three-toothed bevel gears, **3**.

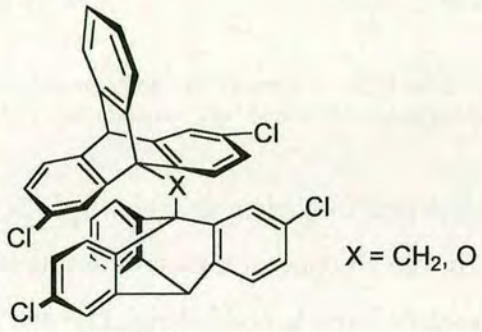

3

The process of dynamic gearing within these molecules was determined by a combination of ^{1}H and ^{13}C NMR spectroscopy and molecular modelling, from which the mechanism and energy barriers to correlated rotation were empirically determined. The mechanism is thought to occur through the clockwise rotation of one triptycyl about the C9–X bond whilst the second triptycyl unit rotates anticlockwise and *vice versa*. The energy barrier to geared rotation was found to be approximately 8 kcal mol^{-1} with a higher energy barrier to *gear slippage* of 30-40 kcal mol^{-1}.

1.2.2 A molecular brake

In pursuit of a molecular motor, Kelly and co-workers set off in the opposite direction by designing a molecular brake in the hopes of attaining insight into control

of motion at the molecular level.[11] As with the molecular gear, the molecular brake was based on a triptycene unit (the 'wheel') attached directly to a conformationally flexible bipyridyl unit, **4** (Scheme 1.1).

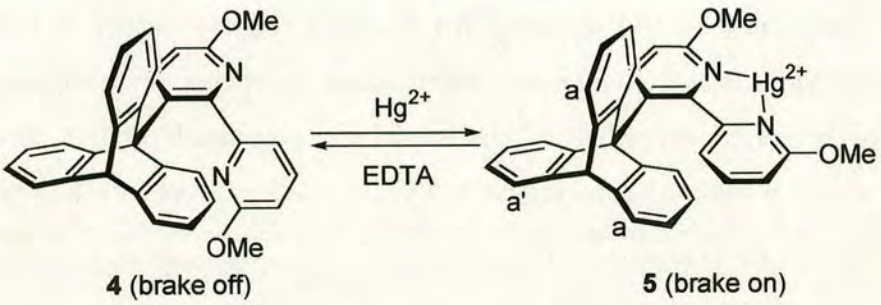

4 (brake off) **5** (brake on)

Scheme 1.1 The molecular brake is turned "on" upon chelation of **4** to Hg^{2+} by the bipyridyl ligand, **5** and subsequently turned "off" on addition of EDTA.

The ability of the bipyridyl unit to chelate to metal ligands formed the basis of the workings of the brake. In the absence of a metal the rotation of the triptycene unit about the central carbon–carbon single bond is rapid on the NMR timescale, even at –70 °C. Treatment of **4** with Hg^{2+} results in chelation of the metal to the bipyridyl unit which in turn forces the aromatic rings of the bipyridyl unit between the rings of the triptycene unit, **5** and at –30 °C rotation of the triptycene unit is prevented. The system is reversible by addition of EDTA and very temperature dependent: on warming **5** from –30 °C the sharp discrete resonances for H_a and $H_{a'}$ begin to broaden and eventually coalesce at room temperature. Thus the molecular brake works but brake slipping also occurs.

1.2.3 Towards a molecular ratchet?

In an attempt to build a molecular ratchet,[12] Kelly and co-workers modified the molecular brake so that the triptycene residue was directly connected to a [3]helicene, **6** and [4]helicene, **7**; with the triptycene acting once again as the 'wheel' and the helicene moiety intended as both a 'pawl' and 'spring'.

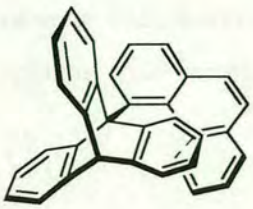

6

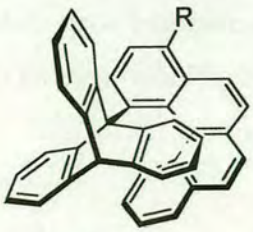

R = H, Me

7

Unexpectedly, calculated barriers to rotation of the triptycene with respect to the helicene *via* the carbon–carbon single bond was found to be *higher* in the case of **6** compared to **7** but it was reasoned later that probably the larger bulk of the [4]helicene moiety means that it is less able to arrive between the blades of the triptycene moiety. Ultimately, the ^{1}H NMR spectra of both molecules at room temperature showed that only **7** gave an unsymmetrical spectrum and had the potential to act as a ratchet. Studies on this compound found the energy barrier to rotation was indeed high, 25 kcal mol^{-1}, but spin polarization transfer NMR experiments showed that the triptycene was rotating in both directions in equal proportion. Although the shapes of the energy barriers to rotation in either direction were different, the heights of the energy barriers must be the same (a molecule at the top of a energy barrier has no 'memory' of how it got there) and since it is the height of an energy barrier – not its shape – that determines how easy it is for it to be passed, the concept of a molecular ratchet powered by the background thermal energy cannot work.

1.3 Unidirectional molecular motors

1.3.1 Chemically driven unidirectional rotational motion

A year later Kelly and co-workers published a molecular motor displaying a 120° *unidirectional* rotation that was chemically driven.[13] The previously described

molecular ratchet was modified such that the triptycene moiety had an amino group attached to one of the blades and an hydroxylalkyl group was attached to the [4]helicene **8a** (Scheme 1.2).

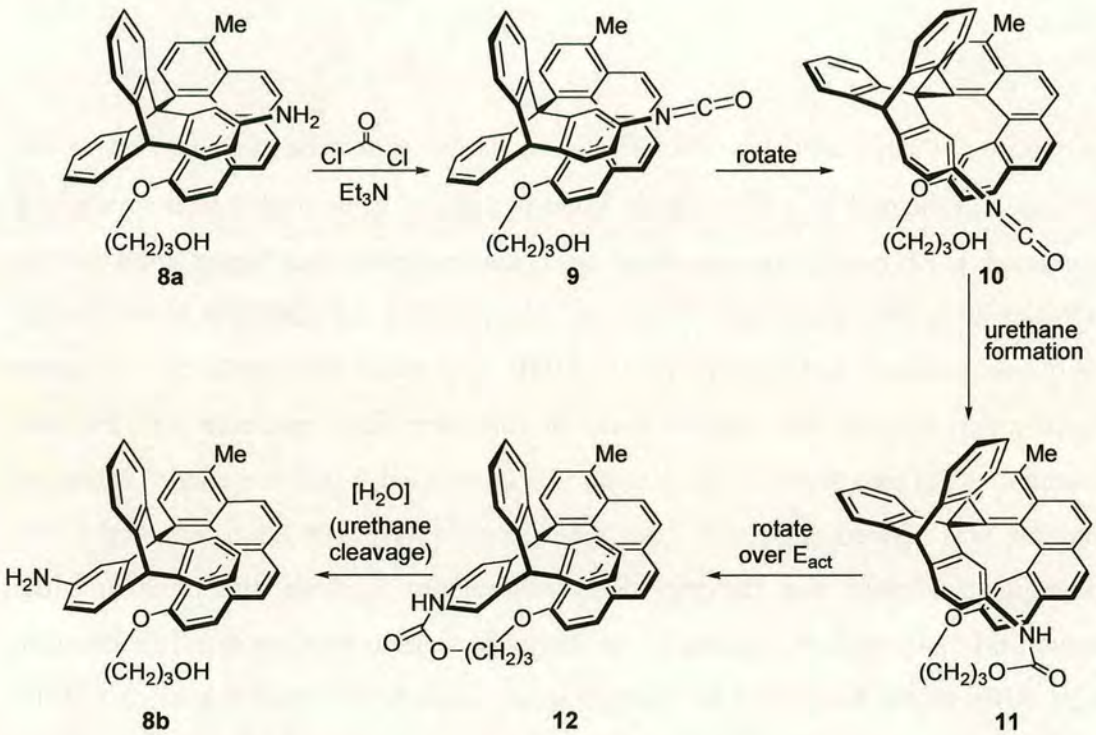

Scheme 1.2 Addition of phosgene and triethylamine triggers 120° unidirectional rotation about a carbon-carbon single bond.

Reaction of **8a** with phosgene yields a triptycene with a pendant isocyanate able to react with the hydroxy group attached to the helicene to form the corresponding urethane. However, the isocyanate derivative, **9** is still physically too far to react with the hydroxy group and it is only in the instances where *clockwise* rotation of the triptycene moiety occurs that a reaction is observed (*anticlockwise* rotation does not yield the urethane since the pendant groups would still be too far apart to react). The progress of the reaction was monitored by ^{1}H NMR spectroscopy and it was found that the reaction was extremely efficient, on addition of phosgene and triethylamine, immediate formation of the urethane was observed (~100%), however, the rate was

too fast on the NMR timescale to be determined. The next step was another clockwise rotation from **11** to **12** that proved to be the rate limiting step since it took ~6 hours to achieve more than 80% conversion. After final cleavage of the urethane with H_2O, an overall 120° unidirectional rotation had been achieved, **8b**.

This chemically driven motor of Kelly represents a significant step towards the construction of molecules which are working mechanical motors. Even so, optimisation of the system still needs to be carried out. At present, only one 120° rotation can be achieved with a system that is initially rotating in *both* directions until forced clockwise rotation is initiated by the addition of phosgene and triethylamine.

1.3.2 A photochemically driven unidirectional molecular rotor

The carbon–carbon single bond between the triptycene and helicene units acted as an axle about which rotation of the attached groups occurred. Feringa and co-workers synthesised the first example of a molecular motor displaying repetitive 360° unidirectional motion around a carbon–carbon double bond in a chiral, helical alkene (Scheme 1.3).[14]

The molecular motor, (3*R*,3'*R*)-(*P*,*P*)-*trans*-1,1',2,2',3,3',4,4'-octahydro-3,3'-dimethyl-4,4'-biphenanthrylidene[15] consisted of two identical halves connected by a central carbon–carbon double bond, bearing axial chirality and two chiral centres. Unidirectional rotation of 360° was achieved by two light-induced *cis-trans* isomerisation reactions, each giving a 180° rotation about the carbon-carbon double bond. Thermally controlled helicity inversions after each isomerisation step ensure the directionality of the rotations.

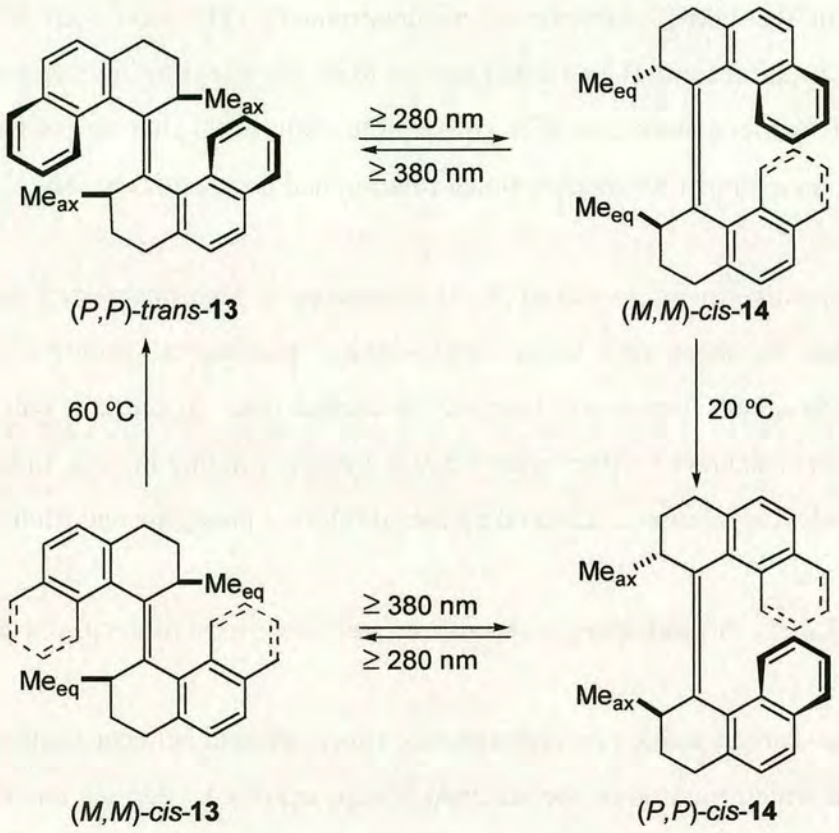

Scheme 1.3 Unidirectional rotational motion of 360° is achieved in a four-step process involving two isomerisation steps and two helical inversions (P = right-handed helicity and M = left-handed helicity; Me_{ax} and Me_{eq} represent the axial and equatorial orientated methyl-substituents respectively).

The four-step rotation was achieved as follows. First irradiation at $\lambda \geq 280$ nm (at –55 °C) of (*P,P*)-*trans*-**13** gave the corresponding (*M,M*)-*cis*-**14** (the reverse process is also possible on irradiation at $\lambda \geq 380$ nm). Raising the temperature of the solution to 20 °C results in a irreversible helical inversion to (*P,P*)-*cis*-**14** since irradiation causes the two methyl substituents to assume less stable equatorial positions in (*M,M*)-*cis*-**14** from the more stable axial positions in (*P,P*)-*trans*-**13**. Thus irreversible helical inversion occurs so that the methyl substituents assume the more stable axial positions in (*P,P*)-*cis*-**14**. A second irradiation step at $\lambda \geq 280$ nm of (*P,P*)-*cis*-**14** gives the corresponding (*M,M*)-*trans*-**13** followed by a second final helical inversion at 60 °C resulting in full 360° rotation in one direction only. The

four-step process was monitored by circular dichroism (CD) each step was accompanied by a change in sign in the CD absorption at 217 nm. The control of temperature is essential in the working of this system since if the irradiation of (*P,P*)-*trans*-**13** was carried out at 60 °C, all three states would be obtained without control.

The use of molecular systems to generate a macroscopic effect would bridge the gap between chemistry at the molecular level and the development of real devices. Recently, Feringa and co-workers demonstrated that if the molecular motor, **13** was doped into a nematic liquid crystal film, followed by irradiation at $\lambda \geq 280$ nm, the rotary motion of the molecular motor induces the motion of the mesogenic molecules and consequently lead to a gradual change colour of the film from purple to red after 80 seconds of irradiation time.[16]

As well as colour tuning, Feringa and co-workers have shown that it is possible to control the speed of rotation, resulting in acceleration of the two halves by lowering the energy barrier of helical inversion in a new series of molecular motors **15–21**.[17]

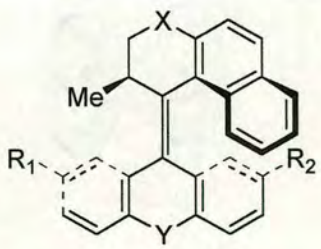

15: X=S, Y=S, R=H
16: X=S, Y=S, R=OMe
17: X=S, Y=O, R=H
18: X=S, Y=$C(CH_3)_2$, R=H
19: X=CH_2, Y=S, R=H
20: X=CH_2, Y=$C(CH_3)_2$, R=H
21: X=CH_2, Y=CHCH, R=H

The change in speed of rotation was achieved by systematically changing the nature of the bridging heteroatoms, X and Y; where a single stereogenic center has been proved sufficient to achieve full control of the direction of motion. The half-lives of the thermal isomerisation steps ranged from $t_{1/2}^{\theta} = 233 \pm 34$ h for **18** to $t_{1/2}^{\theta} = 0.67 \pm 0.02$ h for **19**.

1.4 Molecules with noncovalently-connected moving parts

Many rotaxanes and catenanes can exhibit large amplitude relative motion of their component parts since they are held together by mechanical bonds. A rotaxane consists of a central linear "thread" that passes through a macrocycle. The macrocycle is prevented from falling off the thread by the presence of bulky 'stoppers' (Figure 1.1). In most cases only one ring is interlocked onto the thread (a [2]rotaxane), however, 3, 4 or more (n) rings have been interlocked ([n+1]rotaxane). A catenane is composed of two or more mechanically interlocked rings.

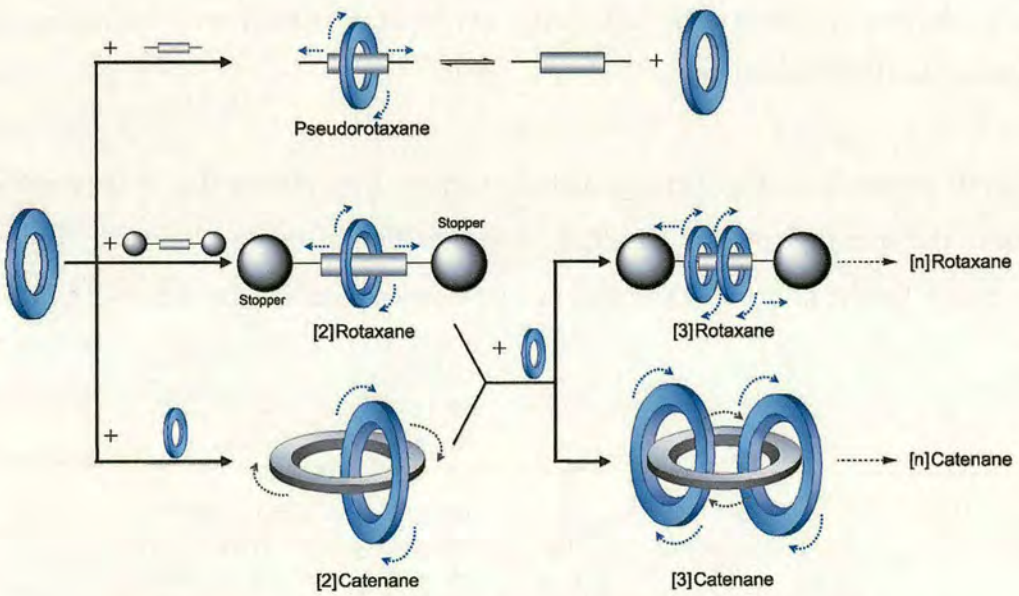

Figure 1.1 Molecular components comprised in rotaxanes and catenanes and the inherent motion possible in these mechanically interlocked molecules.

1.4.1 Synthesis of catenanes and rotaxanes

Template approaches have greatly improved the synthetic route to rotaxanes over statistical[18] (chance interlocking of the macrocycle and thread) and covalently-directed approaches[19] (synthesis of prerotaxanes and precatenanes followed by selective cleavage of covalent bonds to give the mechanical linkages). In template-

directed self-assembly, the two components are mutually-recognising through the formation of favourable intermolecular interactions. By using such noncovalent interactions (including metal ligand, π-donor/π-acceptor interactions, hydrophobic forces and hydrogen bonding) to interlock components, mechanically-linked molecules such as molecular shuttles and switches have been constructed. Of the many forms of supramolecular interactions, hydrogen bonding is arguably the most versatile, since reversibility is limited in metal-ligand interactions and π-π interactions and hydrophobic forces are often weaker and not as directional in nature as hydrogen bonds.

1.4.2 Hydrogen bond-assembled catenanes

The first example of the preparation of a catenane directed through the use of hydrogen bonding was reported by Hunter in 1992, where a double macrocyclisation reaction yielded 34% of [2]catenane **22** from isophthaloyl dichloride and diamine **23** under high dilution conditions (Scheme 1.4).[20] In the same reaction, 51% of the un-interlocked macrocycle **24** and 5% of the corresponding cyclic tetramer were also isolated. Macrocycle **24** had previously been synthesised as a specific macrocyclic host for *p*-benzoquinone through the interaction of four hydrogen bonds and four edge-to-face π-π interactions.[21]

In the same year, Vögtle published the synthesis of an almost identical [2]catenane with a 5-substituted isophthaloyl dichloride in 8% yield.[22] Vögtle later extended the synthesis to include the preparation of hetereocircuit catenanes[23] (a catenane comprised of two differently functionalised macrocycles).

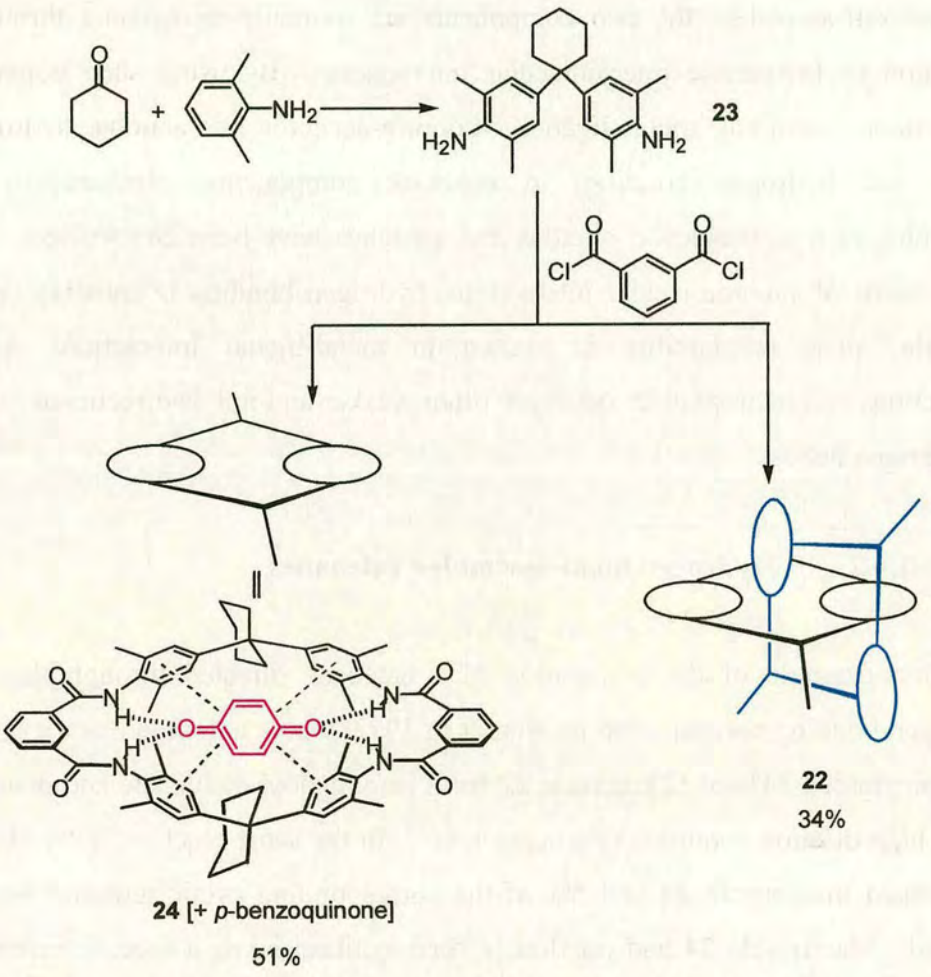

Scheme 1.4 Synthesis of the first catenane **22** formed *via* favourable hydrogen bond and π-π interactions. Macrocycle **24** serves as a host for *p*-benzoquinone.

In 1995, the Leigh group published the synthesis of the benzylic amide [2]catenane, **25** arguably the easiest synthesis of an interlocked architecture, again by chance, from the attempted preparation of benzylic amide macrocycle **26** as a receptor for carbon dioxide.[24] The reaction proceeded *via* an eight-molecule condensation reaction of isophthaloyl dichloride and *p*-xylylene diamine to give the [2]catenane in 20% yield.

The solid-state structure of **25** showed the two macrocyclic rings were held by a total of six intramolecular hydrogen bonds, four of which were involved in two sets of

bifurcated hydrogen bonds (as shown in Scheme 1.5).[7a] The hydrogen bond-directed assembly of catenene, **25** was easily adapted to form [2]rotaxanes (e.g. **27**) when the condensation reaction was carried out in the presence of a suitably stoppered thread.[25]

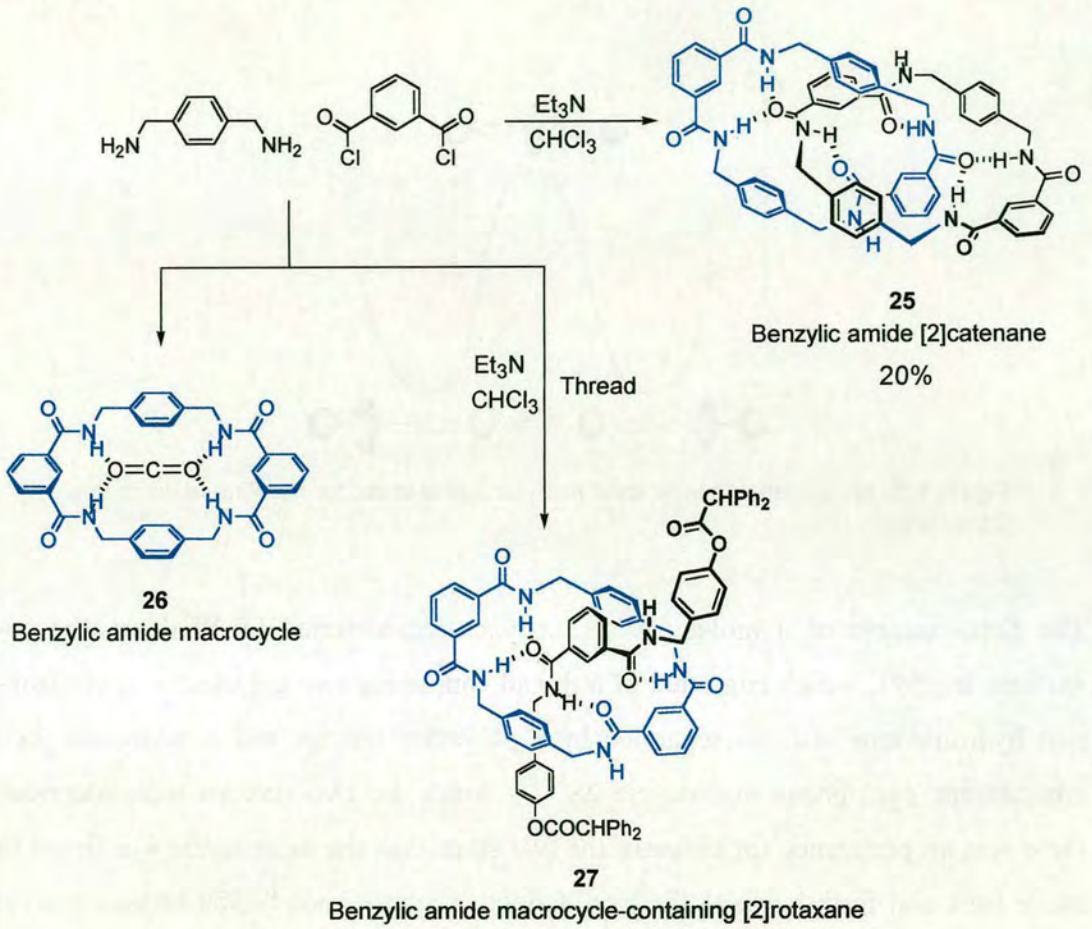

Scheme 1.5 Synthesis of benzylic amide [2]catenane, **25** and [2]rotaxane, **27**. The macrocycle **26** serves as a host for carbon dioxide.

1.5 Molecular shuttles

Rotaxanes offer a more versatile and greater range of systems upon which molecular devices and switches may be derived. Probably no other small molecule system has the ability to show such a large displacement of a single component within a

molecule as the shuttling of a macrocycle along the thread in a [2]rotaxane. Molecular shuttles contain two or more binding sites ('stations') within a thread. If the stations are the same (i.e. of degenerate energies) the macrocycle shuttles between them and populates both stations equally (Figure 1.2).

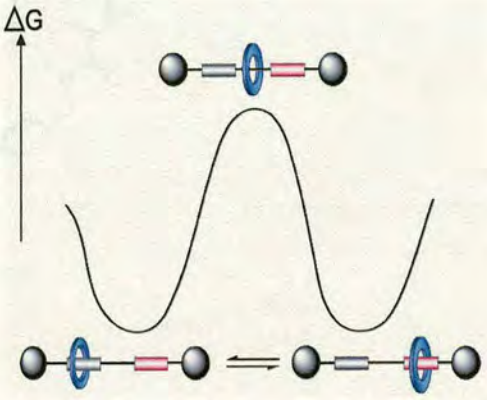

Figure 1.2 An activation barrier must be overcome in order for shuttling to occur in a [2]rotaxane.

The first example of a molecular shuttle was demonstrated by Stoddart and co-workers in 1991, which consisted of a thread containing two degenerate π-electron-rich hydroquinone stations separated by a polyether linkage and a π-electron-poor tetracationic cyclophane macrocycle $\mathbf{28}^{4+}$.[26] Since the two stations were identical, there was no preference for either of the two sites, thus the macrocycle was found to move back and forth between the two stations at approximately 500 times a second in $(CD_3)_2CO$ at room temperature (Scheme 1.6).[27]

Distinct translational isomers may be formed by incorporating two *different* stations on the thread where the macrocycle will have a preference for one over the other under different conditions and environments. Thus shuttling may be induced by application of an external stimulus leading to control over which translational isomer is obtained (stimuli-responsive molecular shuttles). So far, shuttling has been successfully achieved by electrochemical, chemical and photochemical stimuli as well as by solvent changes.

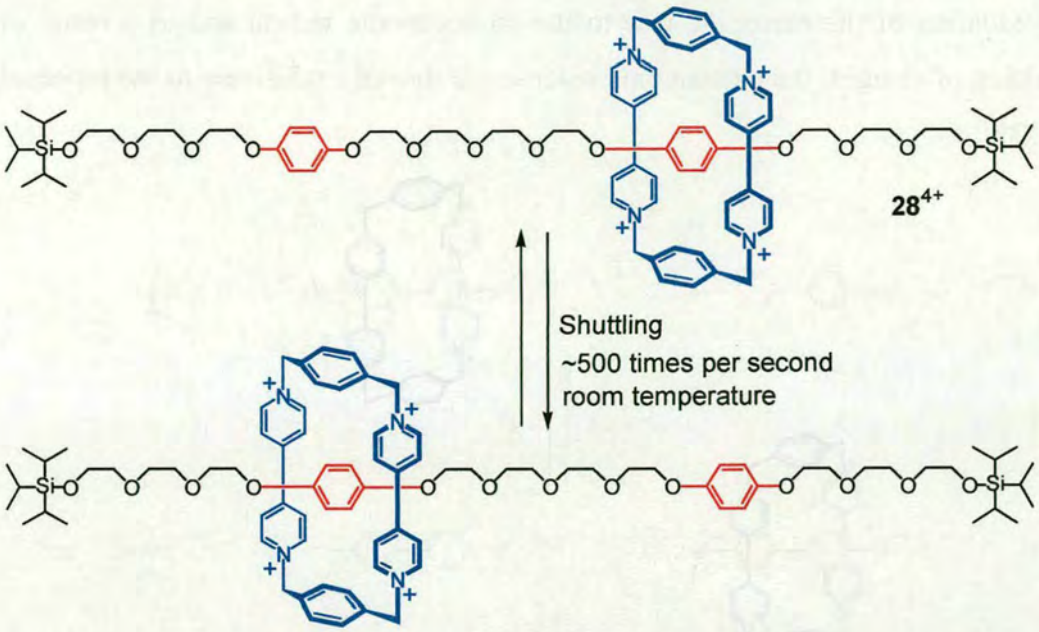

Scheme 1.6 The first molecular shuttle. The cyclophane macrocycle moves rapidly between two hydroquinone stations.

1.5.1 Electrochemically controlled molecular shuttles

Six years after the publication of the first molecular shuttle came the first demonstration of electrochemically controlled motion in a [2]rotaxane. Both Stoddart and Sauvage published molecular shuttles where the macrocycle could be *reversibly* switched between two stations.

In Stoddart's system, two stations with different π-electron-donor abilities were incorporated into the polyether chain $\mathbf{30}^{4+}$ (Scheme 1.7).[28] At equilibrium, the macrocycle was found preferentially to occupy the benzidine station (84% occupation at 229 K in CD_3CN) due to its greater π-electron-donor ability than the biphenol station – setting up stronger π-donor and π-acceptor interactions between the macrocycle and the thread. Control of shuttling was possible by altering the π-electron-donor ability of the two stations. Electrochemical induction resulted in

the oxidation of the benzidine unit to the monocationic radical and as a result of repulsion of charges, the tetracationic macrocycle moved exclusively to the biphenol unit, $\mathbf{29}^{5+}$.

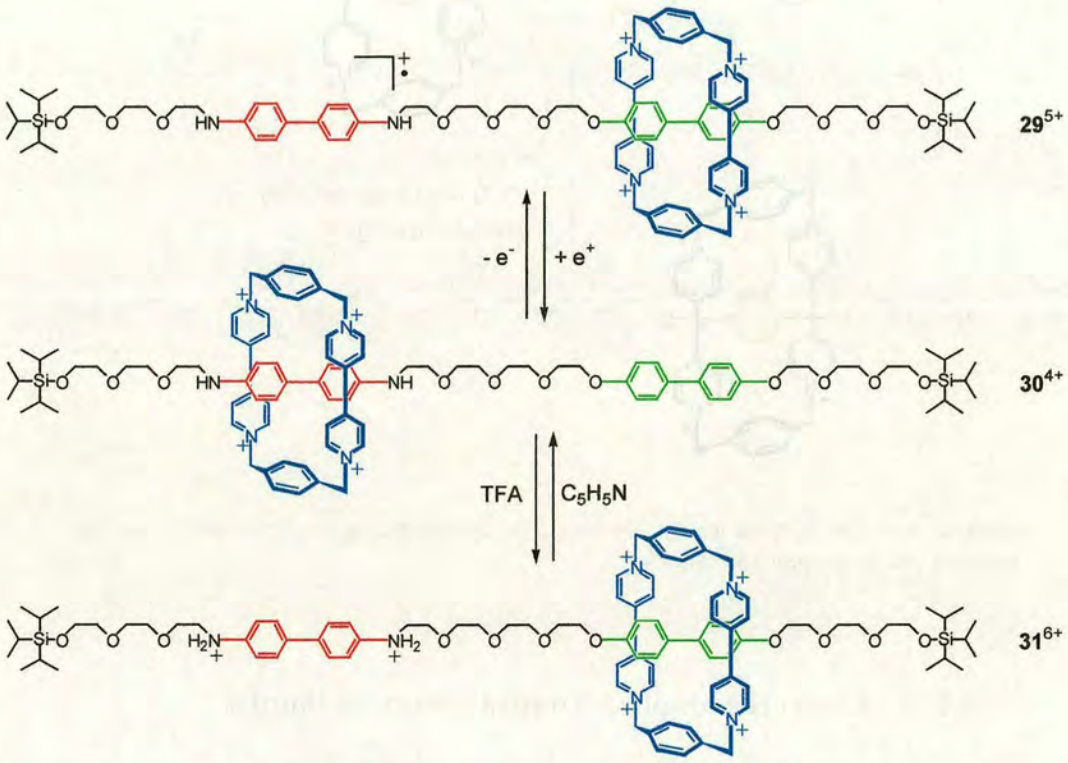

Scheme 1.7 Shuttling of the tetracationic cyclophane macrocycle along the thread is achieved by both electrochemical and chemical stimuli.

The make up of the components meant this molecular shuttle could also be switched chemically. Protonation of the benzidine unit with trifluoroacetic acid (TFA) moves the macrocycle to the biphenol station, $\mathbf{31}^{6+}$. The macrocycle returns to the benzidine unit on addition of pyridine, thus this one molecular shuttle can be controlled by two different stimuli.

Sauvage took a different approach to electrochemically switchable systems.[29] The reduction and oxidation of copper formed the basis of his electrochemically responsive molecular shuttle by taking advantage of the different coordination requirements of copper in its different oxidation states. In its lower oxidation state,

copper(I) is low coordinate and prefers a geometry that is close to tetrahedral; copper(II) on the other hand is high coordinate and prefers to adopt square pyramidal or trigonal bipyrimidal geometries. The molecular shuttle consisted of two distinct binding sites on the thread; a 1,10-phenanthroline (phen) bidentate ligand and 2,2',6',2''-terpyridine (terpy) terdentate ligand with the macrocycle containing a 1,10-phenanthroline unit (Scheme 1.8). The Cu^{+} center prefers tetrahedral geometry thus the translational isomer that is obtained has the Cu^{+} center coordinated to the phenanthroline ligands on both the thread and macrocycle, $\mathbf{32}^{+}$.

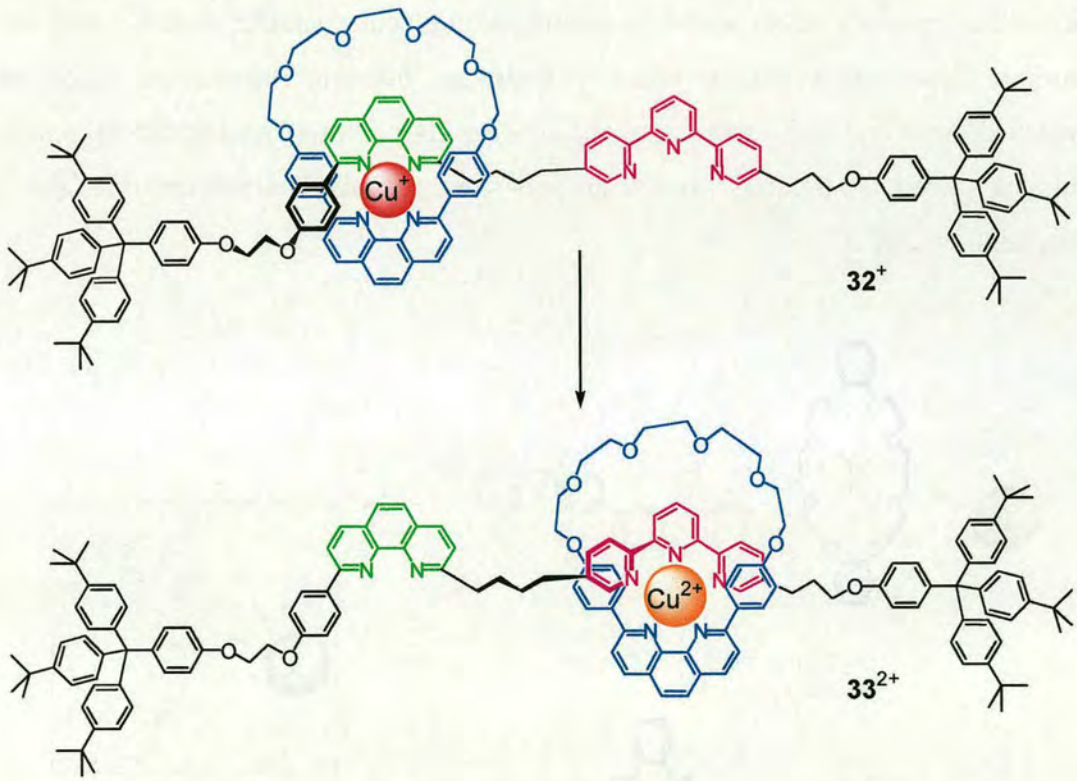

Scheme 1.8 An electrochemically responsive shuttle based on the oxidation and reduction of Cu^{+} and Cu^{2+}.

Shuttling of the phenanthroline-containing macrocycle is brought about by the oxidation of Cu^{+} to Cu^{2+}. The preference for pentacoordination in the Cu^{2+} oxidation state causes the shuttling of the macrocycle so that the Cu^{2+} center is now able to

adopt its preferred trigonal geometry by coordinating to the terpyridine ligand on the thread $\mathbf{33}^{2+}$. From cyclic voltammetry measurements, it was inferred that the motion of the macrocycle after oxidation of to Cu^{2+} is slow (hours). However, the process is reversible, as reduction of the Cu^{2+} center back to Cu^{+} drives the macrocycle back to the phenanthroline ligand on the thread and can be repeated again in a continuous cycle.

1.5.2 Chemically driven molecular shuttles

In another example of an acid-base controlled molecular shuttle, Stoddart and co-workers described a system whereby hydrogen bonding interactions could be switched "on" and "off" and cause the dibenzo[24]crown-8 macrocycle to shuttle along a thread containing two recognition sites: a dialkylammonium unit and a bipyridinium $\mathbf{34}^{3+}$.[30]

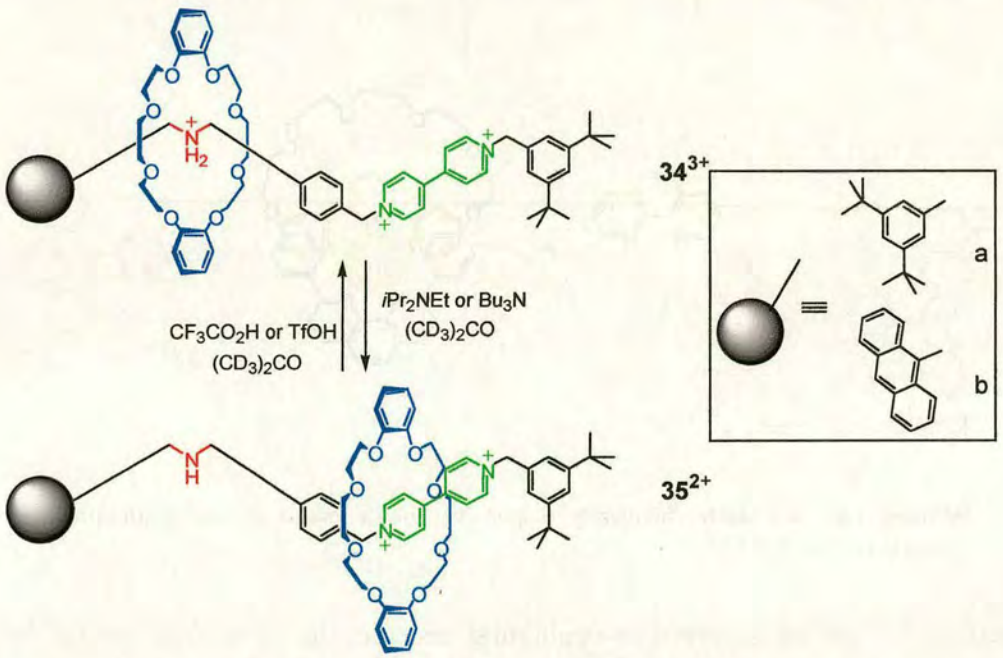

Scheme 1.9 Shuttling of the dibenzo[24]crown-8 macrocycle is achieved by addition of acid and base to switch "on" and "off" hydrogen bonding interactions.

Two-dimensional NMR spectroscopy (NOE) determined the position of the macrocycle to be exclusively upon the ammonium recognition site due to favourable hydrogen bonding interactions (+N–H•••O and C–H•••O) between the $CH_2NH_2^+$ of the dialkylammonium station and the oxygen atoms of the crown macrocycle in $(CD_3)_2CO$ at 298 K. Deprotonation with excess iPr$_2$NEt eliminated the intercomponent hydrogen bonds and caused the macrocycle to shuttle and occupy the second bipyridinium station $\mathbf{35}^{2+}$. The shuttle was reversed by addition of trifluoroacetic acid.

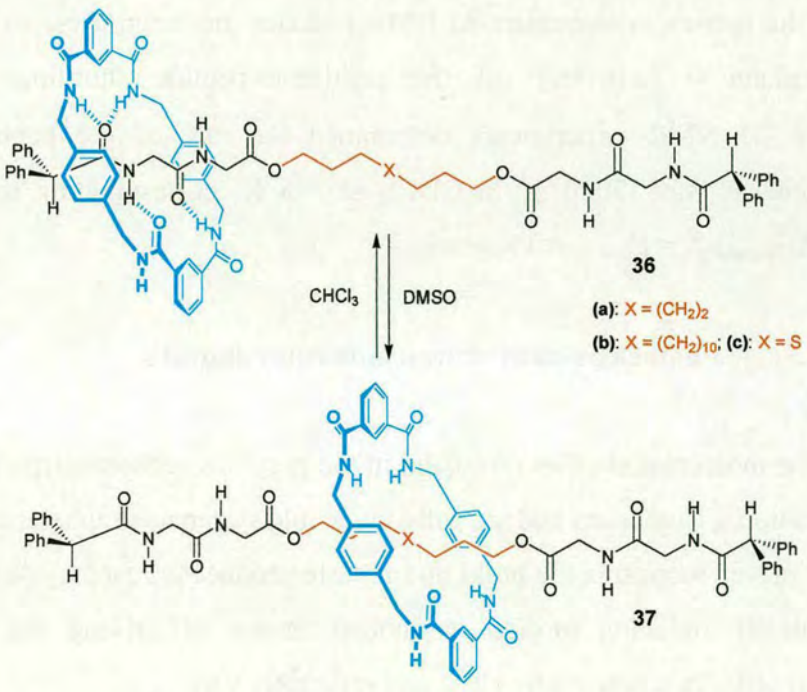

Scheme 1.10 Shuttling of the benzylic amide macrocycle is achieved by changes in polarity of solvent.

A novel type of stimulus used to control shuttling is change of environment as demonstrated in the peptide-based molecular shuttles developed in the Leigh group.[31] The molecular shuttles are made up of two glycylglycine peptide stations[32] separated by lipophilic alkyl chains (Scheme 1.10) and incorporate the standard benzylic amide macrocycle **36**. Since the two stations are degenerate, the macrocycle is found to shuttle between the two indentical peptide stations in nonpolar solvents such as

$CDCl_3$ at 298 K as shown by ^1H NMR spectroscopy. In hydrogen bond disrupting solvents such as DMSO-d_6, however, the macrocycle almost exclusively occupies the lipophilic region of the thread **37**.

An interesting property of this system is that the speed of shuttling can be altered by simple change of polarity of the solvent. Shuttling occurs through the disruption of the hydrogen bonds that hold the macrocyle over the peptide stations. Even addition of amounts of methanol, as small as 0.1% by volume, reduces the strength of the intramolecular bonds and causes a *doubling* in the speed of shuttling. Complete change of the solvent environment to DMSO causes the macrocycle to occupy the lipophilic chain – switching off the peptide-to-peptide shuttling. Variable temperature ^1H NMR experiments determined the rate of the peptide–peptide shuttling process was 37000 s^{-1} in $CDCl_3$ at 298 K, corresponding to an energy barrier of $\Delta G_{shuttling}^{\neq} = 11.2 \pm 0.3$ kcal mol^{-1}.

1.5.3 Photochemically driven molecular shuttles

Although the molecular shuttles discussed in the previous sections display extremely good translational isomerism and are fully reversible systems, an inherent problem of chemically driven motion is the build up of waste products as each cycle is repeated. Photochemically inducing motion is another means of driving the motion of molecular shuttles in a potentially clean and reversible way.

The hydrophobic cavity of cyclodextrins (CyDs) has been used to form host-guest inclusion complexes for many years. In water, they have been known effectively to form complexes with a range of aromatic compounds. This led to the design and synthesis of an α-CyD containing rotaxane by Nakashima and co-workers – using a *E*-azobenzene moiety as the central linear thread component terminated by 2,4-dinitrobenzene units (Scheme 1.11).[33,34]

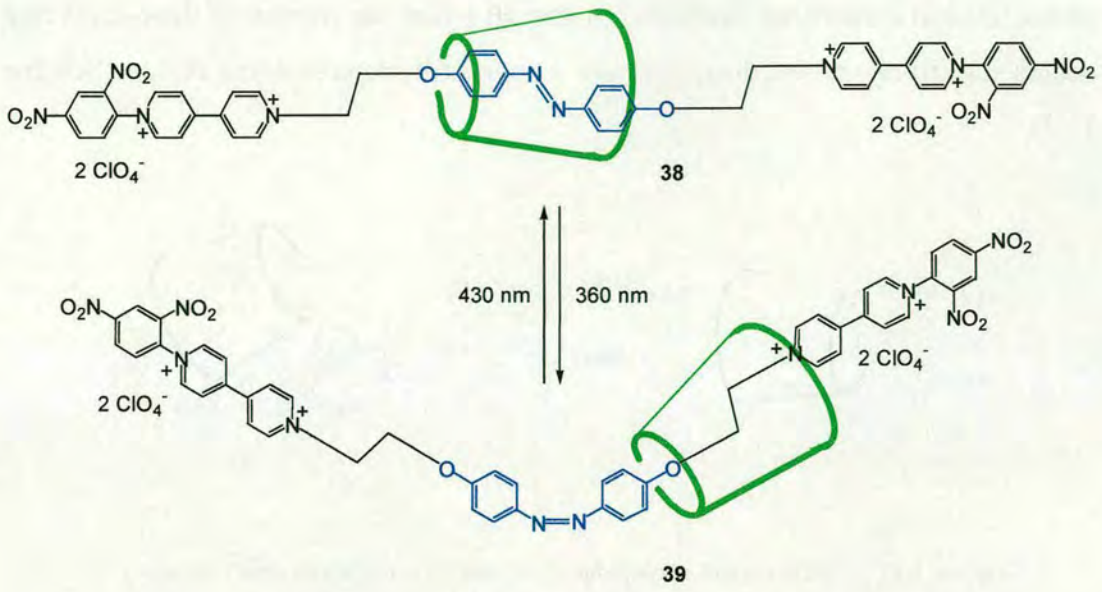

Scheme 1.11 Controlled motion of a α-cyclodextrin ring through *E/Z* photoisomerisation of the azobenzene unit on the thread.

The driving force for the formation of this rotaxane is the hydrophobic interactions between the thread and α-CyD components in water. The location of the α-CyD over the *E*-azobenzene station was determined by comparison of the ^{1}H NMR spectra of the free thread (D_2O, 323 K) and the corresponding rotaxane (DMSO-d_6, 323 K); showing the only two sets of resonances for the protons of the *E*-azobenzene station in the thread, which are split into four separate resonances in the rotaxane owing to the shape of the α-CyD ring. Irradiation at 360 nm causes isomerisation of the *E*-rotaxane **38** to the *Z*-isomer (photostationary state reached after 15 min, 67% *Z*-isomer), whereby shuttling of the α-CyD to the methylene spacer occurs, since the *Z*-azobenzene unit is too sterically demanding to be accommodated within the α-CyD cavity, **39**. Second irradiation at 430 nm moves the α-CyD back upon the *E*-azobenzene unit.

Recent research in the area of cyclodextrin encapsulated rotaxanes coupled with the *E/Z* isomerisation of stilbene units by Anderson *et al* has resulted in the

photochemical responsive molecular shuttle **40** where the motion of the α-CyD ring occurs selectively in *one* direction over a short stilbene-containing thread (Scheme 1.12).[35]

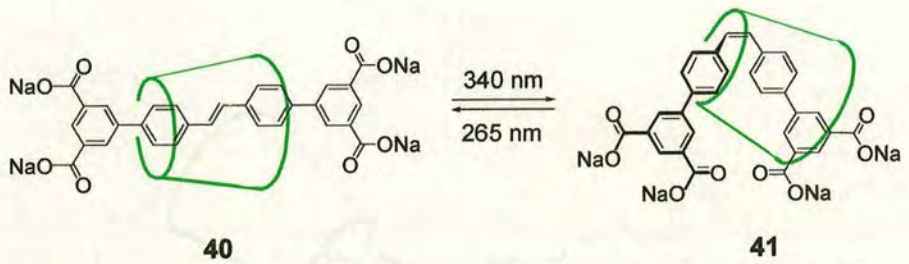

40 **41**

Scheme 1.12 Unidirectional photoinduced motion of a α-cyclodextrin ring along a short stilbene thread.

In much the same principle as the rotaxane developed by Nakashima and co-workers, irradiation at 340 nm produces the *Z*-isomer and induces the cyclodextrin ring to move and occupy selectively one end of the thread with the 6-rim of the cyclodextrin predominately near the *Z*-alkene unit of the stilbene (as confirmed by NOE investigations), **41**. The co-conformer where the cyclodextrin is located on the other side of the olefin is not observed, probably due to the steric hindrance of the stopper.

Recently, the Leigh group synthesised a photochemically responsive molecular shuttle by utilising the different hydrogen bond accepting ability of naphthalimide in the neutral and reduced states.[36] In **42**, a succinamide station is incorporated into the thread with a 3,6-di-*tert*-butyl-1,8-naphthalimide unit to act as both the second station and a stopper for the macrocycle. The two stations are separated by a C12 alkyl chain (Scheme 1.13).

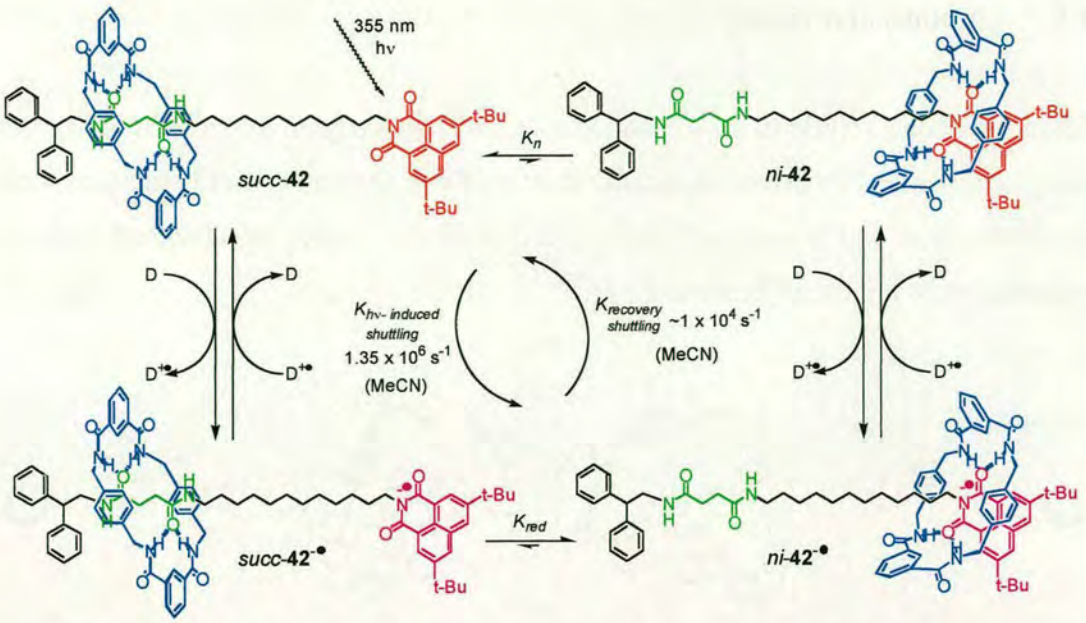

Scheme 1.13 Photoresponsive hydrogen bond-assembled molecular shuttle. Shuttling is triggered by irradiation at 355 nm (D = electron donor, e.g. DABCO).

The hydrogen bond accepting sites on the succinamide station causes the macrocycle to occupy this station, *succ*-**42** (confirmed by comparison of the ^{1}H NMR spectra of the thread and rotaxane), since in its neutral state, the naphthalimide has poor hydrogen bond accepting ability. After photoreduction of the naphthalimide station, initiated using a 355 nm laser pulse and addition of an electron donor (1,4-diazabicyclo[2.2.2]octane, DABCO, 1–10 nM), the reduced state of the naphthalimide station is formed which causes the macrocycle to move to this station over 1 μs, *nu*-**42**$^{\bullet-}$. Charge recombination of the naphthalimide radical anion occurs over a slower time frame, >100 μs, after which the macrocycle shuttles back to the succinamide station and the cycle can be repeated once again. This molecular shuttle can be described to be reminiscent of a working piston whereby the power stroke (application of a laser pulse) produces mechanical work, in the form of shuttling of the macrocycle along the thread (it has been calculated that cycling of the process at 10^4 times per second can generate ~10^{-15} W of mechanical power for each shuttle) with a recovery stroke (charge recombination) that returns the system back to its original state.

1.6 A molecular muscle

From molecular shuttle to molecular muscle, Sauvage adapted the original design of the electrochemically driven molecular shuttle to a molecular assembly that can form both stretched and contracted conformations at the trigger of chemical stimuli; reminiscent of a muscle (Scheme 1.14).[37]

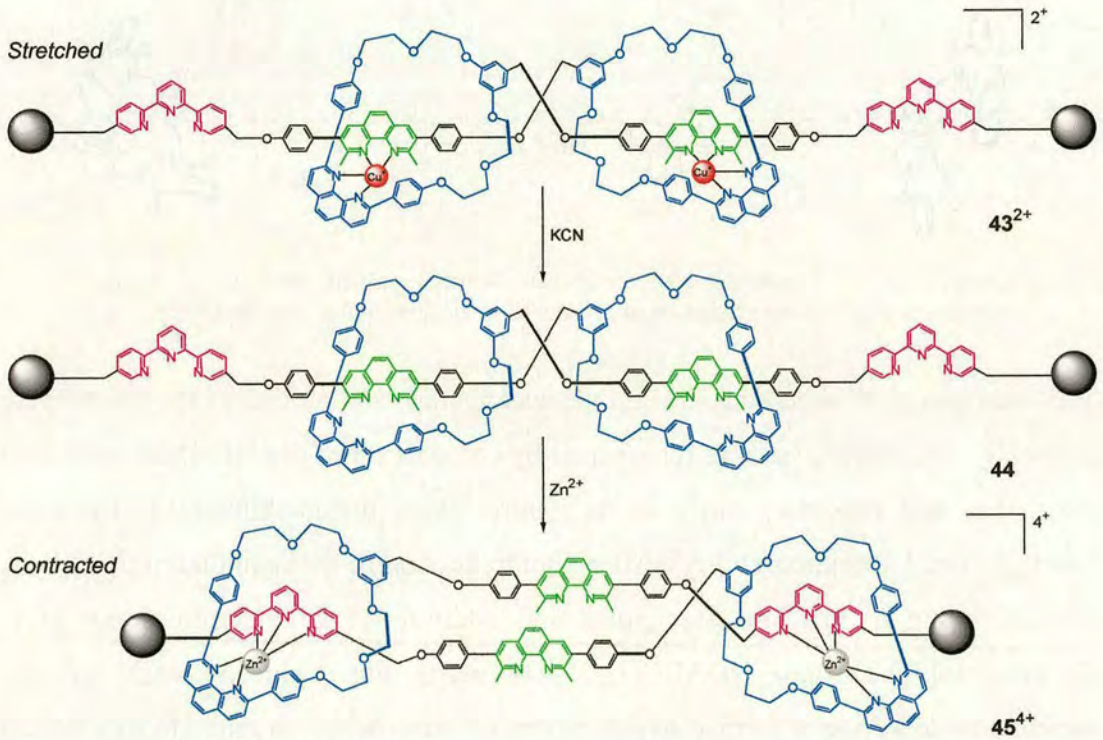

Scheme 1.14 The 'muscle' is stretched when coordinated to Cu^{+} and contracted when coordinated to Zn^{2+}.

The doubly threaded compound containing phenanthroline and terpyridine ligands is a stretched conformation when Cu^{+} is coordinated to the molecule $\mathbf{43}^{2+}$. Demetalation using KCN followed by subsequent remetalation by Zn^{2+} achieves the contracted conformation, $\mathbf{45}^{4+}$.

1.7 Conclusion

In the last thirty years, research has developed from the observation of simple rotary motion in molecules to the first synthetic systems that display controlled unidirectional rotational motion at the trigger of an external stimulus. We have seen the exponential growth of mechanically interlocked architectures, namely, rotaxanes and catenanes and particularly in the past few years, the controlled motion of their molecular components using a wide range of external stimuli. However, although these developments are highly significant, a great distance still has to be travelled to reach the level of accomplishment and utility achieved by Nature – or envisioned by Feynman.

1.8 References

1. Whitesides, G. M.; Simanek, E. E.; Mathias, J. P.; Seto, C. T.; Chin, D. N.; Mammen, M.; Gordon, D. M. *Acc. Chem. Res.* **1995**, *28*, 37–44.
2. For a review of noncovalent synthesis using hydrogen bonding see: Prins, L. J.; Reinhoudt, D. N.; Timmerman, P. *Angew. Chem. Int. Ed.* **2001**, *40*, 2383–2426.
3. (a) Raymo, F. M.; Stoddart, J. F. *Chem. Rev.* **1999**, *99*, 1643–1663. (b) Kim, K. *Chem. Soc. Rev.* **2002**, *31*, 96–107.
4. *Molecular catenanes, Rotaxanes and Knots;* Sauvage, J. -P.; Dietrich-Buchecker, C.; Eds.; Wiley-VCH, Wseinheim, 1999.
5. For examples of molecular machines based on transition metal complexes see: (a) Amendola, V.; Fabbrizzi, L.; Mangano, C.; Pallavicini, P. *Acc. Chem. Res.* **2001**, *34*, 488–493. (b) Colasson, B. X.; Dietrich-Buchecker, C. O.; Jimenez-Molero, M. C.; Sauvage, J. -P. *J. Phys. Org. Chem.* **2002**, *15*, 476–483.
6. For general reviews on rotaxane and catenane-based molecular machines see: (a) Balzani, V.; Gómez-López, M.; Stoddart, J. F. *Acc. Chem. Res.* **1998**, *31*, 405–414. (b) Sauvage, J. -P. *Acc. Chem. Res.* **1998**, *31*, 611–619. (c) Balzani, V.; Credi, A.; Raymo, F. M.; Stoddart, J. F. *Angew. Chem. Int. Ed.* **2000**, *39*, 3349–3391. (d) Pease, A. R.; Jeppesen, J. O.; Stoddart, J. F.; Luo, Y.; Collier, C. P.; Heath, J. R. *Acc. Chem. Res.* **2001**, *34*, 433–444. (e) Ballardini, R.; Balzani, V.; Credi, A.; Gandolfi, M. T.; Venturi, M. *Acc. Chem. Res.* **2001**, *34*, 445–455.
7. For examples of two and three-blade propellers: (a) Gust, D.; Mislow, K, *J. Am. Chem. Soc.* **1973**, *95*, 1535–1547. (b) Finocchiaro, P.; Gust, D.; Mislow, K. *J. Am. Chem. Soc.* **1974**, *96*, 3198–3205. (c) Glaser, R.; Blount, J. F.; Mislow, K. *J. Am. Chem. Soc.* **1980**, *102*, 2777–2786. (d) Biali, S. E.; Nugiel, D. A.; Rappoport, Z. *J. Am. Chem. Soc.* **1989**, *111*, 846–852.
8. Ōki, M. *Angew. Chem. Int. Ed. Engl.* **1976**, *15*, 87–93.
9. (a) Kawada, Y.; Iwamura, H, *J. Am. Chem. Soc.* **1981**, *103*, 958–960. (b) Kawada, Y.; Iwamura, H. *Tetrahedron Lett.* **1981**, *22*, 1533–1536. (c) Koga, N.;

Kawada, Y.; Iwamura, H, *J. Am. Chem. Soc.* **1983**, *105*, 5498–5499. (d) Kawada, Y.; Iwamura, *J. Am. Chem. Soc.* **1983**, *105*, 1449–1459. (e) Kawada, Y.; Iwamura, H.; Okamoto, Y.; Yuki, H, *Tetrahedron Lett.* **1983**, *24*, 791–794. (f) Kawada, Y.; Okamoto, Y.; Iwamura, H. *Tetrahedron Lett.* **1983**, *24*, 5359–5362. (g) Iwamura, H.; Ito, T.; Ito, H.; Toriumi, K.; Kawada, Y.; Osawa, E.; Fujiyoshi, T.; Jamie, C. *J. Am. Chem. Soc.* **1984**, *106*, 4712–4717.

10. (a) Hounshell, W. D.; Johnson, C. D.; Guenzi, A.; Cozzi, F.; Mislow, K. *Proc. Natl. Acad. Sci. USA* **1980**, *77*, 6961–6973. (b) Cozzi, F.; Guenzi, A.; Johnson, C. A.; Mislow, K.; Hounshell, W. D.; Blount, J. F. *J. Am. Chem. Soc.* **1981**, *103*, 957–958. (c) Johnson, C. A.; Guenzi, A.; Mislow, K.; *J. Am. Chem. Soc.* **1983**, *105*, 6240–6242. (d) Johnson, C. A.; Guenzi, A.; Nachbar, R. B.; Blount, J. F.; Wennerström, O.; Mislow, K. *J. Am. Chem. Soc.* **1982**, *104*, 5163–5168. (e) Bürgi, H. -B.; Hounshell, W. D.; Nachbar, R. B.; Mislow, K. *J. Am. Chem. Soc.* **1983**, *105*, 1427–1438. (f) Guenzi, A.; Johnson, C. A.; Cozzi, F.; Mislow, K. *J. Am. Chem. Soc.* **1981**, *103*, 1438–1448.
11. Kelly, T. R.; Bowyer, M. C.; Bhaskar, K. V.; Bebbington, D.; Garcia, A.; Lang, F.; Kim, M. H.; Jette, M. P. *J. Am. Chem. Soc.* **1994**, *116*, 3657–3658.
12. (a) Kelly, T. R.; Tellitu, I.; Sestelo, J. P. *Angew. Chem. Int. Ed. Engl.* **1997**, *36*, 1866–1868. (b) Kelly, T. R.; Sestelo, J. P.; Tellitu, I. *J. Org. Chem.* **1998**, *63*, 3655–3665. (c) Davis, A. P. *Angew. Chem. Int. Ed.* **1998**, *37*, 909–910.
13. (a) Kelly, T. R.; De Silva, H.; Silva, R. A. *Nature* **1999**, *401*, 150–152. (b) Kelly, T. R.; Silva, R. A.; De Silva, H.; Jasmin, S.; Zhao, Y. *J. Am. Chem. Soc.* **2000**, *122*, 6935–6949.
14. Koumura, N.; Zijlstra, R. W. J.; van Delden, R. A.; Harada, N.; Feringa, B. L.; *Nature* **1999**, *401*, 152–155.
15. For synthetic details see: Harada, N.; Koumura, N.; Feringa, B. L. *J. Am. Chem. Soc.* **1997**, *119*, 7256–7264.
16. van Delden, R. A.; Koumura, N.; Harada, N.; Feringa, B. L. *Proc. Natl. Acad.*

Sci. USA **2002**, *99*, 4945–4949.

17. Koumura, N.; Geertsema, E. M.; van Gelder, M. B.; Meetsma, A.; Feringa, B. L. *J. Am. Chem. Soc.* **2002**, *124*, 5037–5051.
18. (a) Wasserman, E. *J. Am. Chem. Soc.* **1960**, *82*, 4433–4434. (b) Frisch, H. L.; Wasserman, E. *J. Am. Chem. Soc.* **1961**, *83*, 3789–3795. (c) Harrison, I. T.; Harrison, S. J. *J. Am. Chem. Soc.* **1967**, *89*, 5723–5724.
19. Schill, G.; Zollenkopf, H. *Liebigs Ann. Chem.* **1969**, *721*, 53–74.
20. Hunter, C. A. *J. Am. Chem. Soc.* **1992**, *114*, 5303–5311.
21. (a) Hunter, C. A. *J. Chem. Soc., Chem. Commun,* **1991**, 749–751. (b) Hunter, C. A. *Chem. Soc. Rev.* **1994**, *23*, 101–109.
22. Vögtle, F.; Meier, S.; Hoss, R. *Angew. Chem. Int. Ed. Engl.* **1992**, *31*, 1619–1622.
23. Ottens-Hildebrandt, S.; Meier, S.; Schmidt, W.; Vögtle, F. *Angew. Chem. Int. Ed. Engl.* **1994**, *33*, 1767–1770.
24. (a) Johnston, A. G.; Leigh, D. A.; Pritchard, R. J.; Deegan, M. D. *Angew. Chem. Int. Ed. Engl.* **1995**, *34*, 1209–1211. (b) Johnston, A. G.; Leigh, D. A.; Nezhat, L.; Smart, J. P.; Deegan, M. D. *Angew. Chem. Int. Ed. Engl.* **1995**, *34*, 1212–1216.
25. Leigh, D. A.; Murphy, A.; Smart, J. P.; Slawin, A. M. Z. *Angew. Chem. Int. Ed. Engl.* **1997**, *36*, 728–732.
26. Anelli, P. -L.; Spencer, N.; Stoddart, J. F. *J. Am. Chem. Soc.* **1991**, *113*, 5131–5133.
27. For other examples of translational motion in rotaxane systems by Stoddart and co-workers see: Amabilino, D. B.; Ashton, P. R.; Boyd, S. E.; Gómez-López, M.; Haynes, W.; Stoddart. J. F. *J. Org. Chem.* **1997**, *62*, 3062–3075.
28. Bissel, R. A.; Córdova, E.; Kaifer, A. E.; Stoddart, J. F. *Nature* **1994**, *369*, 133–137.
29. (a) Gaviña, P.; Sauvage, J. -P. *Tetrahedron Lett.* **1997**, *38*, 3521–3524. (b)

Armaroli, N.; Balzani, V.; Collin, J. -P.; Gaviña, P.; Sauvage, J. -P.; Ventura, B, *J. Am. Chem. Soc.* **1999**, *121*, 4397–4408.

30. (a) Martínez-Díaz, M. -V.; Spencer, N.; Stoddart, J. F. *Angew. Chem. Int. Ed. Engl.* **1997**, *36*, 1904–1907. (b) Ashton, P. R.; Ballardini, R.; Balzani, V.; Baxter, I.; Credi, A.; Fyfe, M. C. T.; Gandolfi, M. T.; Gómez-López, M.; Martínez-Díaz, M. -V.; Piersanti, A.; Spencer, N.; Stoddart, J. F.; Venturi, M.; White, A. J. P.; Williams, D. J. *J. Am. Chem. Soc.* **1998**, *120*, 11932–11942.
31. Lane, A. S.; Leigh, D. A.; Murphy, A. *J. Am. Chem. Soc.* **1997**, *119*, 11092–11093.
32. Leigh, D. A.; Murphy, A.; Smart, J. P.; Slawin, A. M. Z. *Angew. Chem. Int. Ed. Engl.* **1997**, *36*, 728–732.
33. Murakami, H.; Kawabuchi, A.; Kotoo, K.; Kunitake, M.; Nakashima, N. *J. Am. Chem. Soc.* **1997**, *119*, 7605–7606.
34. For other examples of cyclodextrin-based rotaxanes, see: Harada, A. *Acc. Chem. Res.* **2001**, *34*, 456–464.
35. Stainer, C. A.; Alderman, S. J.; Claridge, T. D. W.; Anderson, H. L. *Angew. Chem. Int. Ed.* **2002**, *41*, 1769–1772.
36. Brouwer, A. M.; Frochot, C.; Gatti, F. G.; Leigh, D. A.; Mottier, L.; Paolucci, F.; Roffia, S.; Wurpel, G. W. H. *Science* **2001**, *291*, 2124–2128.
37. (a) Jiménez, M. C.; Dietrich-Buchecker, C.; Sauvage, J. -P. *Angew. Chem. Int. Ed.* **2000**, *39*, 3284–3287. (b) Feringa, B. L. *Nature* **2000**, *408*, 151-153. (c) Collin, J. P.; Dietrich-Buchecker, C. O.; Gaviña, P.; Jimenez-Molero, M. C.; Sauvage, J. -P. *Acc. Chem. Res.* **2001**, *34*, 477–487.

CHAPTER TWO

Rigid Hydrogen Bonding Templates

Published as

"Stiff, and Sticky in the Right Places: Dramatic Influence of Preorganizing Guest Binding Sites on the Hydrogen Bond-directed Assembly of Rotaxanes"

Francesco G Gatti, David A Leigh, Sergey Nepogodiev, Alexandra M Z Slawin, Simon J Teat and Jenny K Y Wong *J. Am. Chem. Soc.* **2001**, *121*, 5983–5989

Acknowledgements

The following people are gratefully acknowledged for their contributions to this paper: the rotaxanes **6-9** were first synthesised by Dr. Francesco Gatti (University of Warwick), rotaxanes **11-12** were synthesised by Dr. Sergey Nepogodiev (University of Warwick). Drs Alex Slawin (University of St Andrews) and Simon Teat (CCLRC Daresbury Laboratory) are thanked for their assistance with the crystal structures.

"The most exciting phrase to hear in science, the one that heralds new discoveries, is not 'Eureka!' but 'That's funny...'"

Isaac Asimov

Rigid Hydrogen Bonding Templates – Synopsis

*Since the serendipitous discovery of benzylic amide catenanes in 1995, the reaction has been adapted to the hydrogen bond-directed assembly of benzylic amide macrocycle-containing rotaxanes. The procedure involves a five-component "clipping" reaction of the macrocycle precursor around the thread template (Scheme I). This route to mechanically interlocked architectures resulted in a whole series of benzylic amide macrocycle-containing [2]rotaxanes being prepared (**I-VII**) where the yield ranges from 28% (**I**) using a isophthalamide thread to 62% (**II**) with a glycylglycine containing thread.*

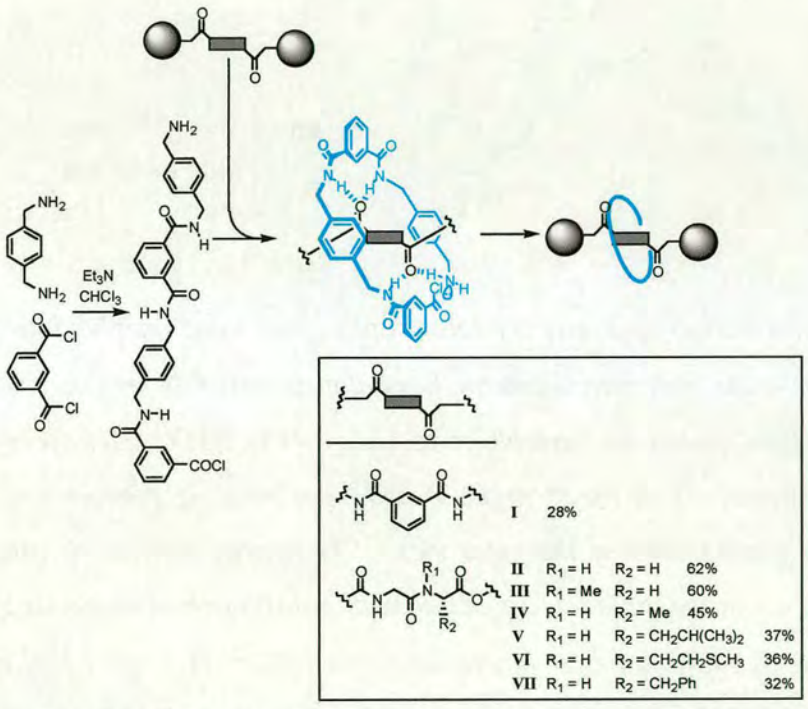

Scheme I *Hydrogen bond-directed assembly of a series of benzylic amide macrocycle-containing [2]rotaxanes.*

Even with a yield of 62%, the dipeptide template is still far from being optimal to template the formation of the benzylic amide macrocycle around it. The inherent flexibility of the template not only gives rise to internal degrees of freedom that need to be restricted on rotaxane formation but also leads to favourable formation of intramolecular hydrogen bonds in the peptide itself.

In this chapter the effect of preorganising the hydrogen bonding sites of the thread to suit the requirements of the benzylic amide macrocycle is examined. The one-step synthesis of a fumaramide rotaxane in 97% yield is the most facile synthesis of a mechanically interlocked molecule described to date. The basis for such an efficient five-component reaction is that the fumaramide double bond not only provides rigidity but also fixes the distance of the hydrogen bonding sites to compliment the forming macrocycle. The preorganisation is so effective that even when the amide groups are substituted for poor hydrogen bond acceptors such as esters, rotaxanes are still isolated.

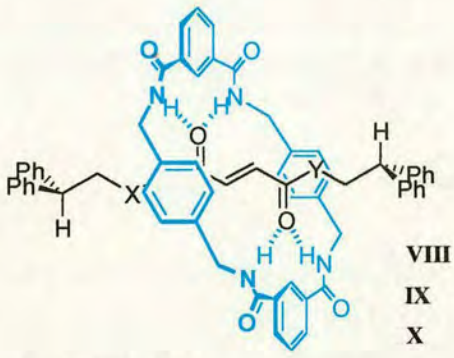

VIII	X, Y = NH	97%
IX	X = NH, Y = O	35%
X	X, Y = O	3%

Structure elucidation by X-ray crystallography gives some insights into the effect of weak amide–ester hydrogen bonds on the conformation of the macrocycle in the solid state. Further studies by variable temperature (VT) NMR spectroscopy provide a quantitative analysis of the strength of hydrogen bonding between the macrocycle and thread components of the rotaxanes. The energy barrier to rotation of the macrocycle about the thread decreases on each substitution of an amide group on the fumaramide thread to an ester functionality from $\Delta G = 11.5 \pm 0.2$ *kcal mol*$^{-1}$ ***(VIII)****,* *to* $\Delta G = 9.3 \pm 0.2$ *kcal mol*$^{-1}$ ***(IX)*** *to* $\Delta G = 7.2 \pm 0.4$ *kcal mol*$^{-1}$ ***(X)****.*

Not only do these results show that the hydrogen bond-directed assembly can be extremely efficient if the thread template is preorganised in such a way so as to maximise its hydrogen bond interactions with forming macrocycle, but the study suggests that in $CDCl_3$ *amide–ester NH···O=C hydrogen bonds are ~1 kcal mol*$^{-1}$ *weaker than the corresponding amide–amide interactions.*

2.1 Introduction

The importance of the preorganization of binding sites in host-guest complexation processes has long been recognized.[1] For example, the structurally rigid spherand **1** binds Li^+ $>10^{12}$ times stronger than the acyclic podand **2** despite near-identical aryl ether–metal ion electrostatic interactions being present in each complex.[2] Whilst the drastically decreased binding of **2** can in part be attributed to the differences in solvation of the free ligands, a significant entropic cost has to be paid to organize the convergent binding sites of the flexible free host into the conformation involved in metal ion complexation. Here we describe how the preorganization of the divergent binding sites of a thread, the "guest"(!), provides a dramatic increase in macrocycle template efficiency, enabling the use of even modest hydrogen bond acceptor groups (esters) in the multicomponent synthesis of hydrogen bond-assembled rotaxanes.[3]

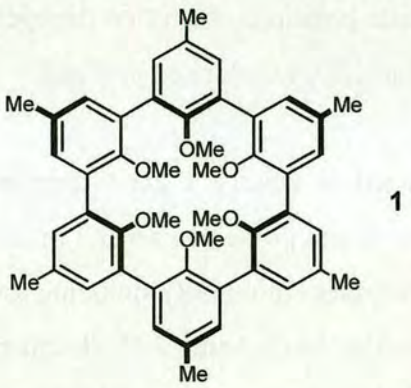

1

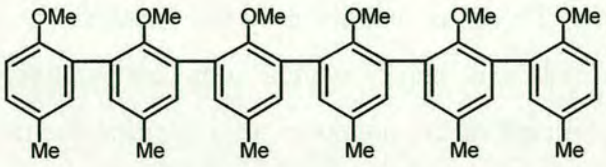

2

Isophthalamide (benzene 1,3-dicarboxyamide) and peptide-based threads have been shown[4] to template the formation of benzylic amide macrocycles about them in nonpolar solvents to give rotaxanes and molecular shuttles in good (typically 28–62%) yields. The five-component "clipping" reactions (Scheme 2.1) are able to

produce rotaxanes because the immediate precursor to macrocycle formation, **3**, preferentially adopts a linear conformation as a consequence of the preference for the aromatic 1,3-diamide unit to adopt a *syn-anti* conformation,[5] which holds the two reactive ends of **3** far apart in a spatial arrangement unsuitable for macrocyclic ring closure. Thus, in the absence of a suitable template, structures such as **3** are long lived in solution and may even dimerize to form larger macrocycles in preference to intramolecular ring closure.[5a] Under the rotaxane-forming reaction conditions, however, cooperative multipoint hydrogen bonding between the precursor and a thread (e.g. **4**) promotes a conformational change in **3** (the *syn-syn* rotamer is stabilized by the bifurcated hydrogen bonding motif shown in **I**, Scheme 2.1) which brings the amine and acid chloride in close proximity leading to rapid cyclization of **3**.[4b] Additional hydrogen bonding interactions between **3** and a *second* site on the thread are important for efficient rotaxane formation since they hold one or both ends of the precusor in appropriate positions, such that the cyclization of **3** occurs around the thread to give the mechanically interlocked product.

Although the dipeptide motif is clearly a good template for the benzylic amide macrocycle system, the free thread possesses several internal degrees of freedom that are lost in the key supramolecular complex **I**, including torsional freedom around the three backbone bonds shown in **4a** (Scheme 2.1). Furthermore, the flexibility of the peptide backbone means that it can adopt additional conformations (e.g. **4b**) reminiscent of γ-turns. These are stabilized by the formation of seven-membered-ring intramolecular hydrogen bonds which, although relatively uncommon in proteins, may be significant in the nonpolar solvents used for promoting rotaxane formation.[6] It seemed likely, therefore, that the unfavorable requirements of breaking intramolecular hydrogen bonds and/or the loss of entropy in going from a flexible thread to the much stricter conformational and co-conformational requirements of the supramolecular transition state could be overcome more efficiently by preorganizing the hydrogen bonding sites of the thread in a spatial arrangement already suited for templating benzylic amide macrocycle formation.

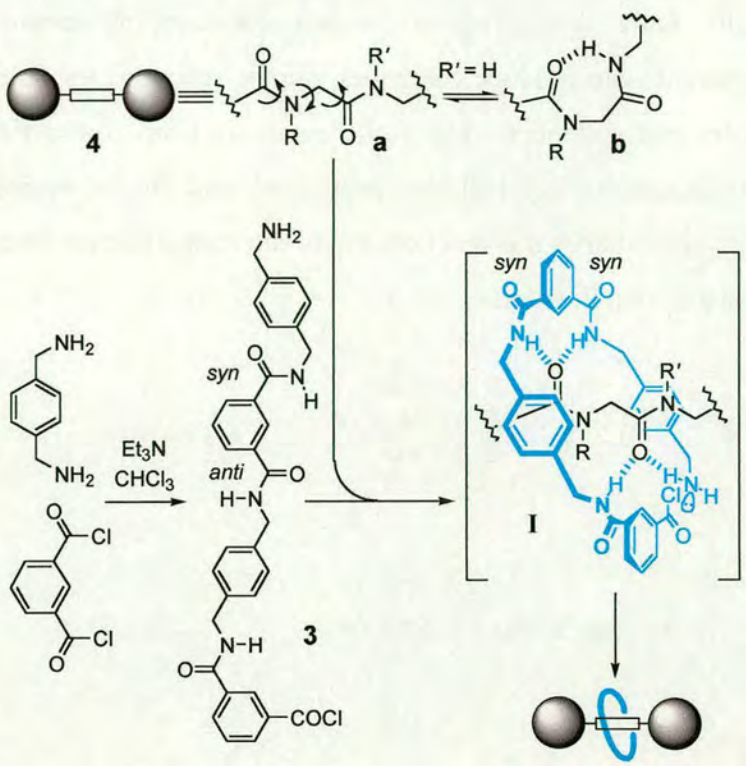

Scheme 2.1 Rotaxane formation *via* flexible, peptide-based hydrogen bond templates (R, R'= H, Me).

2.2 Results and Discussion

The rigid fumaramide thread, **5**, was prepared in one step from the commercially available amine and *bis*-acid chloride. Treatment of **5** with four equivalents of *p*-xylylene diamine and isophthaloyl dichloride (1:9 MeCN:$CHCl_3$, Et_3N, 4 h, high dilution) was sufficient for complete consumption of the thread. Filtration followed by spontaneous crystallization upon addition of water to a dimethylformamide solution of the crude product, led to the rotaxane **6** in 97% yield (Scheme 2.2). The yield is all the more remarkable considering that fumaramide rotaxanes previously prepared by the Vögtle group are formed in much more modest (18–26%) yields,[7] despite being carried out using a presynthesized macrocycle in a three-component "threading" procedure (which can *only* produce free thread or rotaxane) rather than

the intrinsically more demanding five-component clipping method (which, in addition to rotaxane, can produce catenanes, simple macrocycles, linear and higher cyclic oligomers and polymers). The facile synthesis from commerically available reagents, chromatography-free isolation procedure, and "world record" yield for a [2]rotaxane synthesis makes this reaction one of the most effective routes to rotaxane architectures discovered thus far.

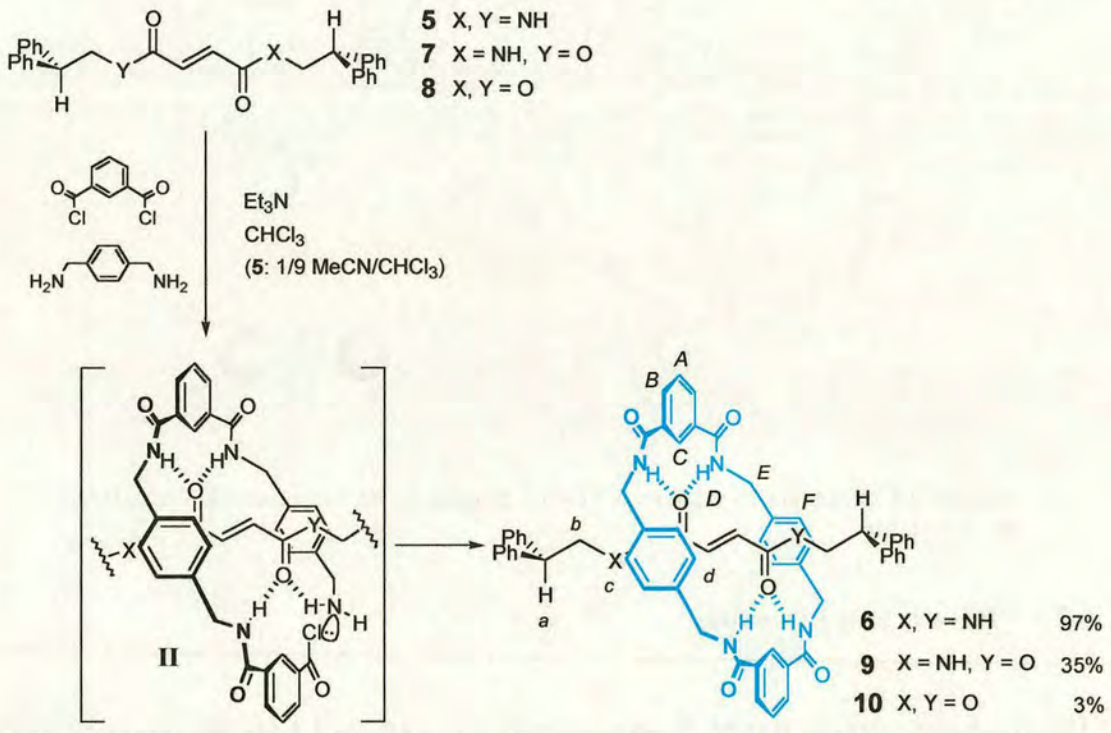

Scheme 2.2 Rotaxane formation *via* preorganized, rigid fumaryl-based hydrogen bond templates.

Single crystals of **6** suitable for investigation by *X*-ray crystallography using a synchrotron source were obtained directly from the work up procedure. The crystal structure (Figure 2.1) shows that the positioning of the amide groups in the fumaramide thread allows them to form four bifurcated intercomponent hydrogen bonds without requiring any distortion in the conjugation of the isophthalamide systems (the amides are close to planar with the aromatic rings) whilst the macrocycle adopts a favorable chair conformation. The two hydrogen bond donor

groups of the thread are satisfied in the solid state by included molecules of DMF, which pack to form additional π-stacks between the phenyl groups of the stoppers and the isophthaloyl rings of the macrocycle. A further characteristic of the system is the lack of sterically demanding sp^3 centres between the two hydrogen bond accepting groups on the thread, previously found[4b,d] to disrupt the complementarity between the flat, close fitting internal surfaces of the mechanically interlocked architecture. Indeed, the proportions of the thread serve to maximize attractive van der Waals interactions between the two components, with the olefin providing an additional π-stacking feature for the xylylene units of the macrocycle.

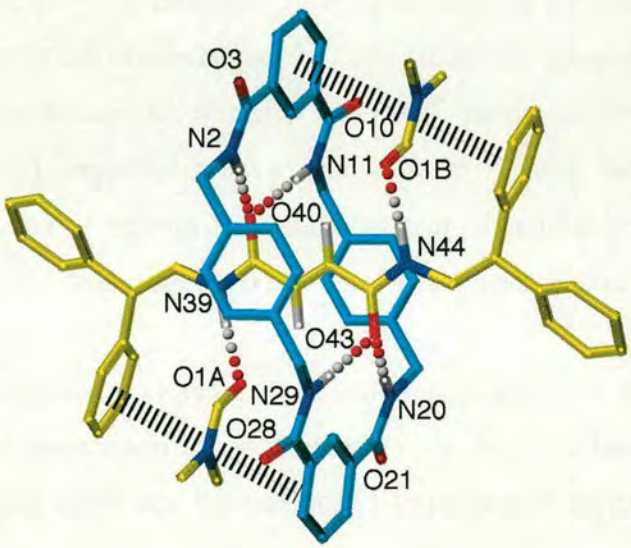

Figure 2.1 *X*-ray crystal structure of the fumaramide [2]rotaxane **6** (for clarity carbon atoms of the macrocycle are shown in blue and the carbon atoms of the thread in yellow; oxygen atoms are depicted in red, nitrogen atoms dark blue and selected hydrogen atoms white). Intramolecular hydrogen bond distances (Å): O40–HN2/O43–HN20 1.98, O40–HN11/O43–HN29 2.06.

The success of the fumaramide template can thus be attributed to:

(i) the spatial arrangement of the co-operative hydrogen bonding sites on the thread which is close-to-ideal as a template for benzylic amide macrocycle formation, i.e. allows a low energy (chair-type) conformation of the

macrocycle precursor **3** to bind efficiently to the hydrogen bonding sites of the thread in the key supramolecular intermediate **II** (Scheme 2.2).

(ii) the rigidity and shape of the template unit. No internal degrees of freedom of the thread are lost upon complexation with **3** to form **II**.

(iii) the inability of the free fumaramide thread **5** to fold and form intramolecular hydrogen bonds.

The use of amide groups in the thread is also significant, of course, because they are excellent hydrogen bond acceptors (H-bond basicity, β^{H}_{2}, typically ~0.66).[8] Indeed, amongst common functional group types the β^{H}_{2} of amides is only exceeded by groups with pronounced mesomeric or ionic character (N^{+}–O^{-}, S^{+}–O^{-}, P^{+}–O^{-} *etc*). However, preorganizing the hydrogen bonding sites of the thread into the ideal geometry illustrated in Figure 2.1 is so effective at enhancing the macrocyclic template effect that esters – significantly weaker hydrogen bond acceptors than amides (β^{H}_{2} ~0.45, similar to that of ethers and nitriles) – can also promote the cyclization of **3** to give mechanically interlocked architectures.

The threads **7** and **8**, replacing one and both secondary amides with ester groups respectively, both act as templates for benzylic amide macrocycle formation (Scheme 2.2), manifested in the formation of [2]rotaxanes **9** and **10** in yields of 35 and 3%, respectively.

Whilst at first sight the yield of the *bis*-ester rotaxane **10** may appear modest at 3%, that the reaction proceeds at all is somewhat remarkable. Rotaxane formation is an entropically unfavorable five-component assembly process, occurring in direct competition with processes such as [2]catenane assembly which is promoted by the formation of up to six amide–amide hydrogen bonds.[9] The reaction takes place in the presence of high concentrations of amines, amides and halide ions (in the form of $Et_3N^{+}HCl^{-}$), all significantly stronger alternative hydrogen bond acceptors to esters,

yet the yield of **10** is only one order of magnitude less than that obtained using the original *bis*-amide isophthalamide thread (28%).[4a] The crucial role played by the second binding site, and thus the full significance of preorganizing the cooperative binding sites in the thread, is evident from the comparative binding constants of di(*p*-butylphenyl)isophthalamide with Cl^- ion ($[PPh_4]^+Cl^-$: $K_a(CD_2Cl_2) = 6.1 \times 10^4\ M^{-1}$)[10] and a single, isolated ester group ($PhCO_2Me$: $K_a(CD_2Cl_2) < 10\ M^{-1}$)!

Gaining an understanding of amide–ester hydrogen bonding is of interest for areas as diverse as the design of peptide mimetics,[11a] D-Ala-D-Lac-binding "super bug" antibiotics,[11b] and the prediction of the structure and folding of commercially important synthetic polyamide/ester polymers.[11c] However, because of the many alternative more energetically favorable ways of satisfying amide hydrogen bonding requirements, amide–ester hydrogen bonds in the solid state are so rare that a recent[12] search found only 16 examples in the Cambridge Crystallographic Database. Together, the three isostructural rotaxanes **6**, **9** and **10** thus provide an unprecedented model series with which to study of the nature of amide–ester hydrogen bonding interactions, both in solution and the solid state.

The *X*-ray crystal structures of **9** and **10** are shown in Figure 2.2. Although the conformations of the central regions of the threads in all three rotaxane crystal structures are virtually superimposable, in the mono-ester (**9**) and *bis*-ester (**10**) rotaxanes the macrocycle is distorted from a chair conformation, and the conjugation of the isophthalamide units disrupted, in order to increase the number of amide–amide hydrogen bonds at the expense of weaker amide–ester hydrogen bonds. In the case of the mono–ester rotaxane, **9**, each macrocycle acts as a donor for three amide-amide hydrogen bonds (including a remarkable intermolecular bifurcated system, e.g. N11'H–O21–HN39', Figure 2.2a) and a single amide–ester one (O43–HN2), with the thread amide also acting as a donor for a further amide–amide hydrogen bond (O21–HN39'). In the *bis*-ester rotaxane, **10**, the

macrocycle acts as the donor for two amide-amide and two amide-ester hydrogen bonds. In both **9** and **10**, only two of the hydrogen bonds are formed *via* intramolecular, intercomponent interactions in the solid state compared to the maximum number possible (four) seen for the fumaramide rotaxane **6**.

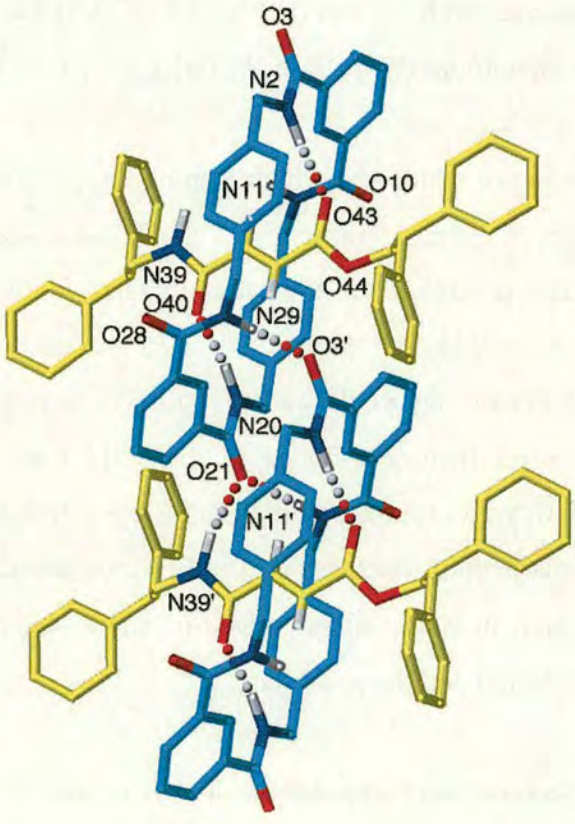

Figure 2.2a *X*-ray crystal structure of the mixed amide-ester [2]rotaxane **9**. Intramolecular hydrogen bond distances (Å): O43–HN2 1.90, O40–HN20 1.87; Intermolecular hydrogen bond distances (Å): O3'–HN29/O21–N11' 2.01, O21–N39' 2.05.

To show that the differences between the fumaramide rotaxane **6** and the ester-containing systems, **9** and **10**, were not a consequence of the number of hydrogen bond donors present in the thread, the *bis*-tertiary amide thread **11** was prepared. As with the *bis*-secondary amide thread, **5**, rotaxane formation proceeds in high yield (67%) to give **12** and the solid-state structure of crystals grown from acetonitrile (Figure 2.3) shows the double bifurcated hydrogen bond motif between the two rotaxane components.

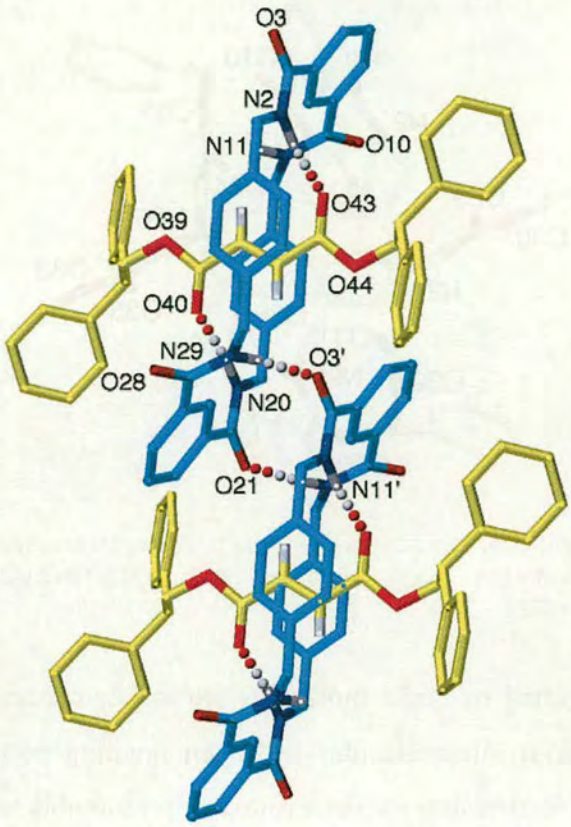

Figure 2.2b *X*-ray crystal structure of the *bis*-ester [2]rotaxane **10**. Intramolecular hydrogen bond distances (Å): O43–HN11/O40–HN20 1.88. Intermolecular hydrogen bond distances (Å): O3'–N29/O21–HN11' 1.93.

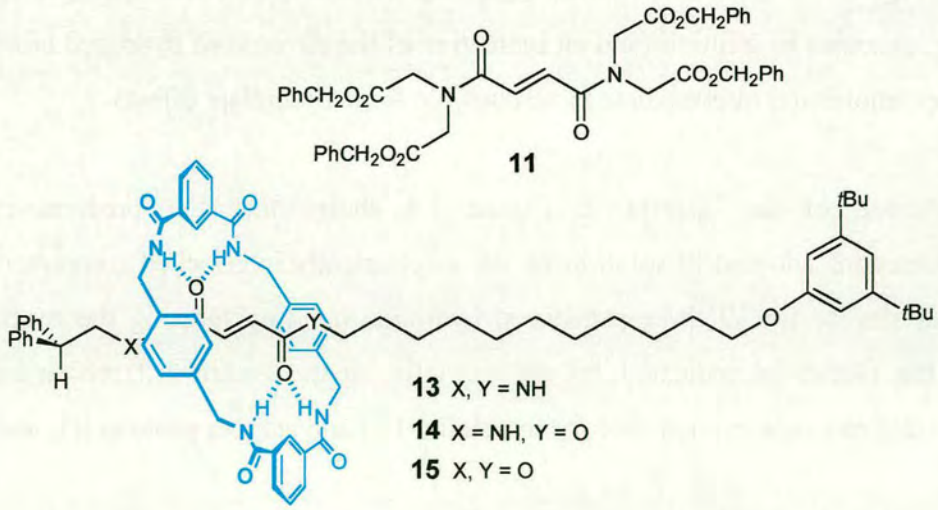

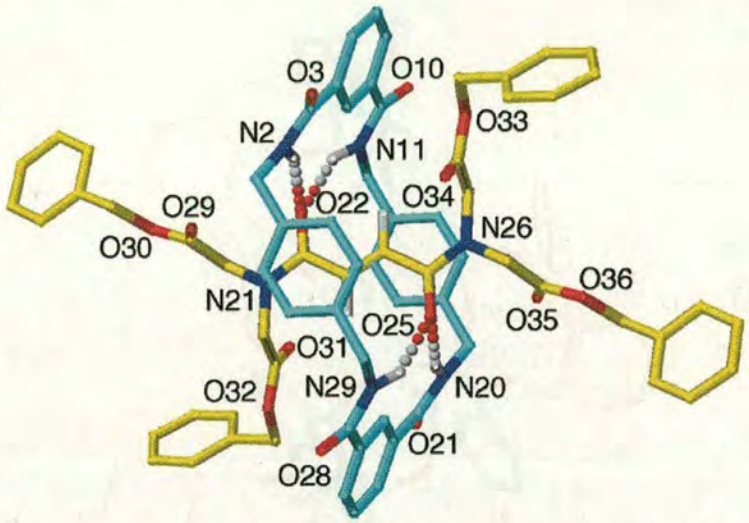

Figure 2.3 *X*-ray crystal structure of the tertiary amide fumaramide [2]rotaxane **12**. Intramolecular hydrogen bond distances (Å): O22–HN2/O25–HN20 2.16, O22–HN11/O25–HN29 2.40.

In solution the individual rotaxane molecules are isolated from each other and the components *must* adopt intramolecular hydrogen bonding patterns to lower their energy, the most stable structure for each rotaxane presumably involving two sets of bifurcated hydrogen bonds analogous to the solid-state structures of **6** and **12**. The ^{1}H NMR spectra ($CDCl_3$, 400 MHz, 298 K) of the isostructural threads and rotaxanes which differ only in the number of amide and ester hydrogen bond acceptors (i.e. **5**–**10**, Figure 2.4) gives information regarding the intercomponent hydrogen bonding in the rotaxanes in solution (and an indication of the strength of hydrogen bonding in the supramolecular intermediate **II** responsible for the template effect).

Comparison of the spectra in Figure 2.4 shows that the predominant co-conformations adopted in solution by the mechanically interlocked components are, indeed, similar for all three rotaxanes, hydrogen bonding locating the macrocycle over the olefin, as indicated by the virtually identical shift-differences between thread and rotaxane in each case for the olefin (H_d) and stopper protons (H_a and H_b).

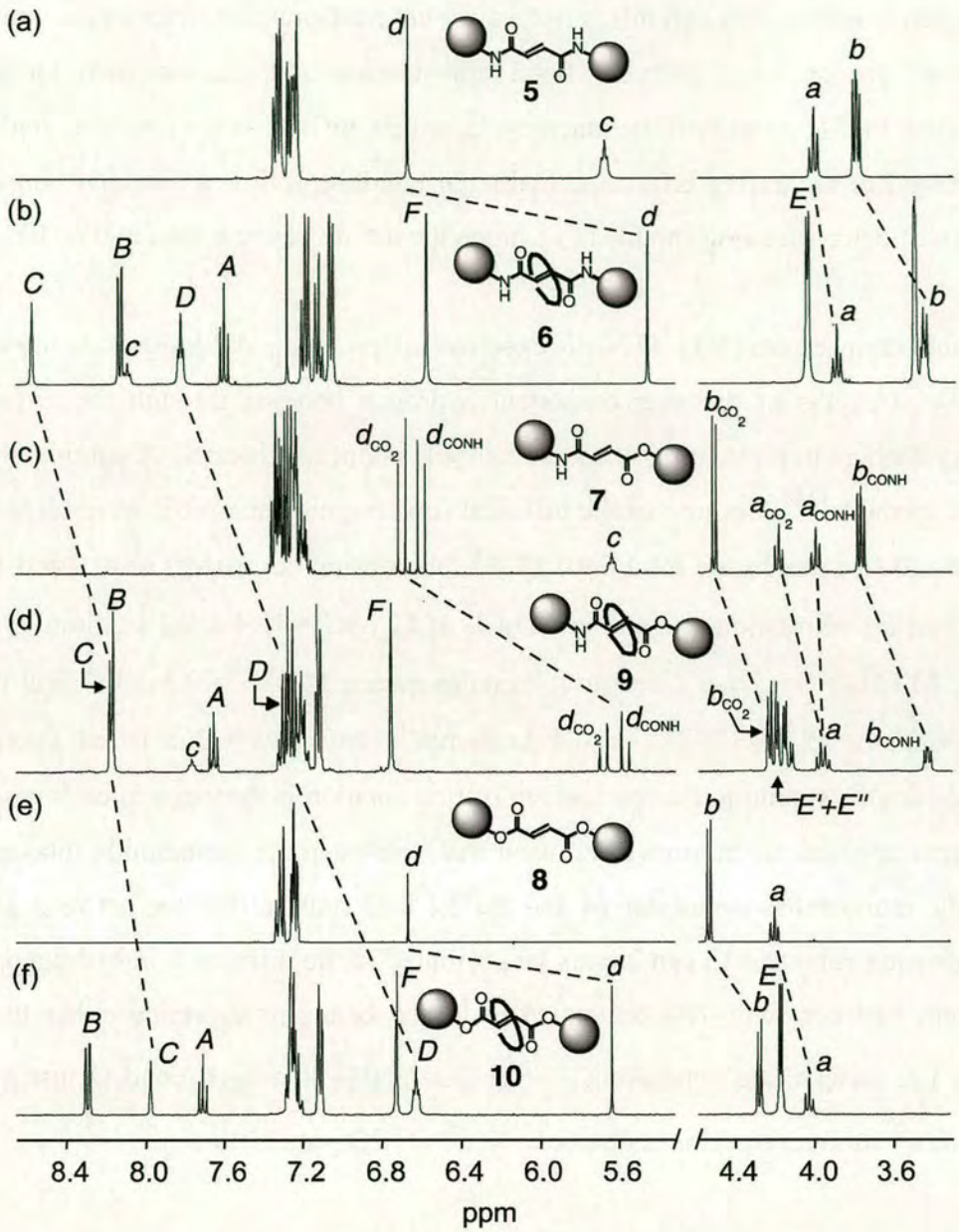

Figure 2.4 ^{1}H NMR Spectra (400 MHz, $CDCl_3$, 298 K) of (a) **5**, (b) **6**, (c) **7**, (d) **9**, (e) **8** and (f) **10**.

The *strength* of the hydrogen bonding between the components in each case, however, is very different. Initially, this is suggested by the relative chemical shifts of the macrocycle amide protons (H_D) in **6** (δ 7.83), **9** (δ 7.15) and **10** (δ 6.66), the downfield position being an indication of the degree of their involvement in

hydrogen bonding, although this is not a clear cut measurement since amide and ester carbonyl groups have different bond anisotropies and electric field strengths. However, the H_C protons of the macrocycle, which are held in the shielding region of a carbonyl group during bifurcated hydrogen bonding, follow a similarly consistent pattern of behavior being shielded to a much greater degree in **6** than in **9** or **10**.

Variable temperature (VT) ^{1}H NMR experiments provide a definitive measure of the relative strengths of the intercomponent hydrogen bonding through the respective energy barriers to pirouetting of the macrocycle about the threads. A combination of NMR methods[13,14] (because of the different time regimes involved) were carried out on **12** and (for reasons of solubility) **13–15**, alkyl chain derivatives of **6**, **9** and **10**, to give barriers of rotation at 298K in CD_2Cl_2 of **12** (ΔG = 13.4 ± 0.1 kcal mol^{-1}; SPT-SIR), **13** (ΔG = 11.5 ± 0.2 kcal mol^{-1}; coalescence), **14** (ΔG = 9.3 ± 0.2 kcal mol^{-1}; coalescence), **15** (ΔG = 7.2 ± 0.4 kcal mol^{-1}; estimated value based upon line broadening). Assuming the mechanism of ring rotation is the same in each case, the differences in energy barriers of 2.2 kcal mol^{-1} between the fumaramide rotaxane **13** and the monoamide-monoester **14** and the 2.1 kcal mol^{-1} difference between **14** and the *bis*-ester rotaxane **15** can largely be attributed to the difference in hydrogen bond strength between two –NH bifurcated hydrogen bonds to an amide rather than an ester, i.e. under these conditions a –NH···O=CNH– hydrogen bond is just over 1 kcal mol^{-1} stronger than the analogous –NH···O=CO– interaction.

The ^{1}H NMR spectroscopy also provides a window through which to observe the remarkable sequence of intra- and intercomponent dynamic processes present in a simple amide-based rotaxane; including (i) macrocycle pirouetting and (ii) amide bond rotamerization, illustrated through the VT ^{1}H NMR spectra of **12** in CD_2Cl_2 (low temperature) and $C_2D_2Cl_4$ (high temperature) given in Figure 2.5. Spin polarization transfer by selective inversion recovery (SPT-SIR)[13] on $H_{a'}$ to $H_{a''}$ and $H_{b'}$ to $H_{b''}$ show that tertiary amide rotamerization in the rotaxane has a significantly

higher energy barrier (20.4 ± 0.1 kcal mol^{-1}) than a conventional tertiary amide (~18.4 kcal mol^{-1}), attributable to intercomponent hydrogen bonding stabilizing the $R_2N^+=C-O^-$ resonance contribution of the tertiary amide group.[4d] Furthermore combination of NMR spectroscopy, Kerr-effect measurements and molecular modeling recently uncovered a remarkable new property of component dynamics in a mechanically interlocked architecture; the rate of macrocycle pirouetting in rotaxanes such as **6** can be varied through the use of an oscillating electric field.[15] This offers a potentially extremely useful method for controlling rotaxane movements in molecular-based devices.

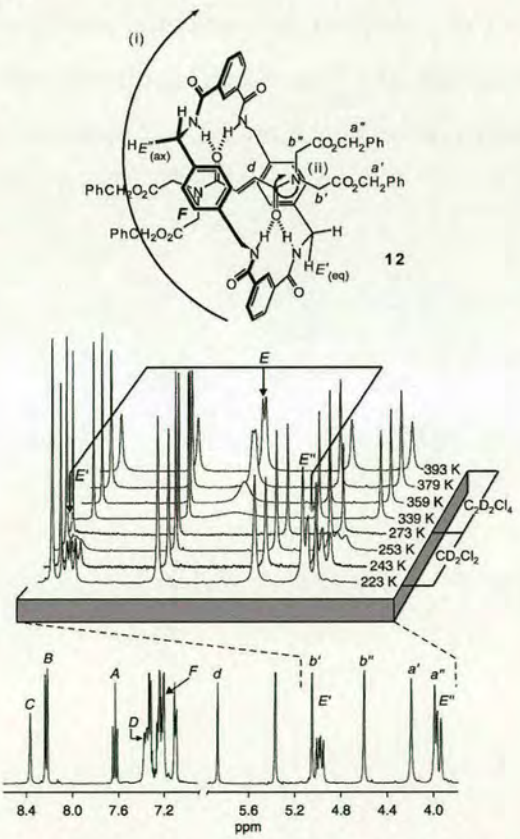

Figure 2.5 Dynamic processes in a [2]rotaxane. The ^1H NMR Spectrum (400 MHz) of **12** in CD_2Cl_2 at 223 K (main trace), showing (i) slow pirouetting of macrocycle about the thread ($H_{E'}$ and $H_{E''}$ resolved) and (ii) slow rotation of tertiary amide N–C bond ($H_{a'}$ and $H_{a''}$/$H_{b'}$ and $H_{b''}$ resolved). The SPT-SIR between resolved signals gives energy barriers for tertiary amide rotation (20.4 ± 0.1 kcal mol^{-1}) and macrocycle pirouetting (13.4 ± 0.1 kcal mol^{-1}). Higher temperature spectra (expansion, 223–273 K (CD_2Cl_2) and 339–393 K ($C_2D_2Cl_4$)) illustrate the wide temperature ranges (170° for $H_{E'}$/$H_{E''}$→H_E!) that can exist between full resolution and coalescence of signals affected by dynamic processes in mechanically interlocked molecules.

2.3 Conclusions

Fixing multiple cooperative binding sites in an ideal spatial arrangement on a structurally rigid backbone is a powerful method for facilitating the hydrogen bond-directed synthesis of rotaxanes, with the fumaramide motif providing one of the most accessible and efficient rotaxane syntheses described to date. Preorganizing the template is so effective that modest hydrogen bonding groups can be used to template multicomponent assembly processes, *even in the presence of far more potent, but not preorganized, hydrogen bonding groups!* It is interesting to note that cooperative interactions, organization and structural rigidity are key elements in the mode of action of LY333328, the "super-bug" antibiotic which binds weakly to the ester-terminated D-Ala-D-Lac sequence on the cell surfaces of vancomycin-resistant enterococci.[11b]

2.4 Experimental Section

General method for the preparation of benzylic amide macrocycle fumaryl based[2]rotaxanes. The threads **5**, **7**, **8** or **11** (1.00 mmol) and triethylamine (2.1 ml, 15.7 mmol) were dissolved in 100 mL chloroform (stabilized with amylenes) or, in the case of **5**, 1:9 acetonitrile:chloroform, and stirred vigorously whilst solutions of the diamine (1.09 g, 4 equiv.) in chloroform (45 mL) and the acid chloride (1.62 g, 4 equiv.) in chloroform (45 mL) were simultaneously added over a period of 2 hours using motor-driven syringe pumps. After a further 2 hours the resulting suspension was filtered and concentrated under reduced pressure to leave, in general, only the unconsumed thread and [2]rotaxane. This mixture was subjected to column chromatography (silica gel, CH_2Cl_2/MeOH as eluent) to yield, in order of elution, the unconsumed thread and the [2]rotaxane. In the case of **6**, the rotaxane was obtained directly from the concentrated reaction filtrate by spontaneous crystallization promoted by the addition of water to a solution of the crude product in dimethylformamide (30 mL).

[2]-(1,7,14,20-tetraaza-2,6,15,19-tetraoxo-3,5,9,12,16,18,22,25-tetrabenzocyclohexacosane)-(*E*)-(*N,N'-bis*(2',2'diphenylethyl)-2'-butendiamide))rotaxane, 6

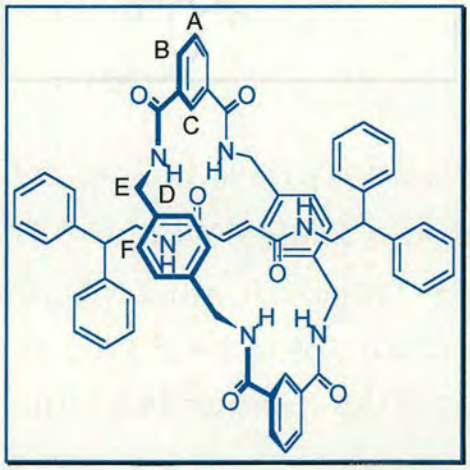

Selected data for (6): Yield 0.97 g (97%); m.p. 355–356 °C (DMF/H_2O); ^{1}H NMR (400 MHz, DMSO-d_6): δ = 8.63 (brs, 2H, ArH_C), 8.53 (t, J = 5.9 Hz, 2H, CONH), 8.15 (t, J = 5.0 Hz, 4H, $N\underline{H}_D$), 8.01 (dd, J = 7.8, 1.4 Hz, 4H, ArH_B), 7.73 (t, J = 7.8 Hz, 2H, ArH_A), 7.35–7.12 (m, 20H, ArH), 6.66 (s, 8H, ArH_F), 5.66 (s, 2H, $C\underline{H}$=$C\underline{H}$), 4.22 (d, J = 5.0 Hz, 8H, CH_{2E}), 4.11 (t, J = 7.9 Hz, 2H, $Ph_2C\underline{H}$), 3.67 (dd, J = 7.9, 5.9 Hz, 4H, $Ph_2CHC\underline{H}_2$); ^{13}C NMR (100 MHz, DMSO-d_6): δ = 166.1, 165.7, 143.0, 136.7, 134.6, 131.1, 129.6, 129.45, 128.89, 128.77, 128.1, 126.9, 125.7, 44.0, 50.3, 43.6; MS (FAB, NBA matrix): *m/z* = 1029 [(rotaxane+Na)$^+$]. Anal. Calcd for $C_{64}H_{58}N_6O_6$: C 76.32, H 5.80, N 8.34. Found: C 76.42, H 5.71, N 8.29.

[2]-(1,7,14,20-tetraaza-2,6,15,19-tetraoxo-3,5,9,12,16,18,22,25-tetrabenzocyclohexacosane)-2,2-diphenyl-(*E*)-4-[(2,2-diphenylethyl)amino]-4-oxo-2-butenoate)rotaxane, 8

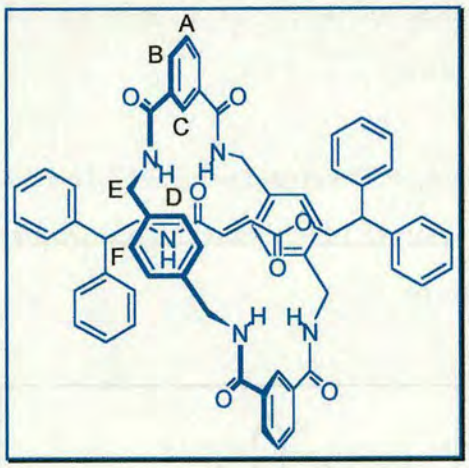

Selected data for (8): Yield 0.35 g (35%); m.p. 246–247 °C; ^{1}H NMR (400 MHz, $CDCl_3$): δ = 8.18 (m, 6H, ArH_B & ArH_C), 7.78 (t, J = 5.9 Hz, 1H, CONH), 7.66 (t, J = 8.1 Hz, 2H, ArH_A), 7.36–7.10 (m, 21H, ArH & $N\underline{H}_D$), 6.67 (s, 8H, ArH_F), 5.71 (d, J = 15.3 Hz, 1H, CH=C$\underline{H}$COO), 5.59 (d, J = 15.3 Hz, 1H, C$\underline{H}$=CHCOO), 4.46 (d, J = 7.5 Hz, $OC\underline{H}_2CHPh_2$), 4.37 (AB system, J = 14.3, 5.0 Hz, 8H, $CH_{2E'/E''}$), 4.20 (t, J =

7.5 Hz, 1H, $OCH_2C\underline{H}Ph_2$), 4.18 (t, J = 7.9 Hz, 1H, $Ph_2C\underline{H}CH_2NH$), 3.67 (dd, J = 7.8, 5.8 Hz, 2H, $Ph_2CHC\underline{H}_2NH$); ^{13}C NMR (100 MHz, $CDCl_3$): δ = 167.34, 167.22, 164.90, 142.00, 140.73, 137.44, 134.97, 134.41, 131.75, 129.80, 129.55, 129.15, 129.13, 128.30, 128.17, 127.63, 127.15, 124.61, 68.84, 50.44, 49.77, 45.28, 44.40, 44.27; MS (FAB, NBA matrix): *m/z* = 1008 [(rotaxane+H)$^+$]. Anal. Calcd for $C_{64}H_{57}N_5O_7$: C 76.25, H 5.82, N 6.95. Found: C 76.37, H 5.82, N 6.85.

[2]-(1,7,14,20-tetraaza-2,6,15,19-tetraoxo-3,5,9,12,16,18,22,25-tetrabenzocyclohexacosane)-*bis*(2,2-diphenylethyl)-(*E*)-2-butenedioate)rotaxane, 10

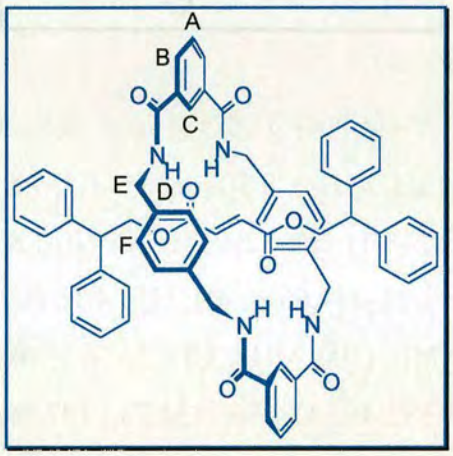

Selected data for (10): Yield 0.03 g (3%); ^1H NMR (400 MHz, $CDCl_3$) δ = 8.32 (d, J = 7.8 Hz, 4H, ArH_B), 8.01 (s, 2H, ArH_C), 7.74 (t, J = 7.8 Hz, 2H, ArH_A), 7.32–7.23 (m, 12H, ArH), 7.15 (d, J = 8.3 Hz, 8H, ArH), 6.76 (s, 8H, ArH_F), 6.66 (t, J = 5.1 Hz, 4H, $N\underline{H}_D$), 5.67 (s, 2H, $C\underline{H}$=$C\underline{H}$), 4.51 (d, J = 7.8 Hz, 4H, $Ph_2CHC\underline{H}_2O$), 4.41 (d, J = 5.3 Hz, 8H, CH_{2E}), 4.26 (t, J = 7.8 Hz, 2H, Ph_2CH); ^{13}C NMR (100 MHz, $CDCl_3$) δ= 166.46, 140.41, 137.73, 134.45, 132.41, 131.18, 130.25, 129.40, 129.35 128.25, 127.87, 122.72, 122.65, 66.25, 49.85, 44.21; MS (FAB, NBA matrix): *m/z* = 1009 [(rotaxane+H)$^+$].

[2](1,7,14,20-tetraaza-2,6,15,19-tetraoxo-3,5,9,12,16,18,22,25-tetrabenzocyclohexacosane)-benzyl-2-[[2-(benzyloxy)-2-oxoethyl]((*E*)-5-(bis[2-(benzyloxy)-2-oxoethyl]amino))2,5-dioxo-3-pentenyl)amino]acetate)rotaxane, 12

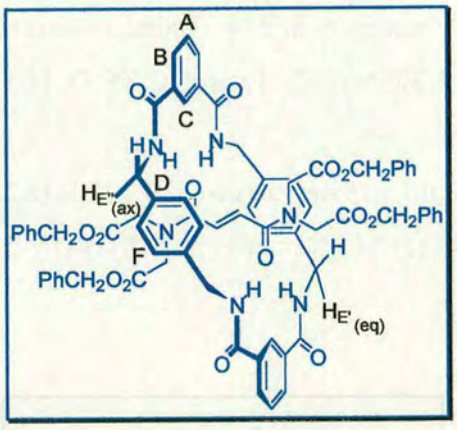

Selected data for (12): Yield 0.83 g (67%); m.p. 268–269 °C; ^{1}H NMR ($CDCl_3$, 400 MHz): δ = 8.39 (brs, 2H, ArH_C), 8.30 (dd, J = 1.5, 7.8 Hz, 4H, ArH_B), 7.58 (t, J = 7.8 Hz, 2H, ArH_A), 7.42–7.11 (m, 32H, ArH & $N\underline{H}_D$ & ArH_F), 5.92 (s, 2H, H_d), 5.12 (s, 4H, $H_{b''}$), 4.95 (brs, $H_{E''}$), 4.66 (s, 4H, $H_{b'}$), 4.16 (s, 4H, $H_{a''}$), 3.90 (brs, $CH_{E'}$), 3.91 (s, 4H, $H_{a'}$); ^{13}C NMR (100 MHz, $CDCl_3$): δ = 49.57, 50.23, 67.94, 68.09, 122.39, 128.58–129.92, 132.46, 134.36, 134.74, 132.46, 138.27, 166.0, 168.63, 166.71, 67.73, 168.27; LSIMS, m/z = 1239 [(rotaxane+H)$^+$], 1262 [(rotaxane+Na)$^+$]. Anal. Calcd for $C_{72}H_{66}N_6O_{14}$: C 69.78, H 5.37, N 6.78. Found C 69.46, H 5.33, N 6.58.

***X*-ray Crystallographic Structure Determinations. 6:** $C_{68}H_{56}N_6O_6$, M = 1007.16, crystal size 0.01 × 0.03 × 0.05 mm, triclinic P-1, a = 15.1820(2), b = 21.2255(2), c = 21.5668(3) Å, α = 65.8240(10), β = 83.8570(10), γ = 78.1380(10)°, V = 6202.83(13) Å^3, Z = 4, ρ_{calcd} = 1.235 Mg m^{-3}; synchrotron radiation (CCLRC Daresbury Laboratory Station 9.8, silicon monochromator, λ = 0.6883 Å), μ = 0.082 mm^{-1}, T = 150(2) K. 36861 data (22685 unique, R_{int} = 0.1774, 1.00 < θ < 27.18°), were

collected on a Siemens SMART CCD diffractometer using narrow frames (0.3° in ω), and were corrected semiempirically for absorption and incident beam decay (transmission 1.00–0.58). The structure was solved by direct methods and refined by full-matrix least-squares on F^2 values of all data (G.M.Sheldrick, SHELXTL manual, Siemens Analytical *X*-ray Instruments, Madison WI, USA, 1994, version 5) to give $wR = \{\Sigma[w(F_o^2-F_c^2)^2]/\Sigma[w(F_o^2)^2]\}^{1/2} = 0.5259$, conventional $R = 0.3240$ for F values of 22635 reflections with $F_o^2 > 2\sigma(F_o^2)$, $S = 1.156$ for 850 parameters. Residual electron density extremes were 0.527 and –0.413 eA^{-3}. Due to the scarcity of observed data, all the oxygen and nitrogen atoms were refined anisotropically whilst all the carbon atoms were refined isotropically. Amide hydrogen atoms were refined isotropically subject to a distance constraint N–H = 0.98 Å, with the remainder constrained. Despite the rather high R factor and wR value due to disorder in the DMF molecules, the results permit an unambiguous determination of connectivity, packing pattern, the spatial relationship between macrocycle, thread and solvent, their conformations and the intercomponent hydrogen bonding motifs.

Experimental details for **9, 10, 12** were the same as for **6** except for the following: **9:** $C_{64}H_{57}N_5O_7$, $M = 1008.15$, crystal size 0.06 × 0.14 × 0.14 mm, monoclinic *Cc*, $a = 11.6650(5)$, $b = 15.6465(8)$, $c = 28.4397(13)$ Å, $\beta = 96.653(2)°$, $V = 5155.8(8)$ Å^3, $Z = 4$, $\rho_{calcd} = 1.299$ Mg m^{-3}; $Mo_{K\alpha}$ radiation (graphite monochromator, $\lambda = 0.71073$ Å), $\mu = 0.085$ mm^{-1}, $T = 298(2)$ K. 11030 data (6202 unique, $R_{int} = 0.0726$, $2.19 < \theta < 23.26°$), were collected on a Siemens SMART CCD diffractometer using narrow frames (0.3° in ω), and were corrected semiempirically for absorption and crystal decay (transmission 1.00–0.31). The structure was solved and refined as described above for **6** to give $wR = \{\Sigma[w(F_o^2-F_c^2)^2]/\Sigma[w(F_o^2)^2]\}^{1/2} = 0.1966$, conventional $R = 0.0667$ for F values of 6202 reflections with $F_o^2 > 2\sigma(F_o^2)$, $S = 0.934$ for 705 parameters. Residual electron density extremes were 0.160 and –0.204 eÅ^{-3}. Amide hydrogen atoms were refined isotropically subject to a distance constraint N–H =

0.98 Å, with the remainder constrained; anisotropic displacement parameters were used for all non-hydrogen atoms. **10:** $C_{64}H_{56}N_4O_8$, M = 1009.13, crystal size 0.04 × 0.13 × 0.2 mm, triclinic P-1, a = 9.7839(7), b = 10.9115(7), c = 15.0045(10) Å, α = 82.5130(10), β = 87.3340(10), γ = 77.8280(10)°, V = 1552.2(2) Å^3, Z = 1, ρ_{calcd} = 1.335 Mg cm^{-3}; $Mo_{K\alpha}$ radiation (graphite monochromator, λ = 0.71073 Å), μ = 0.335 mm^{-1}, T = 298(2) K. 9819 data (4454 unique, R_{int} = 0.0321, 1.92 < θ < 23.29°), were collected on a Siemens SMART CCD diffractometer using narrow frames (0.3° in ω), and were corrected semiempirically for absorption and incident beam decay (transmission 1.00–0.71). The structure was solved and refined as described above for **6** to give $wR = \{\Sigma[w(F_o^2-F_c^2)^2]/\Sigma[w(F_o^2)^2]\}^{1/2}$ = 0.1231, conventional R = 0.0442 for F values of 4454 reflections with $F_o^2 > 2\sigma(F_o^2)$, S = 0.930 for 388 parameters. Residual electron density extremes were 0.321 and –0.277 eÅ^{-3}. Amide hydrogen atoms were refined isotropically subject to a distance constraint N–H = 0.98 Å, with the remainder constrained; anisotropic displacement parameters were used for all non-hydrogen atoms. **12:** $C_{72}H_{66}N_6O_{14}$, M = 1239.31, crystal size 0.12 × 0.13 × 0.24 mm, rhombohedral R-3, a = 41.875(2), b = 41.875(2), c = 10.6871(9) Å, α = 90, β = 90, γ = 120°, V = 16229.4(19) Å^3, Z = 9, ρ_{calcd} = 1.141 Mg cm^{-3}; $Mo_{K\alpha}$ radiation (graphite monochromator, λ = 0.71073 Å), μ = 0.080 mm^{-1}, T = 293(2) K. 23900 data (5187 unique, R_{int} = 0.0900, 1.68 < θ < 23.26°), were collected on a Siemens SMART CCD diffractometer using narrow frames (0.3° in ω), and were corrected semiempirically for absorption and incident beam decay (transmission 1.00–0.15). The structure was solved and refined as described above for **6** to give $wR = \{\Sigma[w(F_o^2-F_c^2)^2]/\Sigma[w(F_o^2)^2]\}^{1/2}$ = 0.3492, conventional R = 0.0984 for F values of 5187 reflections with $F_o^2 > 2\sigma(F_o^2)$, S = 0.805 for 412 parameters. Residual electron density extremes were 0.383 and –0.311 eÅ^{-3}. Amide hydrogen atoms were refined isotropically subject to a distance constraint N–H = 0.98 Å, with the remainder constrained; anisotropic displacement parameters were used for all non-hydrogen atoms.

Crystallographic data for **6**, **9**, **10** and **12** (excluding structure factors) have been deposited with the Cambridge Crystallographic Data Centre as supplementary publication numbers CCDC-140045 (**6**), CCDC-140046 (**9**), CCDC-140047 (**10**) and CCDC-140048 (**12**). Copies of the data can be obtained free of charge on application to The Director, CCDC, 12 Union Road, Cambridge CB2 1EZ, UK (fax: Int. code + (1223)336-033; e-mail: teched@chemcrys.cam.ac.uk).

2.5 References

1. See, for example, (a) Cram, D. J. *Angew. Chem. Int. Ed. Engl.* **1988**, *27*, 1009–1020. (b) Gerbeleu, N. V.; Arion, V. B.; Burgess, J. *Template Synthesis of Macrocyclic Compounds*; Wiley-VCH, Weinheim, **1999**. (c) *Templated Organic Synthesis*, F. Diederich, P. J. Stang, Eds.: Wiley-VCH, Weinheim, **2000**.
2. (a) Cram, D. J.; Lein, G. M. *J. Am. Chem. Soc.* **1985**, *107*, 3657–3668. (b) Cram, D. J.; deGrandpre, M. P.; Knobler, C. B.; Trueblood, K. N. *J. Am. Chem. Soc.* **1984**, *106*, 3286–3292.
3. For reviews on rotaxanes see, for example, (a) Amabilino, D. B.; Stoddart, J. F. *Chem. Rev.* **1995**, *95*, 2725–2828. (b) *Molecular Catenanes, Rotaxanes and Knots*; J. -P. Sauvage, C. Dietrich-Buchecker, Eds.: Wiley-VCH, Weinheim, **1999**. (c) Leigh, D. A.; Murphy, A. *Chem. Ind.* **1999**, 178–183.
4. (a) Johnston, A. G.; Leigh, D. A.; Murphy, A.; Smart, J. P.; Deegan, M. D. *J. Am. Chem. Soc.* **1996**, *118*, 10662–10663. (b) Leigh, D. A.; Murphy, A.; Smart, J. P.; Slawin, A. M. Z. *Angew. Chem. Int. Ed. Engl.* **1997**, *36*, 728–732. (c) Lane, A. S.; Leigh, D. A.; Murphy, A. *J. Am. Chem. Soc.* **1997**, *119*, 11092–11093. (d) Clegg, W.; Gimenez-Saiz, C.; Leigh, D. A.; Murphy, A.; Slawin, A. M. Z.; Teat, S. J. *J. Am. Chem. Soc.* **1999**, *121*, 4124–4129. (e) Leigh, D. A.; Troisi, A.; Zerbetto, F. *Angew. Chem. Int. Ed.* **2000**, *39*, 350–353. (f) Brouwer, A. M.; Frochot, C.; Gatti, F. G.; Leigh, D. A.; Mottier, L.; Paolucci, F.; Roffia, S.; Wurpel, G. W. H. *Science* **2001**, *291*, 2124–2128.
5. (a) Carver, F. J.; Hunter, C. A.; Shannon, R. J. *J. Chem. Soc., Chem. Commun.* **1994**, 1277–1280. (b) Geib, S. G.; Vincent, C.; Fan, E.; Hamilton, A. D. *Angew. Chem. Int. Ed. Engl.* **1993**, *32*, 119–121. (c) Johnston, A. G.; Leigh, D. A.; Nezhat, L.; Smart, J. P.; Deegan, M. D. *Angew. Chem. Int. Ed. Engl.* **1995**, *34*, 1212–1216.
6. Dado, G. P.; Gellman, S. H. *J. Am. Chem. Soc.* **1993**, *115*, 4228–4245.

7. (a) Jäger, R.; Baumann, S.; Fischer, M.; Safarowsky, O.; Nieger, M.; Vögtle, F. *Liebigs Ann./Recueil* **1997**, 2269–2273. (b) Parham, A. H.; Windisch, B.; Vögtle, F. *Eur. J. Org. Chem.* **1999**, 1233–1238.
8. Abraham, M. H. *Chem. Soc. Rev.* **1993**, *22*, 73–83.
9. Johnston, A. G.; Leigh, D. A.; Pritchard, R. J.; Deegan, M. D. *Angew. Chem. Int. Ed. Engl.* **1995**, *34*, 1209–1212.
10. Kavallieratos, K.; de Gala, S. R.; Austin, D. J.; Crabtree, R. H. *J. Am. Chem. Soc.* **1997**, *119*, 2325–2326.
11. (a) *Peptide-based Drug Design*; M.D. Taylor, G.L. Amidon, Eds.: ACS, Washington DC, **1995**. (b) Williams, D. H.; Bardsley, B. *Angew. Chem. Int. Ed.* **1999**, *38*, 1172–1193. (c) *Macromolecular Design of Polymeric Materials*; K. Hatada, T. Kitayama, O. Vogl, Eds.: Marcel-Dekker, Inc., New York, **1997**.
12. Alemán, C.; Navas, J. J.; Muñoz-Guerra, S. *J. Phys. Chem.* **1995**, *99*, 17653–17661.
13. Dahlquist, F. W.; Longmur, K. J.; Du Vernet, R. B. *J. Magn. Reson.* **1975**, *17*, 406. For applications of SPT-SIR to dynamic processes in rotaxanes see ref 4d.
14. Sandström, J. *Dynamic NMR Spectroscopy*; Academic Press, London, 1982.
15. Bermudez, V.; Capron, N.; Gase, T.; Gatti, F. G.; Kajzar, F.; Leigh, D. A.; Zerbetto, F.; Zhang, S. *Nature* **2000**, 406, 608–611.

CHAPTER THREE

Flexible Hydrogen Bonding Templates

Prepared for submission for Journal of American Chemical Society as:

"Flexible Hydrogen Bonding Templates: Hydrogen Bonding Finds a Way!"

Guy J Clarkson, Francesco G Gatti, David A Leigh and Jenny K Y Wong

Acknowledgements

The following people are gratefully acknowledged for their contributions to this chapter: rotaxane **8** was synthesised by Dr. Guy Clarkson (University of Warwick); rotaxanes **13** and **14** were synthesised by Dr. Francesco Gatti (University of Warwick).

> "*You see, wire telegraph is a kind of a very, very long cat. You pull his tail in New York and his head is meowing in Los Angeles. Do you understand this? And radio operates exactly the same way: you send signals here, they receive them there. The only difference is that there is no cat.*"
>
> Albert Einstein

> "*Your theory is crazy, but it's not crazy enough to be true.*"
>
> Niels Bohr

Flexible Hydrogen Bonding Templates – Synopsis

In the previous chapter we saw that the highly efficient fumaramide template for formation of the benzylic amide macrocycle-containing rotaxanes is due to the rigidity provided by the double bond (exemplified by the formation of [2]rotaxane even when the two amides of the thread were substituted for esters). This prompted us to investigate the directing powers of hydrogen bonding during rotaxane synthesis. We explored the effect of eliminating the double bond and introducing flexibility into the thread by gradually increasing the number of methylene groups between the two amide hydrogen bonding sites. Would there be a limit to the directing power of hydrogen bonding between the thread and macrocycle components? And after which point is rotaxane no longer formed?

This chapter describes the synthesis, X-ray structures and $CDCl_3$-solution studies on a series of alkyl diamide [2]rotaxanes ***I–XI****. Introducing flexibility into the thread by eliminating the double bond gives rise to the possibility of forming intramolecular hydrogen bonds (cf. the studies on alkyl diamides by Gellman). The intramolecularly hydrogen bonded cyclic structures are unfavourable for rotaxane formation since the hydrogen bond requirements of the thread are internally satisfied. At the same time, increasing the number of carbons atoms between the amide hydrogen bonding sites of the template leads to increasing numbers of degrees of freedom as the template is lengthened (up to 3^{14} C–C rotamers for fourteen methylene groups). Remarkably, however, it is still possible to isolate rotaxane in every case!*

The yields, coupled with the X-ray crystal structures of each rotaxane, give an indication of the type and effect of competing factors (flexibility, intracomponent hydrogen bonds and non-optimal hydrogen bonding arrangements) on rotaxane formation as the chain length increases.

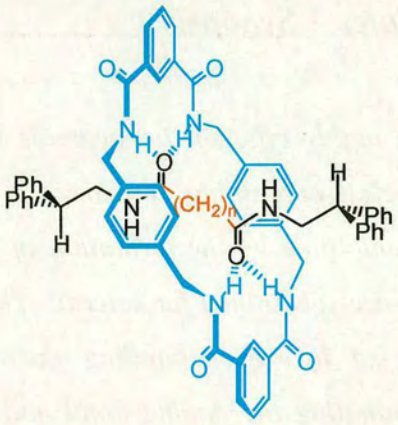

I	n = 1	8 %
II	n = 2	52 %
III	n = 3	3 %
IV	n = 4	8 %
V	n = 5	14 %
VI	n = 6	17 %
VII	n = 7	15 %
VIII	n = 8	18 %
IX	n = 10	12 %
X	n = 12	10 %
XI	n = 14	10 %

Comparison of ^{1}H NMR spectrum of the thread and rotaxane with the X*-ray crystal structures allowed the qualitative assessment of the change in location of the macrocycle in solution along the thread with increasing chain length. The crystal structures also show that as the thread increases in length the macrocycle is able to force the conformation of the thread into one that allows the strongest intramolecular hydrogen bond interactions to be formed.*

3.1 Introduction

Although mechanical interlocking at the molecular level can be achieved through statistical[1] or covalently-directed methods,[2] the most effective routes to rotaxane architectures invoke supramolecular assistance – the use of attractive noncovalent interactions[3] between the macrocycle and thread (or their precursors) – to organize the components prior to interlocking. Hydrogen bonding offers a particularly powerful method for preorganizing precursors in such a way that, with an ideal template, they can direct the formation of rotaxanes in remarkable yields.[4] Here we explore the directing effects of the hydrogen bonding between the forming macrocycle and thread and the efficacy of the assembly process when competing factors (flexibility, intracomponent hydrogen bonding and non-optimal hydrogen bonding arrangements) are introduced.

3.2 Mechanism of rotaxane formation

The synthesis of benzylic amide macrocycle-containing rotaxanes typically occurs *via* a five-component clipping reaction in which the reagents assemble around the thread template (Chapter Two, Scheme 2.1).[4a-f] We have previously described the formation of a fumaramide rotaxane that proceeds in this way in almost quantitative yield (>97%).[4g] The reason the reaction is so efficient is that the double bond holds the H-bonding groups of the thread in a close-to-perfect arrangement for the precursor to the macrocycle to cyclize around it. Not only does the double bond provide rigidity but it also holds the two carbonyls of the thread at the correct distance and orientation to allow the forming macrocycle to adopt a low energy chair-like conformation around it. Indeed, the preorganization of the thread template is so effective that when the amides were substituted for weak hydrogen bond acceptors such as esters, rotaxanes are still formed.

The features of the fumaramide template maximize the number and strength of hydrogen bonds between the thread and the forming macrocycle. We decided to test the directing power of hydrogen bonding in rotaxane synthesis by (i) eliminating the rigidity provided by the double bond in the thread (simultaneously both increasing the number of possible C–C bond rotamers in the thread and introducing the possibility of intracomponent hydrogen bonding which would have to be broken in order to make the hydrogen bond sites of the thread available as a template) and (ii) varying the number of carbon atoms (lengthening the distance) between the hydrogen bonding sites of the thread.

The introduction of flexibility not only leads to an increased number of possible conformations of the thread present in solution but also gives rise to the possibility of intramolecular hydrogen bonding, promoted by the nonpolar solvent environment (e.g. $CHCl_3$), forming cyclic structures (Figure 3.1). A study by Gellman[5] using variable temperature (VT) NMR and IR spectroscopy confirmed the presence of such cyclic structures in alkyl diamide and showed the shift in the equilibrium between the linear conformations of systems containing two amides separated by methylene groups with their cyclic intramolecularly bonded structures as the number of methylene groups between the hydrogen bonding sites increases. The presence of significant quantities of internally hydrogen bonded cyclic structures would be unfavorable for rotaxane formation since the hydrogen bond requirements of the template would be internally satisfied and the hydrogen bond donors and acceptor groups would be poorly predisposed for rotaxane formation.

3.3 Results and discussion

A series of diamide threads **1–11** were prepared (Scheme 3.1), each in one step from the corresponding commercially available *bis*-acid chloride and 2,2-diphenylethylamine (CH_2Cl_2, Et_3N, 16 h, 76–90 % yields). Rotaxane formation was

attempted by simultaneous addition of six equivalents of *para*-xylylene diamine and isophthaloyl dichloride ($CHCl_3$, Et_3N, 4 h, high dilution) to a solution of each thread, followed by filtration of the resulting suspension. The filtrate was concentrated under reduced pressure and subjected to column chromatography (MeOH/$CHCl_3$) to yield unconsumed thread, [2]catenane and – remarkably in *every* case! – the desired [2]rotaxanes **12–22** (Scheme 3.1).

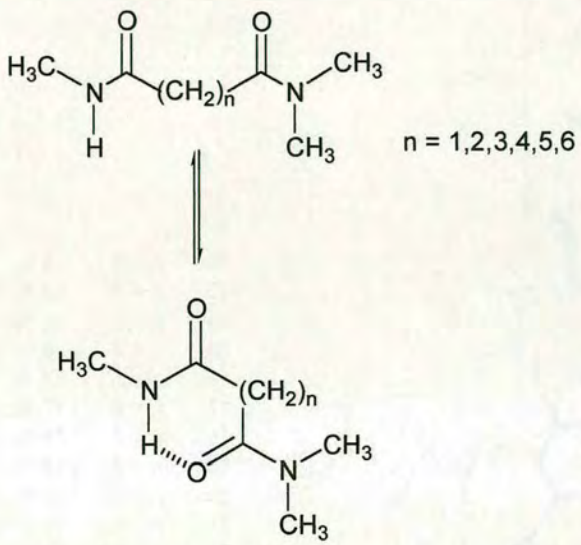

Figure 3.1 Internal hydrogen bonding of flexible diamide threads in nonpolar solvent such as $CHCl_3$

Single crystals were obtained by either slow infusion of diethyl ether or MeOH into a close-to-saturated solution of each rotaxane in chloroform (**16–22**, tetrachloroethane for **19**) or slow infusion of water vapour into a solution of the rotaxane in acetone (**12**), DMF (**13**), or ethanol (**14**) and analyzed by *X*-ray crystallography using either synchrotron or $Mo_{K\alpha}$ radiation sources. Comparing the yields of the various rotaxanes with the *X*-ray crystal structures and the ^1H NMR spectra in $CDCl_3$ provides some interesting insights into the directing influence of hydrogen bonding in these systems.

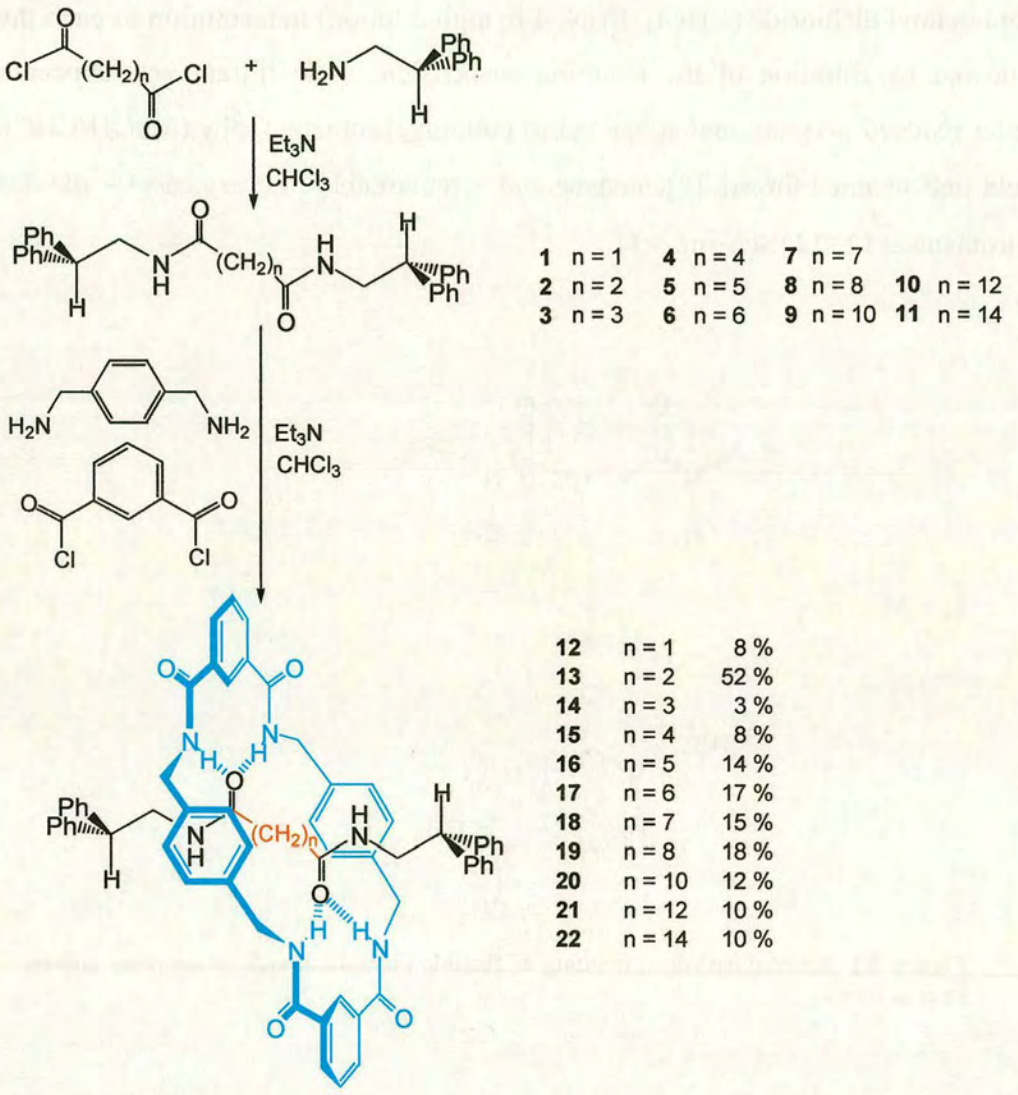

1 n = 1 **4** n = 4 **7** n = 7
2 n = 2 **5** n = 5 **8** n = 8 **10** n = 12
3 n = 3 **6** n = 6 **9** n = 10 **11** n = 14

12	n = 1	8 %
13	n = 2	52 %
14	n = 3	3 %
15	n = 4	8 %
16	n = 5	14 %
17	n = 6	17 %
18	n = 7	15 %
19	n = 8	18 %
20	n = 10	12 %
21	n = 12	10 %
22	n = 14	10 %

Scheme 3.1 Synthesis of diamide threads, **1–11** and rotaxanes, **12–22** containing up to fourteen methylene groups between the two templating sites.

3.3.1 *Succinamide [2]rotaxane,* **13** *(n=2)*

Comparison of the yield and solid-state structure of the succinamide rotaxane **13** (Figure 3.2) with that of the fumaramide rotaxane (Chapter Two, Figure 2.1) shows that eliminating the preorganizing effect of the double bond results in a decrease in

yield of almost half (52%) and reduces the number of intramolecular hydrogen bonds between the macrocycle and the thread in the solid state from four to two. Whilst there is a compensating increase in the number of intermolecular hydrogen bonds in the solid-state structure of **13**, a virtually identical packing architecture could be – but is not – formed by the fumaramide rotaxane and so this can be interpreted as a consequence of weaker hydrogen bonding interactions between the components in the succinamide rotaxane, **13**. It is interesting to note that a similar succinamide rotaxane prepared by the Vögtle group gave only 0.5–1% of rotaxane,[6] although the "threading" method of rotaxane formation used involves only three-components in the assembly reaction compared to the five-component clipping method described here.

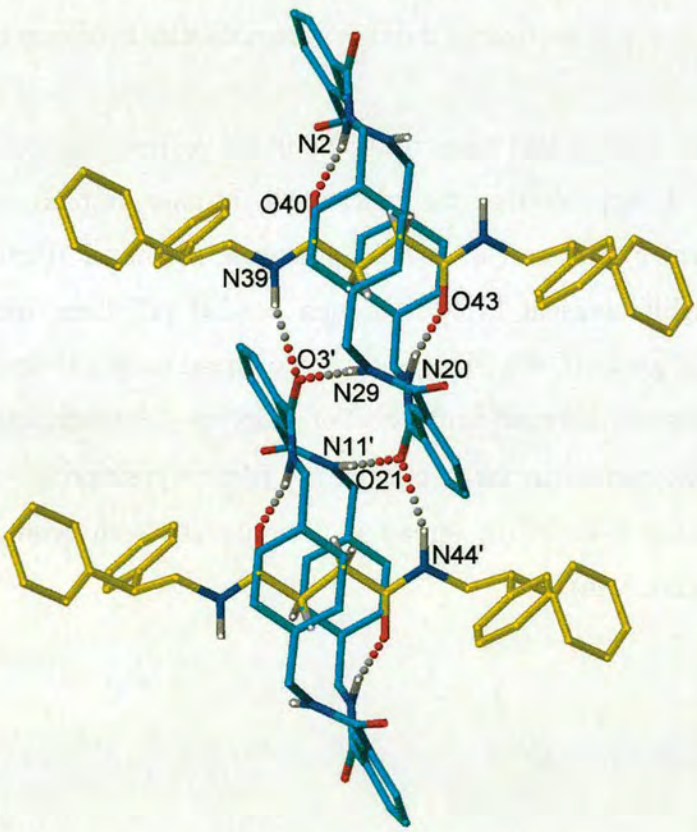

Figure 3.2 *X*-ray crystal structure of succinamide [2]rotaxane, **13**. Intramolecular hydrogen bond distances and angles: O40–HN2/O43–HN20 1.88 Å, 165.3°. Intermolecular hydrogen bond distances: N39H–O3'/O21–HN44' 2.21 Å, 161.8°; N29H–O3'/O21–HN11' 2.00 Å, 162.1°.

3.3.2 *Malonamide [2]rotaxane,* **12** *(n=1) and glutaramide [2]rotaxane,* **14** *(n=3)*

Remarkably, reducing or increasing what we assume is the near-optimum length spacer of two carbon atoms by one to give C_1 and C_3 diamides still results in [2]rotaxane formation! The yields are low, 8 and 3% respectively, but the fact that rotaxane is formed at all is simply extraordinary: not only is the distance between the two binding sites a non-optimal length to hydrogen bond efficiently to the macrocycle but it is hard to envisage any conformation of the thread which is conducive to rotaxane formation. In the standard staggered conformation of C_1 and C_3 alkyl chains the carbonyl groups would be on the same side of the thread and therefore not predisposed to template rotaxane formation; whereas in the cyclic form the hydrogen bond sites are tied up through intramolecular hydrogen bonding.

The solution that each thread takes is shown in the corresponding crystal structures (Figures 3.3). It appears that the macrocycle is able to bind to the internally hydrogen bonded cyclic structure of the malonamide thread (Figure 3.3a). This results in a highly unusual triply hydrogen bonded (all three intramolecular H-bonds!) carbonyl group (O40). The glutaramide thread takes a different solution and the C_3 chain pays the thermodynamic cost of adopting a conformation with a gauche C–C bonding interaction in the backbone in order to position the amide carbonyl groups on opposite sides of the thread so that they can both hydrogen bond to the macrocycle (Figure 3.3b).

(a)

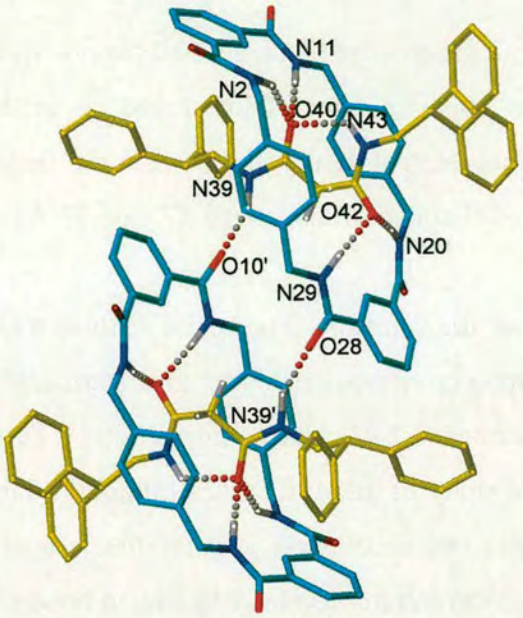

(b)

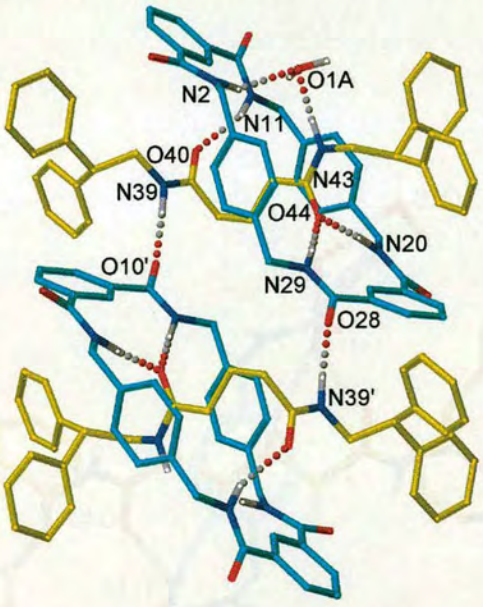

Figure 3.3 *X*-ray crystal structure of (a) malonamide [2]rotaxane, **12**. Intramolecular hydrogen bond distances and angles: O40–HHN2 2.49 Å, 153.1°; O40–HN11 1.89 Å, 168.3°; O40–HN43 2.05 Å, 126.3°; O42–HN20 2.32 Å, 173.7°; O42–HN29 1.95 Å, 173.2°. Intermolecular hydrogen bond distances and angles: N39H–O10'/O28–HN39' 1.94 Å, 148.7°. (b) glutaramide [2]rotaxane, **14**. Intramolecular hydrogen bond distances and angles: O40–HN11 2.01 Å, 138.7°; O44–HN20 2.02 Å, 175.0°; O44–HN29 1.91 Å, 177.3°. Intermolecular hydrogen bond distances and angles: N2H–O1A 2.22 Å, 141.2°; N43H–O1A 1.83 Å, 164.0°; N39H–O10'/O28–HN39' 1.85 Å, 162.8°.

3.3.3 Adipamide [2]rotaxane, **15** (n=4)

Adding a further methylene group to produce a C_4 adipamide thread predisposes the carbonyl groups to be on opposite sides of the thread, as in the fumaramide and succinamide templates, but almost doubles the distance between the hydrogen bonding sites in a staggered chain conformation (3.87 → 6.37 Å).

The solid-state structure of the rotaxane (Figure 3.4) shows that the macrocycle is able to overcome this problem without recourse to a sterically unfavorable thread geometry by adopting a stretched half-chair conformation. The yield of rotaxane is still low (8%). Gellman's study of alkyl diamides (although they studied hydrogen bonding in tertiary amides not secondary) suggest that adipamide has a greater enthalpic driving force to form intramolecularly hydrogen bonded (in this case, nine-membered) rings than most other alkyl diamides, the larger ring size giving rise to more linear intramolecular hydrogen bonds.

(a)

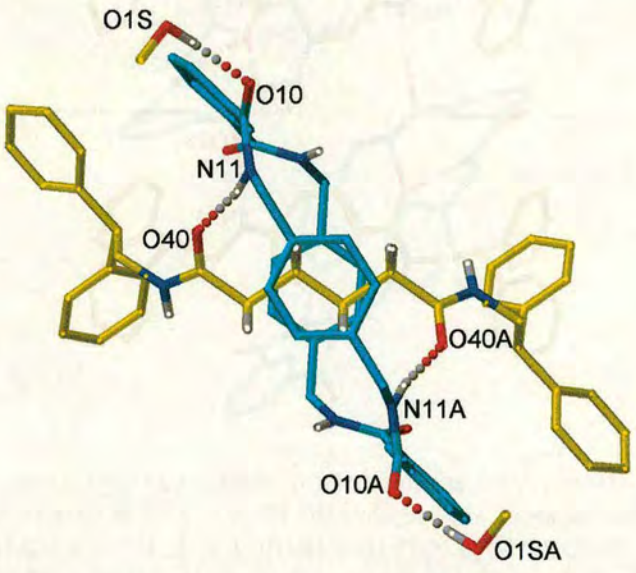

Figure 3.4a *X*-Ray crystal structure of adipamide [2]rotaxane, **15**, crystals grown from $CHCl_3$/MeOH. Intramolecular hydrogen bond distances and angles: O40–HN11/O40A–HN11A 2.00 Å, 168.8°. Intermolecular hydrogen bond distances and angles: O10–HO1S/O10–HO1SA 1.98 Å, 176.7°.

(b)

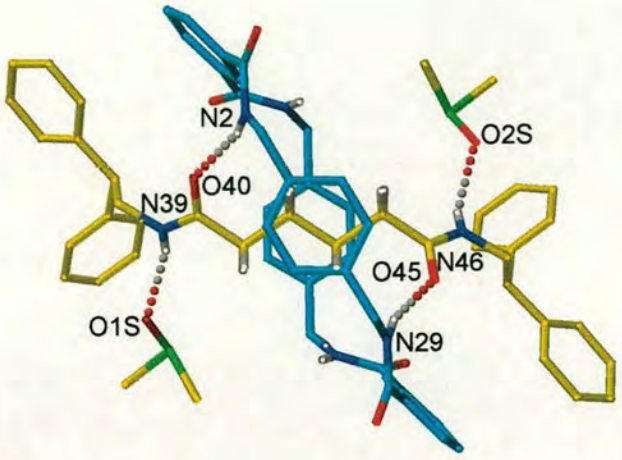

Figure 3.4b *X*-Ray crystal structure of adipamide [2]rotaxane, **15**, crystals grown from DMSO. Intramolecular hydrogen bond distances and angles: O40–HN2 2.22 Å, 163.0°; O45–HN29 2.18 Å, 160.7°. Intermolecular hydrogen bond distances and angles: N39H–O1S 2.20 Å, 155.2°; N46H–O2S 2.23 Å, 153.2°.

It is interesting to note that the solid-state structure of the adipamide rotaxane is virtually identical whether the crystals were grown from a solution of nonpolar $CHCl_3$ (Figure 3.4a) with infusion of MeOH or from a polar medium, DMSO, with infusion of H_2O (Figure 3.4b). The only significant difference in the structures is that solvent molecules bind to the amide NH groups of the thread in the DMSO/H_2O system and to the amide carbonyl groups of the macrocycle with the $CHCl_3$/MeOH system. The conformations and co-conformation of the thread and macrocycle are essentially unaffected by the incorporated solvent molecules, or the nature of the environment that the crystals were grown from, and the position of the macrocycle is best suited to maximize its hydrogen bonding interactions with the adipamide thread. Normally, benzylic amide macrocycle-based rotaxanes and catenanes are extremely sensitive to the polarity of the environment; solvents like DMSO disrupt the intercomponent amide–amide hydrogen bonds and polarophobic effects drive lipophilic groups inside the macrocycle to escape a polar solvent shell.[7] The effect has been used to translocate the macrocycle along the thread in amphiphilic peptide molecular shuttles, e.g. **23** (Figure 3.5).[4c]

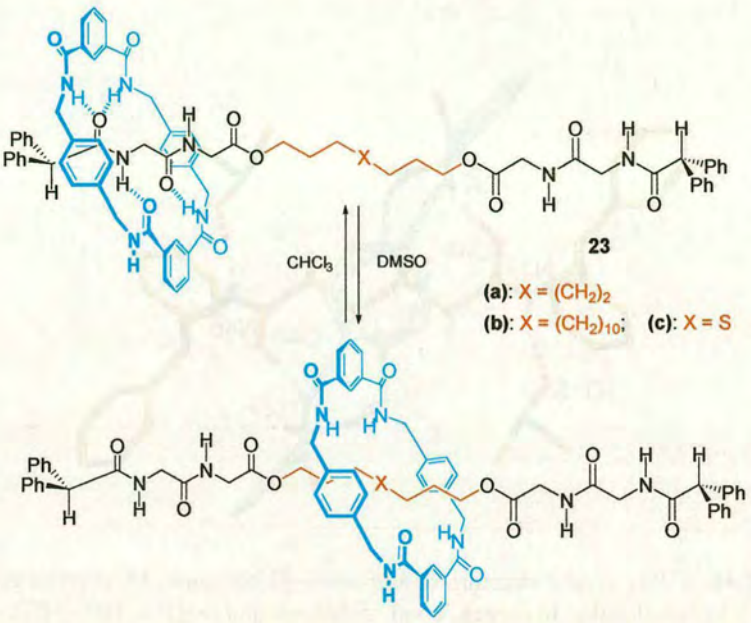

Figure 3.5 Solvent-induced translational isomerism in amphiphilic peptide molecular shuttles.

However, in the adipamide [2]rotaxane **15** the lack of influence of the nature of the solvent of crystallization on the solid-state structure is translated through to the solution structure of the rotaxane in nonpolar and polar media as illustrated by the respective ^{1}H NMR spectra in $CDCl_3$ and DMSO-d_6 (Figure 3.6).

The position of macrocycle in each case can be determined by the upfield shift of the thread protons due to the shielding effects of the xylylene rings of the macrocycle. In $CDCl_3$ both sets of methylene protons in the template region of the thread, H_d and H_e, are shielded upfield by 1.14 and 0.97 ppm respectively (Figure 3.6a and 3.6b). The relative chemical shifts of these protons in the thread and rotaxane in DMSO-d_6 show almost identical shifts, 1.04 and 0.96 ppm respectively (Figure 3.6c and 3.6d). Thus it can be seen that the adipamide binding site is perfectly balanced. Hydrogen bonds to the amide groups of the thread hold it in place in a nonpolar solvent, and the polarophobic nature of the adipyl alkyl chain holds it in the same place in a highly polar solvent!

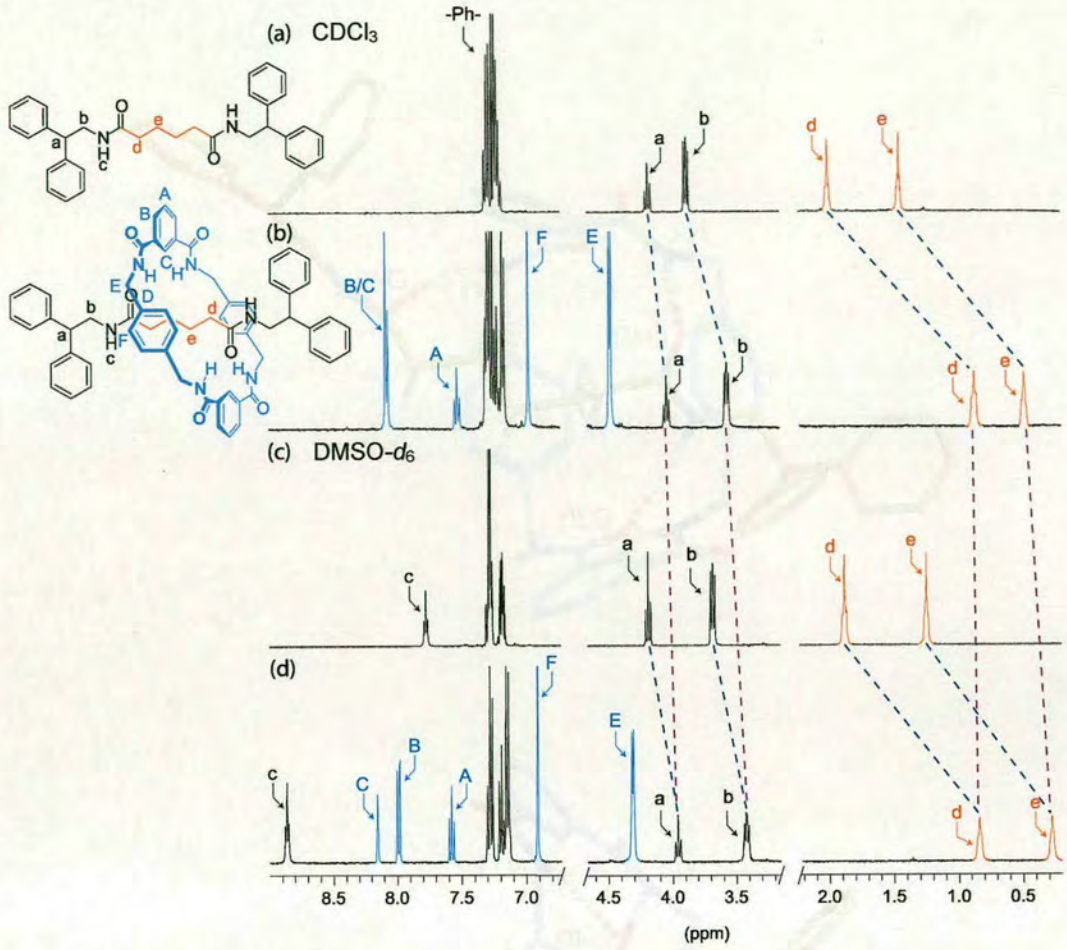

Figure 3.6 ^{1}H NMR spectra (400 MHz, 300 K) of the adipamide thread and [2]rotaxane: (a) **4** $CDCl_3$, (b) **15** $CDCl_3$, (c) **4** DMSO-d_6 and (d) **15** DMSO-d_6.

3.3.4 *Pimelamide [2]rotaxane,* **16** *(n=5), suberamide [2]rotaxane,* **17** *(n=6), azelamide [2]rotaxane,* **18** *(n=7)*

When the number of methylene groups in the template site of the thread increases to n=5, 6 and 7, the crystal structures (Figure 3.7a, 3.7b and 3.7c) of the rotaxanes **16–18** are very different to the solid-state structure of the shorter threads.

(a)

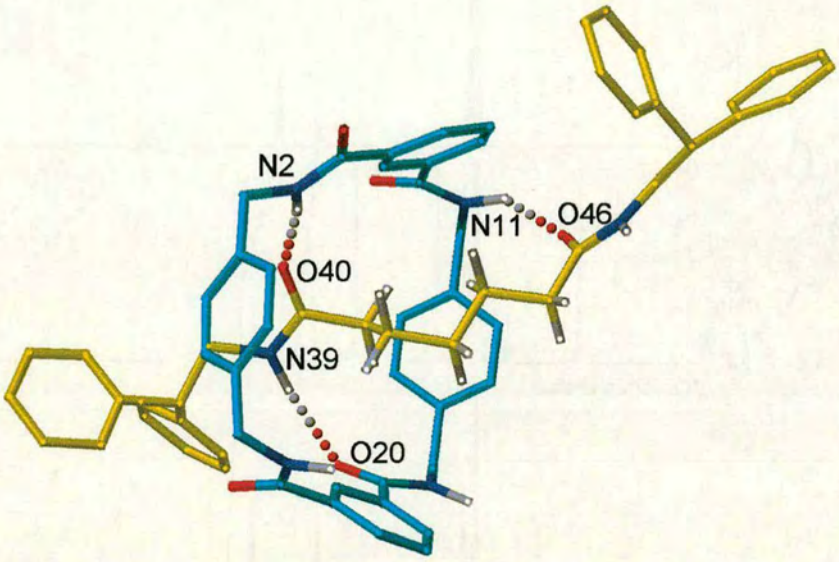

(b)

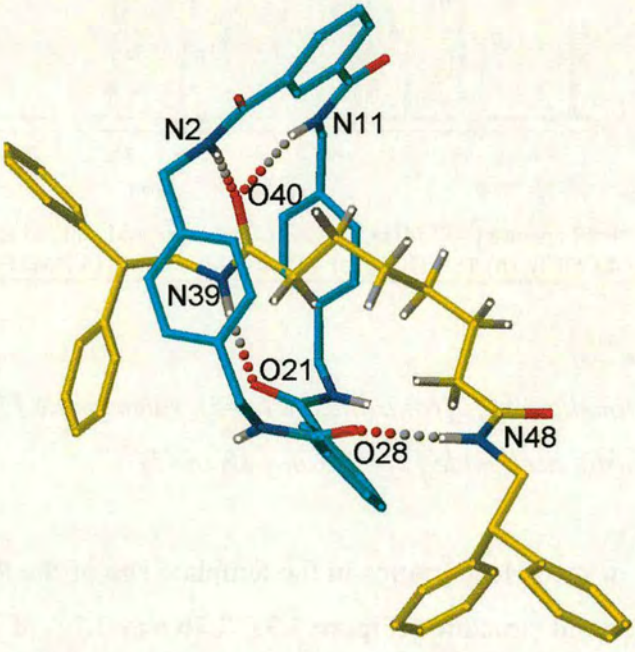

Figure 3.7a and Figure 3.7b *X*-Ray crystal structure of (a) pimelamide [2]rotaxane, **16**. Intramolecular hydrogen bond distances and angles: N39H–O20 2.21 Å, 158.8°; O40–HN2 1.85 Å, 153.4°; O46–HN11 1.97 Å, 144.3°; (b) suberamide [2]rotaxane, **17**. Intramolecular hydrogen bond distances and angles: N39H–O21 2.01 Å, 167.9°; O40–HN2 2.14 Å, 168.1°; O40–HN11 2.42 Å, 164.2°; N48H–O28 2.12 Å, 169.0°;

(c)

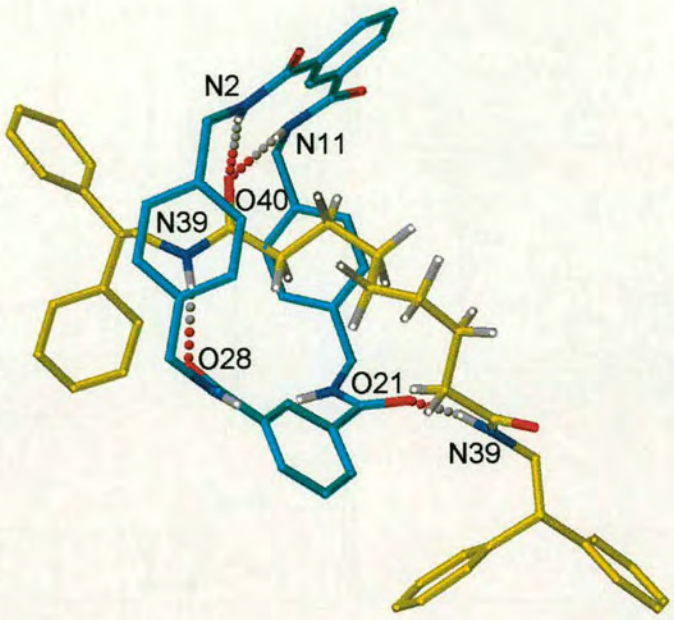

Figure 3.7c *X*-Ray crystal structure of (c) azelamide [2]rotaxane, **18**. Intramolecular hydrogen bond distances and angles: N39H–O28 2.12 Å, 168.5°; O40–HN2 2.42 Å, 162.7°; O40–HN11 2.16 Å, 164.6°; N39H–O21 1.96 Å, 159.5°.

In all three cases, the macrocycle adopts a boat-like conformation, encapsulating one of the two amide groups of the thread, and hydrogen bonds to the second amide binding site by folding of the thread backbone. As the thread increases in length, the folding necessarily becomes more and more pronounced. The ^{1}H NMR spectra (Figure 3.8) show that the corresponding $CDCl_3$ solution structure in all three cases – and in contrast to the adipamide rotaxane – is very different to the snapshot picture captured in the solid-state structure.

The *X*-ray crystal structures of **16–18** show that the macrocycle essentially sits over one amide group in the solid state. The comparison of the shifts of protons in the threads and rotaxanes show that this is not the case in $CDCl_3$.

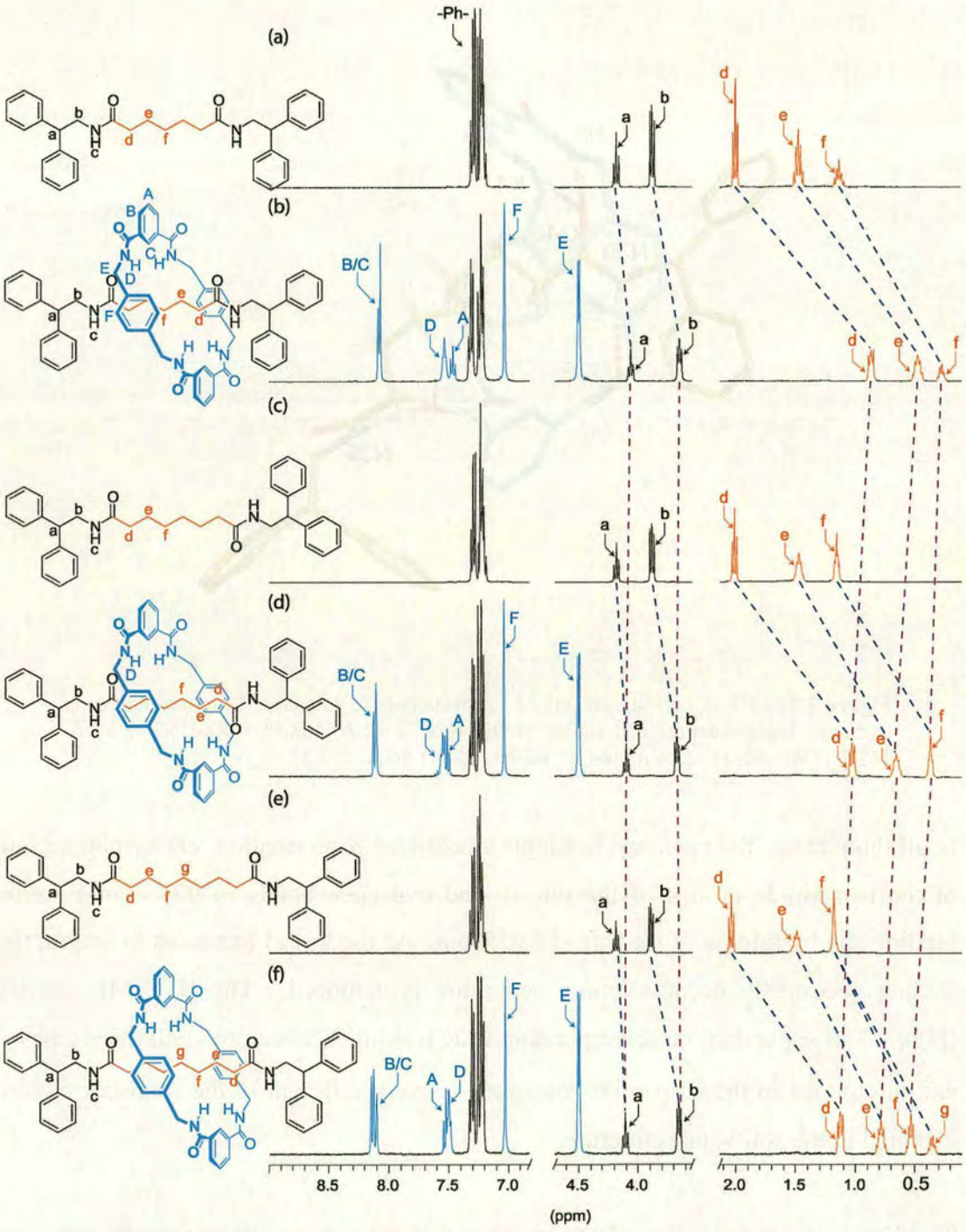

Figure 3.8 ^{1}H NMR spectra (400 MHz, 300 K) in $CDCl_3$ of (a) pimelamide thread, **5**, (b) pimelamide [2]rotaxane, **16**, (c) suberamide thread, **6**, (d) suberamide [2]rotaxane **17**, (e) azelamide thread, **7** and (f) azelamide [2]rotaxane **18**.

In fact, in each rotaxane the shielding of each methylene group is virtually the same as any other indicating that in $CDCl_3$ solution the macrocycle is reasonably evenly distributed all along the diamide thread. This could result from a nonspecific binding mode of the macrocycle to the thread or, more likely, indicates that the type of co-conformations seen in the *X*-ray structures are in equilibrium with another major co-conformation where the macrocycle sits in the centre of the thread and bridges the two thread amide groups. This is discussed further in the next section.

The yield of [2]rotaxane formation for template spacers n=5, 6 and 7 are similar at 14, 17 and 15% respectively. With seven methylene groups between the two amides of the template, there are already more than 2000 (3^7) rotamers of the free thread that can be sampled by the reaction.

3.3.5 *Sebacamide [2]rotaxane* **19** *(n=8), 1,10-decanediamide [2]rotaxane,* **20** *(n=10), 1,12-dodecanediamide [2]rotaxane,* **21** *(n=12), 1,14-tetradecanediamide [2]rotaxane,* **22** *(n=14)*

The hydrogen bond directed-assembly of benzylic amide rotaxanes is so efficient and effective that [2]rotaxane was still obtained on increasing the number of methylene groups between the two amides from n=8 to n=14. With the longer spacer, the solid-state structure of the rotaxanes, **19–22**, is very different to those seen previously (Figure 3.9).

(a)

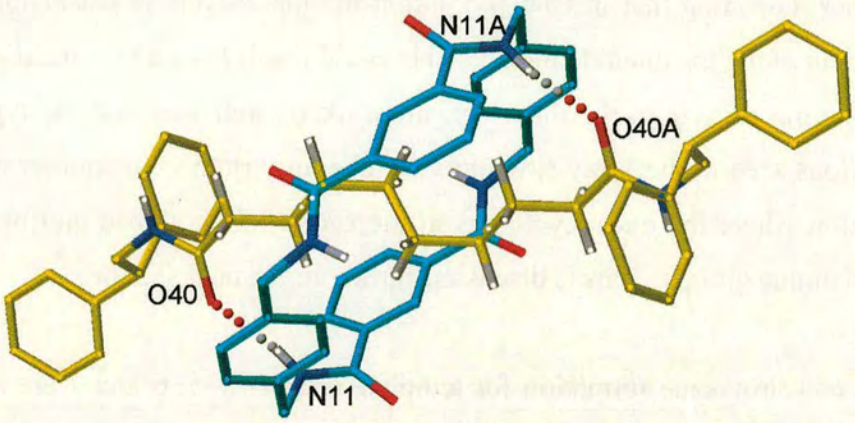

(b)

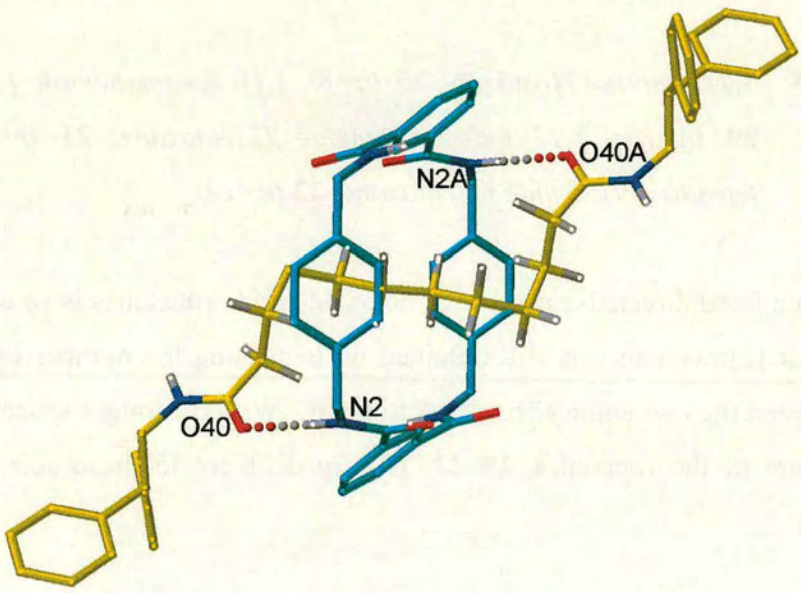

Figure 3.9a and Figure 3.9b *X*-Ray crystal structure of (a) sebacamide [2]rotaxane, **19**, intramolecular hydrogen bond distances and angles: O40–HN11/O40A–N11A 2.05 Å, 168.2°; (b) 1,10-decanediamide [2]rotaxane, **20**, intramolecular hydrogen bond distances and angles: O40–HN2/O40A–HN2A 2.00 Å, 172.3°.

(c)

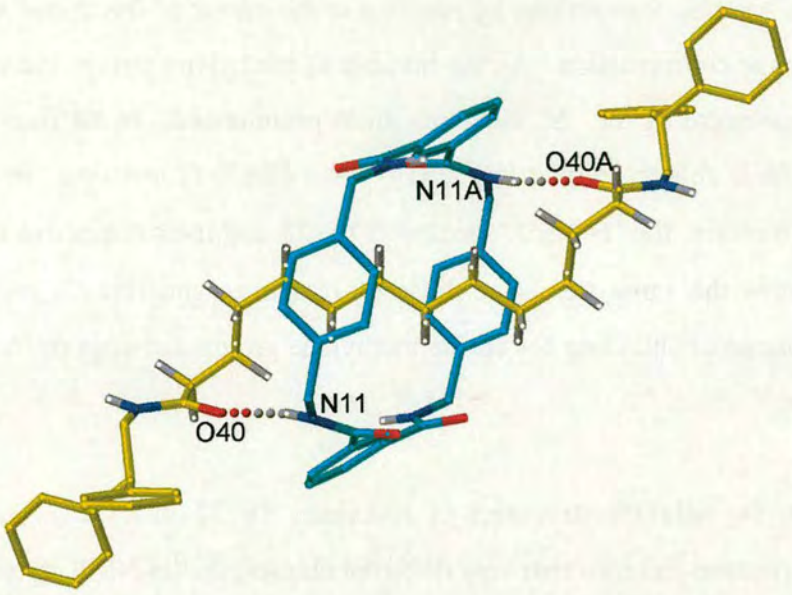

(d)

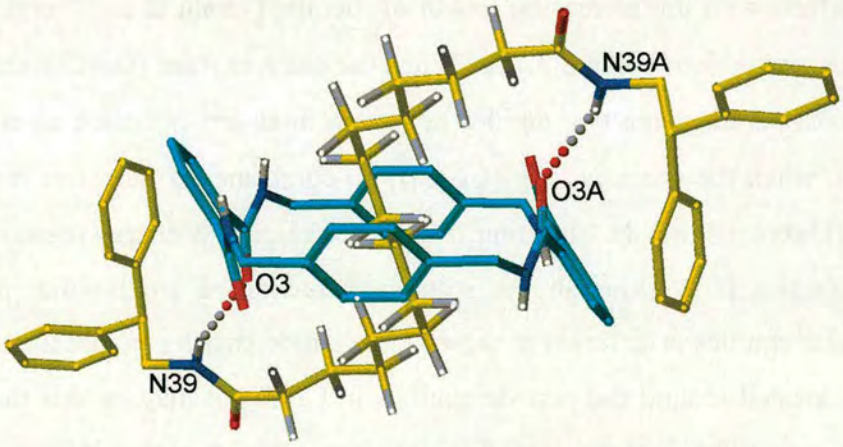

Figure 3.9c and Figure 3.9d *X*-Ray crystal structure of (c) 1,12-dodecanediamide [2]rotaxane, **21**, intramolecular hydrogen bond distances and angles: O40–HN11/O40A–HN11A 1.92 Å, 156.4°; (d) 1,14-tetradecanediamide [2]rotaxane, **22**, intramolecular hydrogen bond distances and angles: O3–HN39/O3A–HN39A 2.24 Å, 151.7°.

With ≥8 methylene groups in the spacer, the size of the ring that would be required for the thread to fold back to hydrogen bond to the macrocycle if it were encapsulating a single amide residue is so large that that co-conformation is no

longer seen in the solid state. Instead, the macrocycle maximizes its intramolecular hydrogen bonding interactions by residing at the center of the thread which assumes an "S"-shape conformation. As the number of methylene groups increases from 8 to 14, the curvature of the "S" becomes more pronounced. In all four rotaxanes, the macrocycle is able to adopt a low energy chair-like conformation. In contrast to the crystal structures, the ^{1}H NMR spectra of **19–22** and their respective threads (Figure 3.10) follow the same trends as those of rotaxanes and threads n=5–7, namely a similar degree of shielding for all the methylene groups between the amide groups of the thread.

What are the solution structures of rotaxanes **16–22** in $CDCl_3$? Although their crystal structures fall into two very different classes, the ^{1}H NMR spectra follow very similar trends. It seems likely that both amide-encapsulated (type **I**) and alkyl chain-encapsulated (type **II**) co-conformations exist in solution for all these rotaxanes and what differs with the increasing length of the alkyl chain is their relative stabilities and thus populations (Figure 3.11). When the chain is short (C_5–C_7), co-conformer **I** dominates (as there are two amides per chain there are two such co-conformers, $\mathbf{I}_a$ and $\mathbf{I}_b$); when the chain is long (C_8–C_{14}) co-conformer **II** becomes relatively more stable (Figure 3.11a). In 'shuttling' from $\mathbf{I}_a$ and $\mathbf{I}_b$, a low energy route is likely to be co-conformer **II**. Although the solution behavior of amphiphilic peptide-based molecular shuttles is different to these single amide shuttles in that the macrocycle is clearly located around the peptide stations in $CDCl_3$, it may be that the low energy route for shuttling in those rotaxanes involves a structure that bridges both peptide units (**IV**, Figure 3.11b).

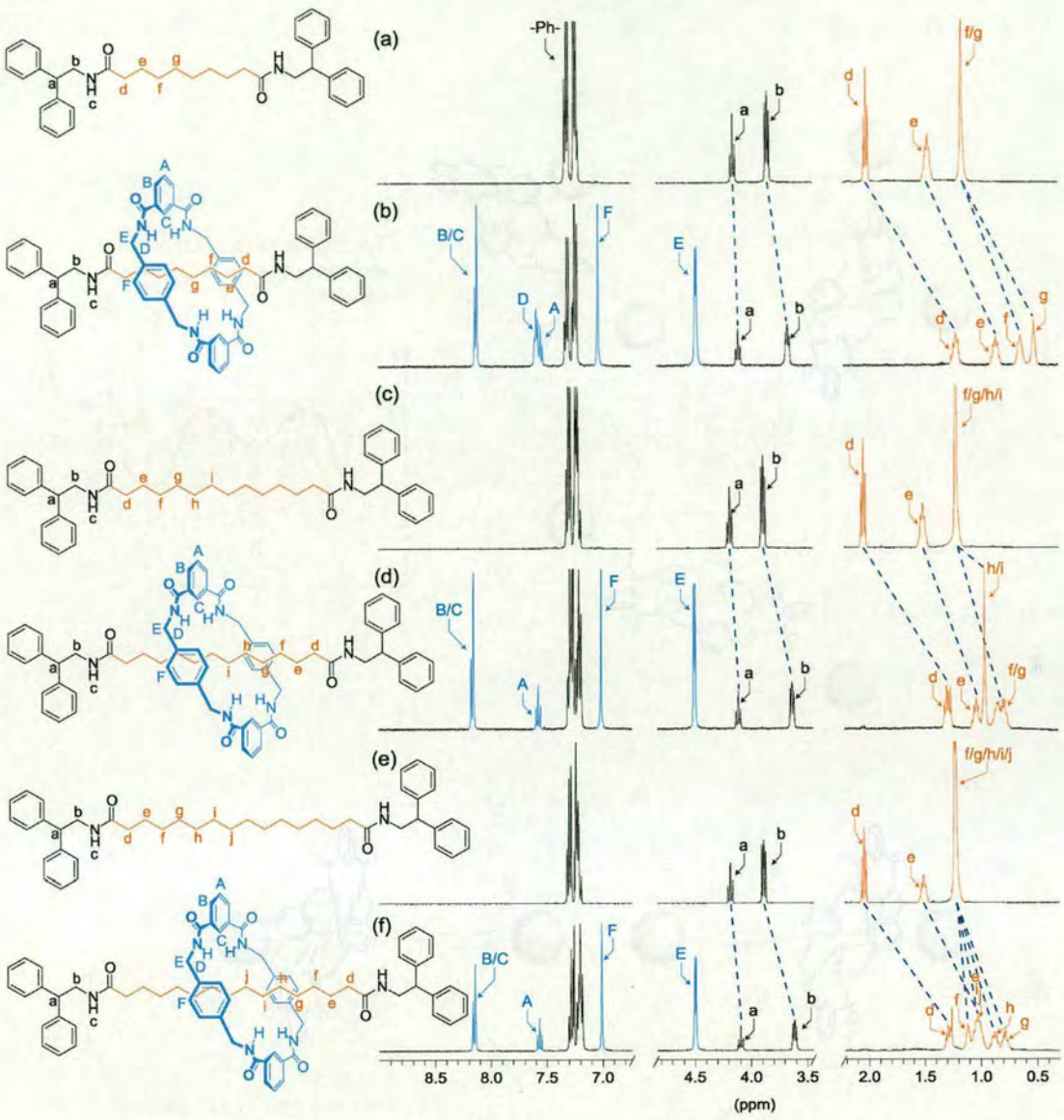

Figure 3.10 ^{1}H NMR spectra (400 MHz, 300 K) in $CDCl_3$ of (a) sebacamide thread, **8**; (b) sebacamide [2]rotaxane, **19**; (c) 1,12-dodecanediamide thread, **10**; (d) 1,12-dodecanediamide thread [2]rotaxane **21**; (e) 1,14-tetradecanediamide thread, **11**; (f) 1,14-tetradocanediamide [2]rotaxane **22**.

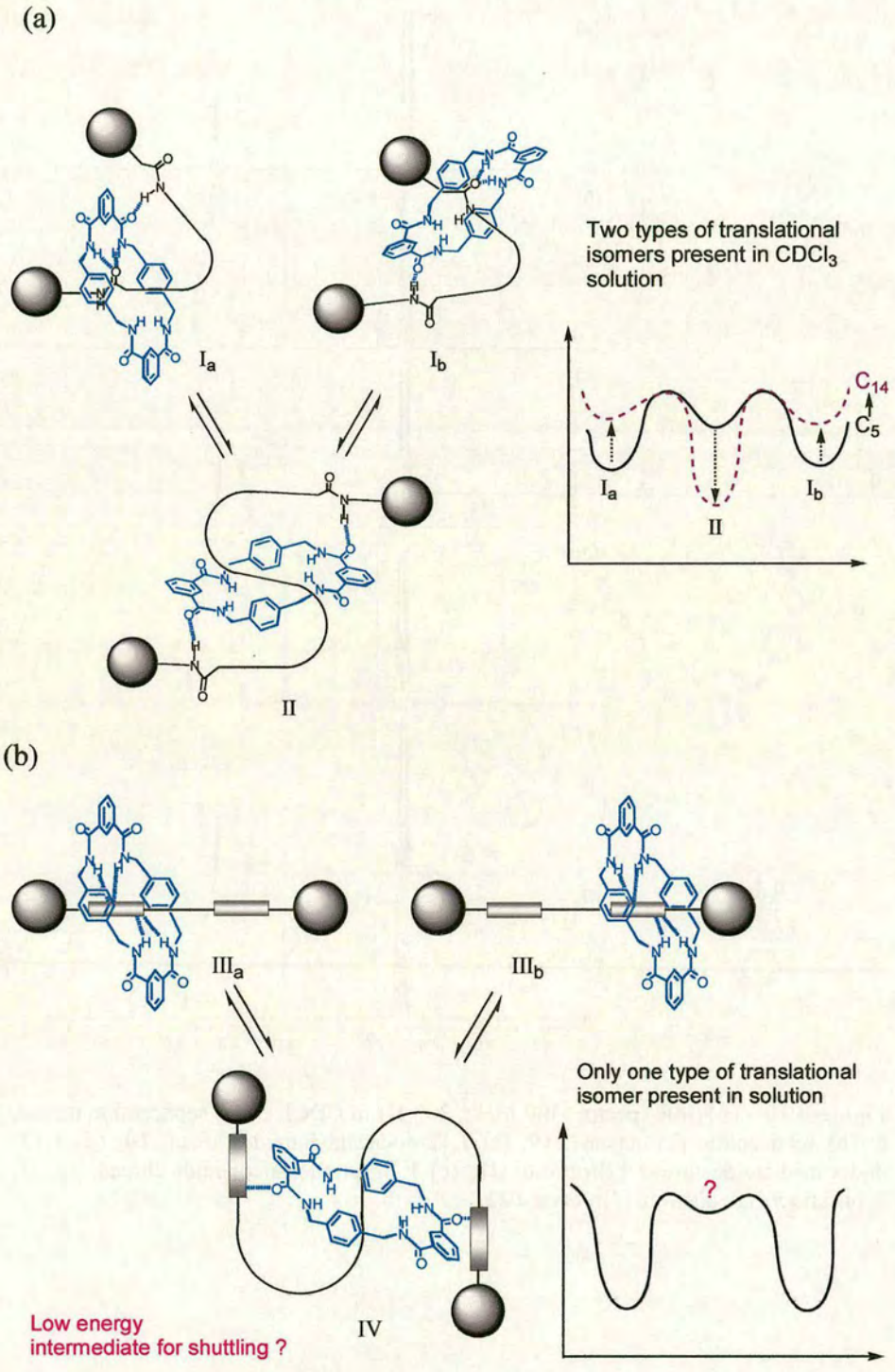

Figure 3.11 Co-conformations existing in solution of (a) amphiphilic amide-based rotaxanes, **12–22**; (b) amphiphilic peptide-based molecular shuttles, **23**.

The number of relatively low energy conformations of the C_{14} spacer template is considerable, with greater than 4 million (3^{14}) C–C rotamers theoretically available. Nevertheless, the yield of the [2]rotaxane is comparable to most of the others in this series. Are all these thread conformations really templates for rotaxane formation? Of course, they do not have to be. If uncatalyzed cyclization of the precursor to macrocycle is very slow but template-induced cyclization about the thread to give rotaxane is very fast then only a small fraction of threads have to be able to adopt a suitable conformation for significant amounts of rotaxane to be formed. However, if the template encompasses the whole length of the alkyl chain in each case, then a decrease in yield of rotaxane formation with increasing chain length would be expected. Since this is not observed in this series, this implies that – in the longer rotaxanes – the macrocycle cyclizes essentially around a single amide group and the part that the second amide plays in the cyclization process is relatively unimportant.

Whatever the mechanism of rotaxane formation, one observation that is clear is that despite the chain length increasing, the benzylic amide macrocycle is able to force the conformation of the thread into one that allows the maximum intramolecular hydrogen bond interactions to be formed. In contrast to the *X*-ray structure of rotaxane **22**, the solid-state structure of **11** (Figure 3.12) shows that the free thread is in a staggered linear form in the solid state and forms structures similar to β-sheets.

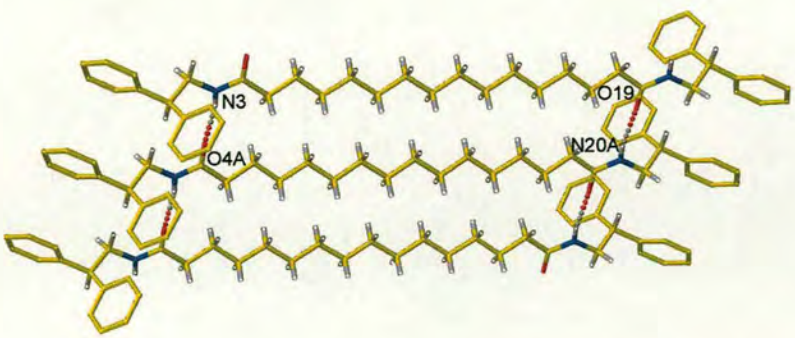

Figure 3.12 *X*-Ray crystal structure of 1,14-tetradecanediamide thread **11**. Intramolecular hydrogen bond distances and angles: N3H–O4A/O19–HN20A 3.08 Å, 170.3°.

3.4 Conclusion

The hydrogen bond-directed assembly of benzylic amide macrocycle-containing rotaxanes is clearly a remarkably efficient process. In a reaction that involves the condensation of four molecules around a thread, in competition with the formation of catenanes, oligomers and larger macrocycles, it is still possible to form rotaxanes in reasonable yields, even with a far from optimized template. The number of degrees of freedom of the templating thread increases with increasing number of methylene groups between the two amide binding sites up to 3^{14} degrees of freedom (n=14)! Despite this, and the possibility of competing formation of intramolecular hydrogen bonds within the thread molecule itself, it was still possible to obtain rotaxanes in all these systems and thus, indeed, *hydrogen bonding does find a way!*

3.5 Experimental

General method for the preparation of diacid chloride. The diacid chloride derivatives for the preparation of threads **1–9** were purchased from Aldich and used without further purification. For **10–11**, the diacid chloride derivatives were prepared from the corresponding diacid purchased from Alrich using the following general method: To a stirred solution of diacid (3.5 mmol, 1 equiv.) in 20 mL of CH_2Cl_2 was added thionyl chloride (2.0 mL, 28 mmol, 8 equiv.), one drop of DMF (cat.) and stirred at 65 °C for 2 hours. Distillation of thionyl chloride and CH_2Cl_2 yielded the acid chloride as a yellow oil which was used immediately.

General method for the preparation of alkyl diamide threads, 1–11. To a solution of 2,2-diphenylethyl amine (2.1 mmol, 2.1 equiv.) and triethylamine (2.5 mmol, 2.5 equiv.) in 10 mL CH_2Cl_2 was added the relevant diacid chloride (1 mmol, 1 equiv.) in 5 mL CH_2Cl_2 over 10 minutes at 0 °C. The reaction mixture was allowed to warm to room temperature and stirred for 16 hours. The resulting mixture was washed with 1 M aqueous HCl (2 x 10 mL), saturated aqueous $NaHCO_3$ (2 x 10 mL), brine (10 mL), dried over anhydrous $MgSO_4$ and concentrated under reduced pressure to give the desired thread as colourless solid.

General method for the preparation of benzylic amide macrocycle alkyl bisamide[2]rotaxanes, 12–22. The threads **1–11** (1.00 mmol, 1 equiv.) and triethylamine (4.2 ml, 30 mmol, 30 equiv.) were dissolved in 100 mL chloroform (stabilised with amylenes) and stirred vigorously whilst solutions of *para*-xylylene diamine (1.63 g, 12 mmol, 12 equiv.) in chloroform (45 mL) and isophthaloyl dichloride (2.33 g, 11.5 mmol, 11.5 equiv.) in chloroform (45 mL) were simultaneously added over a period of 4 hours using motor-driven syringe pumps. The resulting suspension was filtered and concentrated under reduced pressure to leave unconsumed thread and [2]rotaxane in solution. This mixture was subjected to

column chromatography (silica gel, CH_2Cl_2/MeOH as eluent) to yield, in order of elution, the unconsumed thread and the bisamide [2]rotaxane.

***N,N'-bis*(2,2-Diphenylethyl)malonamide, 1**

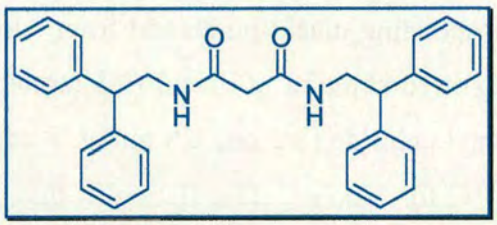

Selected data for *N,N'-bis*(2,2-diphenylethyl)malonamide, 1: Yield 7.23 g (76%); m.p. 174–175 °C; ^{1}H NMR (400 MHz, DMSO-d_6): δ = 7.99 (t, J = 5.6 Hz, 2H, CONH), 7.34–7.17 (m, 20H, ArH, phenyl), 4.14 (t, J = 7.7 Hz, 2H, $Ph_2C\underline{H}$), 3.69 (dd, J = 7.7, 5.6 Hz, 4H, $Ph_2CHC\underline{H}_2$), 2.90 (s, 2H, $CONHC\underline{H}_2$); ^{13}C NMR (100 MHz, DMSO-d_6): δ = 167.33, 142.01, 129.10, 128.42, 127.33, 50.84, 44.33, 43.10; MS (FAB, NBA matrix): *m/z* = 463 $[(M+H)^+]$, 485 $[(M+Na)^+]$; anal. calcd for $C_{31}H_{30}N_2O_2$ (462.58): C 80.49, H 6.54, N 6.06, found: C 80.60, H 6.50, N 5.88.

***N,N'-bis*(2,2-Diphenylethyl)succinamide, 2**

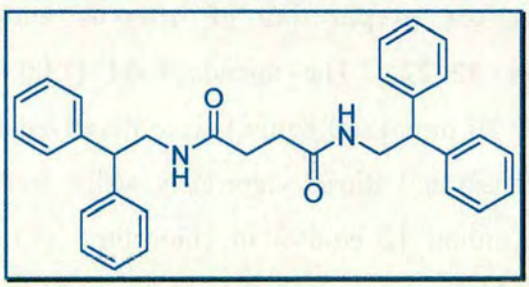

Selected data for *N,N'-bis*(2,2-diphenylethyl)succinamide, 2: Yield 4.00 g (62%); m.p. 280 °C; ^{1}H NMR (400 MHz, $CDCl_3$): δ = 7.32–7.17 (m, 20H, ArH, phenyl), 5.52 (t, J = 5.8 Hz, 2H, CONH), 4.14 (t, J = 8.0 Hz, 2H, $Ph_2C\underline{H}$), 3.82 (dd, J = 8.0,

5.8 Hz, 4H, $Ph_2CHC\underline{H}_2$), 2.27 (s, 4H, $CONHC\underline{H}_2$); ^{13}C NMR (100 MHz, $CDCl_3$): δ = 172.46, 142.26, 129.12, 128.44, 127.24, 50.95, 44.25, 31.90; MS (FAB, NBA matrix): *m/z* = 477 $[(M+H)^+]$, 499 $[(M+Na)^+]$; anal. calcd for $C_{32}H_{32}N_2O_2$ (476.61): C 80.64, H 6.77, N 5.88, found: C 80.51, H 6.76, N 5.67.

***N,N'-bis*(2,2-Diphenylethyl)glutaramide, 3**

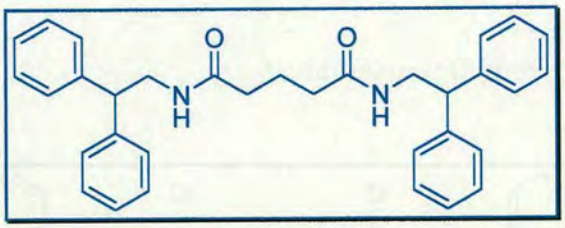

Selected data for *N,N'-bis*(2,2-diphenylethyl)glutaramide, 3: Yield 7.50 g (76%); ^1H NMR (400 MHz, $CDCl_3$): δ = 7.34–7.22 (m, 20H, ArH, phenyl), 5.33 (brt, 2H, CONH), 4.22 (t, *J* = 7.7 Hz, 2H, $Ph_2C\underline{H}$), 3.82 (dd, *J* = 7.7, 5.6 Hz, 4H, $Ph_2CHC\underline{H}_2$), 1.91 (t, *J* = 7.7 Hz, 4H, $CONHC\underline{H}_2$), 1.82 (m, *J* = 7.7 Hz, 2H, $CONHC\underline{H}_2CH_2$); ^{13}C NMR (100 MHz, $CDCl_3$): δ = 172.69, 142.25, 129.17, 128.48, 127.30, 51.02, 44.07, 35.22, 22.05; MS (FAB, NBA matrix): *m/z* = 492 $[(M+H)^+]$; anal. calcd for $C_{33}H_{34}N_2O_2$ (490.64): C 80.78, H 6.98, N 5.71, found: C 80.70, H 6.69, N 5.78.

***N,N'-bis*(2,2-Diphenylethyl)adipamide, 4**

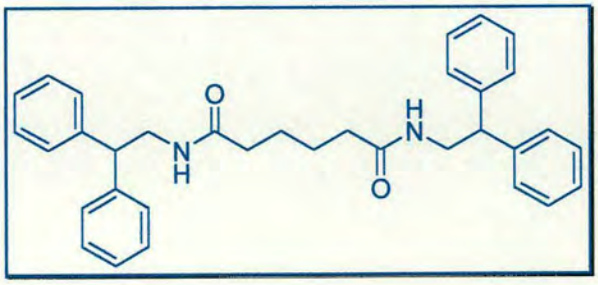

Selected data for *N,N'-bis*(2,2-diphenylethyl)adipamide, 4: Yield 2.18 g (79%); m.p. 183 °C; ^{1}H NMR (400 MHz, $CDCl_3$): δ = 7.31–7.19 (m, 20H, ArH, phenyl), 5.48 (brt, 2H, CONH), 4.18 (t, *J* = 7.8 Hz, 2H, $Ph_2C\underline{H}$), 3.88 (dd, *J* = 7.8, 5.8 Hz, 4H, $Ph_2CHC\underline{H_2}$), 2.01 (m, 4H, $CONHC\underline{H_2}$), 1.45 (m, 4H, $CONHCH_2C\underline{H_2}$); ^{13}C NMR (100 MHz, $CDCl_3$): δ = 172.56, 141.87, 128.71, 128.05, 126.81, 50.62, 43.74, 36.05, 24.72; HRMS (FAB, THIOG matrix): *m/z* = 505.28550 [$(M+H)^+$] (anal. calcd for $C_{34}H_{37}N_2O_2$: *m/z* = 505.28695).

***N,N'-bis*(2,2-Diphenylethyl)pimelamide, 5**

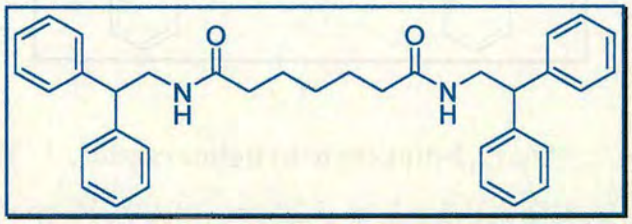

Selected data for *N,N'-bis*(2,2-diphenylethyl)pimelamide, 5: Yield 2.26 g (86%); m.p. 138 °C; ^{1}H NMR (400 MHz, $CDCl_3$): δ = 7.32–7.19 (m, 20H, ArH, phenyl), 5.35 (brt, 2H, CONH), 4.18 (t, *J* = 8.1 Hz, 2H, $Ph_2C\underline{H}$), 3.88 (dd, *J* = 8.1, 5.8 Hz, 4H, $Ph_2CHC\underline{H_2}$), 2.00 (t, *J* = 7.3 Hz, 4H, $CONHC\underline{H_2}$), 1.47 (q, *J* = 7.3 Hz, 4H, $CONHCH_2C\underline{H_2}$), 1.13 (m, 2H, $CONH(CH_2)_2C\underline{H_2}$); ^{13}C NMR (100 MHz, $CDCl_3$): δ = 172.81, 141.87, 128.72, 128.05, 126.82, 50.62, 43.69, 36.27, 28.36, 25.07; HRMS (FAB, THIOG matrix): *m/z* = 519.30115 [$(M+H)^+$] (anal. calcd for $C_{35}H_{38}N_2O_2$: *m/z* = 519.30224).

***N,N'-bis*(2,2-Diphenylethyl)suberamide, 6**

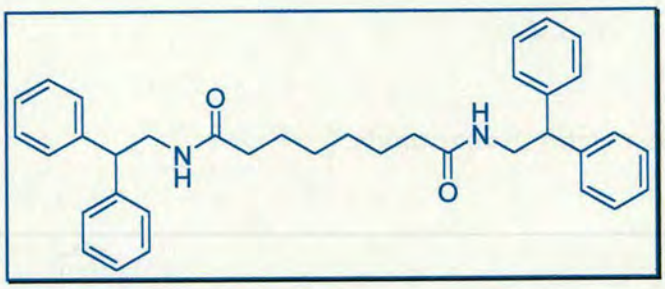

Selected data for *N,N'-bis*(2,2-diphenylethyl)suberamide, 6: Yield 2.20 g (87%); m.p. 137 °C; ^{1}H NMR (400 MHz, $CDCl_3$): δ = 7.32–7.19 (m, 20H, ArH, phenyl), 5.40 (brt, *J* = 5.8 Hz, 2H, CONH), 4.18 (t, *J* = 8.1 Hz, 2H, $Ph_2C\underline{H}$), 3.88 (dd, *J* = 8.1, 5.8 Hz, 4H, $Ph_2CHC\underline{H_2}$), 2.01 (t, *J* = 7.3 Hz, 4H, $CONHC\underline{H_2}$), 1.47 (m, 4H, $CONHCH_2C\underline{H_2}$), 1.15 (m, 4H, $CONH(CH_2)_2C\underline{H_2}$); ^{13}C NMR (100 MHz, $CDCl_3$): δ = 172.96, 141.86, 128.73, 128.05, 126.83, 50.62, 43.69, 36.49, 28.58, 25.34; HRMS (FAB, THIOG matrix): *m/z* = 533.31680 [$(M+H)^+$] (anal. calcd for $C_{36}H_{41}N_2O_2$: *m/z* = 533.31590).

***N,N'-bis*(2,2-diphenylethyl)azelamide, 7**

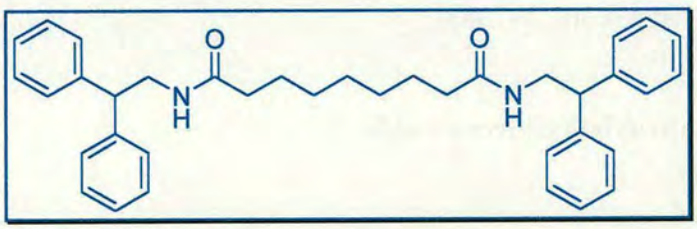

Selected data for *N,N'-bis*(2,2-diphenylethyl)azelamide, 7: Yield 2.14 g (88%); m.p. 144 °C; ^{1}H NMR (400 MHz, $CDCl_3$): δ = 7.32–7.19 (m, 20H, ArH, phenyl), 5.35 (brt, 2H, CONH), 4.18 (t, *J* = 8.1 Hz, 2H, $Ph_2C\underline{H}$), 3.89 (dd, *J* = 8.1, 5.8 Hz, 4H, $Ph_2CHC\underline{H_2}$), 2.03 (t, *J* = 7.6 Hz, 4H, $CONHC\underline{H_2}$), 1.48 (m, 4H, $CONHCH_2C\underline{H_2}$), 1.17 (m, 6H, $CONH(CH_2)_2C\underline{H_2}$ & $CONH(CH_2)_3C\underline{H_2}$); ^{13}C NMR (100 MHz, $CDCl_3$):

δ = 173.05, 141.86, 128.72, 128.05, 126.82, 50.61, 43.70, 36.64, 28.86, 28.79, 25.49; HRMS (FAB, THIOG matrix): *m/z* = 547.33245 $[(M+H)^+]$ (anal. calcd for $C_{37}H_{43}N_2O_2$: *m/z* = 547.33408).

***N,N'-bis*(2,2-diphenylethyl)subacamide, 8**

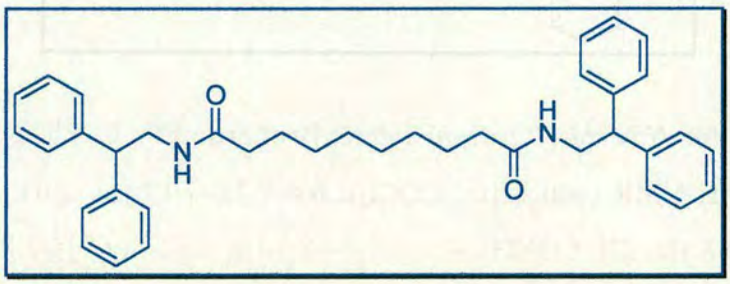

Selected data for *N,N'-bis*(2,2-diphenylethyl)subacamide, 8: Yield 1.92 g (82%); m.p. 138 °C; ^{1}H NMR (400 MHz, $C_2D_2Cl_4$): δ = 7.33–7.21 (m, 20H, ArH, phenyl), 5.37 (brt, 2H, CONH), 4.15 (t, *J* = 7.8 Hz, 2H, $Ph_2C\underline{H}$), 3.85 (dd, *J* = 7.8 Hz, 4H, $Ph_2CHC\underline{H_2}$), 2.01 (t, *J* = 7.6, 5.8 Hz, 4H, $CONHC\underline{H_2}$), 1.46 (m, 4H, $CONHCH_2C\underline{H_2}$), 1.15 (brs, 8H, $CONH(CH_2)_2C\underline{H_2}$ & $CONH(CH_2)_3C\underline{H_2}$); ^{13}C NMR (100 MHz, $CDCl_3$): δ = 173.06, 141.86, 128.72, 128.05, 126.83, 50.61, 43.69, 36.72, 29.18, 29.02, 25.58; HRMS (FAB, THIOG matrix): *m/z* = 561.34810 $[(M+H)^+]$ (anal. calcd for $C_{38}H_{45}N_2O_2$: *m/z* = 561.34738).

***N,N'-bis*(2,2-diphenylethyl)decanamide, 9**

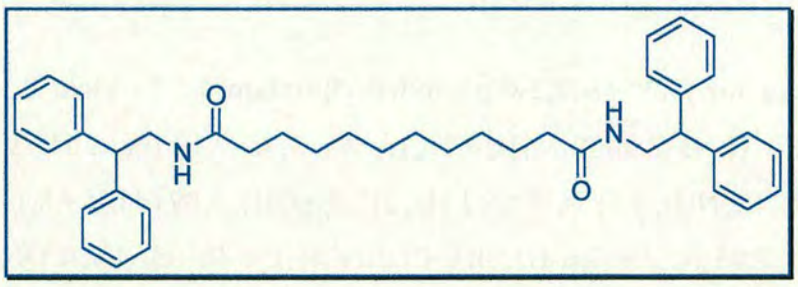

Selected data for *N,N'-bis*(2,2-diphenylethyl)decanamide, 9: Yield 1.87 g (85%); m.p. 137 °C; ^{1}H NMR (400 MHz, $CDCl_3$): δ = 7.32–7.19 (m, 10H, ArH, phenyl), 5.37 (brt, 2H, CONH), 4.18 (t, *J* = 7.8 Hz, $Ph_2C\underline{H}$), 3.88 (dd, *J* = 7.8, 5.8 Hz, 2H, $Ph_2CHC\underline{H_2}$), 2.04 (t, *J* = 7.6 Hz, 4H, $CONHC\underline{H_2}$), 1.50 (m, 4H, $CONHCH_2C\underline{H_2}$), 1.20 (brs, 8H, $CONH(CH_2)_2C\underline{H_2}$ & $CONH(CH_2)_3C\underline{H_2}$ & $CONH(CH_2)_3C\underline{H_4}$); ^{13}C NMR (100 MHz, $CDCl_3$): δ = 173.05, 141.89, 128.70, 128.05, 126.81, 50.63, 43.70, 36.76, 29.30, 29.23, 29.10, 25.63; HRMS (FAB, NBA matrix): *m/z* = 589.37796 $[(M+H)^+]$ (anal. calcd for $C_{40}H_{49}N_2O_2$: *m/z* = 589.37940).

***N,N'-bis*(2,2-diphenylethyl)dodecanamide, <u>10</u>**

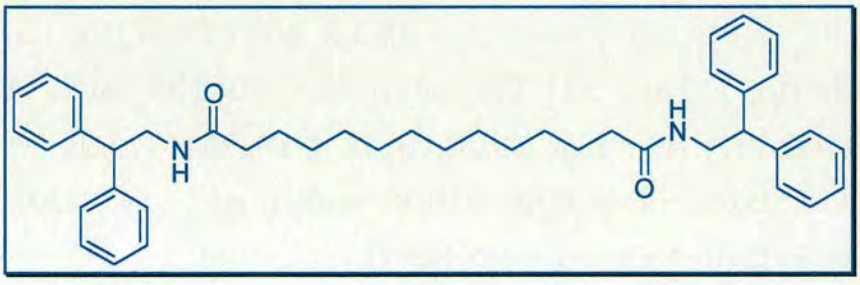

Selected data for *N,N'-bis*(2,2-diphenylethyl)dodecanamide, 10: Yield 1.88 g (90%); m.p. 137 °C; ^{1}H NMR (400 MHz, $CDCl_3$): δ = 7.32–7.19 (m, 20H, ArH, phenyl), 5.37 (brt, *J* = 5.8 Hz, 2H, CONH), 4.18 (t, *J* = 7.8 Hz, 2H, $Ph_2C\underline{H}$), 3.88 (dd, *J* = 7.8, 5.8 Hz, 4H, $Ph_2CHC\underline{H_2}$), 2.04 (t, *J* = 7.6 Hz, 4H, $CONHC\underline{H_2}$), 1.50 (m, 4H, $CONHCH_2C\underline{H_2}$), 1.21 (m, 16H, CH_2, alkyl); ^{13}C NMR (100 MHz, $CDCl_3$): δ = 173.10, 141.89, 128.71, 128.06, 126.82, 50.62, 43.69, 36.79, 29.53, 29.40, 29.30, 29.15, 25.67; HRMS (FAB, THIOG matrix): *m/z* = 617.41070 $[(M+H)^+]$ (anal. calcd for $C_{42}H_{53}N_2O_2$: *m/z* = 617.41106).

***N,N'-bis*(2,2-diphenylethyl)tetradecanamide, 11**

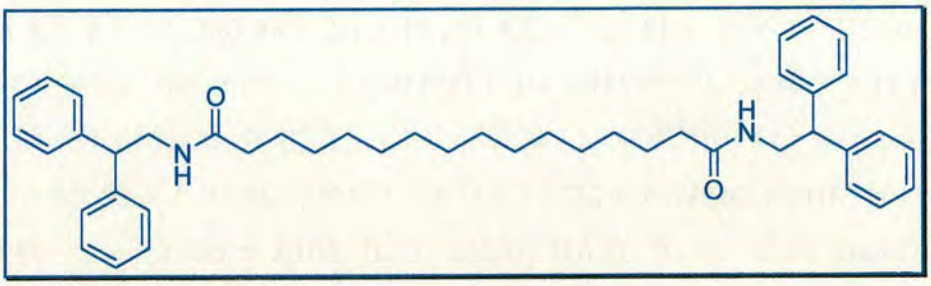

Selected data for *N,N'-bis*(2,2-diphenylethyl)tetradecanamide, 11: Yield 1.64 g (82%); m.p. 140 °C; ^{1}H NMR (400 MHz, $CDCl_3$): δ = 7.32–7.19 (m, 20H, ArH, phenyl), 5.35 (brt, 2H, CONH), 4.18 (t, J = 7.8 Hz, 2H, $Ph_2C\underline{H}$), 3.88 (dd, J = 7.8, 5.8 Hz, 4H, $Ph_2CHC\underline{H_2}$), 2.04 (t, J = 7.8 Hz, 4H, $CONHC\underline{H_2}$), 1.51 (m, 4H, $CONHCH_2C\underline{H_2}$), 1.22 (m, 20H, CH_2, alkyl); ^{13}C NMR (100 MHz, $CDCl_3$): δ = 173.10, 141.88, 128.71, 128.06, 126.82, 50.62, 43.69, 36.80, 29.60, 29.58, 29.43, 29.32, 29.16, 25.68; HRMS (FAB, THIOG matrix): m/z = 645.44200 [$(M+H)^+$] (anal. calcd for $C_{44}H_{57}N_2O_2$: m/z = 645.44251).

***X*-ray crystallographic structure determination, 11**: $C_{44}H_{56}N_2O_2$, M = 644.91, crystal size 0.10 × 0.08 × 0.08 mm, triclinic, P-1, a = 5.1811(2), b = 8.9518(4), c = 19.9950(8) Å, α = 78.2590(10), β = 89.1620(10), γ = 82.8780(10)°, V = 900.91(6) Å^3, Z = 1, ρ_{calcd} = 1.189 Mg m^{-3}; synchrotron radiation (CCLRC Daresbury Laboratory Station 9.8, silicon monochromator, λ = 0.68950 Å), μ = 0.072 mm^{-1}, T = 150(2) K. 9199 data (4877 unique, R_{int} = 0.0249, 2.34 < θ < 30.36°), were collected on a Siemens SMART CCD diffractometer using narrow frames (0.3° in ω), and were corrected semiempirically for absorption and incident beam decay (transmission 1.00–0.74). The structure was solved by direct methods and refined by full-matrix least-squares on F^2 values of all data (G. M. Sheldrick, SHELXTL manual, Siemens Analytical *X*-ray Instruments, Madison WI, USA, 1994, version 5) to give $wR = \{\Sigma[w(F_o^2-F_c^2)^2]/\Sigma[w(F_o^2)^2]\}^{1/2}$ = 0.1490, conventional R = 0.0588 for F

values of 4877 reflections with $F_o^2 > 2\sigma(F_o^2)$, S = 1.027 for 221 parameters. Residual electron density extremes were 0.347 and –0.259 eÅ^{-3}. Amide hydrogen atoms were refined isotropically with the remainder constrained; anisotropic displacement parameters were used for all non-hydrogen atoms.

([2](1,7,14,20-Tetraaza-2,6,15,19-tetraoxo-3,5,9,12,16,18,22,25 cetrabenzocyclohexacosane)-*(N,N'*-Bis-(2,2-diphenyl-ethyl)-malonamide)-rotaxane, 12

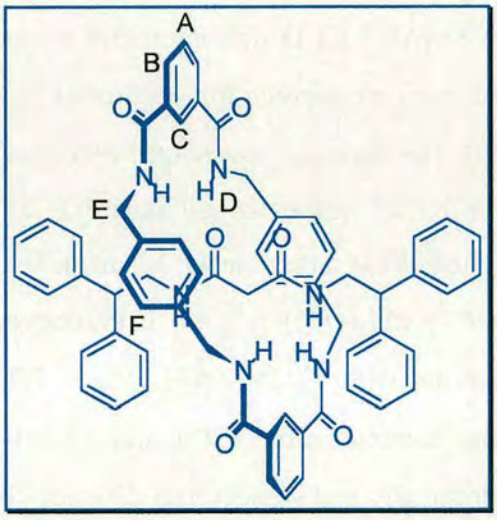

Selected data for ([2](1,7,14,20-Tetraaza-2,6,15,19-tetraoxo-3,5,9,12,16,18,22,25 cetrabenzocyclohexacosane)-*(N,N'*-Bis-(2,2-diphenyl-ethyl)-malonamide)-rotaxane, 11: Yield 0.08 g (8.3%); m.p. 266–267 °C; ^{1}H NMR (400 MHz, DMSO-d_6): δ = 8.59 (t, J = 4.8 Hz, 4H, N$\underline{H}_D$), 8.18 (brs, 2H, ArH_C), 8.08 (d, J = 7.8 Hz, 4H, ArH_B), 7.68 (t, J = 7.8 Hz, 2H, ArH_A), 7.63 (t, J = 5.3 Hz, 2H, CONH), 7.25–7.05 (m, 20H, ArH, phenyl), 6.87 (s, 8H, ArH_F), 4.29 (d, J = 4.8 Hz, 8H, CH_{2E}), 3.80 (t, J = 7.8 Hz, 2H, $Ph_2C\underline{H}$), 3.39 (dd, J = 7.8, 5.3 Hz 4H, $Ph_2CHC\underline{H}_2$), 1.48 (s, 2H, CONHC$\underline{H}_2$); ^{13}C NMR (100 MHz, $CDCl_3$): δ = 167.6, 166.4, 143.2, 137.2, 134.7, 130.6, 129.0, 128.9, 128.7, 127.9, 126.7, 126.5, 50.1, 44.1, 43.4, 40.0; MS (FAB,

NBA matrix): *m/z*= 995 [(rotaxane+H)$^+$], 1017 [(rotaxane+Na)$^+$]; anal. calcd for $C_{63}H_{58}N_6O_6$ (995.17): C 76.03, H 5.87, N 8.45, found C 75.75, H 5.88, N 8.11.

***X*-ray crystallographic structure determination, crystals of rotaxane grown in acetone/H_2O, 12**: $C_{64.50}H_{64}N_6O_{7.50}$, M = 1043.22, crystal size 0.15 × 0.15 × 0.15 mm, triclinic, *P*-1, a = 11.0013(4), b = 14.6086(5), c = 18.5866(6) Å, α = 92.8550(10), β = 95.2040(10), γ = 101.1940(10)°, V = 911.3(2) Å^3, Z = 2, ρ_{calcd} = 1.190 Mg m^{-3}; $Mo_{K\alpha}$ radiation (graphite monochromator, λ = 0.71073 Å), μ = 0.079 mm^{-1}, T = 293(2) K. 16933 data (11048 unique, R_{int} = 0.1247, 1.42 < θ < 26.41°), were collected on a Siemens SMART CCD diffractometer using narrow frames (0.3° in ω), and were corrected semiempirically for absorption and incident beam decay (transmission 1.00–0.09). The structure was solved by direct methods and refined by full-matrix least-squares on F^2 values of all data (G. M. Sheldrick, SHELXTL manual, Siemens Analytical *X*-ray Instruments, Madison WI, USA, 1994, version 5) to give $wR = \{\Sigma[w(F_o^2-F_c^2)^2]/\Sigma[w(F_o^2)^2]\}^{1/2}$ = 0.3019, conventional R = 0.0939 for F values of 11048 reflections with $F_o^2 > 2\sigma(F_o^2)$, S = 1.278 for 344 parameters. Residual electron density extremes were 0.751 and –0.261 eÅ^{-3}. Amide hydrogen atoms were refined isotropically and subject to a distance constraint N–H = 0.98 Å, with the remainder atoms constrained; anisotropic displacement parameters were used for all non-hydrogen atoms.

([2](1,7,14,20-Tetraaza-2,6,15,19-tetraoxo-3,5,9,12,16,18,22,25 cetrabenzocyclohexacosane)-*(N,N'*-Bis-(2,2-diphenyl-ethyl)-succinamide)-rotaxane, 13

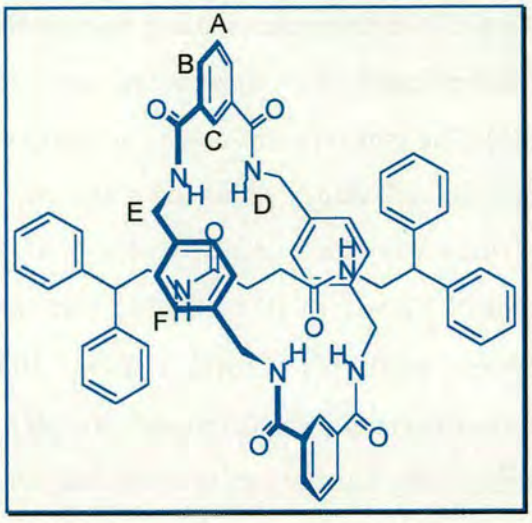

Selected data for ([2](1,7,14,20-Tetraaza-2,6,15,19-tetraoxo-3,5,9,12,16,18,22,25 cetrabenzocyclohexacosane)-*(N,N'*-Bis-(2,2-diphenyl-ethyl)-succinamide)-rotaxane, 13: Yield 0.50 g (52%); m.p. 330 °C, decomposed; ^{1}H NMR (400 MHz, $C_2D_2Cl_4$): δ = 8.33 (brs, 2H, ArH_C), 8.14 (dd, J = 7.8, 1.3 Hz, 4H, ArH_B), 7.59 (t, J = 7.8 Hz, 2H, ArH_A), 7.35 (brt, J = 5.3 Hz, 4H, $N\underline{H}_D$), 7.24–7.10 (m, 20H, ArH, phenyl), 6.71 (s, 8H, ArH_F), 5.53 (brt, 2H, CONH), 4.31 (d, J = 5.0 Hz, 8H, CH_E), 3.93 (t, J = 7.8 Hz, 2H, $Ph_2C\underline{H}$), 3.59 (m, 4H, $Ph_2CHC\underline{H}_2$), 0.74 (brs, 4H, $CONHC\underline{H}_2$); ^{13}C NMR (100 MHz, DMSO-d_6): δ = 173.04, 166.28, 143.10, 137.32, 134.80, 131.52, 129.30, 129.04, 128.80, 128.09, 126.77, 125.89, 50.43, 43.66, 29.14; MS (FAB, NBA matrix): *m/z* = 1010 [(rotaxane+H)$^+$]; anal. calcd for $C_{64}H_{60}N_6O_6$ (1009.20): C 76.17, H 5.99, N 8.33, found C 76.42, H 5.96, N 8.29.

***X*-ray crystallographic structure determinations, crystals of rotaxane grown in DMF/H_2O, 13**: $C_{76}H_{88}N_{10}O_{10}$, M = 1301.56, crystal size 0.24 × 0.06 × 0.06 mm, triclinic, *P*-1, a = 9.8887(5), b = 13.1481(6), c = 15.3131(7) Å, α = 108.0300(10), β = 106.0530(10), γ = 101.9480(10)°, V = 1723.58(14) Å^3, Z = 1, ρ_{calcd} = 1.254 Mg m^{-3}; $Mo_{K\alpha}$ radiation (graphite monochromator, λ = 0.71073 Å), μ = 0.084 mm^{-1}, T = 293(2) K. 8463 data (4770 unique, R_{int} = 0.0628, 1.50 < θ < 23.31°), were collected

on a Siemens SMART CCD diffractometer using narrow frames (0.3° in ω), and were corrected semiempirically for absorption and incident beam decay (transmission 1.00–0.70). The structure was solved by direct methods and refined by full-matrix least-squares on F^2 values of all data (G. M. Sheldrick, SHELXTL manual, Siemens Analytical *X*-ray Instruments, Madison WI, USA, 1994, version 5) to give $wR = \{\Sigma[w(F_o^2-F_c^2)^2]/\Sigma[w(F_o^2)^2]\}^{1/2} = 0.1902$, conventional $R = 0.0866$ for F values of 4770 reflections with $F_o^2 > 2\sigma(F_o^2)$, $S = 1.103$ for 446 parameters. Residual electron density extremes were 0.356 and –0.250 eÅ^{-3}. Amide hydrogen atoms were refined isotropically and subject to a distance constraint N–H = 0.98 Å, with the remainder atoms constrained; anisotropic displacement parameters were used for all non-hydrogen atoms.

([2](1,7,14,20-Tetraaza-2,6,15,19-tetraoxo-3,5,9,12,16,18,22,25 cetrabenzocyclohexacosane)-(*N,N'-bis*(2,2-diphenylethyl)glutaramide)-rotaxne, 14

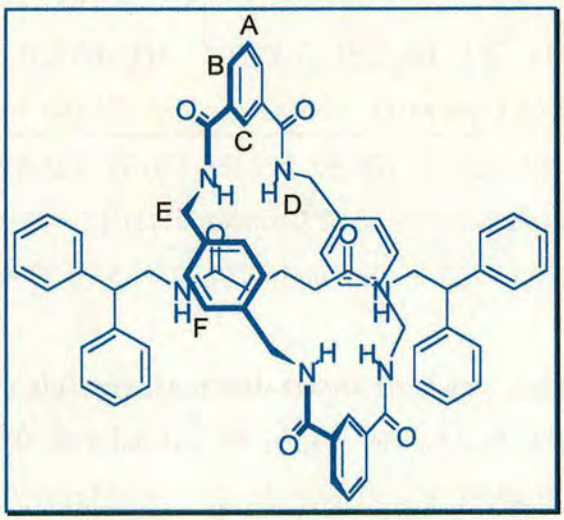

Selected data for ([2](1,7,14,20-Tetraaza-2,6,15,19-tetraoxo-3,5,9,12,16,18,22,25 cetrabenzocyclohexacosane)-(*N,N'-bis*(2,2-diphenylethyl)glutaramide)-rotaxne, 14: Yield 6.3 mg (3%); ^{1}H NMR (400 MHz, $CDCl_3$): δ = 8.17–8.15 (m, 6H, ArH_C &

ArH_B), 7.60 (t, J = 8.2 Hz, 2H, ArH_A), 7.41 (t, J = 5.5 Hz, 4H, $N\underline{H}_D$), 7.30–7.10 (m, 20H, ArH, phenyl), 7.02 (s, 8H, ArH_F), 5.50 (t, J = 5.3 Hz, 2H, CONH), 4.53 (d, J = 5.5 Hz, 8H, CH_{2E}), 3.99 (t, J = 7.9 Hz, 2H, $Ph_2C\underline{H}$), 3.52 (dd, J = 7.9, 5.4 H, $Ph_2CHC\underline{H}_2$), 1.56 (t, J = 7.4 Hz, 4H, $CONHC\underline{H}_2$), 0.65 (m, J = 7.4 Hz, 4H, $CONHC\underline{H}_2CH_2$); ^{13}C NMR (100 MHz, $CDCl_3$): δ = 173.56, 166.94, 141.90, 138.23, 134.79, 131.57, 129.58, 129.28, 129.13, 128.46, 127.45, 125.89, 50.54, 44.50, 44.35, 30.09, 18.73; MS (FAB, NBA matrix): *m/z* = 1024 [(rotaxane+H)$^+$]; anal. calcd for $C_{65}H_{62}N_6O_6$ (1023.20): C 76.30, H 6.11, N 8.21, found C 76.32, H 6.17, N 8.29.

***X*-ray crystallographic structure determinations, crystals of rotaxane grown in EtOH/H_2O, 14**: $C_{67}H_{69}N_6O_8$, M = 1086.28, crystal size 0.20 × 0.18 × 0.15 mm, triclinic, P-1, a = 10.2229(2), b = 17.437, c = 18.3469(3) Å, α = 62.9370(10), β = 89.6630(10), γ = 86.55°, V = 2906.25(7) Å^3, Z = 2, ρ_{calcd} = 1.241 Mg m^{-3}; $Mo_{K\alpha}$ radiation (graphite monochromator, λ = 0.71073 Å), μ = 0.082 mm^{-1}, T = 180(2) K. 18358 data (13260 unique, R_{int} = 0.0290, 2.00 < θ < 29.11°), were collected on a Siemens SMART CCD diffractometer using narrow frames (0.3° in ω), and were corrected semiempirically for absorption and incident beam decay. The structure was solved by direct methods and refined by full-matrix least-squares on F^2 values of all data (G. M. Sheldrick, SHELXTL manual, Siemens Analytical *X*-ray Instruments, Madison WI, USA, 1994, version 5) to give $wR = \{\Sigma[w(F_o^2-F_c^2)^2]/\Sigma[w(F_o^2)^2]\}^{1/2}$ = 0.1877, conventional R = 0.0683 for F values of 13260 reflections with $F_o^2 > 2\sigma(F_o^2)$, S = 1.018 for 750 parameters. Residual electron density extremes were 0.536 and –0.450 eÅ^{-3}. Amide hydrogen atoms were refined isotropically with the remainder constrained; anisotropic displacement parameters were used for all non-hydrogen atoms.

([2](1,7,14,20-Tetraaza-2,6,15,19-tetraoxo-3,5,9,12,16,18,22,25 cetrabenzocyclohexacosane)-(*N,N'-bis*(2,2-diphenylethyl)adipamide)-rotaxane, 15

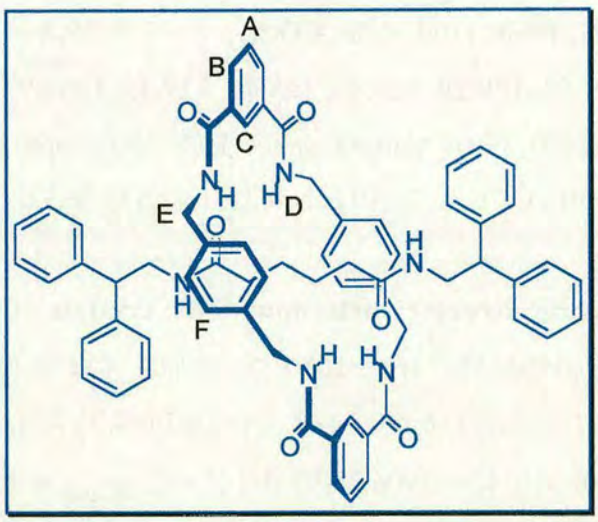

Selected data for ([2](1,7,14,20-Tetraaza-2,6,15,19-tetraoxo-3,5,9,12,16,18,22,25 cetrabenzocyclohexacosane)-(*N,N'-bis*(2,2-diphenylethyl)adipamide)-rotaxane, 15: Yield 164 mg (8%); m.p. 264 °C; ^{1}H NMR (400 MHz, $CDCl_3$): δ = 8.09 (brs, 4H, ArH_B), 8.07 (brs, 2H, ArH_C), 7.53 (t, *J* = 7.8 Hz, 2H, ArH_A), 7.31–7.16 (m, 24H, $N\underline{H}_D$ & ArH, phenyl), 6.98 (s, 8H, ArH_F), 5.76 (brt, 2H, CONH), 4.48 (d, *J* = 5.6 Hz, 8H, CH_{2E}), 4.04 (t, *J* = 7.8 Hz, 2H, $Ph_2C\underline{H}$), 3.57 (dd, *J* = 7.8, 5.6 Hz, 4H, $Ph_2CHC\underline{H}_2$), 0.87 (m, 4H, $CONHC\underline{H}_2$), 0.48 (m, 4H, $CONHCH_2C\underline{H}_2$); ^{13}C NMR (100 MHz, $CDCl_3$): δ = 173.52, 166.51, 141.97, 137.83, 134.11, 131.15, 129.30, 128.80, 128.73, 128.04, 126.95, 124.55, 50.21, 44.18, 43.86, 34.75, 23.83; HRMS (FAB, THIOG matrix): *m/z* = 1037.49656 [(rotaxane+H)$^+$] (anal. calcd for $C_{66}H_{65}N_6O_6$: *m/z* = 1037.49395).

X-ray crystallographic structure determinations:

Crystals of rotaxane grown in $CHCl_3$/MeOH, 15: $C_{68}H_{72}N_6O_6$, M = 1101.32, crystal size 0.10 × 0.06 × 0.05 mm, monoclinic, $C2/c$, a = 30.939(6), b = 11.3129(18), c = 18.568(3) Å, β = 118.147(17)°, V = 5730.5(17) Å^3, Z = 4, ρ_{calcd} = 1.277 Mg m^{-3}; synchrotron radiation (CCLRC Daresbury Laboratory Station 9.8, silicon monochromator, λ = 0.69230 Å), μ = 0.084 mm^{-1}, T = 150(2) K. 18920 data (7604 unique, R_{int} = 0.0348, 2.42 < θ < 29.30°), were collected on a Siemens SMART CCD diffractometer using narrow frames (0.3° in ω), and were corrected semiempirically for absorption and incident beam decay. The structure was solved by direct methods and refined by full-matrix least-squares on F^2 values of all data (G. M. Sheldrick, SHELXTL manual, Siemens Analytical *X*-ray Instruments, Madison WI, USA, 1994, version 5) to give $wR = \{\Sigma[w(F_o^2-F_c^2)^2]/\Sigma[w(F_o^2)^2]\}^{1/2}$ = 0.1361, conventional R = 0.0541 for F values of 7604 reflections with $F_o^2 > 2\sigma(F_o^2)$, S = 1.070 for 384 parameters. Residual electron density extremes were 0.429 and –0.411 eÅ^{-3}. Amide hydrogen atoms were refined isotropically with the remainder constrained; anisotropic displacement parameters were used for all non-hydrogen atoms.

Crystals of rotaxane grown in DMSO/H_2O, 15: $C_{70}H_{80}N_6O_{10}S_2$, M = 1229.52, crystal size 0.15 × 0.12 × 0.10 mm, triclinic P-1, a = 11.6401(3), b = 16.6666(5), c = 18.7274(4) Å, α = 102.8950(10), β = 108.0990(10), γ = 110.3350(10)°, V = 3006.38(14) A^3, Z = 2, ρ_{calcd} = 1.358 Mg m^{-3}; $Mo_{K\alpha}$ radiation (graphite monochromator, λ = 0.71073 Å), μ = 0.157 mm^{-1}, T = 180(2) K. 19537 data (13964 unique, R_{int} = 0.0149, 1.40 < θ < 29.24°), were collected on a Siemens SMART CCD diffractometer using narrow frames (0.3° in ω), and were corrected semiempirically for absorption and incident beam decay. The structure was solved by direct methods and refined by full-matrix least-squares on F^2 values of all data (G. M. Sheldrick, SHELXTL manual, Siemens Analytical *X*-ray Instruments, Madison WI, USA, 1994,

version 5) to give $wR = \{\Sigma[w(F_o^2-F_c^2)^2]/\Sigma[w(F_o^2)^2]\}^{1/2} = 0.2495$, conventional $R = 0.0772$ for F values of 13964 reflections with $F_o^2 > 2\sigma(F_o^2)$, $S = 1.046$ for 817 parameters. Residual electron density extremes were 0.674 and –1.096 eÅ^{-3}. Amide hydrogen atoms were refined isotropically with the remainder constrained; anisotropic displacement parameters were used for all non-hydrogen atoms.

([2](1,7,14,20-Tetraaza-2,6,15,19-tetraoxo-3,5,9,12,16,18,22,25 cetrabenzocyclohexacosane)-(*N,N'-bis*(2,2-diphenylethyl)pimelamide)-rotaxane, 16

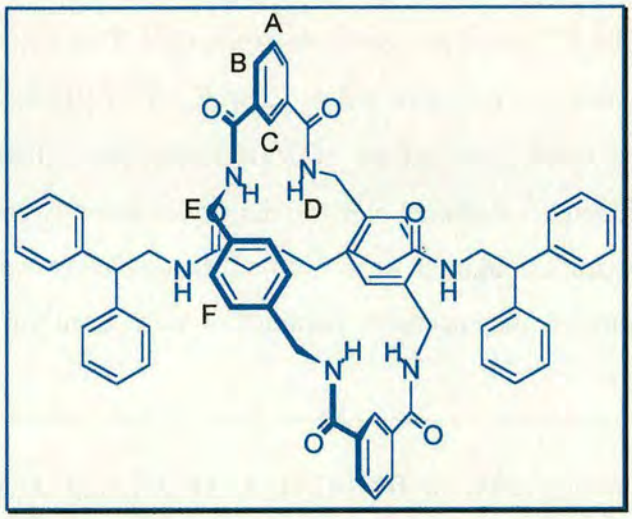

Selected data for ([2](1,7,14,20-Tetraaza-2,6,15,19-tetraoxo-3,5,9,12,16,18,22,25 cetrabenzocyclohexacosane)-(*N,N'-bis*(2,2-diphenylethyl)pimelamide)-rotaxane, 16: Yield 284 mg (14%); m.p. 140 °C; ^{1}H NMR (400 MHz, $CDCl_3$): δ = 8.09 (s, 2H, ArH_C), 8.07 (brm, 4H, ArH_B), 7.54 (brt, 4H, $N\underline{H}_D$), 7.47 (t, J = 8.1 Hz, 2H, ArH_A), 7.33–7.21 (m, 20H, ArH, phenyl), 7.03 (s, 8H, $ArCH_F$), 5.95 (brt, 2H, CONH), 4.49 (d, J = 5.6 Hz, 8H, CH_{2E}), 4.06 (t, J = 7.6 Hz, 2H, $Ph_2C\underline{H}$), 3.65 (dd, J = 7.6, 5.6 Hz, 4H, $Ph_2CHC\underline{H}_2$), 0.86 (m, 4H, $CONHC\underline{H}_2$), 0.47 (m, 4H, $CONHCH_2C\underline{H}_2$), 0.26 (m, 2H, $CONH(CH_2)_2C\underline{H}_2$); ^{13}C NMR (100 MHz, $CDCl_3$): δ = 173.83, 166.51, 157.59,

142.00, 137.62, 133.95, 131.28, 128.99, 128.79, 128.07, 126.95, 124.65, 50.24, 44.23, 43.94, 34.85, 27.62, 23.28; HRMS (FAB, THIOG matrix): *m/z* = 1051.51221 [(rotaxane+H)$^+$] (anal. calcd for $C_{67}H_{67}N_6O_6$: *m/z* = 1051.51236).

Crystals of rotaxane grown in $CHCl_3$/MeOH, 16: $C_{69}H_{69}N_6O_6Cl_5$, M = 1255.55, crystal size 0.08 × 0.03 × 0.03 mm, monoclinic, $C2/c$, a = 18.6031(9), b = 23.8302(12), c = 29.7448(14) Å, β = 103.876(10)°, Z = 8, ρ_{calcd} = 1.227 Mg m^{-3}; synchrotron radiation (CCLRC Daresbury Laboratory Station 9.8, silicon monochromator, λ = 0.69230 Å), μ = 0.24 mm^{-1}, T = 150(2) K. 32135 data (26166 unique, R_{int} = 0.0840, 2.97 < θ < 25.63°), were collected on a Siemens SMART CCD diffractometer using narrow frames (0.3° in ω), and were corrected semiempirically for absorption and incident beam decay (transmission 1.00–0.65). The structure was solved by direct methods and refined by full-matrix least-squares on F^2 values of all data (G. M. Sheldrick, SHELXTL manual, Siemens Analytical *X*-ray Instruments, Madison WI, USA, 1994, version 5) to give $wR = \{\Sigma[w(F_o^2-F_c^2)^2]/\Sigma[w(F_o^2)^2]\}^{1/2}$ = 0.4326, conventional R = 0.2057 for F values of 26166 reflections with $F_o^2 > 2\sigma(F_o^2)$, S = 2.443 for 717 parameters. Residual electron density extremes were 2.40 and –1.30 eÅ^{-3}. Amide hydrogen atoms were refined isotropically with the remainder constrained; anisotropic displacement parameters were used for all non-hydrogen atoms.

([2](1,7,14,20-Tetraaza-2,6,15,19-tetraoxo-3,5,9,12,16,18,22,25 cetrabenzocyclohexacosane)-(*N,N'-bis*(2,2-diphenylethyl)suberamide)-rotaxane, 17

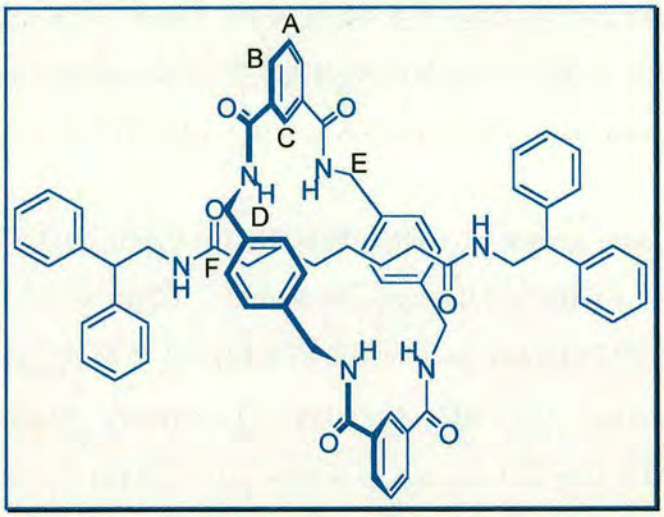

Selected data for ([2](1,7,14,20-Tetraaza-2,6,15,19-tetraoxo-3,5,9,12,16,18,22,25 cetrabenzocyclohexacosane)-(*N,N'-bis*(2,2-diphenylethyl)suberamide)-rotaxane, 17: Yield 331 mg (17%); m.p. 242 °C; ^{1}H NMR (400 MHz, $CDCl_3$): δ = 8.13 (s, 2H, ArH_C), 8.11 (m, 4H, ArH_B), 7.55 (brt, 4H, $N\underline{H}_D$), 7.52 (t, J = 8.1 Hz, 2H, $ArCH_A$), 7.32–7.21 (m, 20H, ArH, phenyl), 7.04 (s, 8H, ArH_F), 5.97 (brt, 2H, CONH), 4.50 (d, J = 5.6 Hz, 8H, CH_{2E}), 4.10 (t, J = 7.8 Hz, 2H, $Ph_2C\underline{H}$), 3.67 (m, 4H, $Ph_2CHC\underline{H}_2$), 1.02 (t, J = 7.6 Hz, 4H, $CONHC\underline{H}_2$), 0.65 (m, 4H, $CONHCH_2C\underline{H}_2$), 0.36 (m, 4H, $CONH(CH_2)_2C\underline{H}_2$); ^{13}C NMR (100 MHz, $CDCl_3$): δ = 174.17, 166.51, 158.36, 142.04, 137.59, 133.90, 131.36, 129.09, 128.77, 128.09, 126.92, 124.74, 50.17, 44.32, 44.02, 35.39, 27.61, 24.03; HRMS (FAB, THIOG matrix): *m/z* = 1065.52786 [(rotaxane+H)$^+$] (anal. calcd for $C_{68}H_{69}N_6O_6$: *m/z* = 1065.52656).

***X*-ray crystallographic structure determination, crystals of rotaxane grown in $CDCl_3$/ether, 17**: $C_{68}H_{68}N_6O_6$, M = 1065.28, crystal size 0.15 × 0.12 × 0.10 mm, monoclinic, $P2_1/c$, a = 10.10930(10), b = 24.2595(4), c = 22.8433(2) Å, β = 90.0710(10)°, V = 5602.24(12) Å^3, Z = 4, ρ_{calcd} = 1.263 Mg m^{-3}; $Mo_{K\alpha}$ radiation (graphite monochromator, λ = 0.71073 Å), μ = 0.081 mm^{-1}, T = 150(2) K. 55201 data (15270 unique, R_{int} = 0.0366, 1.78 < θ < 30.18°), were collected on a Siemens

SMART CCD diffractometer using narrow frames (0.3° in ω), and were corrected semiempirically for absorption and incident beam decay. The structure was solved by direct methods and refined by full-matrix least-squares on F^2 values of all data (G. M. Sheldrick, SHELXTL manual, Siemens Analytical *X*-ray Instruments, Madison WI, USA, 1994, version 5) to give $wR = \{\Sigma[w(F_o^2-F_c^2)^2]/\Sigma[w(F_o^2)^2]\}^{1/2} = 0.1866$, conventional $R = 0.0699$ for F values of 15270 reflections with $F_o^2 > 2\sigma(F_o^2)$, $S = 1.078$ for 763 parameters. Residual electron density extremes were 0.403 and –0.508 eÅ^{-3}. Amide hydrogen atoms were refined isotropically with the remainder constrained; anisotropic displacement parameters were used for all non-hydrogen atoms.

([2](1,7,14,20-Tetraaza-2,6,15,19-tetraoxo-3,5,9,12,16,18,22,25 cetrabenzocyclohexacosane)-(*N,N'-bis*(2,2-diphenylethyl)azelamide)-rotaxane, 18

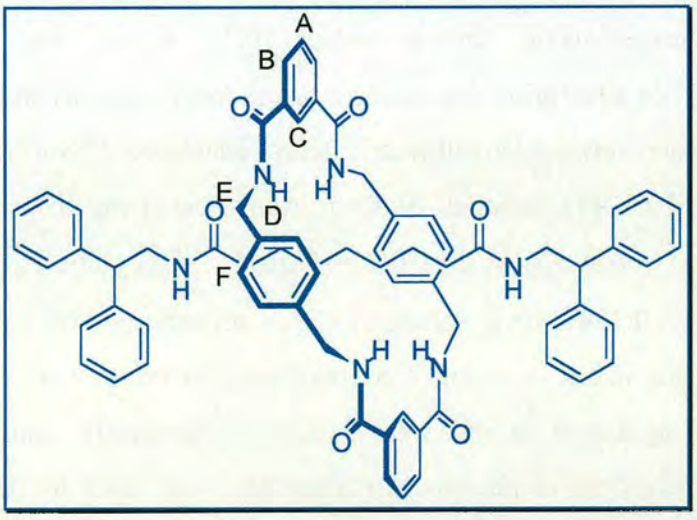

Selected data for ([2](1,7,14,20-Tetraaza-2,6,15,19-tetraoxo-3,5,9,12,16,18,22,25 cetrabenzocyclohexacosane)-(*N,N'-bis*(2,2-diphenylethyl)azelamide)-rotaxane, 18: Yield 296 mg (15%); m.p. 204 °C; ^{1}H NMR (400 MHz, $CDCl_3$): $\delta = 8.13$ (d, $J =$ 7.8 Hz, 4H, ArH_B), 8.10 (s, 2H, ArH_C), 7.52 (brm, 6H, $N\underline{H}_D$ & ArH_A), 7.33–7.21 (m,

20H, ArH, phenyl), 7.03 (s, 8H, ArH_F), 6.06 (brt, 2H, CONH), 4.49 (d, J = 5.3 Hz, 8H, CH_E), 4.10 (t, J = 7.8 Hz, 2H, $Ph_2C\underline{H}$), 3.65 (dd, J = 7.8, 5.6 Hz, 4H, $Ph_2CHC\underline{H_2}$), 1.12 (t, J = 8.1 Hz, 4H, $CONHC\underline{H_2}$), 0.78 (quintet, J = 8.1 Hz, 4H, $CONHCH_2C\underline{H_2}$), 0.53 (m, 4H, $CONH(CH_2)_2C\underline{H_2}$), 0.34 (m, 2H, $CONH(CH_2)_3C\underline{H_2}$); ^{13}C NMR (100 MHz, $CDCl_3$): δ = 174.20, 166.35, 142.07, 137.63, 133.83, 131.28, 129.06, 128.75, 128.67, 128.10, 126.90, 124.77, 50.12, 44.35, 44.06, 35.19, 27.53, 26.74, 23.93; MS (FAB, THIOG matrix): m/z = 1079.54351 [(rotaxane+H)$^+$] (anal. calcd for $C_{69}H_{71}N_6O_6$: m/z = 1079.54387).

***X*-ray crystallographic structure determination, crystals of rotaxane grown in $CHCl_3$/ether, 18:** $C_{69}H_{70}N_6O_6$, M = 1079.31, crystal size 0.20 × 0.18 × 0.15 mm, monoclinic, $P2_1/c$, a = 10.2440(2), b = 24.234, c = 23.2044(5) Å, β = 92.4800(10)°, V = 5755.19(17) A^3, Z = 4, ρ_{calcd} = 1.246 Mg m^{-3}; $Mo_{K\alpha}$ radiation (graphite monochromator, λ = 0.71073 Å), μ = 0.080 mm^{-1}, T = 180(2) K. 34761 data (13923 unique, R_{int} = 0.01673, 1.76 < θ < 29.09°), were collected on a Siemens SMART CCD diffractometer using narrow frames (0.3° in ω), and were corrected semiempirically for absorption and incident beam decay. The structure was solved by direct methods and refined by full-matrix least-squares on F^2 values of all data (G. M. Sheldrick, SHELXTL manual, Siemens Analytical *X*-ray Instruments, Madison WI, USA, 1994, version 5) to give $wR = \{\Sigma[w(F_o^2-F_c^2)^2]/\Sigma[w(F_o^2)^2]\}^{1/2}$ = 0.2355, conventional R = 0.1247 for F values of 13923 reflections with $F_o^2 > 2\sigma(F_o^2)$, S = 1.012 for 754 parameters. Residual electron density extremes were 0.425 and –0.309 $eÅ^{-3}$. Amide hydrogen atoms were refined isotropically with the remainder constrained; anisotropic displacement parameters were used for all non-hydrogen atoms.

([2](1,7,14,20-Tetraaza-2,6,15,19-tetraoxo-3,5,9,12,16,18,22,25 cetrabenzocyclohexacosane)-(*N,N'-bis*(2,2-diphenylethyl)subacamide)-rotaxane, 19

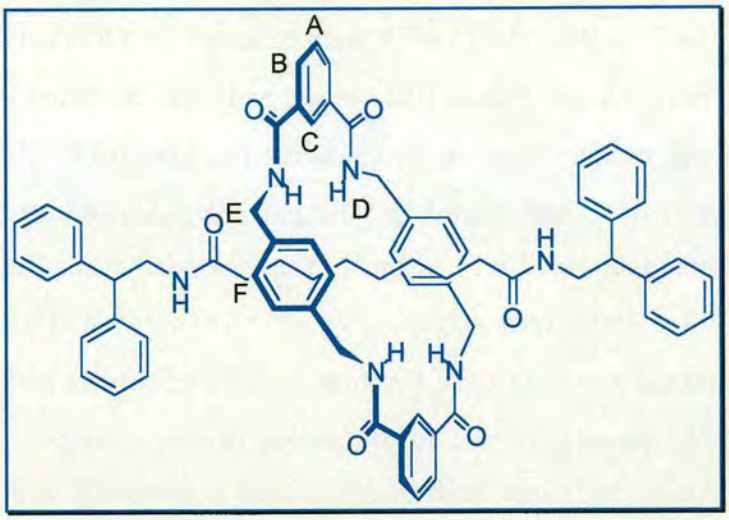

Selected data for ([2](1,7,14,20-Tetraaza-2,6,15,19-tetraoxo-3,5,9,12,16,18,22,25 cetrabenzocyclohexacosane)-(*N,N'-bis*(2,2-diphenylethyl)subacamide)-rotaxane, 19: Yield 351 mg (18%); m.p. 249 °C; ^{1}H NMR (400 MHz, $C_2D_2Cl_4$): δ = 8.14 (brs, 2H, Ar$\underline{H}_C$), 8.12 (brs, 4H, Ar$\underline{H}_B$), 7.59 (br, 4H, N$\underline{H}_D$), 7.55 (brt, *J* = 7.8 Hz, 4H, Ar$\underline{H}_B$), 7.33–7.22 (m, 20H, ArH, phenyl), 7.04 (s, 8H, Ar$\underline{H}_F$), 6.21 (brt, 2H, CONH), 4.48 (d, *J* = 5.3 Hz, 8H, C$\underline{H}_E$), 4.10 (t, *J* = 7.8 Hz, 2H, $Ph_2C\underline{H}$), 3.66 (m, 4H, $Ph_2CHC\underline{H}_2$), 1.21 (m, 4H, CONHC$\underline{H}_2$), 0.85 (m, 4H, CONHCH$_2$C$\underline{H}_2$), 0.63 (m, 4H. CONH(CH$_2$)$_2$C$\underline{H}_2$), 0.51 (m, 4H, CONH(CH$_2$)$_3$C$\underline{H}_2$); ^{13}C NMR (100 MHz, $CDCl_3$): δ = 174.19, 166.35, 142.11, 137.64, 133.86, 131.27, 129.06, 128.75, 128.67, 128.27, 128.12, 126.90, 124.78, 50.13, 44.37, 44.08, 35.21, 27.58, 26.79, 23.97; HRMS (FAB, THIOG matrix): *m/z* = 1093.55916 [(rotaxane+H)$^+$] (anal. calcd for $C_{67}H_{67}N_6O_6$: *m/z* = 1093.55790).

***X*-ray crystallographic structure determination, crystals of rotaxane grown in $C_2H_2Cl_4$/ether:** $C_{70}H_{72}N_6O_6$, *M* = 1093.34, crystal size 0.08 × 0.07 × 0.05 mm,

triclinic, *P*-1, a = 8.1440(8), b = 10.5732(10), c = 17.8480(17) Å, α = 105.545(2), β = 98.001(2), γ = 99.427(2)°, V = 1433.3(2) Å^3, Z = 1, ρ_{calcd} = 1.267 Mg m^{-3}; synchrotron radiation (CCLRC Daresbury Laboratory Station 9.8, silicon monochromator, λ = 0.68950 Å), μ = 0.081 mm^{-1}, T = 150(2) K. 11416 data (5454 unique, R_{int} = 0.0471, 1.98 < θ < 25.00°), were collected on a Siemens SMART CCD diffractometer using narrow frames (0.3° in ω), and were corrected semiempirically for absorption and incident beam decay (transmission 1.00–0.77). The structure was solved by direct methods and refined by full-matrix least-squares on F^2 values of all data (G. M. Sheldrick, SHELXTL manual, Siemens Analytical *X*-ray Instruments, Madison WI, USA, 1994, version 5) to give $wR = \{\Sigma[w(F_o^2-F_c^2)^2]/\Sigma[w(F_o^2)^2]\}^{1/2}$ = 0.2176, conventional R = 0.1001 for F values of 5454 reflections with $F_o^2 > 2\sigma(F_o^2)$, S = 1.200 for 382 parameters. Residual electron density extremes were 0.740 and –0.387 eÅ^{-3}. Amide hydrogen atoms were refined isotropically with the remainder constrained; anisotropic displacement parameters were used for all non-hydrogen atoms.

([2](1,7,14,20-Tetraaza-2,6,15,19-tetraoxo-3,5,9,12,16,18,22,25 cetrabenzocyclohexacosane)-(*N,N'-bis*(2,2-diphenylethyl)decanamide)-rotaxane, 20

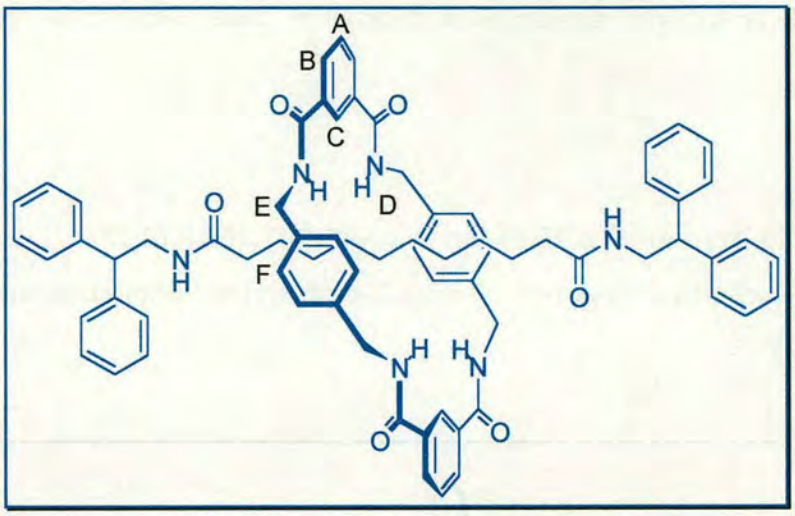

Selected data for ([2](1,7,14,20-Tetraaza-2,6,15,19-tetraoxo-3,5,9,12,16,18,22,25 cetrabenzocyclohexacosane)-(*N,N'-bis*(2,2-diphenylethyl)decanamide)-rotaxane, 20: Yield 229 mg (12%). Compound could only be characterized by *X*-ray crystallography: ***X*-ray crystallographic structure determination, crystals of rotaxane grown in $CHCl_3$/ether, 20**: $C_{72}H_{76}N_6O_6$, M = 1121.39, crystal size 0.12 × 0.05 × 0.05 mm, triclinic, *P*-1, a = 8.5024(9), b = 10.4249(11), c = 17.5264(19) Å, α = 99.719(2), β = 100.927(2), γ = 99.733(2)°, V = 1470.6(3) Å^3, Z = 1, ρ_{calcd} = 1.266 Mg m^{-3}; synchrotron radiation (CCLRC Daresbury Laboratory Station 9.8, silicon monochromator, λ = 0.68830 Å), μ = 0.081 mm^{-1}, T = 150(2) K. 14617 data (7777 unique, R_{int} = 0.0310, 2.07 < θ < 29.21°), were collected on a Siemens SMART CCD diffractometer using narrow frames (0.3° in ω), and were corrected semiempirically for absorption and incident beam decay (transmission 1.00–0.77). The structure was solved by direct methods and refined by full-matrix least-squares on F^2 values of all data (G. M. Sheldrick, SHELXTL manual, Siemens Analytical *X*-ray Instruments, Madison WI, USA, 1994, version 5) to give $wR = \{\Sigma[w(F_o^2-F_c^2)^2]/\Sigma[w(F_o^2)^2]\}^{1/2}$ = 0.1435, conventional R = 0.0565 for F values of 7777 reflections with $F_o^2 > 2\sigma(F_o^2)$, S = 0.957 for 391 parameters. Residual electron density extremes were 0.600 and –0.296 eÅ^{-3}. Amide hydrogen atoms were refined isotropically with the remainder

constrained; anisotropic displacement parameters were used for all non-hydrogen atoms.

([2](1,7,14,20-Tetraaza-2,6,15,19-tetraoxo-3,5,9,12,16,18,22,25 cetrabenzocyclohexacosane)-(*N,N'-bis*(2,2-diphenylethyl)dodecanamide)-rotaxane, 21

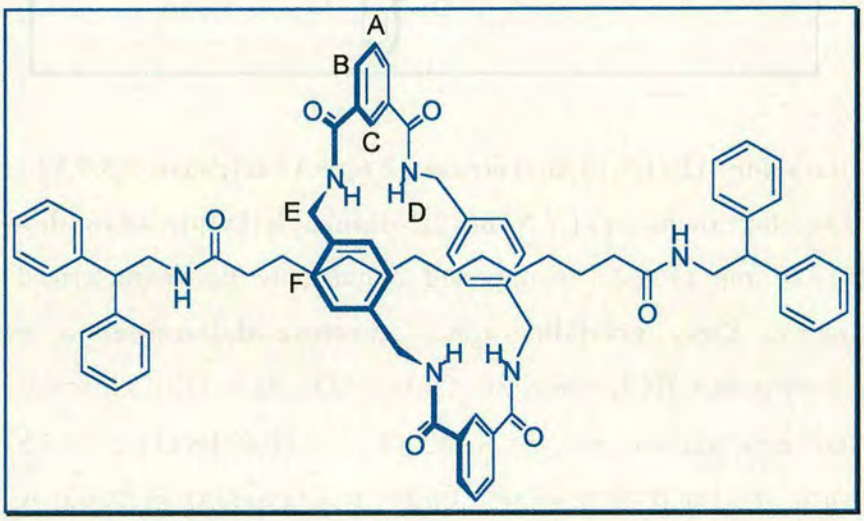

Selected data for ([2](1,7,14,20-Tetraaza-2,6,15,19-tetraoxo-3,5,9,12,16,18,22,25 cetrabenzocyclohexacosane)-(*N,N'-bis*(2,2-diphenylethyl)dodecanamide) rotaxane, 21: Yield 186 mg (10%); m.p. 201 °C; ^{1}H NMR (400 MHz, $CDCl_3$): δ = 8.18 (s, 2H, ArH_C), 8.16 (m, 4H, ArH_B), 7.57 (t, *J* = 8.1 Hz, 2H, ArH_A), 7.31–7.19 (m, 24H, ArH, phenyl & NH_D), 7.01 (s, 8H, ArH_F), 6.11 (brt, 2H, CONH), 4.49 (d, *J* = 5.1 Hz, 8H, CH_{2E}), 4.11 (t, *J* = 7.8 Hz, 2H, Ph_2CH), 3.63 (dd, *J* = 7.8, 5.6 Hz, 4H, Ph_2CHCH_2), 1.29 (t, *J* = 7.6 Hz, 4H, $CONHCH_2$), 1.03 (m, 4H, $CONHCH_2CH_2$), 0.95 (brs, 8H, $CONH(CH_2)_4CH_2$ & $CONH(CH_2)_5CH_2$), 0.81 (m, 8H, $CONH(CH_2)_2CH_2$ & $CONH(CH_2)_3CH_2$); ^{13}C NMR (100 MHz, $CDCl_3$): δ = 174.11, 166.15, 142.15, 137.53, 133.76, 131.03, 129.24, 128.71, 128.61, 128.10, 126.84, 124.86, 50.04, 44.36, 44.17, 35.64, 28.64, 28.59, 28.39, 24.66; HRMS (FAB, NBA

matrix): *m/z* = 1149.62103 [(rotaxane+H)$^+$] (anal. calcd for $C_{74}H_{81}N_6O_6$: *m/z* = 1149.62176).

***X*-ray crystallographic structure determination, crystals of rotaxane grown in $CHCl_3$/ether, 21**: $C_{74}H_{80}N_6O_6$, M = 1149.44, crystal size 0.10 × 0.05 × 0.05 mm, monoclinic, $P2_1/c$, a = 11.4490(18), b = 8.8620(14), c = 31.166(5) Å, β = 94.141(4)°, V = 3153.9(9) Å^3, Z = 2, ρ_{calcd} = 1.210 Mg m^{-3}; synchrotron radiation (CCLRC Daresbury Laboratory Station 9.8, silicon monochromator, λ = 0.68950 Å), μ = 0.077 mm^{-1}, T = 150(2) K. 10273 data (3210 unique, R_{int} = 0.0846, 2.07 < θ< 20.00°), were collected on a Siemens SMART CCD diffractometer using narrow frames (0.3° in ω), and were corrected semi-empirically for absorption and incident beam decay. The structure was solved by direct methods and refined by full-matrix least-squares on F^2 values of all data (G. M. Sheldrick, SHELXTL manual, Siemens Analytical *X*-ray Instruments, Madison WI, USA, 1994, version 5) to give wR = $\{\Sigma[w(F_o^2-F_c^2)^2]/\Sigma[w(F_o^2)^2]\}^{1/2}$ = 0.2654, conventional R = 0.1046 for F values of 3210 reflections with $F_o^2 > 2\sigma(F_o^2)$, S = 1.142 for 393 parameters. Residual electron density extremes were 0.563 and –0.765 eÅ^{-3}. Amide hydrogen atoms were refined isotropically with the remainder constrained; anisotropic displacement parameters were used for all non-hydrogen atoms.

([2](1,7,14,20-Tetraaza-2,6,15,19-tetraoxo-3,5,9,12,16,18,22,25 cetrabenzocyclohexacosane)-(*N,N'-bis*(2,2-diphenylethyl)tetradecanamide)-rotaxane, 22

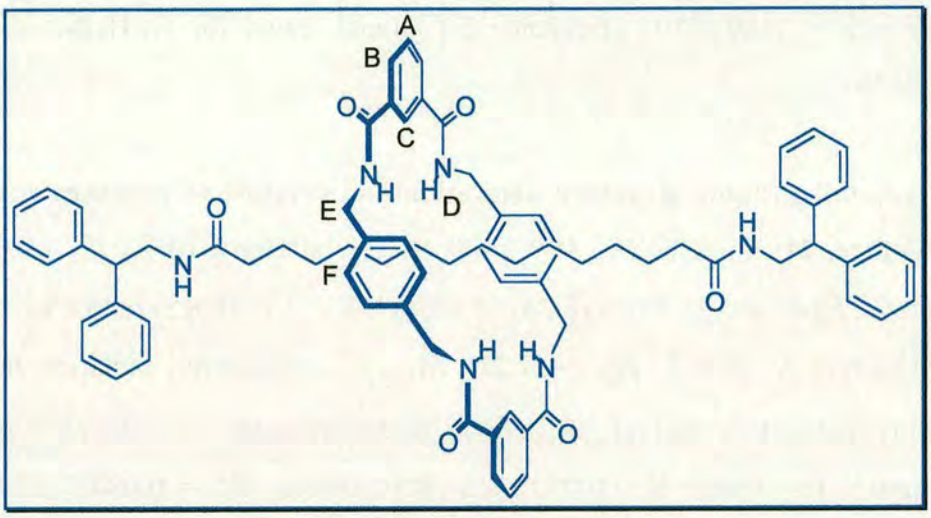

Selected data for ([2](1,7,14,20-Tetraaza-2,6,15,19-tetraoxo-3,5,9,12,16,18,22,25 cetrabenzocyclohexacosane)-(N,N'-bis(2,2-diphenylethyl)tetradecanamide) rotaxane, 22: Yield 183 mg (10%); m.p. 163 °C; ^{1}H NMR (400 MHz, $CDCl_3$): δ = 8.17 (s, 2H, ArH_C), 8.15 (m, 4H, ArH_B), 7.57 (t, J = 7.8 Hz, 2H, ArH_A), 7.30–7.18 (m, 24H, ArH, phenyl & $N\underline{H}_D$), 7.01 (s, 8H, ArH_F), 6.05 (brt, 2H, CONH), 4.49 (d, J = 5.1 Hz, 8H, CH_E), 4.09 (t, J = 7.8 Hz, 2H, $Ph_2C\underline{H}$), 3.61 (dd, J = 7.8, 5.6 Hz, 4H, $Ph_2CHC\underline{H}_2$), 1.29 (m, 4H, $CONHC\underline{H}_2$), 1.12 (m, 4H, $CONH(CH_2)_2C\underline{H}_2$), 1.02 (m, 12H, $CONHCH_2C\underline{H}_2$ & $CONH(CH_2)_5C\underline{H}_2$ & $CONH(CH_2)_6C\underline{H}_2$), 0.87 (m, 4H, $CONH(CH_2)_4C\underline{H}_2$), 0.77 (m, 4H, $CONH(CH_2)_3C\underline{H}_2$); ^{13}C NMR (100 MHz, $CDCl_3$): δ = 174.01, 166.13, 142.18, 137.51, 133.80, 131.01, 129.23, 128.68, 128.62, 128.10, 126.80, 124.82, 50.05, 44.36, 44.19, 35.74, 29.21, 29.10, 29.04, 28.84, 24.79; MS (FAB, NBA matrix): m/z = 1177.65315 [(rotaxane+H)$^+$] (anal. calcd for $C_{76}H_{85}N_6O_6$: m/z = 1177.65306).

***X*-ray crystallographic structure determination, crystals of rotaxane grown in $CHCl_3$/ether, 22**: $C_{78}H_{86}Cl_3N_6O_6$, M = 1309.88, crystal size 0.12 × 0.08 × 0.05 mm, monoclinic, $P2_1/c$, a = 20.5947(5), b = 9.2683(2), c = 19.1134(4) Å, β = 92.3500(10)°, V = 3645.26(14) A^3, Z = 2, ρ_{calcd} = 1.193 Mg m^{-3}; $Mo_{K\alpha}$ radiation (graphite monochromator, λ = 0.71073 Å), μ = 0.181 mm^{-1}, T = 180(2) K. 22137

data (8833 unique, R_{int} = 0.0607, 1.98 < θ < 29.16°), were collected on a Siemens SMART CCD diffractometer using narrow frames (0.3° in ω), and were corrected semiempirically for absorption and incident beam decay. The structure was solved by direct methods and refined by full-matrix least-squares on F^2 values of all data (G. M. Sheldrick, SHELXTL manual, Siemens Analytical *X*-ray Instruments, Madison WI, USA, 1994, version 5) to give $wR = \{\Sigma[w(F_o^2-F_c^2)^2]/\Sigma[w(F_o^2)^2]\}^{1/2} = 0.2063$, conventional $R = 0.0739$ for F values of 8833 reflections with $F_o^2 > 2\sigma(F_o^2)$, S = 1.025 for 445 parameters. Residual electron density extremes were 0.534 and –0.549 eÅ^{-3}. Amide hydrogen atoms were refined isotropically with the remainder constrained; anisotropic displacement parameters were used for all non-hydrogen atoms.

3.6 References

1. Harrison, I. T.; Harrison, D. J. *J. Am. Chem. Soc.* **1967**, *89*, 5723–5725.
2. Schill, G.; Zollenkopf, H. *Liebig. Ann. Chem.* **1979**, *721*, 53–74.
3. (a) Leigh, D. A.; Murphy, A. *Chem. Ind*, **1999**, 178–183. (b) Sauvage, J. -P.; Dietrich-Buchecker, C.; Eds. *Molecular Catenanes, Rotaxanes and Knots*; VCD-Wiley, Weinheim, **1999**.
4. (a) Johnston, A. G.; Leigh, D. A.; Murphy, A.; Smart, J. P.; Deegan, M. D. *J. Am. Chem. Soc.* **1996**, *118*, 10662–10663. (b) Leigh, D. A.; Murphy, A.; Smart, J. P.; Slawin, A. M. Z. *Angew. Chem. Int. Ed. Engl.* **1997**, *36*, 728–732. (c) Lane, A. S.; Leigh, D. A.; Murphy, A. *J. Am. Chem. Soc.* **1997**, *119*, 11092–11093. (d) Clegg, W.; Gimenez-Saiz, C.; Leigh, D. A.; Murphy, A.; Slawin, A. M. Z.; Teat, S. J. *J. Am. Chem. Soc.* **1999**, *121*, 4124–4129. (e) Leigh, D. A.; Troisi, A.; Zerbetto, F. *Angew. Chem. Int. Ed.* **2000**, *39*, 350–353. (f) Brouwer, A. M.; Frochot, C.; Gatti, F. G.; Leigh, D. A.; Mottier, L.; Paolucci, F.; Roffia, S.; Wurpel, G. W. H. *Science* **2001**, *291*, 2124–2128. (g) Gatti, F. G.; Leigh, D. A.; Nepogodiev, S. A.; Slawin, A. M. Z.; Teat, S. J.; Wong, J. K. Y. *J. Am. Chem. Soc.* **2001**, *123*, 5983–5989.
5. (a) Gellman, S. H.; Gregory, P. D.; Liang, G. -B.; Adams, B. R. *J. Am. Chem. Soc.* **1991**, *113*, 1164–1173. (b) Liang, G. B.; Desper, J. M.; Gellman, S. H. *J. Am. Chem. Soc.* **1993**, *115*, 925–938.
6. Jäger, R.; Baumann, S.; Fischer, M.; Safarowsky, O.; Nieger, M.; Vögtle, F. *Liebigs Ann./Recueil* **1997**, 2269–2273.
7. Leigh, D. A.; Moody, K.; Smart, J. P.; Watson, K. J.; Slawin, A. M. Z. *Angew. Chem. Int. Ed. Engl.* **1996**, *35*, 306–310.

CHAPTER FOUR

From Synthesis to Control of Motion...

Accepted for publication in Proceedings of the National Acadamy of Science, USA

as:

"Photoisomerization of a Rotaxane Hydrogen Bonding Template: Light-induced Acceleration of a Large Amplitude Rotational Motion

Francesco G Gatti, Salvador León, Jenny K Y Wong, Giovanni Bottari, Andrea Altieri, Angeles M Farran, Simon J Teat, Céline Frochot, David A Leigh, Albert M Brouwer, Francesco Zerbetto

Acknowledgements

The following people are gratefully acknowledged for their contributions to this paper: the first versions of the photochemical experiments were carried out by Dr. Céline Frochot and Dr. Fred Brouwer (University of Amsterdam); Giovanni Bottari and Andrea Altieri came up with the idea for reversing the isomerisation thermally and the molecular modelling simulations were carried out by Dr. Salvador León and Prof. Francesco Zerbetto (University of Bologna).

"*Before the beginning of great brilliance and beauty there first must be a period of complete chaos.*"

I-Ching

From Synthesis to Control of Motion... – Synopsis

Having investigated the directing power of hydrogen bonding in synthesis, we turned our attention to attempting to use it to control large amplitude molecular motion. In this chapter, the investigation of E- *to* Z- *photoisomerisation of fumaramide-based [2]rotaxanes leads to the discovery that the rate of pirouetting of the macrocycle around the thread can be photochemically-induced to accelerate by more than six orders of magnitude.*

A series of E- *and* Z-*fumaramide-based [2]rotaxanes were synthesised,* E-***I–III*** *and* Z-***I–III*** *(Scheme I). The double bond of the fumaramide thread not only makes it an effective template for the formation of the benzylic amide macrocycle (Chapter Two) but also opens up the possibility of* E- *to* Z- *photoinduced isomerisation after rotaxane formation; where the corresponding change in geometry, changes the nature and strength of the intracomponent hydrogen bonds between the macrocycle and thread. The back reaction was possible by heating to give the more thermodynamically stable* E-*isomer.*

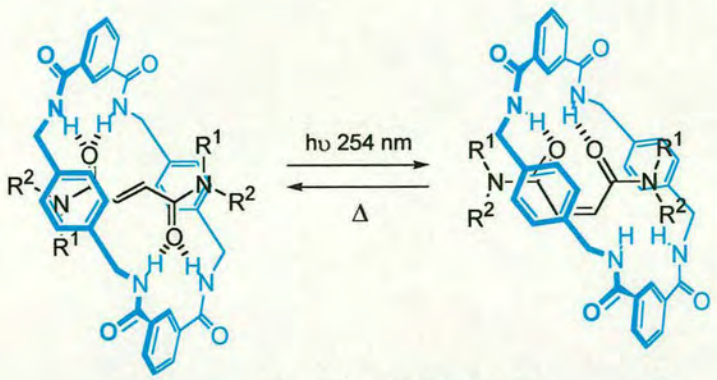

E-**I**	$R^1 = R^2 = CH_2CO_2CH_2Ph$	*Z*-**I**
E-**II**	R^1 = Me, $R^2 = CH_2CHPh_2$	*Z*-**II**
E-**III**	R^1 = H, $R^2 = CH_2CHPh_2$	*Z*-**III**

Scheme I *Synthesis of E-**I–III** by clipping strategy followed by photoisomerisation at 254 nm to give the corresponding Z-**I–III**.*

Variable temperature (VT) NMR experiments determined the energy barrier to macrocycle pirouetting for the fumaramide rotaxane, E-***1*** $\Delta G^{\ddagger} = 13.4 \pm 0.1$ *kcal* mol^{-1} *corresponding to a macrocycle spinning rate of ~1* s^{-1} *at 223 K compared to the maleamide rotaxane,* Z-***1,*** $\Delta G^{\ddagger} = 6.8 \pm 0.8$ *kcal* mol^{-1} *giving a spin rate of ~1.2 x* 10^{-6} s^{-1} *at 223 K. Computational simulations using MM3 forcefield and the TINKER program were in good agreement to the experimental values, giving energy barriers to rotation of 13.51 kcal* mol^{-1} *and 6.53 kcal* mol^{-1} *for fumaramide and maleamide [2]rotaxanes respectively.*

4.1 Introduction

Large amplitude internal rotations which resemble to some extent processes found in authentic machinery have recently inspired analogic molecular versions of gears[1], turnstiles[2], brakes[3], ratchets[4,5], rotors[6] and unidirectional spinning motors[7-10], and are an inherent characteristic of many catenanes and rotaxanes[11-13]. Establishing methods for controlling aspects of such movements is a prerequisite for the development of artificial devices that function through rotary motion at the molecular level.[‖] In this regard, we recently reported the unexpected discovery that the rate of rotation of the interlocked components of benzylic amide macrocycle-containing nitrone and fumaramide [2]rotaxanes can be slowed ("dampened") by 2–3 orders of magnitude by applying a modest (~1 Vcm^{-1}) external oscillating electric field[14]. Here we demonstrate that the rate of rotation of the interlocked components of the olefin-based rotaxanes can also be accelerated – by more than *six* orders of magnitude – using another broadly useful stimulus, light.

4.2 Results and discussion

Fumaramide threads template the assembly of benzylic amide macrocycles around them to form rotaxanes in high yields[15]. This cheap and simple preparative procedure (suitable threads are prepared in a single step from fumaryl chloride and a bulky primary or secondary amine) is particularly efficient because the *trans*-olefin fixes the two hydrogen bond-accepting groups of the thread in an arrangement which is complementary to the geometry of the hydrogen bond-donating sites of the forming macrocycle. However, the feature of the fumaramide unit that makes it such an

[‖] For wonderful examples of the use of submolecular rotational motion to bring about macroscopic property changes in materials see (22) and (23). Examples of controlling the frequency of large amplitude internal rotary motions include the redox-mediated acceleration/deceleration of the spinning of porphyrin ligands in cerium and zirconium sandwich complexes(24), the environment-dependent rate of circumrotation in hydrogen bonded [2]catenanes(25), and the electrochemically-induced pirouetting of a macrocycle in a rotaxane(26).

effective template also provides an opportunity to enforce a geometrical change in the thread *after* rotaxane formation, thus altering the nature and strength of the interactions between the interlocked components. Isomerization of the olefin from *E*- to *Z*- must necessarily disrupt the near-ideal hydrogen bonding motif between macrocycle and thread and therefore also change any internal dynamics governed by those interactions.

To test this idea, the photochemical isomerization of three fumaramide-based threads (*E*-**1**–**3**) and rotaxanes (*E*-**4**–**6**) was investigated. The synthesis of rotaxanes *E*-**4** and *E*-**6** has previously been described[15] and *E*-**5** was prepared in analogous fashion from the corresponding thread, *E*-**2**, isophthaloyl dichloride and *p*-xylylene diamine (Scheme 4.1).** Under the same reaction conditions the *cis*-olefin (maleamide) threads, *Z*-**1**–**3**, did not give detectable quantities of the corresponding *Z*-rotaxanes.

Single crystals suitable for investigation by *X*-ray crystallography were obtained for each of the three *E*-rotaxanes. In each case the solid-state structure shows two sets of bifurcated hydrogen bonds between the amide groups of the macrocycle and the carbonyl groups of the fumaramide system[15]. The crystal structure of *E*-**5** is typical (Figure 4.1), and shows the macrocycle in a chair conformation forming short, close-to-linear, hydrogen bonds orthogonal to the lone pairs of the fumaramide carbonyl groups. Of the three different tertiary amide rotamers present in solution (as observed by NMR) only the {*ZZ*}amide rotamer of *E*-**5** is found in the crystal.

** The modest yield (33%) of *E*-**5** is probably a consequence of the {*E*,*E*}- and/or {*E*,*Z*}- tertiary amide rotamers being sterically mismatched with the forming macrocycle. Interestingly, a small amount (2%) of rotaxane *E*-**6**, presumably arising from *p*-xylylene diamine-catalyzed isomerization of the thread, was isolated from the reaction of pristine *Z*-**3**, again indicating the extraordinary efficiency of the *E*-**3** template for rotaxane formation.

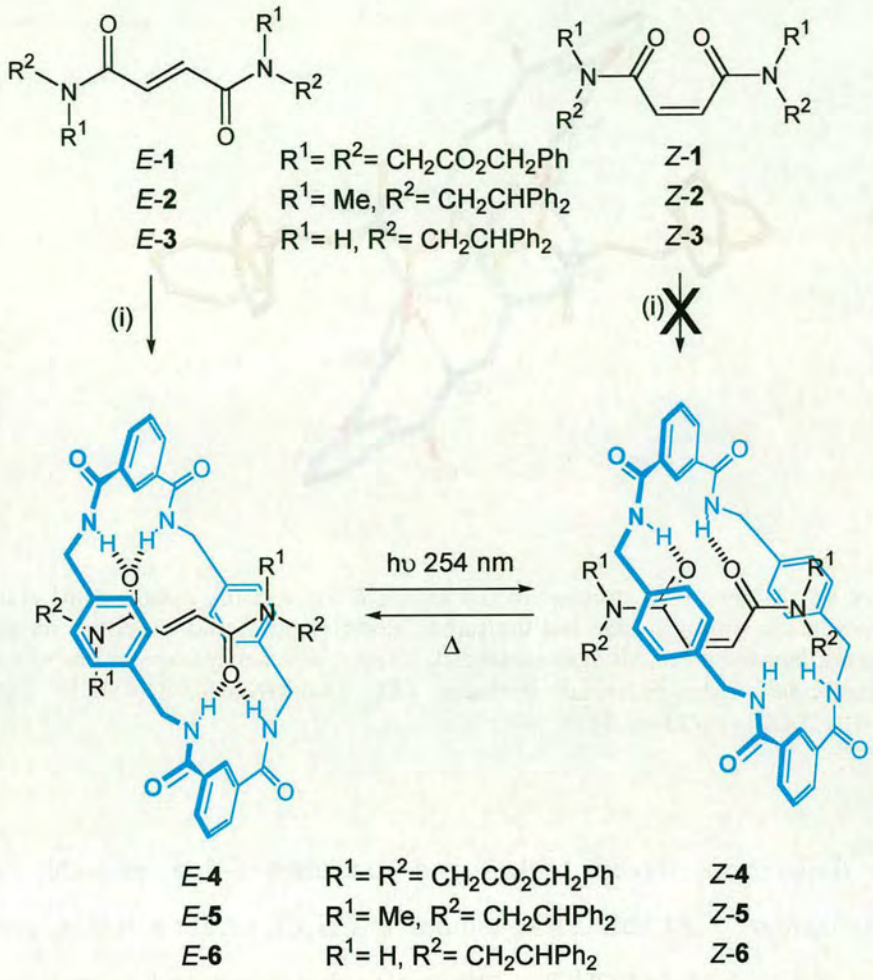

Scheme 4.1 Synthesis of [2]rotaxanes *E*/*Z*-**4**–**6**. (i) 4 equiv. isophthaloyl dichloride, 4 equiv. *p*-xylylene diamine, Et_3N, 4 h, high dilution; $CHCl_3$ for *E*-**4** (67%) and *E*-**5** (33%), 1/9 MeCN/$CHCl_3$ for *E*-**6** (97%). Direct irradiation (254 nm, 30 min.) of a solution of an *E*-rotaxane (0.1 M, RT, CH_2Cl_2 [1:9 MeOH/$CHCl_3$ for *E*-**6**]) yields the "accelerated" *Z*-isomer (45–50% single experiment; >90% from 4 successive cycles). Heating a 0.02 M solution of a *Z*-rotaxane at 400 K reforms the "dampened" *E*-isomer (*E*-**6**: $C_2D_2Cl_4$, 7 days, 84% or DMSO-d_6, 4 days, 100%).

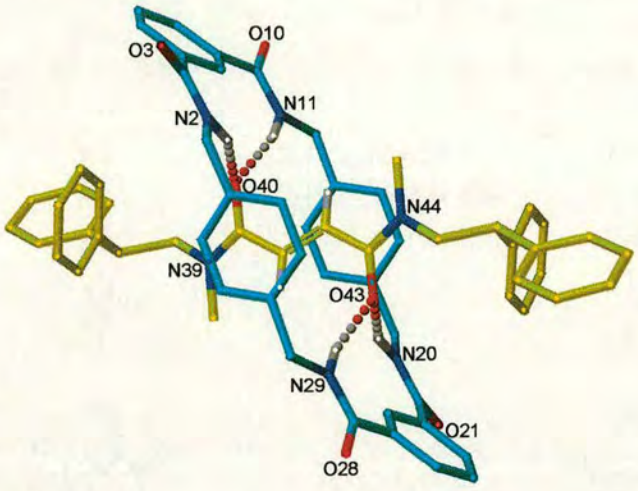

Figure 4.1 *X*-Ray crystal structure of [2]rotaxane *E*-**5** (for clarity carbon atoms of the macrocycle are shown in blue and the carbon atoms of the thread in yellow; oxygen atoms are depicted in red, nitrogen atoms dark blue and selected hydrogen atoms white). Intramolecular hydrogen bond distances (Å): O40–HN2/O43–HN20 = 2.22, O40–HN11/O43–HN29 = 1.94.

All three fumaramide threads *E*-**1–3** and rotaxanes *E*-**4–6** smoothly undergo photoisomerization[16] (254 nm; 0.1 M solution in CH_2Cl_2 or, for solubility reasons in the case of *E*-**6**, 1:9 MeOH/$CHCl_3$; 30 min.) to the corresponding maleamide (*Z*-olefin) systems. The yields for the rotaxanes, 45–50%, are remarkably good considering the confined cavity that the molecular rearrangement has to occur in and that the intercomponent hydrogen bonding between the thread and macrocycle is complementary to the positions of the amide groups only in the *E*-olefin. Unanticipated enhanced solubility of the *Z*-rotaxanes in nonpolar solvents allowed the separation of the *E*/*Z* photochemical reaction mixtures into the individual isomers by simple trituration (PhMe/CH_2Cl_2, 1:1). The photoisomerization reaction produces few byproducts so *E*-rotaxanes recovered in this way could be recycled leading to >90% overall conversion to the *Z*-isomer from a series of irradiation experiments.

The ^{1}H NMR spectra of each pair of *E*- and *Z*-olefin rotaxanes gives insight regarding their structure and relative dynamic properties in nonpolar solvents. The trends are similar in all cases but the clearest information is provided by *E/Z*-**4**.[††]

The variable temperature ^{1}H NMR spectra of *E*-**4** and *Z*-**4** in CD_2Cl_2 (223–273 K) and $C_2D_2Cl_4$ (339–393 K) are shown in Figure 4.2 (the wide temperature range involved meant different non-hydrogen bond-disrupting solvents were required to monitor the dynamic processes at high and low temperatures). Pirouetting, a 180° rotation of the macrocycle about the axis of the arrow plus formal chair-chair flip of the macrocycle, is the simplest process that must occur in order to translate the equatorial macrocycle methylene protons, H_{E_2} onto the axial, H_{E_1} sites. In the fumaramide system the H_E protons coalesce at 273 K and are fully resolved into the H_{E_1} and H_{E_2} resonances at 223 K (Figure 4.2a). The coupling constants confirm the axial and equatorial assignments of H_{E_1} and H_{E_2}. Spin polarization transfer by selective inversion recovery (SPT-SIR) experiments provided a direct measure of the rate of the exchange process I (i.e. half circumrotation of the macrocycle) at 298 K corresponding to an energy barrier $\Delta G^{\ddagger} = 13.4 \pm 0.1$ kcal mol^{-1} which extrapolates to a rate of macrocycle rotation of ~1 s^{-1} at 223 K[15]. In contrast, the macrocycle methylene protons (H_E) in *Z*-**4** remain sharp and well resolved throughout this temperature range and only begin to broaden significantly at 223 K (Figure 4.2b); remarkably, the broadening of H_E in *Z*-**4** at 223 K is comparable to that in *E*-**4** at 359 K – a 136° temperature difference between the two rotaxane isomers! Exchange is so fast in *Z*-**4** that it is not possible to resolve the signals and prove unequivocally by experiment that the process responsible for the broadening at this temperature is,

[††] The spectra of *Z*-**6** are complicated because intracomponent hydrogen bonding of the maleamide group desymmetrizes the rotaxane (the macrocycle methylene groups appear as an ABX system because the two faces of the macrocycle experience different environments). Similarly, the temperature-dependent equilibrium between the populations of the different amide rotamers present in the methylated rotaxanes *E/Z*-**5** makes their study nontrivial, whereas the symmetrical tertiary amides means *E/Z*-**4** suffers no such complication.

in fact, macrocycle pirouetting (it could be occurring at even lower temperatures). However, making the assumption (*vide infra*) that this is the process responsible for broadening, line shape analysis gives an energy barrier of 6.8 ± 0.8 kcal mol^{-1}, i.e. a macrocycle spinning rate > 1.2 x 10^6 s^{-1} at 223 K.

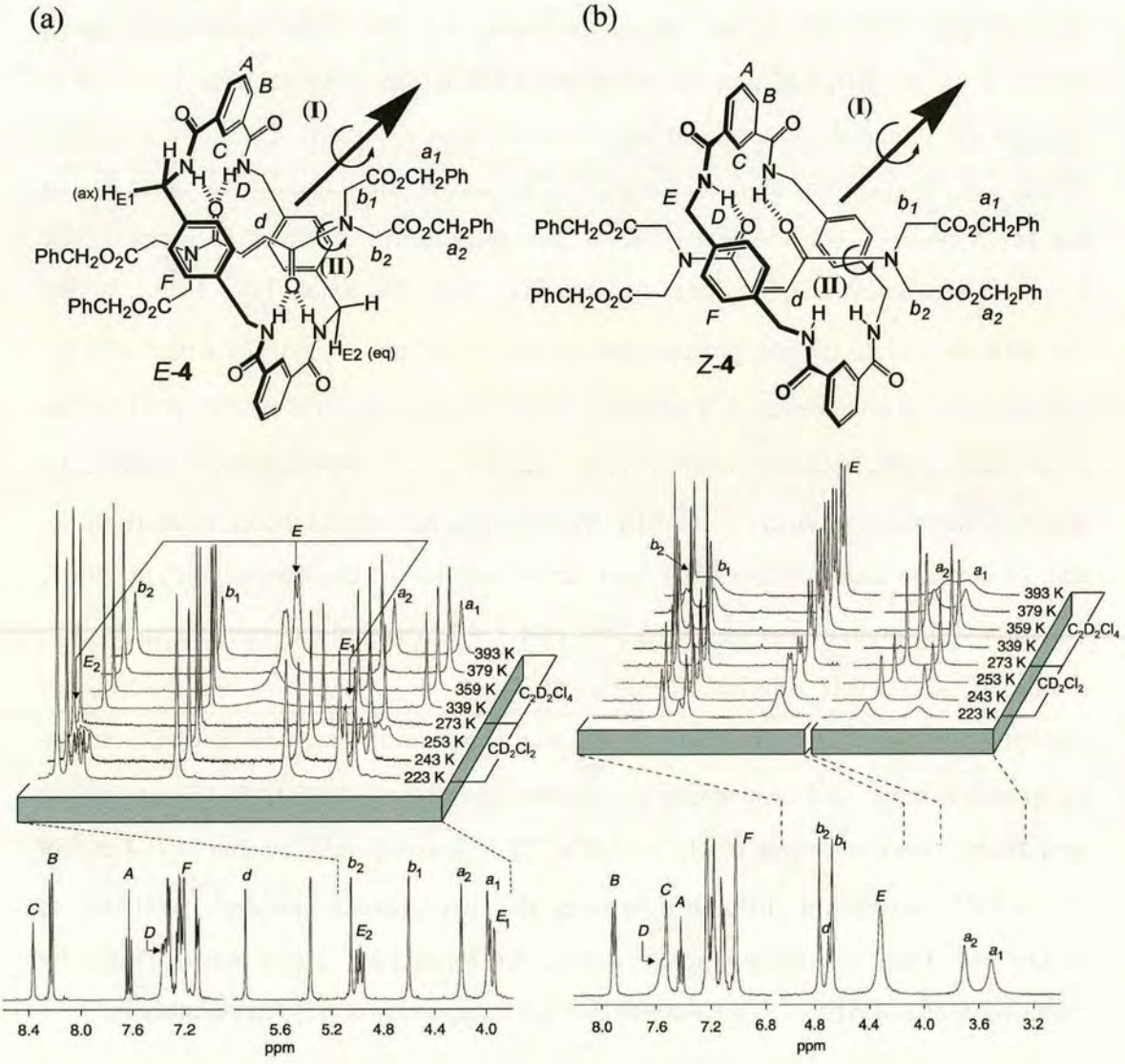

Figure 4.2 Variable temperature ^{1}H NMR spectra (400 MHz) of (a) *E*-**4** and (b) *Z*-**4** in CD_2Cl_2 at 223 K (main traces) and 223–273 K (stackplot expansions) and $C_2D_2Cl_4$ 339–393 K (stackplot expansions). Lettering corresponds to selected non-equivalent proton environments. A 180° rotation of the macrocycle about the axis of the arrow, plus chair-chair flipping of the macrocycle, translates the H_{E_2} (equatorial) protons onto the H_{E_1} (axial) sites. The NMR spectra in (a) reveal slow pirouetting of the macrocycle

about the thread in *E*-**4**, (H_{E_1} and H_{E_2} coalesce at 273 K, $\Delta G^{\ddagger} = 13.4 \pm 0.1$ kcal mol^{-1}; process I) and slow rotation of the thread tertiary amide bonds ($H_{a_1}$and H_{a_2}/H_{b_1} and H_{b_2} fully resolved even at 393 K, $\Delta G^{\ddagger} = 21.1 \pm 0.1$ kcal mol^{-1}; process II). The NMR spectra in (b) show that process I is much lower in energy for *Z*-**4** ($\Delta G^{\ddagger} = 6.8 \pm 0.8$ kcal mol^{-1}) than *E*-**4** and that process II is also more facile ($H_{a_1}$and H_{a_2}/H_{b_1} and H_{b_2} broadening at higher temperatures, $\Delta G^{\ddagger} = 20.0 \pm 0.1$ kcal mol^{-1})[28].

Remarkably, it was possible to obtain an *X*-ray crystal structure of one of the rotaxanes with a 'switched off' recognition motif. Small crystals of *Z*-**5** suitable for investigation using a synchrotron source were grown from slow evaporation of a saturated solution in $CHCl_3$/MeOH. In contrast to the crystal structure of *E*-**5**, two of the three tertiary amide rotamers, i.e. {*ZE*} and {*EE*} rotamers are present in the unit cell of *Z*-**5** (Figure 4.3a and 4.3b, respectively). Both forms are consistent with the dramatic increase in the rate of rotation in solution for the *cis*-rotaxanes observed experimentally by ^{1}H NMR spectroscopy; the consequence of isomerizing the double bond is that the amide groups of the thread are held in positions such that they can hydrogen bond to only one of the two isophthalamide groups of the macrocycle. It is interesting to note that the energy barrier for the *trans*-rotaxane with four intercomponent hydrogen bonds (13.4 kcal mol^{-1}) is almost exactly twice the value for the *cis*-rotaxane with two intercomponent hydrogen bonds (~6.8 kcal mol^{-1}).

In order to obtain a more detailed understanding of the dynamic properties of these systems and, in particular, to confirm that the low energy dynamic process measured by NMR in the maleamide rotaxane was circumrotation, we carried out simulations of the dynamic processes present in both *E*- and *Z*-**4**.

Using a computational procedure which employs the MM3 forcefield[17] and the TINKER program[18], and has previously proved successful in describing the circumrotation pathway in catenanes[19], macrocycle pirouetting in rotaxanes[13] and other properties in mechanically-interlocked molecules[20,21], it was possible to locate the saddle points for macrocycle circumrotation in *E*-**4** and *Z*-**4**. Figure 4.4 shows the transition states, the arrows indicating the initial motion that macrocycle and

thread would undergo away from the saddle point. The calculated activation energies (13.51 kcal mol^{-1} for *E*-**4** and 6.53 kcal mol^{-1} for *Z*-**4**) compare well with the NMR determined ΔG's of 13.4 ± 0.1 and 6.8 ± 0.8 kcal mol^{-1}, respectively, and thus confirm that macrocycle pirouetting is probably a major contributor to the broadening of resonances observed in the low temperature NMR spectra of *Z*-**4**. The good agreement of calculations and experiments also allows one to take a closer look at the contributions of various kinds of interactions to the dynamic process of pirouetting. Table 4.1 shows the different energy contributions to the *E*-**4** and *Z*-**4** minima and transition states. Interestingly, from the calculations the ~7 kcal mol^{-1} difference between the activation barriers of circumrotation in the two molecules can be ascribed to contributions from *all* the energy components, not just H-bonding.

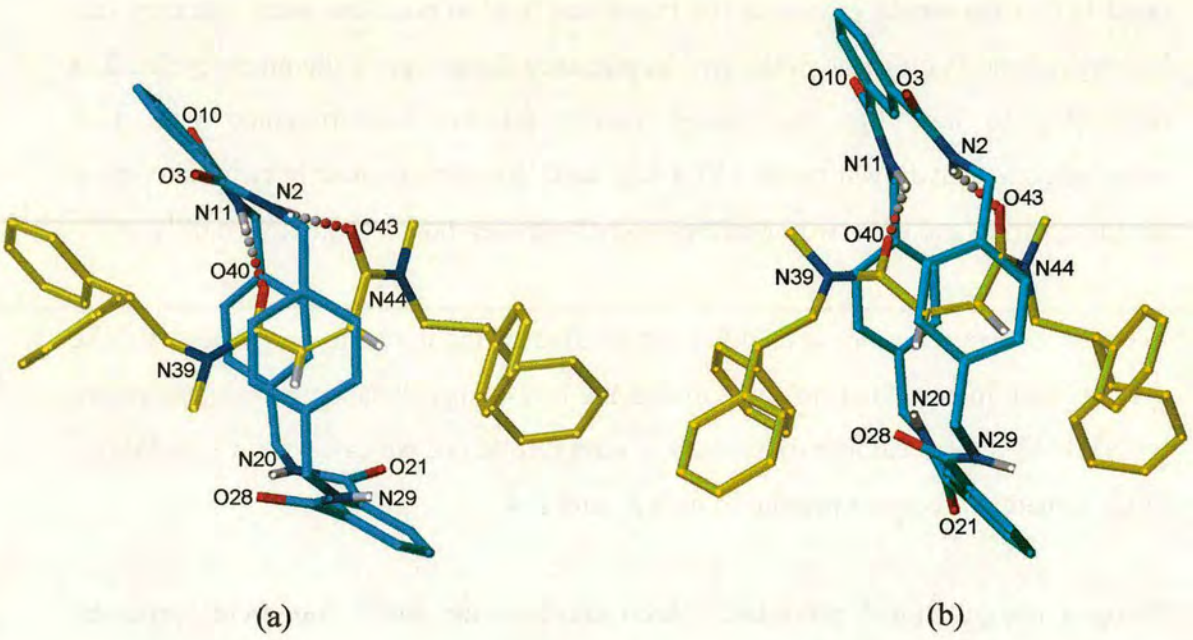

Figure 4.3 *X*-ray crystal structures of (a) {*ZE*} and (b) {*EE*} rotamers of *N,N'*-dimethylmaleamide [2]rotaxane *Z*-**5**. Intramolecular hydrogen bond distances (Å): (a) O40–HN11 = 2.08, O43–HN2 = 2.05; (b) O40–HN11 = 1.76, O43–HN2 = 2.08.

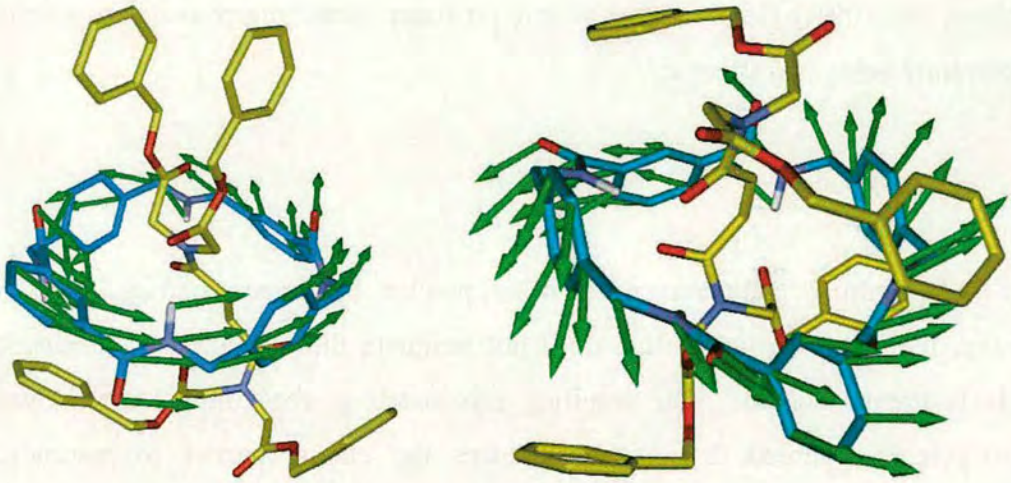

(a) (b)

Figure 4.4 Calculated transition-state structures for the macrocycle ring motions for rotaxanes (a) *Z*-**4** and (b) *E*-**4**. Green arrows represent the corresponding atomic motion vectors connecting the transition states to their minima.

	E_v	$E_{H\text{-bonding}}$	$E_{\pi\text{-stacking}}$	E_{vdW}
E-**4**[a]	29.18	-20.14	-15.36	-24.91
E-**4**[b]	33.09	-13.75	-12.65	-24.40
	(3.91)	(6.39)	(2.71)	(0.51)
Z-**4**[a]	38.11	-16.84	-14.89	-30.97
Z-**4**[b]	44.66	-15.99	-16.73	-29.99
	(6.55)	(0.85)	(-1.84)	(0.98)

(a) energy minimum (b) transition state energy

Table 4.1 Molecular energy contributions (kcal mol^{-1}) divided into four components: (i) a valence term, E_V, which includes stretchings and in-plane and out-of-plane bendings, (ii) a hydrogen bond contribution, $E_{H\text{-bonding}}$, (iii) π-π stacking energy, $E_{\pi\text{-stacking}}$, and (iv) the remaining van der Waals components, E_{vdW}. The energy differences between the minima and the transition states are given in parentheses.

Preliminary studies show that it is possible to reverse the photoisomerization process thermally. Heating each of *Z*-**4**–**6** ($C_2D_2Cl_4$ or DMSO-d_6, 400 K, 4–7 days) resulted

in re-conversion to the more thermodynamically stable *E*-rotaxanes in good-to-excellent (80–100%) yields. Other simple *cis-trans* olefin interconversion reactions are currently being investigated.[‡‡]

4.3 Conclusion

The post-assembly photoconversion of a precise hydrogen bonding, rotaxane-forming, template to a motif that does not template the formation of mechanical bonds is unprecedented. The resulting mis-match in recognition sites between macrocycle and thread dramatically reduces the energy barrier to macrocycle pirouetting in the rotaxane. Such control could be useful for the future construction of synthetic molecular machines that utilize large amplitude internal rotary motions.

[‡‡] Attempts to grow crystals of *Z*-**6** resulted in significant yields of crystalline *E*-**6** although no *E*-**6** could be detected at any stage in solution! It appears that the growing crystal surface of *E*-**6** is able to catalyze the *cis-trans* isomerization process. Such a phenomenon is not unprecedented (27).

4.4 Experimental Section

Preparation of thread *(E)-N,N'*- dimethyl-*bis*(2,2-diphenylethyl)-butendiamide, *E*-2.

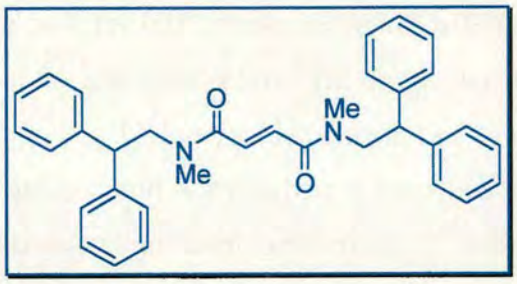

To a stirred ice-cooled solution of *bis*-(2,2-diphenylethyl) fumaramide (1 g, 2.01 mmol) in dry THF (20 mL) under nitrogen was added NaH (0.2 g, 60% dispersion in oil, excess) portion-wise under nitrogen. After the effervescence had subsided, methyl iodide (0.3 mL, excess) was added in one portion. The reaction was allowed to warm to room temperature and stirred overnight and water (20 mL) and ammonia solution (10 mL) added drop-wise to quench the reaction. Most of the solvent was removed under reduced pressure, and the remainder partitioned between water and CH_2Cl_2 (3x20 mL). The organic extracts were washed with sodium hydroxide (1N, 20 mL) and dried over anhydrous magnesium sulfate. The filtered solution was concentrated under reduced pressure to give an oil that slowly solidified. Recrystallization from CH_2Cl_2/diisopropyl ether afforded colorless needles.

Selected data for (*E*-**2**): Yield 0.87g, 87%; m.p. 134–136 °C; ^{1}H NMR (400 MHz, $C_2D_2Cl_4$ at 90 °C): δ = 7.34–7.19 (m, 20H, ArH), 6.99 (s, 2H, C<u>H</u>=C<u>H</u>), 4.37 (t, J = 8.8 Hz, 2H, Ph_2CH), 4.04 (d, J = 8.0 Hz, 4H, $Ph_2CHC\underline{H}_2$), 2.79 (s, 6H, NCH_3); ^{13}C NMR (100 MHz, $C_2D_2Cl_4$ at 120 °C): δ = 166.70, 143.0, 132.14, 129.71, 128.9, 127.2, 55.52, 51.01, 37.5; MS (FAB, mNBA): *m/z* (%) = 502 [$(M+H)^+$]. Anal. Calcd for $C_{32}H_{36}N_2O_2$: C 81.24, H 6.82, N 5.57%. Found: C 81.61, H 6.68, N 5.43%.

General Method for the Preparation of Benzylic Amide Macrocycle Fumaramide [2]Rotaxanes.

The threads *E*-**1**–**3** (1.00 mmol) and triethylamine (2.1 mL, 15.7 mmol) were dissolved in $CHCl_3$ (stabilized with amylenes, 100 mL) or, in the case of *E*-**3**, 1:9 MeCN:$CHCl_3$, and stirred vigorously whilst solutions of the diamine (1.09 g, 4 equiv.) in $CHCl_3$ (45 mL) and the acid chloride (1.62 g, 4 equiv.) in $CHCl_3$ (45 mL) were simultaneously added over a period of 2 hours using motor-driven syringe pumps. After a further 2 hours the resulting suspension was filtered and concentrated under reduced pressure. The rotaxanes *E*-**4** and **5** were purified by trituration of the respective solids in dichloromethane (to remove the polar impurities – catenane, macrocycles, $Et_3HN^+Cl^-$ etc), and subsequently separating the rotaxane from unreacted thread through trituration in hot toluene. Rotaxane *E*-**6** was obtained by spontaneous crystallization from the reaction mixture as previously described.[10]

([2](1,7,14,20-tetraaza-2,6,15,19-tetraoxo-3,5,9,12,16,18,22,25-cetrabenzocyclohexacosane)-((E)-N,N'-(dimethyl)-bis{2',2'-diphenylethyl}-butendiamide)-rotaxane, *E*-5

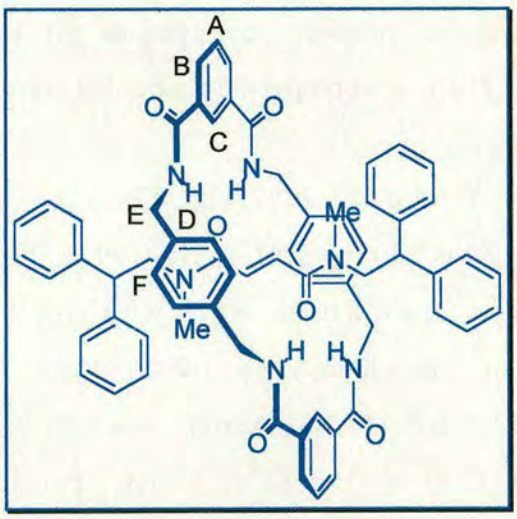

Selected data for (*E*-**5**): Yeld 0.34 g (33%); m.p. 320–323 °C; ^{1}H NMR (400 MHz, DMSO-d_6 at 130 °C): δ = 8.51 (brs, 2H, ArH_C), 8.09 (dd, *J* = 7.8, 1.8 Hz, ArH_B), 7.78 (brt, 4H, NH_D), 7.60 (t, *J* = 7.8 Hz, 2H, ArH_A), 7.35–7.11 (m, 20H, ArH), 6.96 (s, 8H, ArH_F), 5.92 (bs, 2H, C<u>H</u>=C<u>H</u>), 4.40 (brd, *J* = 5.4 Hz, 8H, CH_{2E}), 4.26 (brt, 2H, Ph_2CH), 3.91 (brd, 4H, $Ph_2CHC\underline{H}_2$), 2.41 (s, 6H, NCH_3); ^{13}C NMR (100 MHz, $CDCl_3$): δ = 166.99–165.99, 142.91, 138.18, 134.89, 129.27–127.63, 125.05, 53.9–53.10, 49.79, 44.61–44.09, 46.27–36.14; MS (FAB, *m*NBA): *m/z* 1036 [(rotaxane+H)$^+$]. Anal. Calcd for $C_{66}H_{62}N_6O_6$: C 76.57, H 6.04, N 8.12 %. Found: C 76.88, H 6.20, N 8.30 %.

General Method for the Photoisomerization of Fumaramide [2]Rotaxanes.

The rotaxanes *E*-**4–6** (0.60 g) were dissolved in CH_2Cl_2 [except for solubility reasons *E*-**6**, MeOH/$CHCl_3$ (1/9)] (1000 mL) in a quartz vessel. The solutions were directly irradiated at 254 nm using a multilamp photoreactor model MLU18 manufactured by Photochemical Reactors Ltd, UK. The progress of photoisomerization was monitored by TLC (silica, $CHCl_3$/ EtOAc 4:1) or NMR with the photostationary state typically reached after 30 min after which the reaction mixture was concentrated under reduced pressure to afford the crude products (*Z*-**4–6**). The unconverted *trans* isomers were isolated by triturating the solids with toluene/CH_2Cl_2 (1:1, ~20 mL) and, because the photoisomerization process produces few byproducts, could be recycled eventually leading to >90% conversion of each rotaxane to the corresponding *cis*-isomer. The solutions were then passed through a pad of silica ($CHCl_3$/EtOAc, 4:1) to afford the *cis* isomers *E*-**4–6** in 50, 47 and 45% yields, respectively, from a single photoisomerization experiment.

[2](1,7,14,20-tetraaza-2,6,15,19-tetraoxo-3,5,9,12,16,18,22,25-tetrabenzocyclohexacosane)- benzyl 2-[[2-(benzyloxy)-2-oxoethyl]((*Z*)-5-(bis[2-(benzyloxy)-2-oxoethyl]amino})2,5-dioxo-3-pentenyl)amino]acetate-rotaxane, *Z*-4

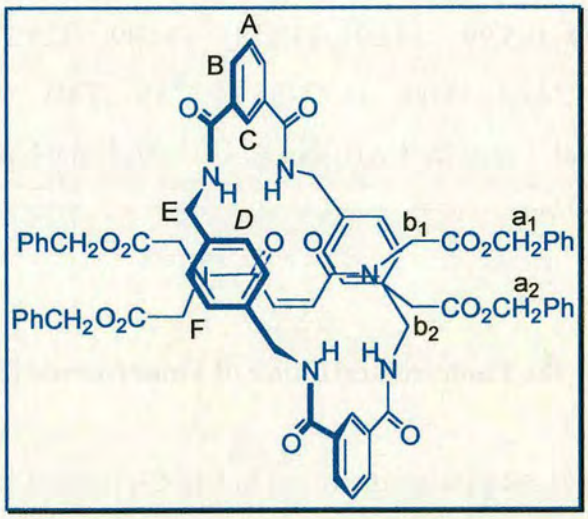

Selected data for (*Z*-**4**): Yield 0.3 g (50%); m.p. 243–244 °C; ^{1}H NMR (CD_2Cl_2, 400 MHz): δ = 8.92 (dd, *J* = 7.8, 1.7 Hz, 4H, ArH_B), 7.60 (t, *J* = 1.7 Hz, 2H, ArH_C), 7.40 (t, *J* = 7.8 Hz, 2H, ArH_A), 7.30 (t, *J* = 5.1 Hz, 4H, NH_D), 7.23–7.11 (m, 20H, ArH), 7.03 (s, 8H, ArH_F), 4.89 (s, 4H, H_{b2}), 4.83 (s, 2H, H_d), 4.78 (s, 4H, H_{b1}), 4.36 (d, *J* = 5.1 Hz, 8H, H_E), 3.63 (s, 4H, H_{a2}), 3.58 (s, 4H, H_{a1}); ^{13}C NMR (100 MHz, $CDCl_3$): δ = 168.37, 167.63, 166.57, 166.23, 137.27, 131.96, 134.54, 134.36, 132.46, 129.92–128.58, 123.39, 68.79, 68.34, 50.94, 50.57; LSIMS, m/z = 1239 [(rotaxane+H)$^+$], 1262 [(rotaxane+Na)$^+$]. Anal. Calcd for $C_{72}H_{66}N_6O_{14}$: C 69.78, H 5.37, N 6.78%. Found C 69.56, H 5.32, N.6.68%.

([2](1,7,14,20-tetraaza-2,6,15,19-tetraoxo-,5,9,12,16,18,22,25-cetrabenzocyclohexacosane)-((*Z*)-*N*,*N*'-(dimethyl)-*bis*{2',2'-diphenylethyl}-butendiamide)-rotaxane, *Z*-5

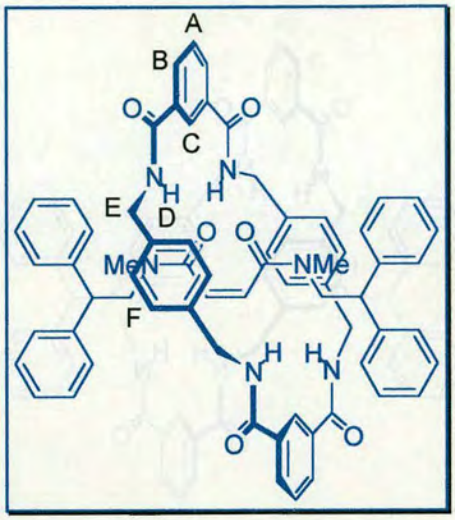

Selected data for (*Z*-**5**): Yield 0.28 g (47%); m.p. >300°C (decompose); ^{1}H NMR (400 MHz, $C_2D_2Cl_4$ at 130 °C): δ = 8.13 (dd, *J* = 7.8 Hz, ArH_B), 7.91 (brs, 2H, ArH_C), 7.63 (t, *J* = 7.8 Hz, 2H, ArH_A), 7.35–7.11 (m, 24H, ArH & NH_D), 6.98 (s, 8H, ArH_F), 4.92 (brs, 2H, C<u>H</u>=C<u>H</u>), 4.40 (brd, *J* = 5.4 Hz, 8H, CH_{2E}), 4.07 (brt, 2H, Ph_2CH), 3.51 (brd, 4H, $Ph_2CHC\underline{H}_2$), 2.21 (s, 6H, NCH_3); ^{13}C NMR (100 MHz, $CDCl_3$): δ = 166.99–165.99, 142.91, 138.18, 134.89, 129.27–127.63, 125.05, 53.9–53.10, 49.79, 44.61–44.09, 46.27–36.14; MS (FAB, mNBA): *m/z* 1036 [(rotaxane+H)$^+$]. Anal. calcd for $C_{66}H_{62}N_6O_6$: C 76.57, H 6.04, N 8.12 %. Found: C 76.98, H 6.30, N 8.23 %.

([2](1,7,14,20-tetraaza-2,6,15,19-tetraoxo-3,5,9,12,16,18,22,25-cetrabenzocyclohexacosane)-((*Z*)-*N*,*N*'-(dimethyl)-*bis*{2',2'-diphenylethyl}-butendiamide)-rotaxane, *Z*-6

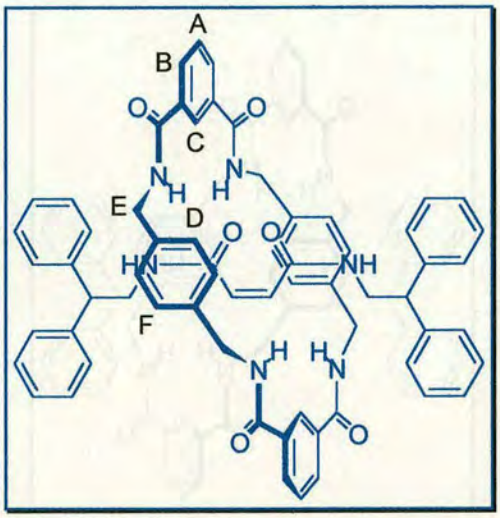

Selected data for (*Z*-**6**): Yield 0.27 (45%); m.p. >300°C (decompose); ^{1}H NMR (400 MHz, $CDCl_3$) δ = 8.22 (d, *J* = 7.8 Hz, ArH_B), 8.13 (s, 2H, ArH_C), 7.73 (t, *J* = 5.4 Hz, 4H, NH_D), 7.62 (t, *J* = 7.8 Hz, 2H, ArH_A), 7.27–7.11 (m, 18H, ArH & NH), 6.98 (d, *J* = 7.5 Hz, 4H, ArH), 6.83 (s, 8H, ArH_F), 5.11 (s, 2H, C<u>H</u>=C<u>H</u>), 4.38 (d, *J* = 5.4 Hz, 8H, CH_{2E}), 3.87 (t, 2H, Ph_2CH), 3.41 (dd, 4H, $Ph_2CHC\underline{H}_2$); ^{13}C NMR (100 MHz, $CDCl_3$): δ = 166.8, 165.5, 141.8, 137.4, 134.3, 131.9, 131.2, 129.9, 129.3, 129.2, 128, 127.5, 124.8, 50.32, 44.9, 44.81; MS (FAB, mNBA): *m/z*=1029 [(rotaxane+Na)$^{+}$]. Anal. Calcd for $C_{64}H_{58}N_6O_6$: C 76.32, H 5.80, N 8.34%. Found: C 76.39, H 5.91, N 8.19%.

X-ray Crystallographic Structure Determinations. :

E-**5:** $C_{66}H_{62}N_6O_6$, *M* = 1035.22, crystal size 0.30 × 0.14 × 0.08 mm, monoclinic, $P2_1/c$, *a* = 10.5696(3), *b* = 27.7157(9), *c* = 10.7503(3) Å, *β* = 115.2530(10), *V* = 2848.27(15) Å^3, *Z* = 2, ρ_{calcd} = 1.207 Mg m^{-3}; $Mo_{K\alpha}$ radiation (graphite monochromator, *λ* = 0.71073 Å), *μ* = 0.078 mm^{-1}, *T* = 293(2) K. 13437 data (4049

unique, R_{int} = 0.1701, 1.47 < θ < 23.29°), were collected on a Siemens SMART CCD diffractometer using narrow frames (0.3° in ω), and were corrected semiempirically for absorption and incident beam decay (transmission 1.00–0.20). The structure was solved by direct methods and refined by full-matrix least-squares on F^2 values of all data (G. M. Sheldrick, SHELXTL manual, Siemens Analytical *X*-ray Instruments, Madison WI, USA, 1994, version 5) to give $wR = \{\Sigma[w(F_o^2-F_c^2)^2]/\Sigma[w(F_o^2)^2]\}^{1/2}$ = 0.2136, conventional R = 0.0811 for F values of 4049 reflections with $F_o^2 > 2\sigma(F_o^2)$, S = 0.754 for 361 parameters. Residual electron density extremes were 0.355 and –0.337 eÅ^{-3}. Amide hydrogen atoms were refined isotropically subject to a distance constraint N–H = 0.98 Å, with the remainder constrained; anisotropic displacement parameters were used for all non-hydrogen atoms.

***Z*-5:** $C_{64}H_{58}N_6O_6$, M = 1039.22, crystal size 0.18 × 0.04 × 0.02 mm, triclinic *P*-1, a = 13.4337(13), b = 16.2778(16), c = 29.964(3) Å, α = 75.716(2), β = 87.934(2), γ = 71.880(2)°, V = 6028.9(10) Å^3, Z = 4, ρ_{calcd} = 1.145 Mg m^{-3}; synchrotron radiation (CCLRC Daresbury Laboratory Station 9.8, silicon monochromator, λ = 0.69290 Å), μ = 0.107 mm^{-1}, T = 150(2) K. 23260 data (12003 unique, R_{int} = 0.0466, 1.73 < θ < 20.00°), were collected on a Siemens SMART CCD diffractometer using narrow frames (0.3° in ω), and were corrected semiempirically for absorption and incident beam decay (transmission 1.00–0.60). The structure was solved solved with SIR97 (A. Altomare, M. C. Burla, M. Camalli, G. L. Cascarano, C. Giacovazzo, A. Guagliardi, A. G. G. Moliterni, G. Polidori, R. Spagna *J. Appl. Cryst.* **32**, 115–119 (1999)) and refined using SHELXTL and refined by full-matrix least-squares on F^2 values of all data (G. M. Sheldrick, SHELXTL manual, Siemens Analytical *X*-ray Instruments, Madison WI, USA, 1994, version 5) to give $wR = \{\Sigma[w(F_o^2-F_c^2)^2]/\Sigma[w(F_o^2)^2]\}^{1/2}$ = 0.2771, conventional R = 0.0952 for F values of 12003 reflections with $F_o^2 > 2\sigma(F_o^2)$, S = 1.050 for 1480 parameters. Residual electron density extremes were 1.093 and –0.420 eÅ^{-3}.

Crystallographic data for (excluding structure factors) have been deposited with the Cambridge Crystallographic Data Centre as supplementary publication numbers CCDC-149673 and 149672 (*E*-**5** and *Z*-**5**). Copies of the data can be obtained free of charge on application to The Director, CCDC, 12 Union Road, Cambridge CB2 1EZ, UK (fax: +44-1223-336-033; e-mail: teched@chemcrys.cam.ac.uk).

4.5 References

1. Iwamura, H. & Mislow, K. (1988) *Acc. Chem. Res.* **21**, 175–182.
2. Bedard, T. C. & Moore, J. S. (1995) *J. Am. Chem. Soc.* **117**, 10662–10671.
3. Kelly, T. R., Bowyer, M. C., Bhaskar, K. V., Bebbington, D., Garcia, A., Lang, F., Kim, M. H. & Jette, M. P. (1994) *J. Am. Chem. Soc.* **116**, 3657–3658.
4. Kelly, T. R., Tellitu, I. & Sestelo, J. P. (1997) *Angew. Chem. Int. Ed. Engl.* **36**, 1866–1868.
5. Kelly, T. R., Sestelo, J. P. & Tellitu, I. (1998) *J. Org. Chem.* **63**, 3655–3665.
6. Schoevaars, A. M., Kruizinga, W., Zijlstra, R. W. J., Veldman, N., Spek, A. L. & Feringa, B. L. (1997) *J. Org. Chem.* **62**, 4943–4948.
7. Kelly, T. R., De Silva, H. & Silva, R. A. (1999) *Nature* **401**, 150–152.
8. Koumura, N., Zijlstra, R. W. J., van Delden, R. A., Harada, N. & Feringa, B. L. (1999) *Nature* **401**, 152–155.
9. Kelly, T. R., Silva, R. A., De Silva, H., Jasmin, S. & Zhao, Y. (2000) *J. Am. Chem. Soc.* **122**, 6935–6949.
10. Koumura, N. L., Geertsema, E. M., van Gelder, M. B., Meetsma, A. & Feringa, B. L. (2002) *J. Am. Chem. Soc.* **124**, 5037–5051.
11. Balzani, V., Credi, A., Raymo, F. M. & Stoddart, J. F. (2000) *Angew. Chem. Int. Ed.* **39**, 3348–3391.
12. Special issue on *Molecular Machines* (2001) *Acc. Chem. Res.* **34**, 409–522.
13. *Molecular Machines and Motors*. Structure and Bonding, Vol. 99, ed. by J.-P. Sauvage (Springer, Berlin 2001).
14. Bermudez, V., Capron, N., Gase, T., Gatti, F. G., Kajzar, F., Leigh, D. A., Zerbetto, F. & Zhang, S. (2000) *Nature* **406**, 608–611.
15. Gatti, F. G., Leigh, D. A., Nepogodiev, S. A., Slawin, A. M. Z., Teat, S. J. & Wong, J. K. Y. (2001) *J. Am. Chem. Soc.* **123**, 5983–5989.
16. Campari, G., Fagnoni, M., Mella, M. & Albini, A. (2000) *Tetrahedron Asym.*

11, 1891–1906.

17. Allinger, N. L., Yuh, Y. H. & Lii, J.-H. (1989) *J. Am. Chem. Soc.* **111**, 8551–8556.
18. Dudek, M. J. & Ponder, J. (1995) *J. Comput. Chem.* **16**, 791–816.
19. Deleuze, M. S., Leigh, D. A. & Zerbetto, F. (1999) *J. Am. Chem. Soc.* **121**, 2364–2379.
20. Biscarini, F., Cavallini, C., Leigh, D. A., León, S., Teat, S. J., Wong, J. K. W. & Zerbetto, F. (2002) *J. Am. Chem. Soc.* **124**, 225–233.
21. Fustin, C.-A., Leigh, D. A., Rudolf, P., Timpel, D. & Zerbetto, F. (2000) *ChemPhysChem* **1**, 97–100.
22. van Delden, R. A., Koumura, N., Harada, N. & Feringa, B. L. (2002) *Proc. Natl. Acad. Sci. USA* **99**, 4945–4949.
23. Collier, C. P., Mattersteig, G., Wong, E. W., Luo, Y., Beverly, K., Sampaio, J., Raymo, F. M., Stoddart, J. F. & Heath, J. R. (2000) *Science* **289**, 1172–1175.
24. Tashiro, K., Konishi, K. & Aida, T. (2000) *J. Am. Chem. Soc.* **122**, 7921–7926.
25. Leigh, D. A., Murphy, A., Smart, J. P., Deleuze, M. S. & Zerbetto, F. (1998) *J. Am. Chem. Soc.* **120**, 6458–6467.
26. Raehm, L., Kern, J.-M. & Sauvage, J.-P. (1999) *Chem. Eur. J.* **5**, 3310–3317.
27. Chatterjee, S., Pedireddi, V. R. & Rao, C. N. R. (1998) *Tetrahedron Lett.* **39**, 2843–2846.
28. Clegg, W., Gimenez-Saiz, C., Leigh, D. A., Murphy, A., Slawin, A. M. Z. & Teat, S. J. (1999) *J. Am. Chem. Soc.* **121**, 4124–4129.

CHAPTER FIVE

From Rotational To Translational Control...

Submitted to Angewandte Chemie as:

"Remarkable Positional Discrimination in Bistable Light and Heat-Switchable, Hydrogen Bonded Molecular Shuttles"

Andrea Altieri, Giovanni Bottari, David A Leigh, Jenny K Y Wong

Acknowledgements

The following people are gratefully acknowledged for their contributions to this paper: rotaxanes *Z*-**1** and *E*-**1** were synthesised by Giovanni Bottari and rotaxanes *Z*-**2** and *E*-**2** were synthesised by Andrea Altieri.

"Sometimes a scream is better than a thesis."

Ralph Waldo Emerson

From Rotational to Translational Control... – Synopsis

Having used light to control the rate of rotational motion in rotaxanes, we turned our attention to the possibility of using the same photochemical reaction to control the position of the macrocycle on a thread – i.e. controlling translational motion. In this chapter, the synthesis and properties of three molecular shuttles where a macrocycle displays remarkable positional discrimination between two binding sites is described.

The basis of the shuttling mechanism combines our understanding of the fumaramide groups ability to act as a highly efficient template (Chapter Two) coupled with its potential to isomerise to the maleamide form which has only weak binding affinity for the macrocycle (Chapter Four). By incorporating a nonphotoreactive second station of binding affinity in-between the fumaramide and maleamide groups, translational isomerism of the macrocycle between the stations was achieved by a combination of photochemical and thermal stimuli. The intermediate binding stations were determined by their ability to template the formation of the macrocycle. Thus succinic amide ester, succiniamide (Chapter Three, page 68) and adipamide (Chapter Three, page 72) groups where chosen as the counterparts to the fumaramide/maleamide stations (Scheme I).

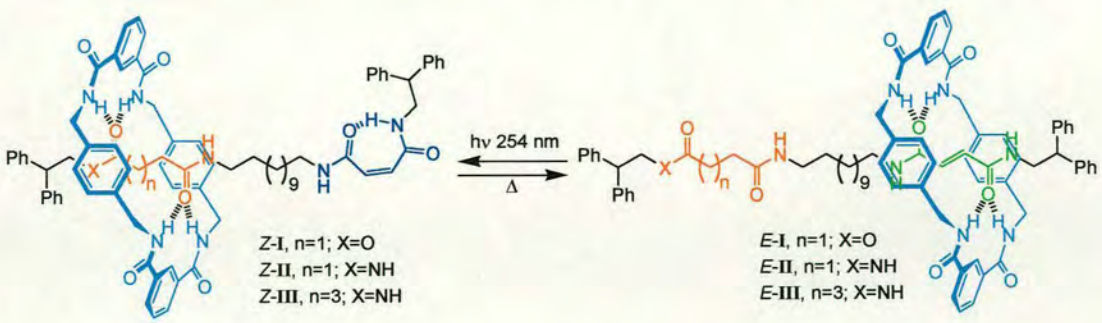

Scheme I *Synthesis of* Z-***I–III*** *by clipping strategy followed by thermal isomerisation at 120 °C to give the corresponding* E-***I–III***.

*The position of the macrocycle in $CDCl_3$ was determined for each shuttle by ^1H NMR spectroscopy where the protons of the stations occupied by the macrocycle experienced the greatest upfield shift. For Z-**I** and Z-**II** extremely good positional discrimination of the stations was observed. The predictions of the relative binding affinities were not completely accurate as in Z-**III**, the positional discrimination between the adipamide and maleamide stations is surprisingly poor.*

5.1 Introduction

Stimuli-responsive molecular 'shuttles',[1-11] mechanically interlocked molecules where a macrocycle can be translocated between different sites in response to an external signal, all operate through the same basic principle. The external stimulus does not induce directional motion of the macrocycle *per se*, rather it alters the equilibrium between different translational co-conformers (a Boltzmann distribution determined by the difference in binding affinities of the macrocycle for the two sites at a given temperature), either by increasing the binding strength of the less populated station or destabilizing the initially preferred binding site. The motion of the components arises from the background thermal energy, the net result being a change in the position of the macrocycle through biased Brownian motion (Figure 5.1).

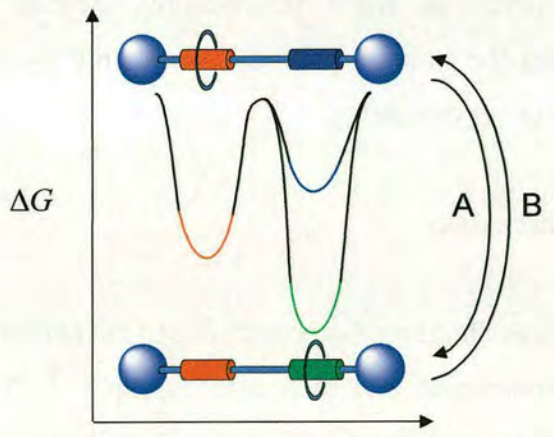

Figure 5.1 Macrocycle translation in a stimuli-responsive molecular shuttle. Stimulus A induces a blue-to-green transformation, stimulus B, a green-to-blue transformation. The equilibrium distribution of the macrocycle between two stations is determined by the difference in their binding energies and the temperature.

Trying to design synthetic systems where photons initiate such processes is fraught with technical difficulties.[2-10] A major problem is finding ways of generating sufficiently large, long lived, binding energy differences between two positional

isomers in two different states by modifying only non-covalent – i.e. intrinsically weak – binding modes. One solution is to use photochemistry, sterically to block what are essentially 'one station' rotaxanes, systems where the macrocycle is only able to sit on an azobenzene[5] or stilbene unit[10] in the *E*-diastereomer of the rotaxane and so must reside elsewhere in the *Z*-form. Another is to compromise on the timescales involved; the binding strength of poorly hydrogen bonding groups can be dramatically increased by photo-production of an excited state if it is a better hydrogen bonding motif than the ground state[9] or can be reduced to one[8]. However, such processes are transient (or require a sacrifical chemical reductant) and in the rotaxanes described to date the macrocycle returns to its original position over millisecond and nanosecond timescales, respectively. Here we describe a new class of hydrogen bonded shuttles (**1–3**) where each translational form is stable until a particular destabilizing stimulus is applied. The macrocycle moves over a relatively large distance (~1.5 nm) between two discrete stations with almost complete positional integrity (even at room temperature), despite the fact that the discrimination between the binding sites is caused only by 'matched' and 'mis-matched' hydrogen bonding motifs.

5.2 Results and discussion

The basis for this bistable shuttling mechanism lies in the photochemical and thermal interconversion of fumaramide and maleamide groups.[12] The *trans*-olefin *bis*-amide acts as an excellent template for the formation of benzylic amide macrocycle-based rotaxanes (e.g *E*-**4**) because the amide carbonyl groups of the thread are rigidly held in positions that fit the hydrogen bond-donating sites of the forming macrocycle (an arrangement maintained even in crystals of *E*-**4** obtained from DMSO, Figure 5.2a).[13] Somewhat remarkably however, given the tight encapsulated binding site and that only the *trans*-olefin has hydrogen bonding sites complementary to the macrocycle, we found that irradiation at 254 nm[14] of fumaramide rotaxanes produces the corresponding maleamide rotaxane in which the numbers of

intercomponent hydrogen bonds is reduced from four to two (Figure 5.2b), considerably reducing the strength of binding[15] between macrocycle and thread. By incorporating a second binding site ('station') into the thread, of macrocycle binding affinity in-between those of the fumaramide and maleamide groups, we reasoned it might be possible to generate photoinduced, thermally reversible, translation of the macrocycle along the thread.

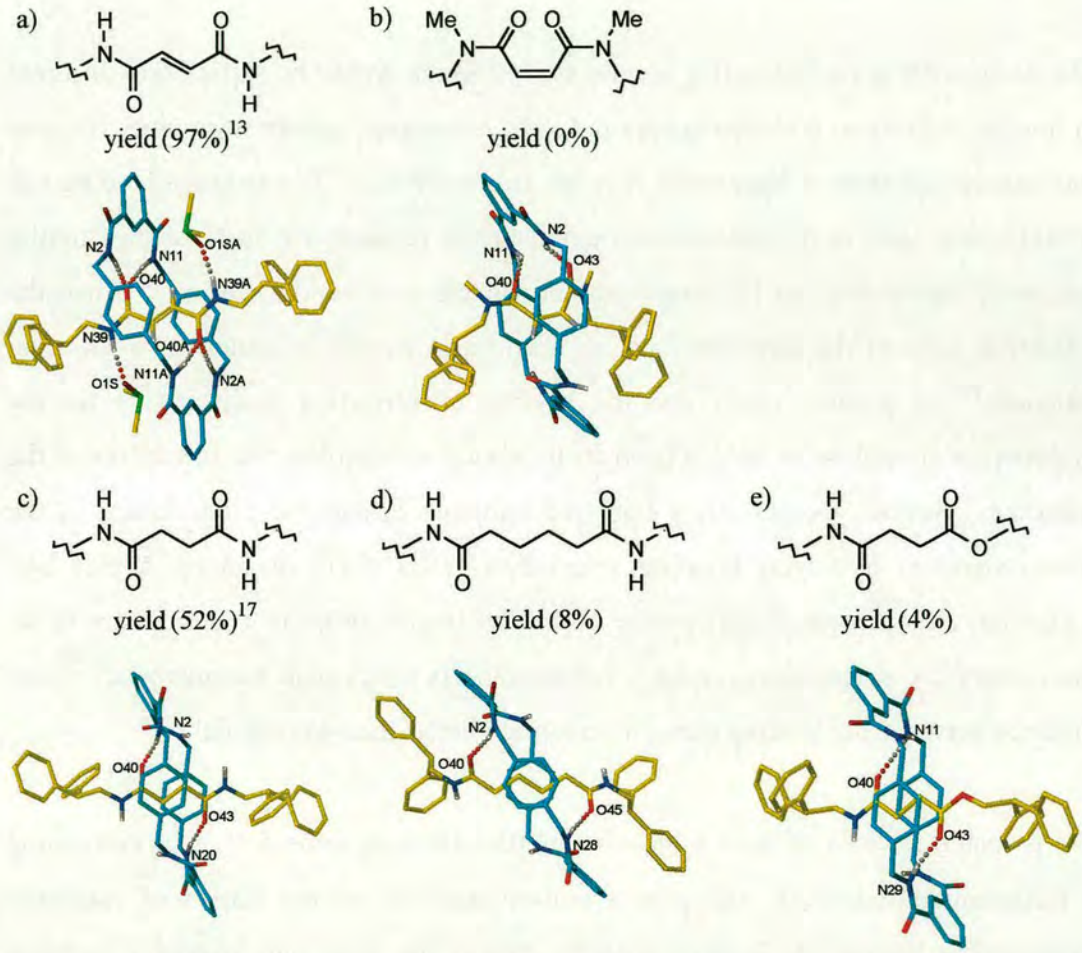

Figure 5.2 *X*-ray structures of model single binding site [2]rotaxanes showing hydrogen bonding characteristics of predicted (a) 'strong', (b) 'weak' and (c)–(e) 'intermediate strength' hydrogen bonding stations. (a) fumaramide rotaxane *E*-**4** crystallized from DMSO; (b) *N,N'*-dimethyl derivative of the corresponding maleamide (*Z*) rotaxane; (c) succinamide analogue of *E*-**4**; (d) adipamide analogue of *E*-**4**; (e) succinic amide ester analogue of *E*-**4**. Intramolecular

hydrogen bond distances and angles: (a) O40–HN2/O40A–HN2A 2.13 Å, 173.7°; O40–HN11/O40A–HN11A 1.89 Å, 169.3°; (b) O40–HN11 2.08 Å, 139.3°; O43–HN2 2.00 Å, 142.1°; (c) O40–HN2/O43–HN20 1.88 Å, 165.3°; (d) O40–HN2/O45–HN28 2.00 Å, 168.8°; (e) O40–HN11/O43–HN29 1.89 Å, 156.1°. For clarity the carbon atoms of the macrocycles are shown in blue and the carbon atoms of the threads in yellow; oxygen atoms are red, nitrogen atoms dark blue and selected hydrogen atoms white. In all cases the rotaxane 'stoppers' are $-CH_2CHPh_2$.

The design of a non-photoactive second station which would be sufficiently different in binding affinity to both the fumaramide and maleamide groups to produce discrete translational isomers in both states requires subtle choices. Too strong a binding site would cause poor positional discrimination in the fumaramide form of the shuttle; too weak would lead to the same problem in the maleamide isomer. Since the transition state of the rotaxane-forming reaction is similar in structure to the final rotaxane,[16] it seemed likely that the binding affinity of a given station for the macrocycle should be closely related to its ability to template the formation of the rotaxane. Several factors affect both the template efficacy and the nature of the intercomponent hydrogen bonding interactions (NH···O=C distances, angles *etc*) including; the hydrogen bond basicity of the functional groups (e.g. amides are better than esters[13]), preorganization (e.g. fumaramide is better than succinamide[17]) and distance between the binding sites (succinamide better than adipamide[18]).

We prepared a series of three molecular shuttles (**1–3**, Scheme 5.1), each containing a fumaramide/maleamide site plus a non-photoactive second station of predicted intermediate macrocycle binding affinity. Where the solid state hydrogen bonding characteristics of the stations were not known we also prepared the model 'one station' [2]rotaxanes and determined their structures by *X*-ray crystallography (Figure 5.2). The synthetic routes to **1–3** are worthy of note: Although *E*-**1** was prepared from the corresponding thread, *E*-**5**, in good yield (*p*-xylylene diamine, isophthaloyl dichloride, $CHCl_3/CH_3CN$ (9/1), Et_3N, RT, 4 h, 57%), the other *E*-

threads were insufficiently soluble in non-hydrogen bond-disrupting solvents to be utilized in this way. Therefore rotaxanes **2** and **3** were prepared from the corresponding *Z*-threads ($CHCl_3$, Et_3N, RT, 4 h, 40 and 20%, respectively, the lower yields a consequence of the lack of a fumaramide template in the thread) and the *Z*-rotaxanes converted to the *E*-isomers thermally (120 °C, 1–7 days, $C_2H_2Cl_4$, 80–95%).

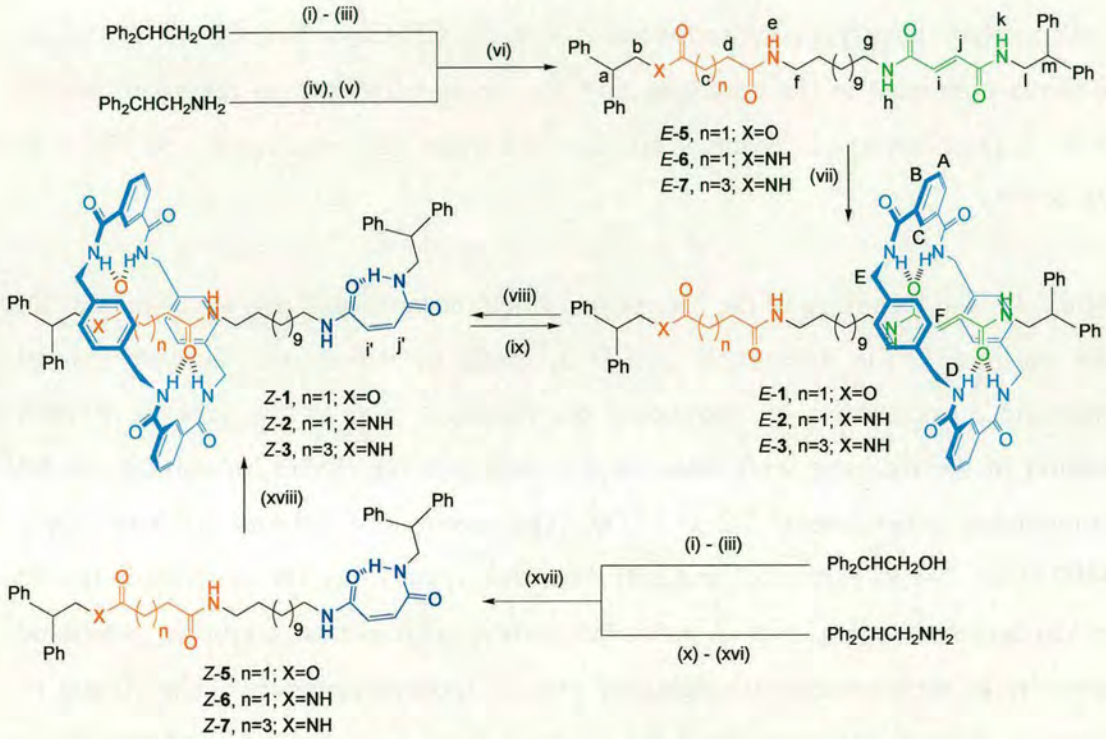

Scheme 5.1 Synthesis of bistable molecular shuttles **1**–**3**. (i) succinic anhydride, Et_3N, CH_2Cl_2, 90%. (ii) $H_2N(CH_2)_{12}NHBoc$, 4-dimethylaminopyridine (DMAP), 1-(3-dimethylaminopropyl)-3-ethyl-carbodiimide hydrochloride (EDCI.HCl), CH_2Cl_2, 68%. (iii) trifluoroacetic acid, $CHCl_3$, quantitative. (iv) fumaric acid monoethylester, DMAP, EDCI.HCl, CH_2Cl_2, 85%. (v) NaOH in H_2O, EtOH, 91%. (vi) *E*-**5**, DMAP, EDCI.HCl, DMF, 76%. (vii) *E*-**1**, isophthaloyl dichloride, *p*-xylylene diamine, Et_3N, $CHCl_3$, 57%. (viii) *E*-**1**, hν at 254 nm for 30 min., CH_2Cl_2, 54%; *E*-**2**, 48%; *E*-**3**, 39%. (ix) *Z*-**1**, $C_2H_2Cl_4$ at 120 °C for 7 days, 80%; *Z*-**2**, 80%; or 1 day, *Z*-**3**, 95%. (x) maleic anhydride, anhydrous THF, 75%. (xi) succinic anhydride, anhydrous THF, 95%. (xii) 1,12-diaminododecane, thionyl chloride, CH_2Cl_2, 35%. (xiii) adipic acid

monoethylester, DMAP, EDCI.HCl, CH_2Cl_2, 86%. (xiv) KOH in H_2O, EtOH, 95%. (xv) $H_2N(CH_2)_{12}NHBoc$, DMAP, EDCI.HCl, $CHCl_3$, 92%. (xvi) trifluoroacetic acid, $CHCl_3$, quantitative. (xvii) *Z*-**5**, DMAP, EDCI.HCl, $CHCl_3$, 70%; *Z*-**6**, 70%; *Z*-**7**, 70%; (xviii) Z-**1**, isophthaloyl dichloride, *p*-xylylene diamine, Et_3N, $CHCl_3$, 2%, *Z*-**2**, 40% and *Z*-**3**, 20%.

Pleasingly, in fact, the *E*-isomers of each molecular shuttle could be converted to the *Z*-form with light (*E*→*Z*, direct radiation at 254 nm, CH_2Cl_2, 30 min, 39–54% or with catalytic benzophenone sensitizer at 350 nm, CH_2Cl_2, 5 min, 60–65%) and the *Z*-forms converted to the corresponding *E*-isomers with heat (as described above, 80% *E*-**1**) or reversible Michael addition (catalytic ethylenediamine, 60 °C, 4 h, 75–85%).

Since the xylylene rings of the macrocycle shield encapsulated regions of the thread, the position of the macrocycle in $CDCl_3$ could be determined for each pair of rotaxane diastereomers by comparing the chemical shift of the protons of each station in the rotaxane with those of the corresponding thread (or suitable model compounds in the case of *E*-2 and *E*-**3**). The spectra of *E*/*Z*-**1** and *E*/*Z*-**5** in $CDCl_3$ (400 MHz, 298 K, Figure 5.3 and 5.4) show that, remarkably, the macrocycle is held by hydrogen bonding over a particular station with almost complete positional integrity in each rotaxane diastereomer even at room temperature! The H_i and H_j protons of the fumaramide group are shielded in the rotaxane *E*-**1** compared to the thread *E*-**5** by 1.09 and 1.02 ppm, respectively, whereas the chemical shifts of the H_c and H_d protons of the succinic amide-ester group are almost identical in both compounds (Figure 5.3). Furthermore, the H_h and H_k fumaramide amide protons are deshielded by ~1.7 ppm in the rotaxane, indicating their involvement in hydrogen bonding to the macrocycle in some co-conformers of *E*-**1**. The slight downfield shift of H_e is probably a result of intramolecular hydrogen bonding indicating some folding in the *E*-rotaxane.

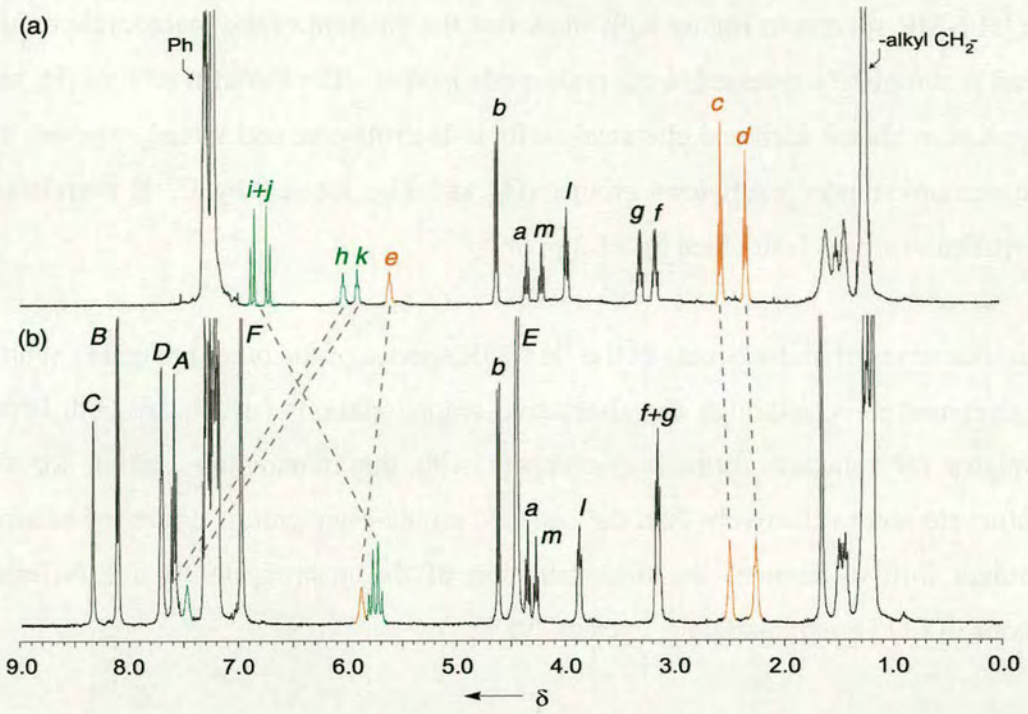

Figure 5.3 400 MHz ^{1}H NMR spectra of (a) thread *E*-**5** and (b) rotaxane *E*-**1** in $CDCl_3$ at 298 K. The assignments correspond to the lettering shown in Scheme 5.1.

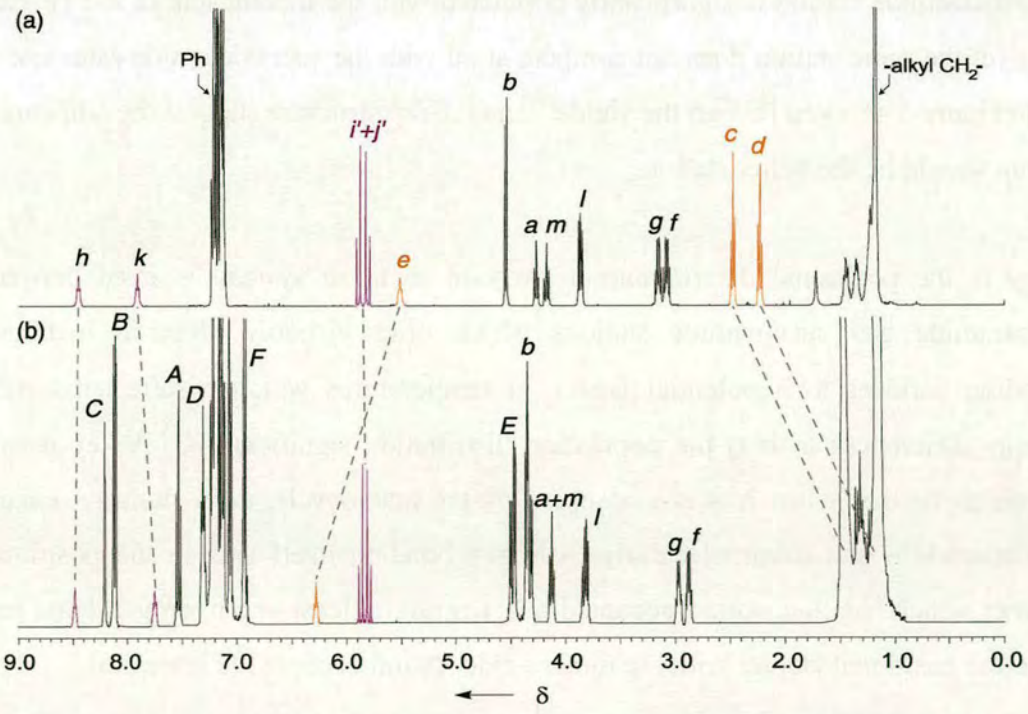

Figure 5.4 400 MHz ^{1}H NMR spectra of (a) thread *Z*-**5** and (b) rotaxane *Z*-**1** in $CDCl_3$ at 298 K. The assignments correspond to the lettering shown in Scheme 5.1.

The ^{1}H NMR spectra in Figure 5.4b show that the position of the macrocycle on the thread is completely reversed in the maleamide isomer. The *Z*-olefin protons ($H_{i'}$ and $H_{j'}$) occur at almost identical chemical shifts in the rotaxane and thread, whereas the succinic amide-ester methylene groups ($H_{c'}$ and $H_{d'}$, located by C, H correlation experiments) are each shielded by >1.3 ppm.

A similar series of shifts occurs in the ^{1}H NMR spectra of the other molecular shuttle diastereomer pairs, although the alternative second stations (which are both better templates for rotaxane formation) compete with the fumaramide station for the macrocycle more effectively than the succinic amide-ester group. From the relative chemical shift differences the discrimination of the macrocycle for the different stations in $CDCl_3$ is remarkable, even at 298 K.

It is interesting to note that the estimates of relative station binding affinities from either rotaxane yield or hydrogen bond distances/angles are not completely accurate. The maleamide station is significantly populated with the macrocycle in Z-**3** (Figure 5.5) yet the same station does not compete at all with the succinic amide ester site in Z-**1** (Figure 5.4), even though the yields[19] and *X*-ray structure suggest the adipamide group should be the better station.

Why is the positional discrimination so good in these systems – even between fumaramide and succinamide stations which offer virtually identical hydrogen bonding surfaces to a potential host – at temperatures which require substantial energy differences to bias the population distribution significantly? A key reason seems to be that when it is not occupied by the macrocycle, each station – except fumaramide – can intramolecularly hydrogen bond to itself and so the positional isomer which has that station occupied has, overall, at least one hydrogen bond less than the positional isomer with the fumaramide station occupied (Figure 5.6).

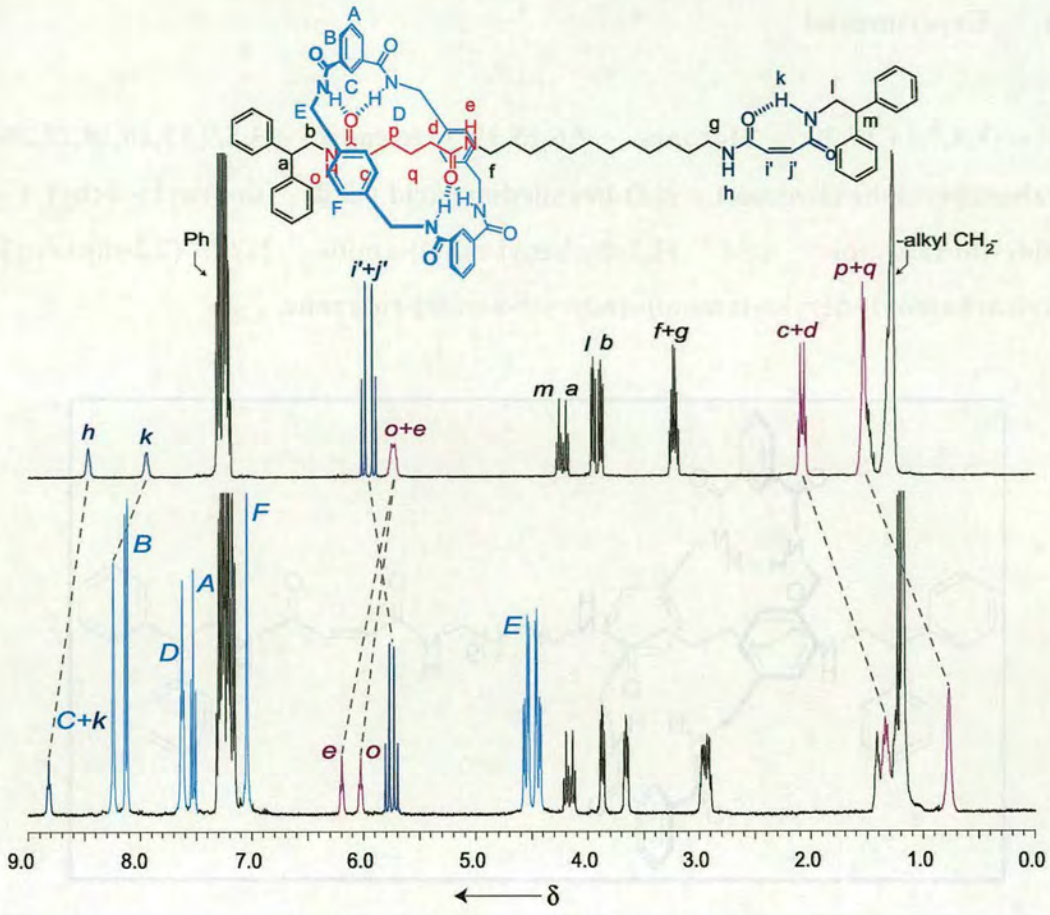

Figure 5.5 400 MHz ^{1}H NMR spectra of (a) maleamide-adipamide thread *Z*-**7** and (b) rotaxane *Z*-**3** in $CDCl_3$ at 298 K.

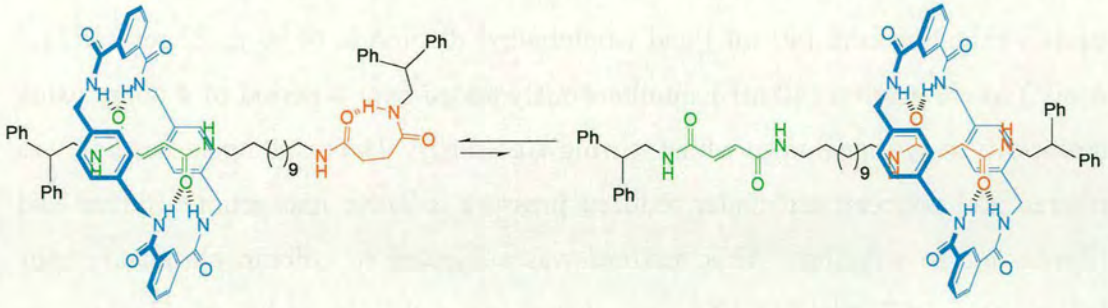

Figure 5.6 Translational isomerism in fumaramide-succinamide shuttle *E*-**2**.

5.3 Experimental

[2] - (1,4,7,14,17,20, - Hexaaza - 2,6,15,19 - tetraoxo - 3,5,9,12,16,18,22,25-terabenzocyclohexacosane) - ((*Z*)-hexanedioic acid (2,2 - diphenyl - ethyl) – amide-(hexanedioic acid (2,2-diphenyl-ethyl)-amide {12-[3-(2,2-diphenyl-ethylcarbamoyl)-acryloylamino]-dodecyl}-amide)-rotaxane, *Z*-3

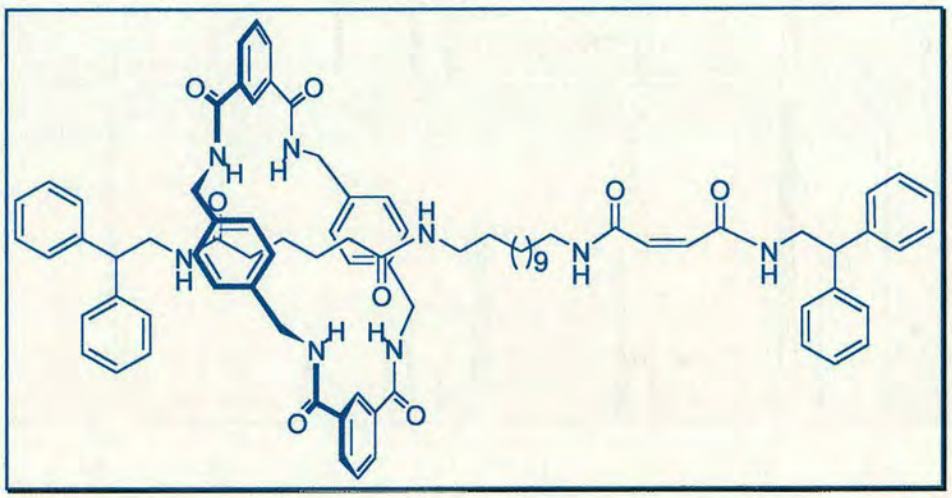

To a solution of hexanedioic acid (2,2-diphenyl-ethyl)-amide {12-[3-(2,2-diphenyl-ethylcarbamoyl)-acryloylamino]-dodecyl}-amide, *Z*-7 (1.50 g, 1.9 mmol, 1 equiv.) with triethylamine (8 mL, 57 mmol, 30 equiv.) in 80 mL chloroform (stabilized with amylenes) was added solutions of *para*-xylylene diamine (3.10 g, 22.9 mmol, 12 equiv.) in chloroform (40 mL) and isophthaloyl dichloride (4.50 g, 22 mmol, 11.5 equiv.) in chloroform (40 mL) simultaneously added over a period of 4 hours using motor-driven syringe pumps whilst stirring vigorously. The resulting suspension was filtered and concentrated under reduced pressure to leave unconsumed thread and [2]rotaxane in solution. This mixture was subjected to column chromatography (silica gel, 3:97 MeOH:$CHCl_3$ as eluent) to yield, in order of elution, the unconsumed thread and the [2]rotaxane.

Selected data for ([2](1,7,14,20-Tetraaza-2,6,15,19-tetraoxo-3,5,9,12,16,18,22,25 cetrabenzocyclohexacosane)-(hexanedioic acid (2,2-diphenyl-ethyl)-amide {12-[3-(2,2-diphenyl-ethylcarbamoyl)-acryloylamino]-dodecyl}-amide)-rotaxane,

***Z*-3**: Yield 0.5 g, (20%): m.p. 115 °C; ^{1}H NMR (400 MHz, $CDCl_3$): δ = 8.82 (brt, 1H, NHCOCH=CH), 8.24 (brs, 3H, ArH_C & CH=CHCONH), 8.13 (dd, *J* = 7.8, 1.5 Hz, 4H, ArH_B), 7.63 (t, *J* = 5.3 Hz, 4H, NH_D), 7.53 (t, *J* = 7.8 Hz, 2H, ArH_A), 7.32–7.15 (m, 20H, ArH, phenyl), 7.05 (s, 8H, ArH_F), 6.20 (brt, *J* = 5.6 Hz, 1H, $(CH_2)_4CONH$), 6.03 (brt, *J* = 5.1 Hz, 1H, $NHCO(CH_2)_4$), 5.79 (d, *J* = 13.4 Hz, 1H, CH=CH), 5.71 (d, *J* = 13.4 Hz, 1H, CH=CH), 4.55 (dd, *J* = 14.2, 5.8 Hz, 4H, CH_{2E}), 4.45 (dd, *J* = 14.4, 5.3 Hz, 4H, CH_{2E}), 4.19 (t, *J* = 7.8 Hz, 1H, $CH=CHCONHCH_2CHPh_2$), 4.13 (t, *J* = 7.8 Hz, 1H, $Ph_2CHCH_2NHCO(CH_2)_2$), 3.87 (2d, *J* = 7.8 Hz, 2H, $CH=CHCONHCH_2CHPh_2$), 3.66 (2d, *J* = 7.8 Hz, 2H, $Ph_2CHCH_2NHCO(CH_2)_2$), 2.94 (m, 4H, 2 x $CONHCH_2$), 1.41 (brm, 2H, CH_2, alkyl), 1.33 (brm, 4H, $NHCOCH_2(CH_2)_3$ and $(CH_2)_3CH_2CONH$), 1.25–1.18 (m, 22H, CH_2, alkyl), 0.76 (brm, 4H, $NHCOCH_2(CH_2)_2CH_2CONH$); ^{13}C NMR (100 MHz, $CDCl_3$): δ = 173.4, 173.3, 166.4, 165.4, 164.6, 142.1, 141.5, 137.6, 133.9, 133.2, 131.9, 131.8, 131.4, 129.2, 128.4, 128.0, 126.91, 124.4, 50.7, 50.2, 44.4, 44.3, 44.0, 40.1, 39.7, 35.5, 35.4, 29.4, 29.3, 29.2, 29.1, 29.0, 28.9, 28.6, 26.8, 26.7, 24.7, 24.5; HRMS (FAB, NBA matrix): *m/z* = 1317.70829 $[(M+H)^+]$ (anal. calcd for $C_{82}H_{93}N_8O_8$: *m/z* = 1317.71164).

Hexanedioic acid (2,2-diphenyl-ethyl)-amide {12-[3-(2,2-diphenyl-ethylcarbamoyl)-acryloylamino]-dodecyl}-amide, *Z*-7

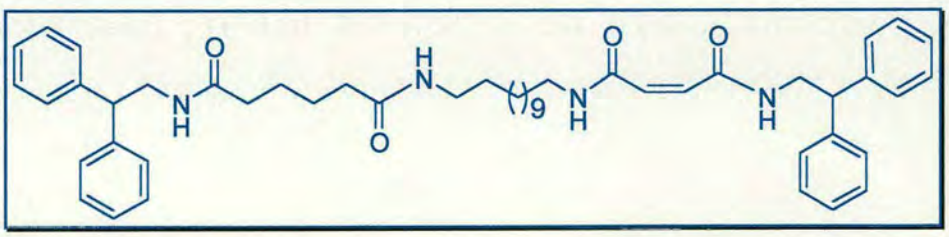

A solution of *cis*-3-(2,2-diphenyl-ethylcarbamoyl)-acrylic acid, **S8** (1.59 g, 5.37 mmol, 1 equiv.), hexanedioic acid (12-amino-dodecyl)-amide (2,2-diphenyl-ethyl)-amide, **S5** (3 g, 5.91 mmol, 1.1 equiv.) and DMAP (0.66 g, 5.37 mmol, 1 equiv.) in 200 mL of $CHCl_3$ was stirred at 0 °C for ten minutes followed by addition of EDCI.HCl (1.03 g, 5.37 mmol, 1 equiv.). The reaction mixture was stirred for 16 hours at room temperature. The resulting solution was washed with 1 M aqueous HCl (3 x 150 mL), saturated $NaHCO_3$ (3 x 150 mL), brine (150 mL), dried over anhydrous $MgSO_4$ and concentrated under reduced pressure to give the product as a white solid.

Selected data for hexanedioic acid (2,2-diphenyl-ethyl)-amide {12-[3-(2,2-diphenyl-ethylcarbamoyl)-acryloylamino]-dodecyl}-amide, *Z*-7: Yield 3.5 g, (83%): ^{1}H NMR (400 MHz, $CDCl_3$): δ = 8.45 (brt, 1H, NHCOCH=CH), 7.88 (brt, 1H, CH=CHCONH), 7.33–7.20 (m, 20H, ArH, phenyl), 6.02 (d, *J* = 13.3 Hz, 1H, CH=CH), 5.92 (d, *J* = 13.3 Hz, 1H, CH=CH), 5.72 (m, 2H, $NHCO(CH_2)_4$ & $(CH_2)_4CONH$), 4.26 (t, *J* = 8.0 Hz, 1H, $CH=CHCONHCH_2CHPh_2$), 4.20 (t, *J* = 8.0 Hz, 1H, $Ph_2CHCH_2NHCO(CH_2)_2$), 3.96 (2d, *J* = 8.0 Hz, 2H, $CH=CHCONHCH_2CHPh_2$), 3.89 (2d, *J* = 8.0 Hz, 2H, $Ph_2CHCH_2NHCO(CH_2)_2$), 3.23 (m, 4H, 2 x $CONHCH_2$), 2.10 (t, *J* = 7.3 Hz, 4H, $NHCOCH_2(CH_2)_3$ and $(CH_2)_3CH_2CONH$), 2.07 (t, *J* = 7.3 Hz, 2H, $NHCOCH_2(CH_2)_3$ or $(CH_2)_3CH_2CONH$), 1.55–1.47 (m, 8H, $NHCOCH_2(CH_2)_2CH_2CONH$ and CH_2, alkyl), 1.32–1.27 (m, 16H, CH_2, alkyl); ^{13}C NMR (100 MHz, $CDCl_3$): δ = 172.79, 172.63, 165.01, 164.58, 141.87, 141.81, 133.43, 131.36, 128.70, 128.67, 128.04, 126.81, 50.59, 50.30, 44.18, 43.77, 39.81, 39.53, 36.20, 36.07, 29.54, 29.33, 29.13, 29.03, 26.89, 26.84, 24.92; HRMS (FAB, NBA matrix): *m/z* = 785.49929 [$(M+H)^+$] (anal. calcd for $C_{50}H_{64}N_4O_4$: *m/z* = 785.50058).

Hexanedioic acid (2,2-diphenyl-ethyl)-amide {12-[3-(2,2-diphenyl-ethylcarbamoyl)-acryloylamino]-dodecyl}-amide, *E*-7

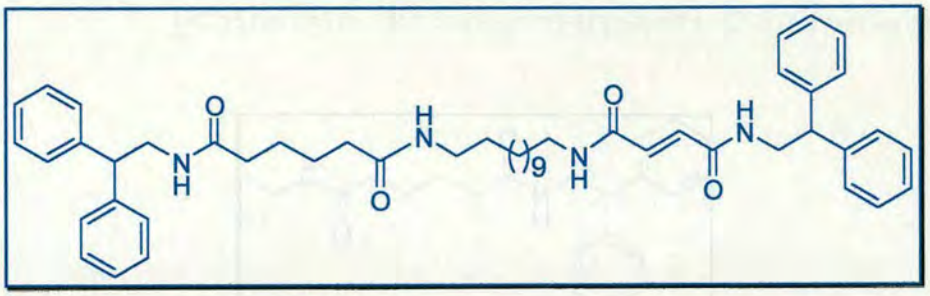

A solution of *trans*-3-(2,2-diphenyl-ethylcarbamoyl)-acrylic acid, **S7** (0.053 g, 0.18 mmol, 1 equiv.), hexanedioic acid (12-amino-dodecyl)-amide (2,2-diphenyl-ethyl)-amide, **S5** (0.10 g, 0.20 mmol. 1.1 equiv.) and DMAP (0.022 g, 0.18 mmol, 1 equiv.) in 10 mL of $CHCl_3$ was stirred at 0 °C for 10 minutes followed by addition of EDCI.HCl (0.034 g, 0.18 mmol, 1 equiv.). The reaction mixture was stirred for 16 hours at room temperature. To this was added 10 mL of $CHCl_3$ and the combined organic phase was washed with 1 M aqueous HCl (3 x 10 mL), saturated $NaHCO_3$ (3 x 10 mL), brine (10 mL), dried over anhydrous $MgSO_4$ and concentrated under reduced pressure to give the product as a white solid.

Selected data for hexanedioic acid (2,2-diphenyl-ethyl)-amide {12-[3-(2,2-diphenyl-ethylcarbamoyl)-acryloylamino]-dodecyl}-amide, *E*-7: Yield (could not be determined due to poor solubility – only ^{1}H NMR could be obtained); ^{1}H NMR (400 MHz, DMSO-d_6): δ = 8.47 (brt, 1H, CONH), 8.34 (brt, 1H, CONH), 7.82 (brt, 1H, CONH), 7.69 (brt, 1H, CONH), 7.31–7.19 (m, 20H, ArH, phenyl), 6.80 (d, J = 15.3 Hz, 1H, CH=CH), 6.73 (d, J = 15.3 Hz, 1H, CH=CH), 4.24 (t, J = 8.3 Hz, 1H, $CH_2CONHCH_2CHPh_2$), 4.19 (t, J = 8.2 Hz, 1H, $Ph_2CHCH_2NHCOCH{=}CH$), 3.82 (m, 2H, $CH_2CONHCH_2CHPh_2$), 3.69 (m, 2H, $Ph_2CHCH_2NHCOCH{=}CH$), 3.10 (m, 2H, $CH{=}CHCONHCH_2$ or CH_2NHCO), 3.01 (m, 2H, $CH{=}CHCONHCH_2$ or

$C\underline{H_2}NHCO$), 1.96 (m, 2H, $NHCOC\underline{H_2}$ or $C\underline{H_2}CONHCH_2CHPh_2$), 1.35 (m, 8H, CH_2, alkyl), 1.25 (m, 16H. CH_2, alkyl).

5-(2,2-Diphenyl-ethylcarbamoyl)-pentanoic acid ethyl ester, S1

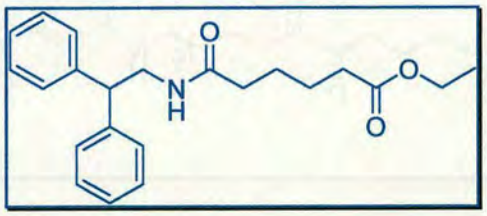

A solution of adiptic acid monoethyl ester (4.01 g, 23 mmol, 1 equiv.), 2,2-diphenylethyl amine (5.00 g, 25 mmol, 1.1 equiv.) and DMAP (2.81 g, 23 mmol, 1 equiv.) in 250 mL of CH_2Cl_2 was stirred at 0 °C for 10 minutes followed by addition of EDCI.HCl (4.42 g, 23 mmol, 1 equiv.). The reaction mixture was stirred for 16 hours at room temperature. The organic phase was washed with 1 M aqueous HCl (3 x 70 mL), saturated aqueous $NaHCO_3$ (3 x 70 mL), brine (70 mL), dried over anhydrous $MgSO_4$ and concentrated under reduced pressure to give the product as a white solid.

Selected data for 5-(2,2-diphenyl-ethylcarbamoyl)-pentanoic acid ethyl ester, S1: Yield 7.03 g (86%); m.p. 44 °C; ^{1}H NMR (400 MHz, $CDCl_3$): δ = 7.34–7.21 (m, 10H, ArH, phenyl), 5.70 (brt, 1H, NHCO), 4.23 (t, J = 8.0 Hz, 1H, $Ph_2C\underline{H}$), 4.13 (q, J = 7.0 Hz, $C\underline{H_2}CH_3$), 3.91 (2d, J = 8.0 Hz, 2H, $Ph_2CHC\underline{H_2}$), 2.26 (t, J = 7.0 Hz, 2H, $C\underline{H_2}CO_2$), 2.09 (t, J = 7.0 Hz, 2H, $NHCOC\underline{H_2}$), 1.56 (m, 4H, $NHCOCH_2C\underline{H_2}$ & $C\underline{H_2}CH_2CO_2$), 1.27 (t, J = 7.0 Hz, 3H, $CH_2C\underline{H_3}$); ^{13}C NMR (100 MHz, $CDCl_3$): δ = 173.83, 172.94, 142.34, 129.09, 128.46, 127.19, 60.68, 51.00, 44.17, 36.55, 34.31, 25.41, 24.69, 14.66; HRMS (FAB, THIOG matrix): *m/z* = 354.20660 [$(M+H)^+$] (anal. calcd for $C_{22}H_{28}NO_3$: *m/z* = 354.20692).

5-(2,2-Diphenyl-ethylcarbamoyl)-pentanoic acid, S2

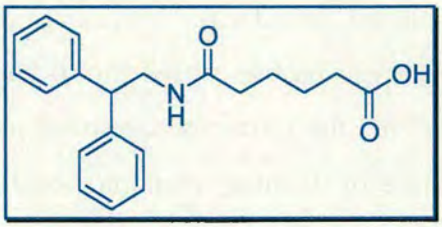

To a solution of 5-(2,2-diphenyl-ethylcarbamoyl)-pentanoic acid ethyl ester, **S1** (7.03 g, 19.9 mmol, 1 equiv.) in 50 mL of EtOH was added aqueous KOH (5.58 g in 9 mL of H_2O, 99.4 mmol, 5 equiv.) and stirred for 2 hours at 78 °C. A yellow solution was obtained that was cooled to room temperature and poured into water followed by acidifying with dropwise addition of concentrated HCl which resulted in a white precipitate. This was filtered and dried to give the product.

Selected data for 5-(2,2-diphenyl-ethylcarbamoyl)-pentanoic acid, S2: Yield 6.12 g (95%); m.p. 124 °C; ^{1}H NMR (400 MHz, $CDCl_3$): δ = 7.36–7.23 (m, 10H, ArH, phenyl), 5.55 (brt, 1H, NHCO), 4.21 (t, J = 7.8 Hz, 1H, $Ph_2C\underline{H}$), 3.92 (2d, J = 7.8 Hz, 2H, $Ph_2CHC\underline{H_2}$), 2.33 (t, J = 6.8 Hz, 2H, $C\underline{H_2}CO_2H$), 2.12 (t, J = 6.8 Hz, 2H, $NHCOC\underline{H_2}$), 1.59 (m, 4H, $NHCOCH_2C\underline{H_2}$ & $C\underline{H_2}CH_2CO_2H$); ^{13}C NMR (100 MHz, $CDCl_3$): δ = 178.22, 172.79, 141.75, 128.74, 128.04, 126.87, 50.55, 43.79, 36.16, 33.53, 24.86, 24.05; HRMS (FAB, THIOG matrix): *m/z* = 326.17637 [$(M+H)^+$] (anal. calcd for $C_{20}H_{24}NO_3$: *m/z* = 326.17562).

(12-Amino-dodecyl)-carbamic acid *tert*-butyl ester, S3

To a solution of 1,12-diaminododecane (20 g, 100 mmol, 1 equiv.) in 600 mL of $CHCl_3$ (slight suspension) was added a solution of di-*tert*-butyl dicarbonate (10.9 g, 50 mmol, 0.5 equiv.) in 200 mL of $CHCl_3$. Immediate precipitation occurred on addition and the resulting suspension was stirred for 16 hours at room temperature. The precipitate was filtered and the filtrate concentrated under reduced pressure to give a white solid (a mixture of diamine, monoprotected and diprotected amine). The white solid was subjected to column chromatography (silica gel, 5:95 MeOH:$CHCl_3$ to elute the diprotected amine and 1:10:89 NH_4OH:MeOH:$CHCl_3$ to yield the monoprotected amine).

Selected data for (12-amino-dodecyl)-carbamic acid *tert*-butyl ester, S3: Yield 8.53 g (57%); m.p. 96 °C; ^1H NMR (400 MHz, $CDCl_3$): δ = 4.54 (brs, 1H, OCONH), 3.09 (m, 2H, OCONHC$\underline{H}_2$), 2.67 (t, J = 6.8 Hz, 2H, C$\underline{H}_2NH_2$), 1.43 (brs, 13H, CH_3, *t*-butyl & CH_2, alkyl), 1.38 (brs, 2H, NH_2), 1.25 (brs, 16H, CH_2, alkyl); ^{13}C NMR (100 MHz, $CDCl_3$): δ = 157.64, 79.69, 42.24, 40.63, 33.86, 30.06, 29.60, 29.55, 29.53, 29.48, 29.28, 28.42, 26.88, 26.80; HRMS (FAB, THIOG matrix): *m/z* = 301.28491 $[(M+H)^+]$ (anal. calcd for $C_{17}H_{37}N_2O_2$: *m/z* = 301.28550).

Diprotected:

Selected data for (12-*tert*-butoxycarbonylamino-dodecyl)-carbamic acid *tert*-butyl ester, S3b: Yield 3.7 g (43%); m.p. 115 °C; ^1H NMR (400 MHz, $CDCl_3$): δ = 4.51 (brs, 2H, OCONH), 3.10 (m, 4H, OCONHC$\underline{H}_2$), 1.45 (brs, 13H, CH_3, *t*-butyl & CH_2, alkyl), 1.27 (m, 16H, CH_2, alkyl); ^{13}C NMR (100 MHz, $CDCl_3$): δ = 157.62, 79.69, 40.63, 30.06, 29.51, 29.27, 28.43, 26.79, 20.60; HRMS (FAB, THIOG

matrix): m/z = 401.33864 [$(M+H)^+$] (anal. calcd for $C_{22}H_{45}N_2O_4$: m/z = 401.33793).

(12-[5-(2,2-Diphenyl-ethylcarbamoyl)-pentanoylamino]-dodecyl}-carbamic acid *tert*-butyl ester, S4

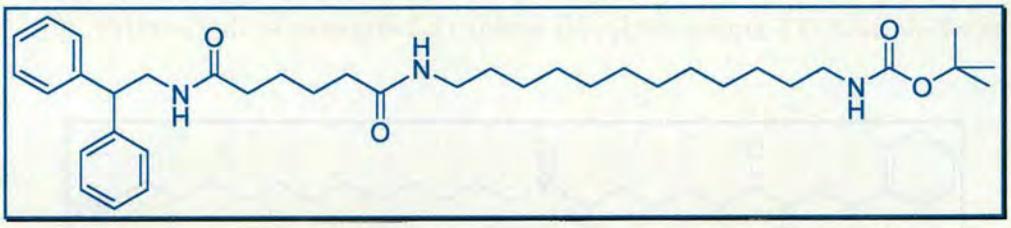

A solution of 5-(2,2-diphenyl-ethylcarbamoyl)-pentanoic acid, **S2** (0.50 g, 1.54 mmol, 1 equiv.), (12-amino-dodecyl)-carbamic acid *tert*-butyl ester, **S3** (0.51 g, 1.69 mmol, 1.1 equiv.) and DMAP (0.19 g, 1.54 mmol, 1 equiv.) in 20 mL of $CHCl_3$ was stirred at 0 °C for 10 minutes followed by addition of EDCI.HCl (0.29 g, 1.54 mmol, 1 equiv.). The reaction mixture was stirred for 16 hours at room temperature. The reaction mixture was diluted with 10 mL of $CHCl_3$ and the organic phase was washed with 1 M aqueous HCl (3 x 10 mL), saturated $NaHCO_3$ (3 x 10 mL), brine (10 mL), dried over anhydrous $MgSO_4$ and concentrated under reduced pressure to give the product as a white solid.

Selected data for (12-[5-(2,2-diphenyl-ethylcarbamoyl)-pentanoylamino]-dodecyl}-carbamic acid *tert*-butyl ester, S4: Yield 0.85 g (92%); m.p. 114 °C; ^{1}H NMR (400 MHz, $CDCl_3$): δ = 7.33–7.20 (m, 10H, ArH, phenyl), 5.84 (t, J = 5.5 Hz, 1H, $(CH_2)_4CONH$), 5.79, (t, J = 5.5 Hz, 1H, Ph_2CHCH_2NHCO), 4.57 (brt, 1H, $NHCO_2$), 4.22 (t, J = 8.0 Hz, 1H, Ph_2CH), 3.90 (2d, J = 8.0 Hz, 2H, Ph_2CHCH_2), 3.23 (q, J = 7.3 Hz, 2H, $(CH_2)_4CONHCH_2$), 3.11 (m, 2H, CH_2NHCO_2), 2.10 (dt, J = 7.0 Hz, 4H, $Ph_2CHCH_2CONHCH_2$ & $(CH_2)_3CH_2CONH$), 1.56 (m, 4H, $Ph_2CHCH_2CONHCH_2CH_2$ & $(CH_2)_2CH_2CH_2CO_2$), 1.46 (s, 13H, $CONHCH_2CH_2$ & $CH_2CH_2NHCO_2$ & CH_3, *t*-butyl), 1.27 (brs, 16H, CH_2, alkyl); ^{13}C NMR (100 MHz,

$CDCl_3$): δ = 172.72, 172.55, 157.65, 141.86, 128.70, 128.05, 126.80, 50.60, 43.74, 40.64, 39.56, 36.19, 36.08, 30.06, 29.62, 29.50, 29.26, 28.43, 26.93, 26.79, 24.87, 24.85; HRMS (FAB, THIOG matrix): *m/z* = 326.44148 $[(M+H)^+]$ (anal. calcd for $C_{37}H_{58}N_3O_4$: *m/z* = 608.44273).

Hexanedioic acid (12-amino-dodecyl)-amide (2,2-diphenyl-ethyl)-amide, S5

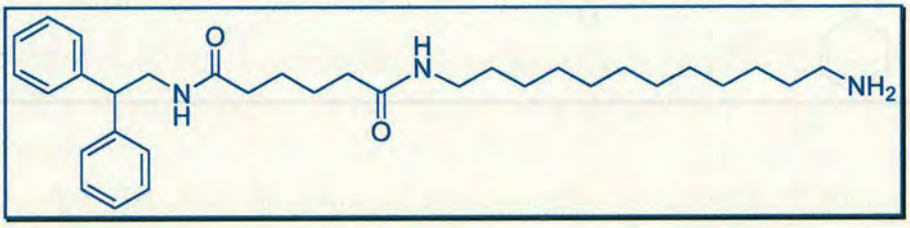

A solution of (12-[5-(2,2-diphenyl-ethylcarbamoyl)-pentanoylamino]-dodecyl}-carbamic acid *tert*-butyl ester, **S4** (0.40 g, 6.58 mmol, 1 equiv.) in 15 mL of trifluoroacetic acid was stirred at room temperature for 30 minutes. The reaction mixture was concentrated under reduced pressure and 20 mL of CH_2Cl_2 was added. The organic phase was washed with 0.1 M aqueous NaOH (2 x 10 mL), brine (10mL), dried over anhydrous $MgSO_4$ and concentrated under reduced pressure to give the product as a white solid.

Selected data for hexanedioic acid (12-amino-dodecyl)-amide (2,2-diphenyl-ethyl)-amide, S5: Yield 0.22 g (66%); m.p. 91 °C; ^{1}H NMR (400 MHz, $CDCl_3$): δ = 7.35–7.22 (m, 10H, ArH, phenyl), 5.77 & 5.75 (m, 2H, Ph_2CHCH_2CONH & $(CH_2)_4CONH$), 4.22 (t, *J* = 7.8 Hz, 1H, Ph_2CH), 3.91 (2d, *J* = 7.78 Hz, 2H, Ph_2CHCH_2), 3.24 (q, *J* = 7.8 Hz, 2H, $CONHCH_2$), 2.69 (m, 2H, NH_2), 2.12 (dt, *J* = 6.8 Hz, 4H, $Ph_2CHCH_2CONHCH_2$ & $(CH_2)_3CH_2CONH$), 1.58 (m, 4H, $Ph_2CHCH_2CONHCH_2CH_2$ & $(CH_2)_2CH_2CH_2CO_2$), 1.51 (m, 2H, $CONHCH_2CH_2$), 1.45 (m, 2H, CH_2NH_2), 1.28 (brs, 18H, CH_2, alkyl); ^{13}C NMR (100 MHz, $CDCl_3$): δ = 172.75, 172.58, 141.88, 128.70, 128.05, 126.80, 50.60, 43.75, 42.19, 39.55,

36.19, 36.07, 33.67, 29.62, 29.56, 29.51, 29.49, 29.45, 29.26, 26.92, 26.86, 24.89, 24.87; HRMS (FAB, THIOG matrix): *m/z* = 508.39143 [$(M+H)^+$] (anal. calcd for $C_{32}H_{50}N_3O_2$: *m/z* = 508.39030).

3-(2,2-Diphenyl-ethylcarbamoyl)-acrylic acid ethyl ester, S6

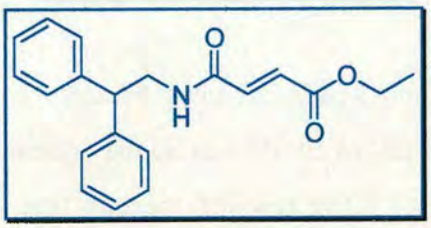

To a solution of 2,2-diphenylamine (5.00 g, 25 mmol, 1.1 equiv.) in 150 mL of CH_2Cl_2 was added fumaric acid monoethyl ester (3.32 g, 23 mmol, 1 equiv.), followed by addition of DMAP (2.81 g, 23 mmol, 1 equiv.). The resulting mixture was cooled to 0 °C and EDCI.HCl (4.42 g, 23 mmol, 1 equiv.) was added and stirred at room temperature for 16 hours. The reaction mixture was washed successively with 2 M aqueous HCl (50 mL), saturated $NaHCO_3$ (2 x 50 mL), brine (50 mL), dried over anhydrous $MgSO_4$ and concentrated under reduced pressure to give the product as a white solid.

Selected data for 3-(2,2-diphenyl-ethylcarbamoyl)-acrylic acid ethyl ester, S6: Yield 7.48 g, (91%); m.p. 112 °C; ^{1}H NMR (400 MHz, $CDCl_3$): δ = 7.67–7.1 (m, 10H, ArH, phenyl), 6.78 (2d, *J* = 15.3 Hz, 2H, CH=CH), 6.03 (brt, 1H, NHCO), 4.3–4.1 (m, 3H, Ph_2CH & CH_2CH_3), 4.01 (2d, *J* = 7.9 Hz, 2H, Ph_2CHCH_2), 1.32 (t, *J* = 7.2 Hz, 3H, CH_2CH_3); ^{13}C NMR (100 MHz, $CDCl_3$): δ = 165.0, 164.0, 141.92, 136.5, 130.9, 129.2, 128.4, 127.4, 61.57, 50.8, 44.55, 14.51; MS (FAB, NBA matrix): *m/z* = 324 [$(M+H)^+$]. Anal. calcd for $C_{20}H_{21}NO_3$: C 74.28, H 6.55, N 4.33. Found C 74.83, H 6.91, N 4.38.

***Trans*-3-(2,2-diphenyl-ethylcarbamoyl)-acrylic acid, S7**

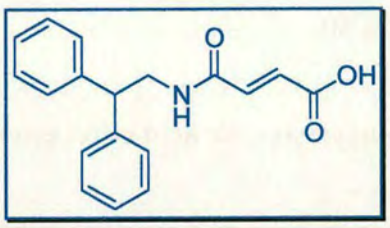

To a solution of 3-(2,2-diphenyl-ethylcarbamoyl)-acrylic acid ethyl ester, **S6** (1.00 g, 3.09 mmol, 1 equiv.) in 20 mL of EtOH was added aqueous NaOH (0.14 g in 1 mL H_2O, 3.40 mmol, 1.1 equiv.). The reaction mixture was left to stir for 3 hours at room temperature. The resulting pink solution was poured into water (20 mL) and precipitated by addition of small amounts of concentrated HCl to give the product as a white solid which was filtered and dried.

Selected data for *trans*-3-(2,2-diphenyl-ethylcarbamoyl)-acrylic acid, S7: Yield 0.93 g, (98%); m.p. >270 °C (decompose); ^{1}H NMR (400 MHz, DMSO-d_6): δ = 12.8 (brs, CO_2H), 8.56 (t, J = 5.8 Hz, 1H, NHCO), 7.32–7.16 (m, 10H, ArH, phenyl), 6.89 (d, J = 15.3 Hz, 1H, CH=CH), 6.48 (d, J = 15.3 Hz, 1H, CH=CH), 4.23 (t, J = 8.0 Hz, 1H, Ph_2CH), 3.83 (2d, J = 8.0 Hz, 2H, Ph_2CHCH_2); ^{13}C NMR (100 MHz, DMSO-d_6): δ = 166.8, 163.6, 143.1, 137.3, 132.9, 128.8, 128.2, 126.66, 50.3, 43.8; MS (FAB, NBA matrix): *m/z* = 296 [$(M+H)^+$]. Anal. calcd for $C_{18}H_{17}NO_3$: C 73.20, H 5.80, N 4.70. Found C 73.10, H 5.20, N 4.73.

***Cis*-3-(2,2-diphenyl-ethylcarbamoyl)-acrylic acid, S8**

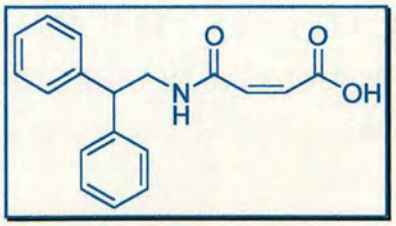

To a solution of maleic anhydride (2.50 g, 25 mmol, 1 equiv.) and triethylamine (5.3 mL, 38 mmol, 1.5 equiv.) in 80 mL of $CHCl_3$ was added 2,2-diphenylamine (5.50 g, 28 mmol, 1.1 equiv.) and left to stir at room temperature for 16 hours. The organic layer was washed with 1 M HCl (3 x 80 mL), saturated $NaHCO_3$ (3 x 80 mL), brine (80 mL), dried over anhydrous $MgSO_4$ and evaporated under reduced pressure to give a white solid.

Selected data for *cis*-3-(2,2-diphenyl-ethylcarbamoyl)-acrylic acid, S8: Yield 6.56 g, (87%): m.p. 209 °C; ^{1}H NMR (400 MHz, $CHCl_3$): δ = 7.29–7.23 (m, 4H, ArH, phenyl), 7.20–7.14 (m, 6H, ArH, phenyl), 6.43 (brt, J = 5.7 Hz, 1H, NHCO), 6.19 (d, J = 12.6 Hz, 1H, CH_2CO_2H), 6.02 (d, J = 12.6 Hz, 1H, $NHCOCH_2$), 4.18 (t, J = 8.0 Hz, 1H, $Ph_2C\underline{H}_2$), 3.95 (dd, J = 8.0 Hz, 5.7 Hz, 2H, $Ph_2CH_2C\underline{H}$); ^{13}C NMR (100 MHz, $CDCl_3$): δ = 166.0, 164.5, 140.7, 137.1, 130.2, 129.0, 127.9, 127.4, 50.0, 44.6; HRMS (FAB, THIOG matrix): m/z = 262.12884 $[(M+H)^+]$ (anal. calcd for $C_{18}H_{18}NO_3$: m/z = 296.12867). Anal. calcd for $C_{18}H_{17}NO_3$: C 73.20, H 5.80, N 4.74. Found C 73.13, H 5.85, N 4.61.

5.4 References

[1] For recent reviews see a) V. Balzani, A. Credi, F. M. Raymo, J. F. Stoddart, *Angew. Chem. Int. Ed.* **2000**, *39*, 3349–3391. b) Special issue on *Molecular Machines*, *Acc. Chem. Res.* **2001**, *34*, 409–522. c) Special issue on *Molecular Machines and Motors*. Structure and Bonding *Vol. 99* (Ed.: J. -P. Sauvage), Springer, Berlin, **2001**.

[2] A. C. Benniston, A. Harriman, *Angew. Chem. Int. Ed. Engl.* **1993**, *32*, 1459–1461.

[3] A. C. Benniston, A. Harriman, V. M. Lynch, *J. Am. Chem. Soc.* **1995**, *117*, 5275–5291.

[4] A. C. Benniston, *Chem. Soc. Rev.* **1996**, *25*, 427–436.

[5] H. Murakami, A. Kawabuchi, K. Kotoo, M. Kunitake, N. Nakashima, *J. Am. Chem. Soc.* **1997**, *119*, 7605–7606.

[6] P. R. Ashton, R. Ballardini, V. Balzani, A. Credi, K. R. Dress, E. Ishow, C. J. Kleverlaan, O. Kocian, J. A. Preece, N. Spencer, J. F. Stoddart, M. Venturi, S. Wenger, *Chem. Eur. J.* **2000**, *6*, 3558–3574.

[7] N. Armaroli, V. Balzani, J. P. Collin, P. Gaviña, J. -P. Sauvage, B. Ventura, *J. Am. Chem. Soc.* **1999**, *121*, 4397–4408.

[8] A. M. Brouwer, C. Frochot, F. G. Gatti, D. A. Leigh, L. Mottier, F. Paolucci, S. Roffia, G. W. H. Wurpel, *Science* **2001**, *291*, 2124–2128.

[9] G. W. H. Wurpel, A. M. Brouwer, I. H. M. van Stokkum, A. Farran, D. A. Leigh, *J. Am. Chem. Soc.* **2001**, *123*, 11327–11328.

[10] C. A. Stanier, S. J. Alderman, T. D. W. Claridge, H. L. Anderson, *Angew. Chem. Int. Ed.* **2002**, *41*, 1769–1772.

[11] For examples featuring the use of stimuli other than light to induce shuttling in rotaxanes see a) R. A. Bissell, E. Córdova, A. E. Kaifer, J. F. Stoddart, *Nature* **1994**, *369*, 133–137. b) J. P. Collin, P. Gaviña, J. -P. Sauvage, *New J. Chem.* **1997**, *21*, 525–528. c) P. R. Ashton, R. Ballardini, V. Balzani, S. E.

Boyd, A. Credi, M. T. Gandolfi, M. Gómez-López, S. Iqbal, D. Philp, J. A. Preece, L. Prodi, H. G. Ricketts, J. F. Stoddart, M. S. Tolley, M. Venturi, A. J. P. White, D. J. Williams, *Chem. Eur. J.* **1997**, *3*, 152–170. d) M. -V. Martínez-Díaz, N. Spencer, J. F. Stoddart, *Angew. Chem. Int. Ed. Engl.* **1997**, *36*, 1904–1907. e) C. Gong, H. W. Gibson, *Angew. Chem. Int. Ed. Engl.* **1997**, *36*, 2331–2333. f) A. S. Lane, D. A. Leigh, A. Murphy, *J. Am. Chem. Soc.* **1997**, *119*, 11092–11093. g) P. R. Ashton, R. Ballardini, V. Balzani, I. Baxter, A. Credi, M. C. T. Fyfe, M. T. Gandolfi, M. Gómez-López, M. -V. Martínez-Díaz, A. Piersanti, N. Spencer, J. F. Stoddart, M. Venturi, A. J. P. White, D. J. Williams, *J. Am. Chem. Soc.* **1998**, *120*, 11932–11942. h) C. P. Collier, E. W. Wong, M. Belohradsky, F. M. Raymo, J. F. Stoddart, P. J. Kuekes, R. S. Williams, J. R. Heath, *Science* **1999**, *285*, 391–394. i) H. Shigekawa, K. Miyake, J. Sumaoka, A. Harada, M. Komiyama, *J. Am. Chem. Soc.* **2000**, *122*, 5411–5412. j) C. P. Collier, J. O. Jeppesen, Y. Luo, J. Perkins, E. W. Wong, J. R. Heath, J. F. Stoddart, *J. Am. Chem. Soc.* **2001**, *123*, 12632–12641. k) M. C. Jimenez-Molero, C. Dietrich-Buchecker, J. -P. Sauvage, *Chem. Eur. J.* **2002**, *8*, 1456–1466. l) Y. Luo, C. P. Collier, J. O. Jeppesen, K. A. Nielsen, E. Delonno, G. Ho, J. Perkins, H. R. Tseng, T. Yamamoto, J. F. Stoddart, J. R. Heath, *Chem. Phys. Chem.* **2002**, *3*, 519–525. For recent accounts from the UCLA and Strasbourg groups see m) A. R. Pease, J. O. Jeppesen, J. F. Stoddart, Y. Luo, C. P. Collier, J. R. Heath, *Acc. Chem. Res.* **2001**, *34*, 433–444. n) J. P. Collin, C. Dietrich-Buchecker, P. Gaviña, M. C. Jimenez-Molero, J. -P. Sauvage, *Acc. Chem. Res.* **2001**, *34*, 477–487.

[12] G. Campari, M. Fagnoni, M. Mella, A. Albini, *Tetrahedron Asym.* **2000**, *11*, 1891–1906.

[13] F. G. Gatti, D. A. Leigh, S. A. Nepogodiev, A. M. Z. Slawin, S. J. Teat, J. K. Y. Wong, *J. Am. Chem. Soc.* **2001**, *123*, 5983–5989.

[14] The wavelength for the reaction has not yet been optimized.

[15] ^{1}H NMR experiments show that the macrocycle spins >10^6 times faster in the *Z*-form of the rotaxane than the *E*-form in CD_2Cl_2 at 233 K!

[16] G. Brancato, F. Coutrot, D. A. Leigh, A. Murphy, J. K. Y. Wong, F. Zerbetto, *Proc. Natl. Acad. Sci. USA* **2002**, *99*, 4967–4971.

[17] V. Bermudez, N. Capron, T. Gase, F. G. Gatti, F. Kajzar, D. A. Leigh, F. Zerbetto, S. W. Zhang, *Nature* **2000**, *406*, 608–611.

[18] D. A. Leigh and J. K. Y. Wong, unpublished results.

[19] The yield of the adipamide-maleamide rotaxane *Z*-**3** (20%) is reproducibly higher than that of the model single site adipamide rotaxane shown in Figure 2 (8%). The significant differences in yield might indicate that the intramolecularly hydrogen bonded 9 membered ring conformer [S. H. Gellman, G. P. Dado, G. -B. Liang, B. R. Adams, *J. Am. Chem. Soc.* **1991**, *113*, 1164–1173] for the adipamide unit has very different stabilities in both the one- and two-station adipamide threads and possibly also rotaxane *Z*-**3**.

CHAPTER SIX

The Ultimate Challenge: Unidirectional Rotation in a [2]Catenane

Prepared as:

An abbreviated form to be submitted to Nature:

Unidirectional Ring Rotation in a Mechanically-linked Molecule

David A Leigh and Jenny K Y Wong

"Do, or do not. There is no try."

Yoda

The Ultimate Challenge: Unidirectional Rotation in a [2]Catenane – Synopsis

Having established a method for controlling the translation of the macrocycle along the thread in a [2]rotaxane using light, we applied the same principles in an attempt to control the direction of rotation in a [2]catenane. The design criteria of such a molecule is rather challenging; it requires five different stations (including two sets of interchangeable pairs), four of which must have considerably different binding affinities.

The 21-step synthesis and characterisation of three [2]catenane diastereomers which can be interconverted in the sequence E,E-***I***→Z,E-***I***→Z,Z-***I***→E,E-***I*** *using light of two wavelengths and heat to drive the motion is described. Comparison of the* ^1H *NMR spectra of the various [2]catenane diastereomers with those of the corresponding macrocycles show unambiguously that the benzylic amide macrocycle moves from station to station as outlined in Scheme I. The question of whether this is really unidirectional motion is discussed.*

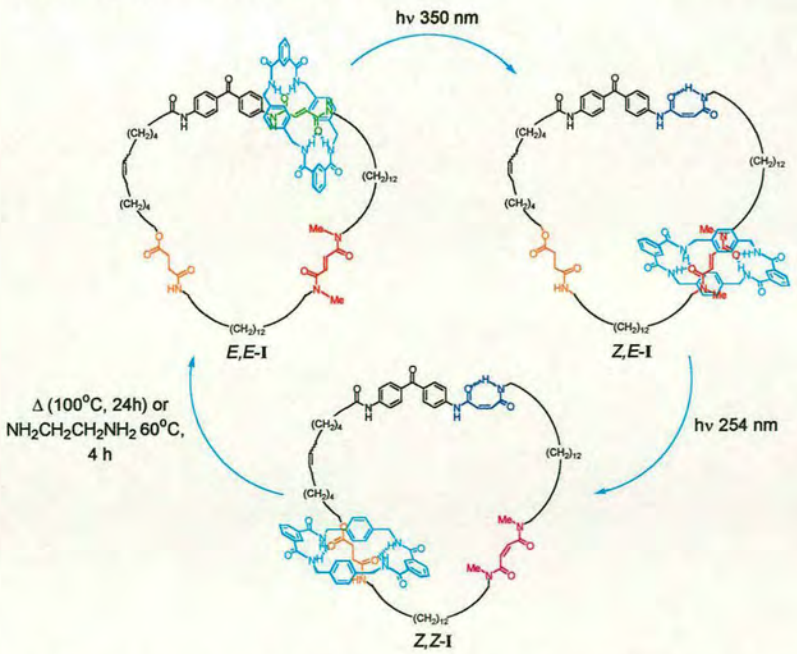

Scheme I *Unidirectional rotation of the benzylic amide macrocycle in a three-station [2]catenane.*

6.1 Introduction

F_1-ATPase is part of the multiprotein ATP-synthase assembly that synthesises ATP from ADP and inorganic phosphate in mitochondria, bacteria and chloroplasts.[1,2] The enzyme acts as a rotary molecular motor (Figure 6.1) in which the γ subunit turns unidirectionally within the central core of the C_3-symmetric $\alpha_3\beta_3$ hexamer when ATP is formed (or hydrolysed). The rotation consists of discrete 120° steps, each associated with an ATP binding event in one of the catalytic β subunits, and is powered by proton flow across the membrane to which the ATPsynthase is attached.

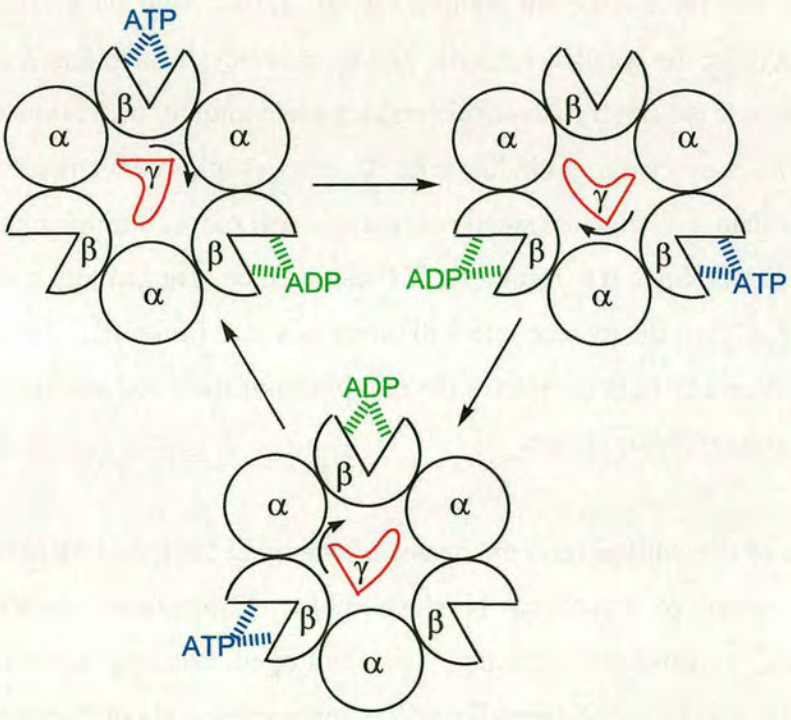

Figure 6.1 Rotation of the γ-subunit inside the central core of F_1-ATPase during the synthesis of ATP from ADP.

Inspired by the sublime control of molecular motion in biology, the first reports of designed unidirectional rotation of submolecular fragments about carbon-carbon single[3,4] and double[5-8] bonds in synthetic molecules have recently appeared. Here we report the first example of stimuli-driven directional rotation in a molecule where the

components are not connected by covalent bonds. We describe the design, synthesis and characterisation of a mechanically interlocked molecular assembly (a [2]catenane) in which a ring can be made to move around another sequentially, from one binding site ('station') to another in discrete 120° steps, driven by changes in binding energy induced by light and heat.

6.2 Results and discussion

The design of the [2]catenane is shown in cartoon form in Figure 6.2 and consists of two different macrocycles which are mechanically interlocked. The larger macrocycle has three different stations, A, B and C, each with different binding affinities (K_a) for the smaller, benzylic amide, macrocycle such that K_aA>K_aB>K_aC. Thus, in State I, the small macrocycle resides preferentially on station A. If binding site A can be converted to a binding site, A', that has a lower binding affinity for the macrocycle than K_aC then the small macrocycle will move, through biased Brownian motion, to site B (State II). Similarly, if B can then be changed into a station B' such that K_aB'<K_aC then the macrocycle will move to site C (State III). Finally, changing A' back to A and B' to B completes the revolution of the small macrocycle about the larger one and resets the system.

The choice of the stations (and the means of changing their binding affinities) comes from the series of hydrogen bond-assembled [2]rotaxanes developed in our laboratories.[9-17] Threads containing two hydrogen bonding sites (e.g. amides) template the formation of benzylic amide macrocycles about themselves to form rotaxanes. The yields of rotaxane vary from 0–97% depending upon the complimentarity between the macrocycle and the template. Several factors (Figure 6.3) affect both the template efficacy and the nature of the intercomponent hydrogen bonding interactions (NH···O=C distances, angles *etc*) including; the hydrogen bond basicity of the functional groups (e.g. amides are better than esters), preorganisation (e.g. fumaramide is better than succinamide) and distance between the binding sites

(succinamide better than adipamide), steric hindrance (fumaramide better than *N,N*-dimethylfumaramide).

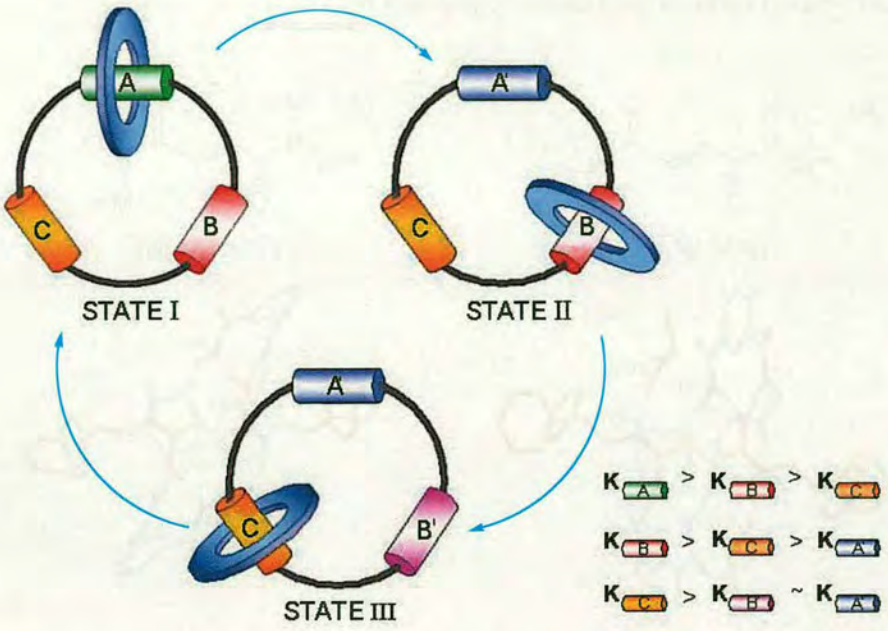

Figure 6.2 Unidirectional rotational motion in a three-station [2]catenane.

Fumaramide (Figure 6.3a) is a particularly good template because the double bond holds the amide groups of the thread rigidly in a close-to-ideal arrangement to hydrogen bond to the amide groups of the forming macrocycle.[13] However, after rotaxane formation, these strong interactions can be 'switched off' by photoisomerisation (either through direct irradiation at 254 nm or at 350 nm with an appropriate sensitizer such as benzophenone) of the *trans*-olefin to the *cis*-(maleamide) diastereomer. In this form (Figure 6.3d) only two hydrogen bonds can be formed between the macrocycle and the thread and so it is far more weakly held. *N,N'*-Dimethylfumaramide is a poorer binding template, probably because of the steric bulk of the methyl groups and the possibility of tertiary amide rotamers which are sterically mis-matched with the macrocycle. The succinic amide ester is a poorer station than the fumaramide derivatives because of the lack of rigidity in the template

and because ester groups are poorer hydrogen bond acceptors than amides. The succinic amide ester station has previously been shown to display excellent positional discrimination between the fumaramide and maleamide sites in two-station [2]rotaxane-based molecular shuttles (Chapter Five).

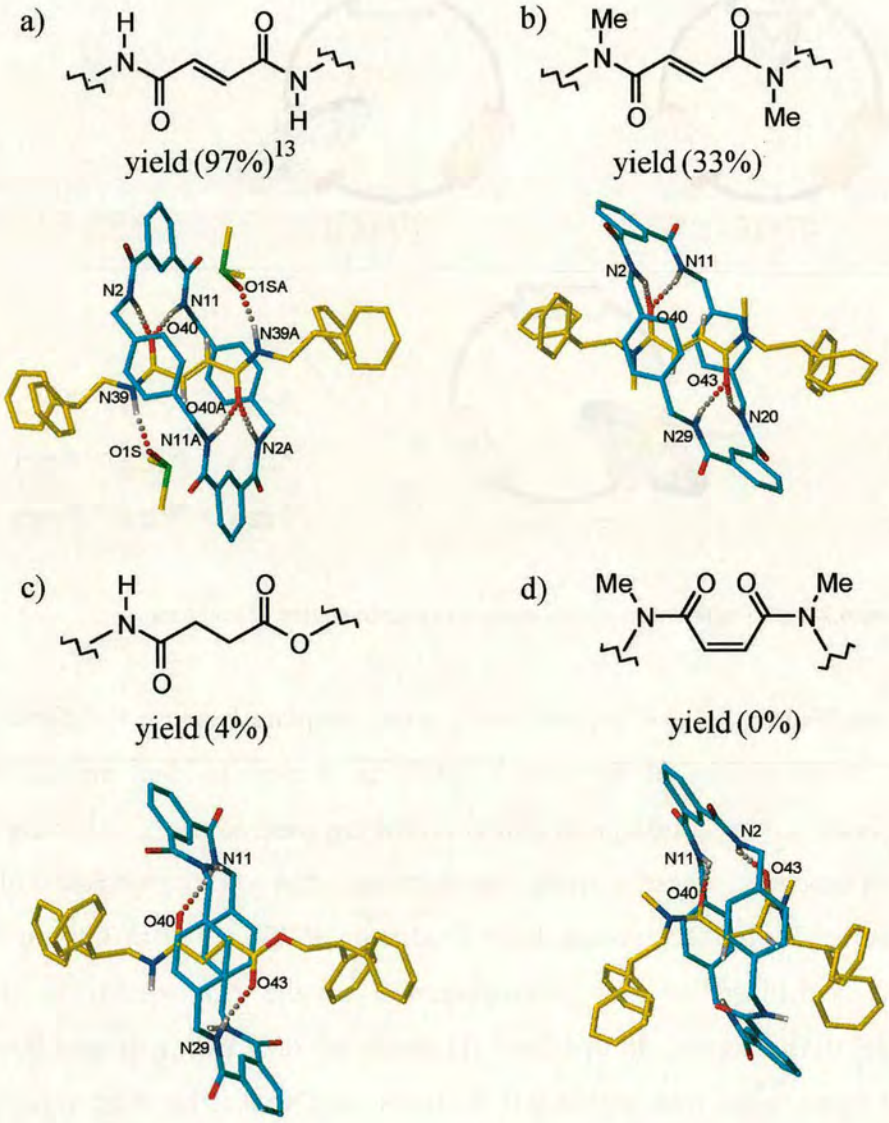

Figure 6.3 *X*-ray structures of model single binding site [2]rotaxanes showing hydrogen bonding characteristics of various hydrogen bonding stations in order of macrocycle binding affinity – (a) strongest → (d) weakest: (a) fumaramide; (b) *N,N'*-dimethylfumaramide; (c) succinic amide ester; (d) *N,N'*-dimethylmaleamide.

The design of the [2]catenane in chemical structure terms is shown in Figure 6.4. The three stations chosen are, in predicted order of binding affinity for the macrocycle: (i) a secondary amide fumaramide group (shown in green); (ii) a tertiary amide fumaramide group (shown in red); and (iii) a succinic amide ester group (shown in orange). To the highest affinity fumaramide station was attached a benzophenone unit to enable sensitized isomerisation of that station at 350 nm. Studies on a model [2]rotaxane **2** (Scheme 6.1) showed that (i) the benzylic amide macrocycle exhibits excellent positional discrimination between the different fumaramide stations and (ii) the difference in distances between the benzophenone and the two fumaramide groups was sufficient to allow complete discrimination between the sites in the sensitized photoisomerism reaction.

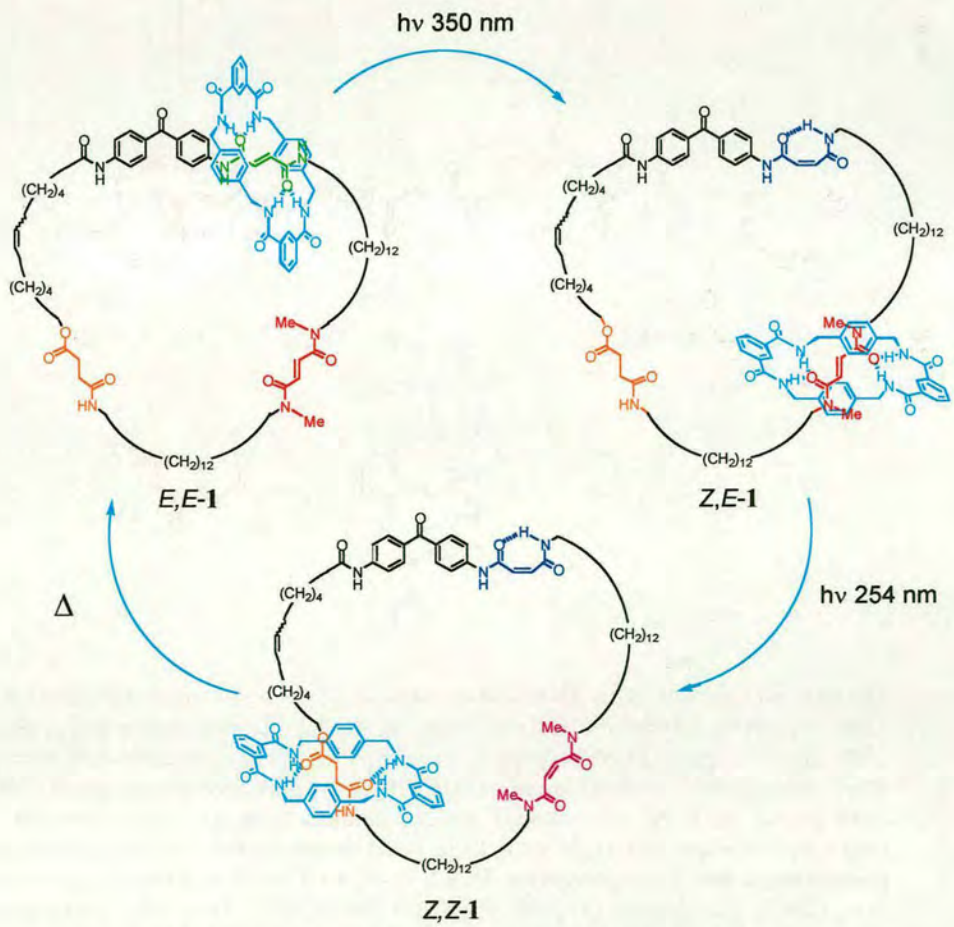

Figure 6.4 Design of a unidirectional rotating [2]catenane, **1**.

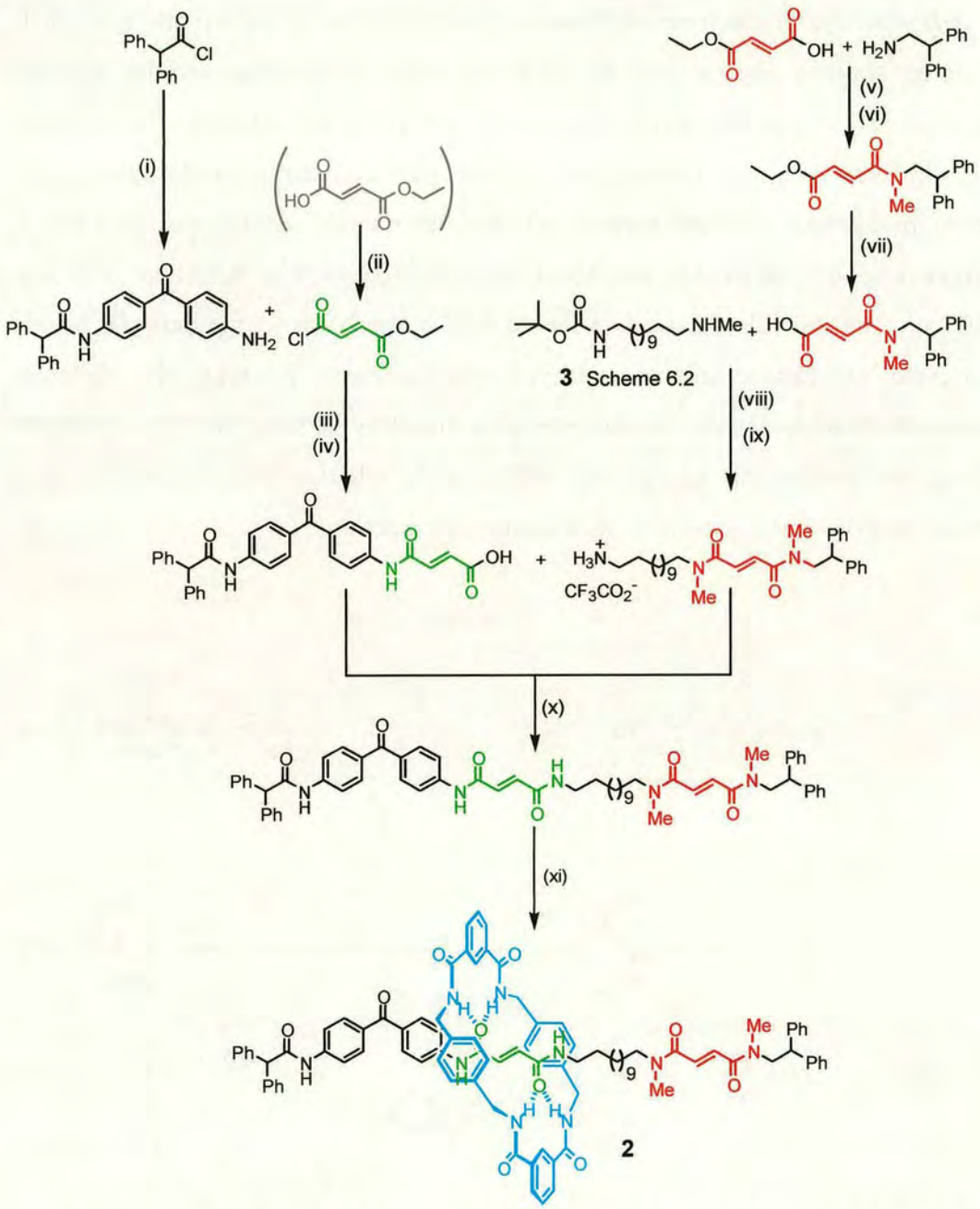

Scheme 6.1 Synthesis of molecular shuttle, **2**. (i) 4,4'-diaminobenzophenone, Et_3N, THF, 2 h, 90%. (ii) thionyl chloride, CH_2Cl_2, 40 °C, 40 min., quantitative. (iii) Et_3N, THF, 2h, 77%. (iv) 1 M NaOH(aq), THF, 22 h, 98%. (v) 1-(3-dimethylaminopropyl)-3-ethyl-carbodiimide hydrochloride (EDCI.HCl), 4-dimethylaminopyridine (DMAP), CH_2Cl_2, 16 h, 91%. (vi) methyl iodide, sodium hydride, DMF, 30 min., 76%. (vii) 1 M NaOH(aq), EtOH, 30 min., 84%. (viii) benzotriazol-1-yloxytris(dimethylamino) phosphonium hexafluorophosphate (BOP), Et_3N, $CHCl_3$, 16 h, 94%. (ix) trifluoroacetic acid, $CHCl_3$, quantitative. (x) BOP, Et_3N, 1/9 DMF/$CHCl_3$, 16 h, 24%. (xi) isophthaloyl dichloride, *p*-xylylene diamine, Et_3N, 1/9 MeCN/$CHCl_3$, 2 h, 22 %.

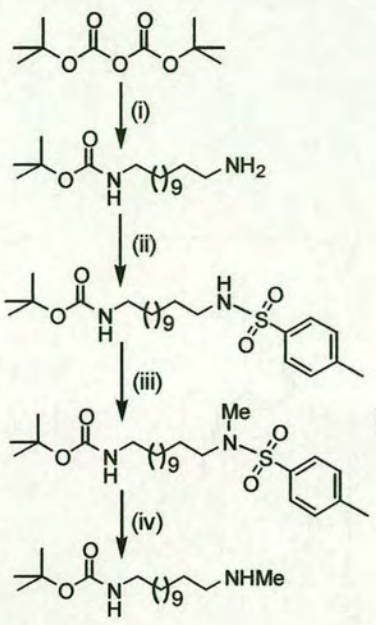

3

Scheme 6.2 Synthesis of lipophilic spacer, **3**. (i) 1,12-diaminododecane, $CHCl_3$, 16 h, 57%. (ii) *p*-toluenesulfonyl chloride, Et_3N, 1/5 THF/$CHCl_3$, 16 h, 88%. (iii) methyl iodide, K_2CO_3, acetone, 40 °C, 48 h, 98%. (iv) sodium/naphthalene, DME, –35 °C, 40 min., 85%.

The three station [2]catenane, **1**, was synthesised according to scheme 6.3. The main features of the synthesis are the two cyclisation reactions that form each ring. Closure of the large macrocycle, *E,E*-**4**, proceeds in 59% yield *via* ring closing metathesis with Grubbs' catalyst, a remarkable yield for formation of a 63-membered ring. The hydrogen bond templated cyclisation of the benzylic amide macrocycle around the bigger macrocycle to form the [2]catenane, *E,E*-**1**, proceeds in 50% yield and is accompanied by formation of 21% of the corresponding [3]catenane (two of the small rings locked onto the bigger ring), *E,E*-**5**. [4]Catenane could be detected in the product distribution by mass spectrometry but was not isolated.

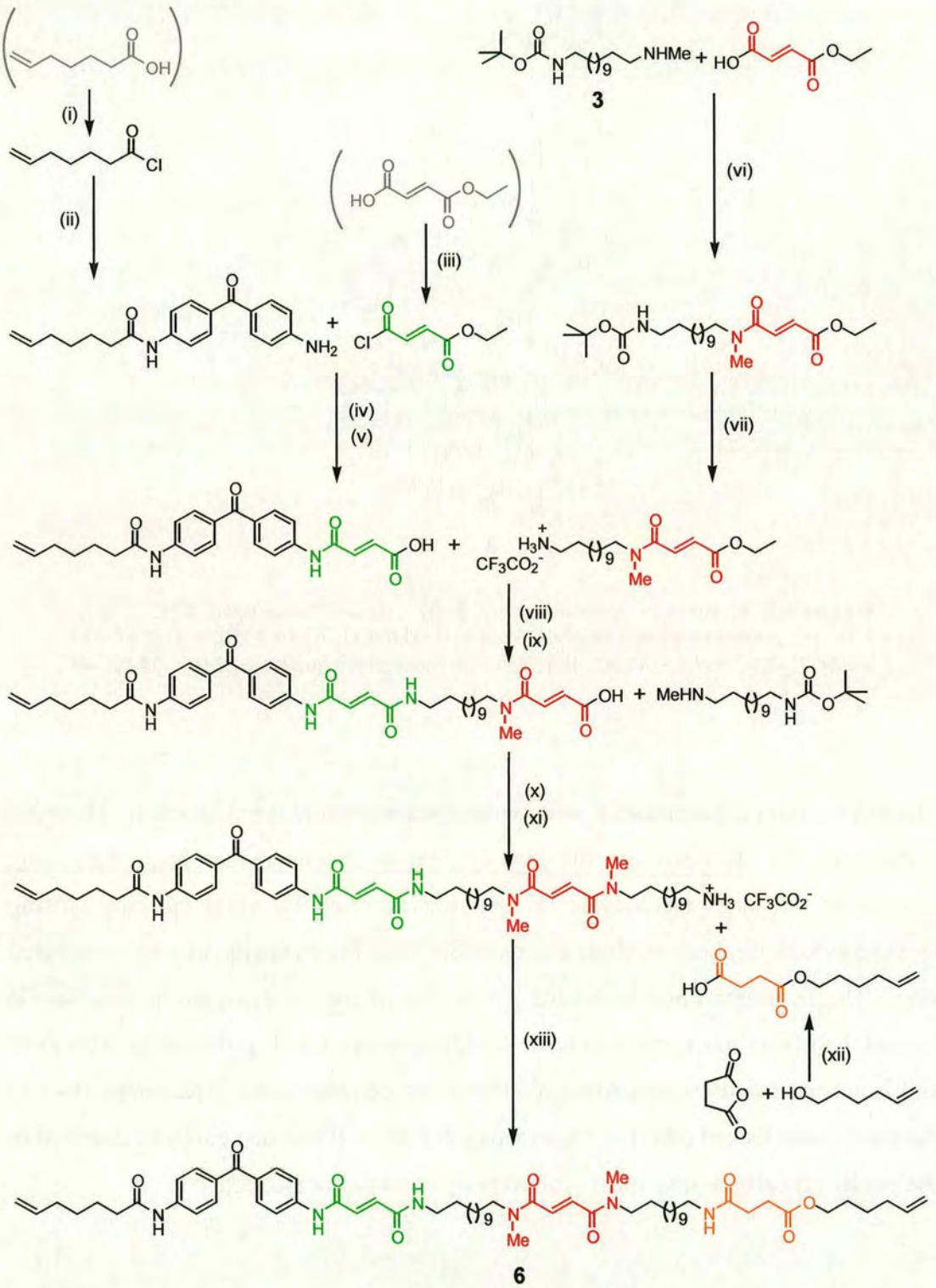

Scheme 6.3a Synthesis of three-station macrocycle precursor, **6**. (i) thionyl chloride, CH_2Cl_2, 65 °C, 2 h, quantitative. (ii) 4,4'-diaminobenzophenone, Et_3N, THF, 2 h, 96%.

(iii) thionyl chloride, CH_2Cl_2, 40 °C, 2 h, quantitative. (iv) Et_3N, THF, 2 h, 90%. (v) 1M NaOH(aq), THF, 16 h, 83 %. (vi) EDCI.HCl, DMAP, CH_2Cl_2, 16 h, 89%. (vii) trifluoroacetic acid, $CHCl_3$, 30 min., quantitative. (viii) BOP, Et_3N, 1/5 THF/$CHCl_3$, 1 h, 69%. (ix) 1 M NaOH(aq), THF, 16 h, quantitative. (x) BOP, Et_3N, 1/5 THF/$CHCl_3$, 1 h, 74%. (xi) trifluoroacetic acid, $CHCl_3$, 30 min., 95%. (xii) Et_3N, $CHCl_3$, 16 h, 98%. (xiii) BOP, Et_3N, 1/5 THF/$CHCl_3$, 2 h, 86%.

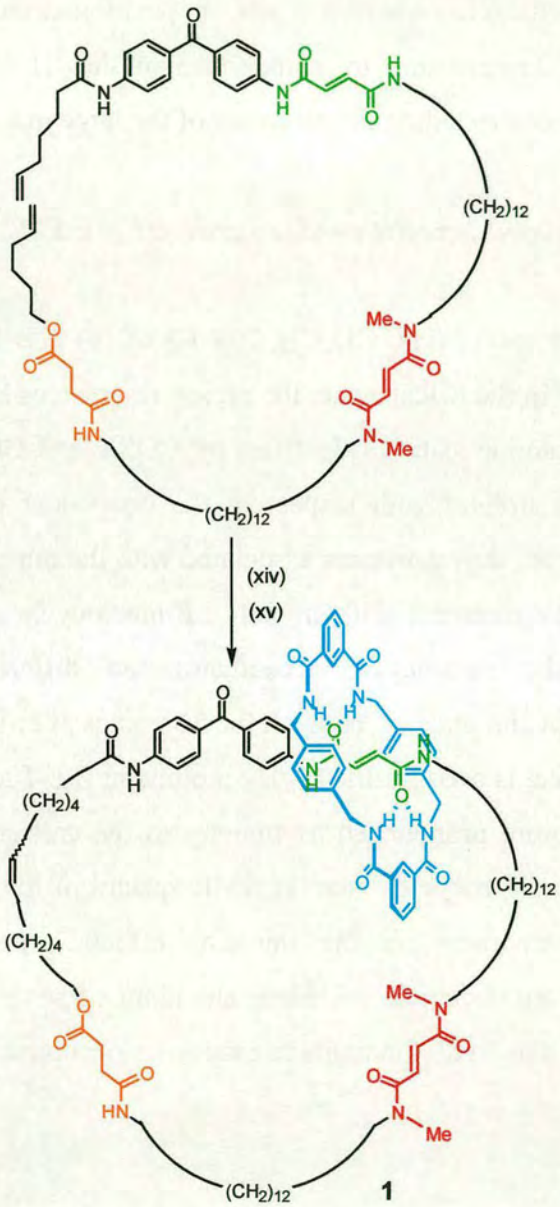

Scheme 6.3b Synthesis of three-station catenane, **1**. (xiv) Grubbs' catalyst, 1/9 THF/CH_2Cl_2, 16 h, 59%. (xv) isophthaloyl dichloride, *p*-xylylene diamine, Et_3N, 1/9 MeCN/$CHCl_3$, 2 h, 50%.

Interconversion of the diastereomers of the [2]catenane was carried out in the sequence *E,E*-**1** → *Z,E*-**1** (350 nm, 5 min., 67%) → *Z,Z*-**1** (254 nm, 30 min., 50%) → *E,E*-**1** (Δ, 100 °C, 24h, ~100%) and authentic samples of each diastereomer isolated at each stage. Since the xylylene rings of the benzylic amide macrocycle shield the part of the larger macrocycle on which it sits, its position could be unambiguously determined for each diastereomer by comparison of the ^{1}H NMR spectra of the [2]catenane with the corresponding diastereomer of the large macrocycle.

6.2.1 *Where is the benzylic amide macrocycle in* E,E-*1?*

The ^{1}H NMR spectra (600 MHz, CD_2Cl_2, 298 K) of (a) *E,E*-**1** and (b) *E,E*-**4** are shown in Figure 6.5. In the [2]catenane, the proton resonances H_a and H_b associated with the green fumaramide station (identified by COSY and GOESY experiments) are shielded ~1 ppm upfield with respect to the equivalent protons in the *E,E*-macrocycle. In contrast, the resonances associated with the other stations, H_c/H_d and H_e/H_f, appear at similar chemical shifts in both *E,E*-macrocycle and *E,E*-[2]catenane. The presence of the macrocycle accentuates the differences in magnetic environments between the ends of both olefin *bis*amides (i.e. the H_a/H_b and H_c/H_d protons; a similar effect is seen for the $H_{a'}/H_{b'}$ protons in *Z,E*-**1** and **4**), probably as a consequence of the more pronounced asymmetry in the catenane compared to the *pseudo*-C_3-symmetric macrocycle. The ^{1}H NMR spectra of the [3]catenane (Figure 6.5c) provides a comparison for the shielding effects experienced when both fumaramide stations are occupied, including shielding of some rotamers of the *N*-methyl groups when the 'red' fumaramide station is occupied (not seen in Figure 6.5b).

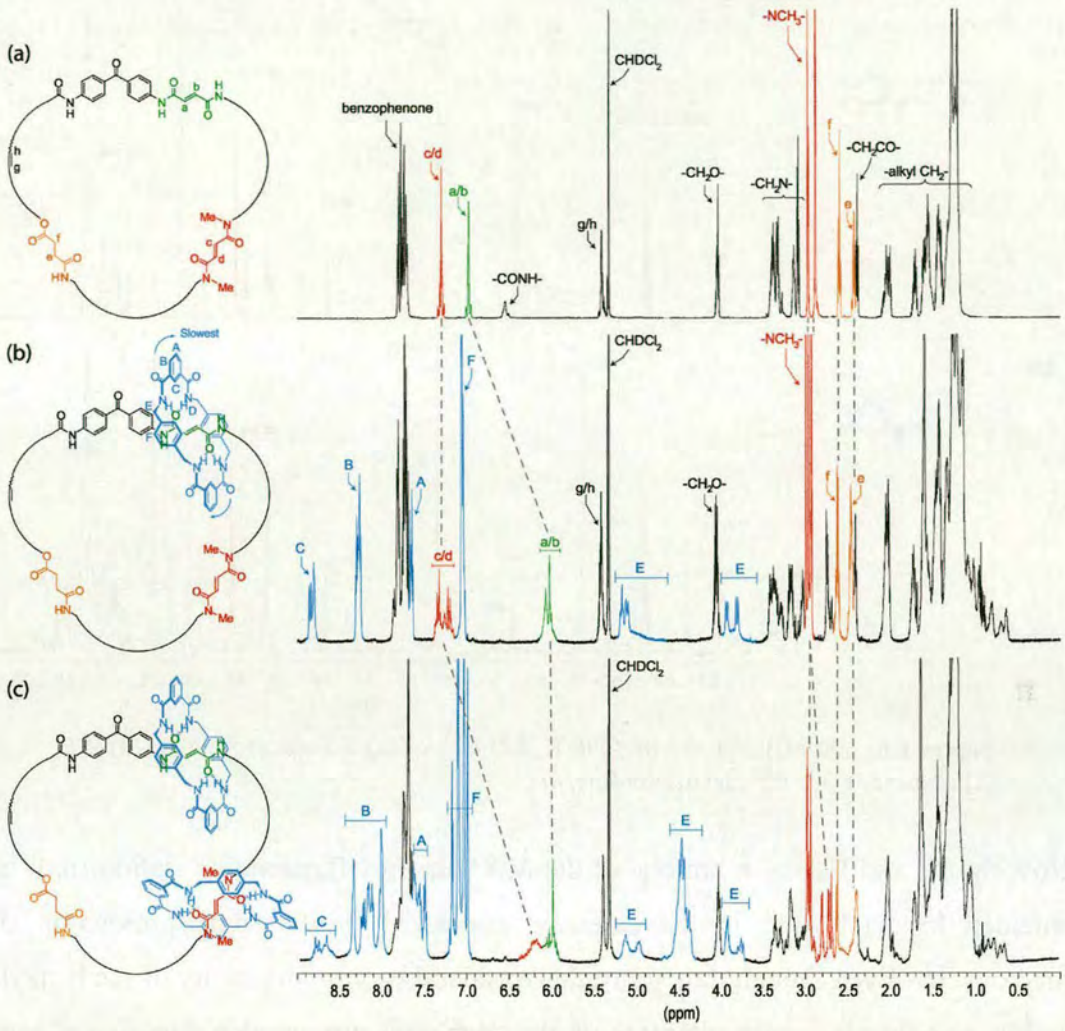

Figure 6.5 600 MHz ^{1}H NMR spectra (298 K, CD_2Cl_2) of (a) three-station macrocycle, **4**; (b) three-station [2]catenane, **1**; (c) three-station [3]catenane, **5**.

6.2.2 *Where is the benzylic amide macrocycle in* Z,E-*1?*

The ^{1}H NMR spectra (600 MHz, CD_2Cl_2, 298 K) of the macrocycle and [2]catenane with one station isomerised, *Z,E*-**1** and *Z,E*-**4**, respectively, are shown in Figure 6.6.

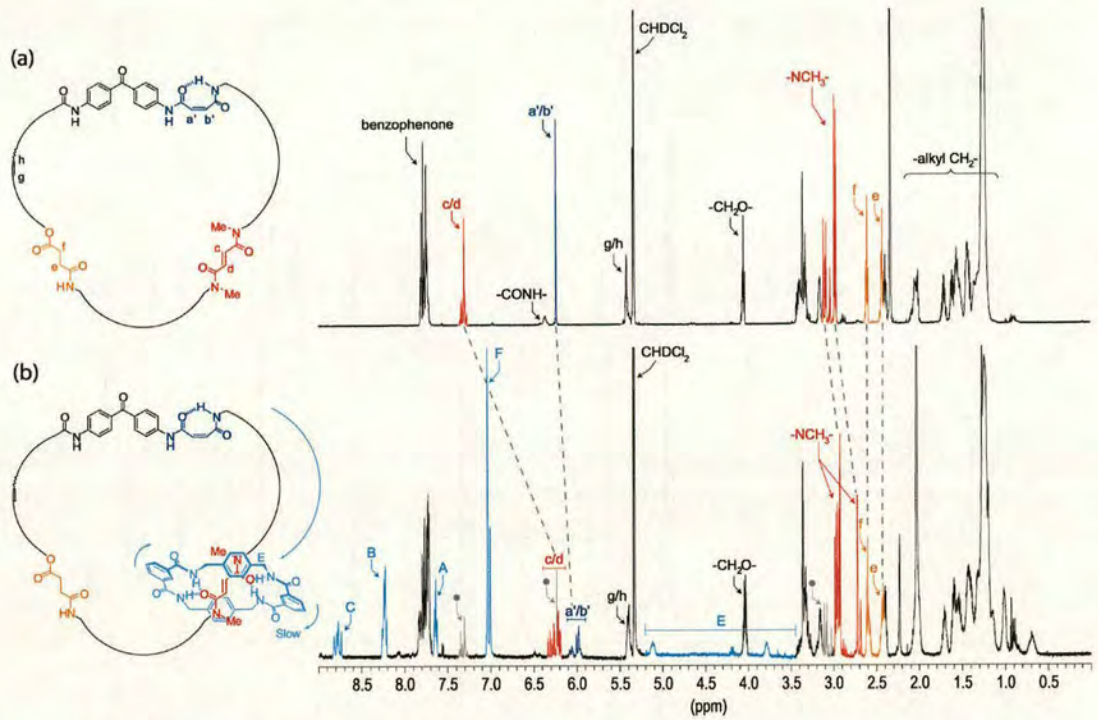

Figure 6.6 600 MHz ^{1}H spectra (298 K, CD_2Cl_2) of (a) *Z*/*E*-macrocycle, **4**; (b) *Z*/*E*-[2]catenane, **1** (• = residual macrocycle, **4**).

Now the H_c and H_d olefin protons of the *N,N'*-dimethylfumaramide station (red) are shielded by ~1.1 ppm in the catenane compared to the same protons in the macrocycle. Even though they protrude considerably from the cavity of the benzylic amide macrocycle, some rotamers of the *N*-methyl groups also experience some shielding in the *Z,E*-catenane. In contrast, the $H_{a'}/H_{b'}$ protons of the isomerised maleamide (*cis*-olefin) group (shown in blue) appear at similar shifts in *Z,E*-**1** and *Z,E*-**4** indicating that the station is not occupied in the *Z,E*-[2]catenane. Again, the H_e/H_f protons of the succinic amide ester group appear at similar chemical shifts in both macrocycle and catenane.

6.2.3 *Where is the benzylic amide macrocycle in Z,Z-1?*

The ^{1}H NMR spectra (600 MHz, CD_2Cl_2, 298 K) of the macrocycle and [2]catenane with both stations isomerised, *Z,Z*-**1** and *Z,Z*-**4**, respectively, are shown in Figure 6.7.

The shifts in the resonances of H_e and H_f (–0.91 and –0.83 ppm, respectively) confirm the benzylic amide macrocycle resides on the succinic amide ester station in *Z,Z*-**1**. The $H_{a'}/H_{b'}$ and $H_{c'}/H_{d'}$ resonances for the two maleamide stations appear at almost identical chemical shifts in both macrocycle and catenane.

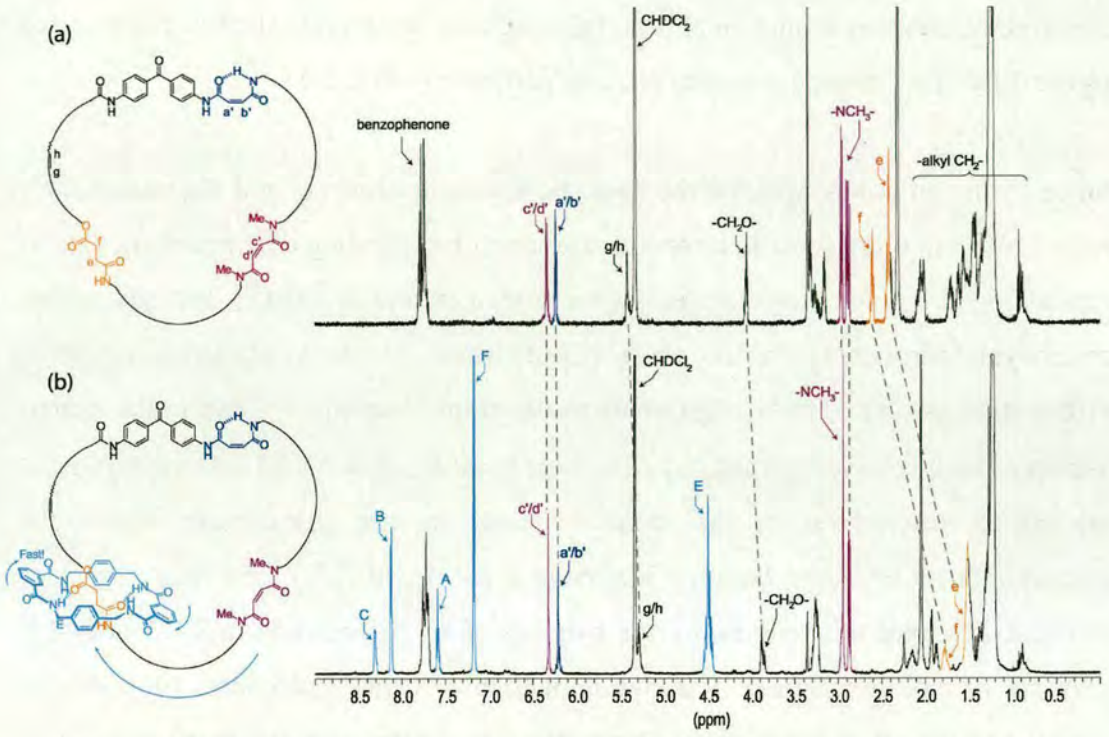

Figure 6.7 600 MHz ^{1}H spectra (298 K, CD_2Cl_2) of (a) *Z/Z*-macrocycle, **4**; (b) *Z/Z*-[2]catenane, **1**.

A further interesting property of this [2]catenane system that is apparent from the ^{1}H NMR spectra of the three [2]catenane diastereomers (repeated for convenience as Figure 6.8) is that as the small macrocycle moves successively from a stronger binding station to a weaker one, its rate of pirouetting around the axis of the larger macrocycle speeds up! A definitive illustration of this can be seen from the different resonance patterns of the H_E protons in the three catenanes. In a static 'snap-shot' of the [2]catenane the eight H_E protons of the benzylic amide macrocycle (as a chair conformation on a given station) exist in four different environments that could give rise to four resonances in the ^{1}H NMR spectra. However, because of the symmetry

of the benzylic amide macrocycle, a 180° pirouette around the axis of the other macrocycle groups the eight H_E protons into only two different sets of averaged environments. Thus, if benzylic amide macrocycle pirouetting is fast on the NMR timescale only two (or one if they are accidentally isochronous) resonances should be observed for the H_E protons. However, if pirouetting is slow on the NMR timescale then four resonances should be present [although the situation is slightly complicated by the different *N*-methyl rotamers present, particularly in *Z,E*-**1**].

Since hydrogen bonds between the benzylic amide macrocycle and the station have to be broken in order for it to pirouette, the strength of binding determines the rate of pirouetting at a given temperature. At room temperature in CD_2Cl_2, benzylic amide macrocycle pirouetting in the three [2]catenanes is clearly occurring on three different timescales. The H_E signals are resolved into four signals (two of the signals appear as well resolved portions of ABx systems at δ 3.9 and δ 5.1; the other protons are broad resonances in the same regions) in the [2]catenane where the intercomponent hydrogen bonding is strongest, *E,E*-**1**. In *Z,E*-**1**, 298 K is very close to the coalescence temperature for the two sets of H_E protons and in *Z,Z*-**1** at 298 K they are in rapid exchange. Variable temperature NMR experiments (in $C_2D_2Cl_4$) established the activation barrier to pirouetting of the benzylic amide macrocycle by the coalescence method of ΔG = 14.2 ± 0.3 kcal mol^{-1} (coalescence temperature = 323 K) for *E,E*-**1** (green fumaramide station); ΔG = 13.0 ± 0.3 kcal mol^{-1} (coalescence temperature = 298 K) for *Z,E*-**1** (red *N,N*-dimethylfumaramide station); and ΔG <9 kcal mol^{-1} for *Z,Z*-**1** (orange succinic amide ester station).

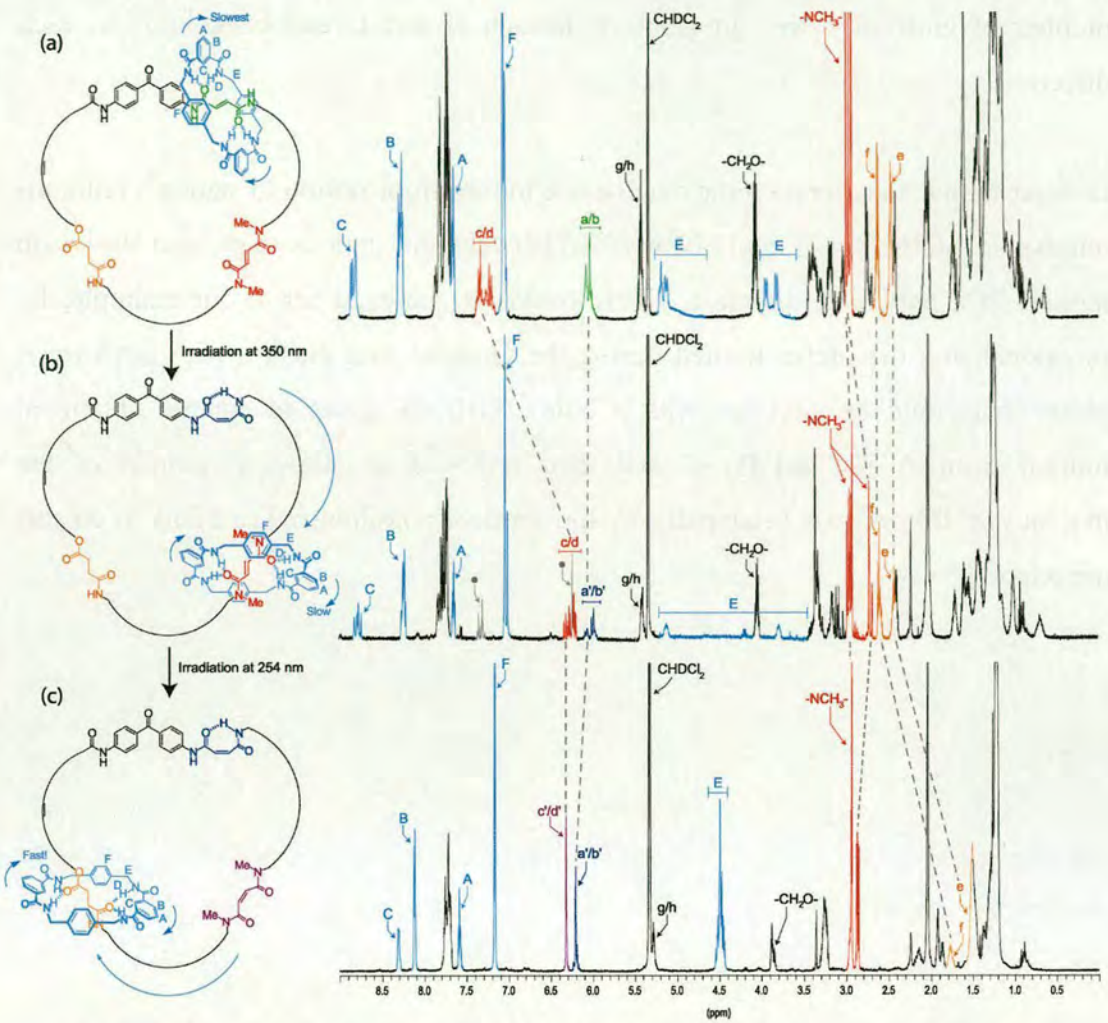

Figure 6.8 600 MHz ^{1}H spectra (298 K, CD_2Cl_2) of (a) *E/E*-[2]catenane, **1**; (b) *Z/E*-[2]catenane, **1**; (c) *Z/Z*-[2]catenane, **1**.

Is the rotation of the benzylic amide macrocycle in [2]catenane truly unidirectional? Although the averaged position of the benzylic amide macrocycle changes in response to the external stimuli (through biased Brownian motion) in discrete 120° steps, the route it takes to get there is not directionally biased. Although most of the rings will move from station A to station B *via* the shortest route, some (approximately ⅓ in **1**) will get there by going round the other way (i.e. *via* C in Figure 6.2). Similarly, only ⅔ will then go the correct way from B to C and the other fraction from B to A to C. In fact, for the complete sequence A→B→C→A an equal

number of molecules will go from A through B and C and back to A in each direction.

In order to bias the direction the macrocycle moves from station to station a (stimuli-removable) steric barrier could be inserted between the stations to prevent Brownian motion in a particular direction. This could be achieved for **1**, for example, by functionalising the olefin formed during the Grubbs' ring closure with a hydroxyl group that could be silylated with a bulky TBDMS group to ensure directional motion from A→B and B→C and then removed to allow movement of the macrocycle from C→A principally by the shortest possible route. Plans to do this are ongoing.

6.3 Experimental

Three-station [2]catenane, *E,E*-1

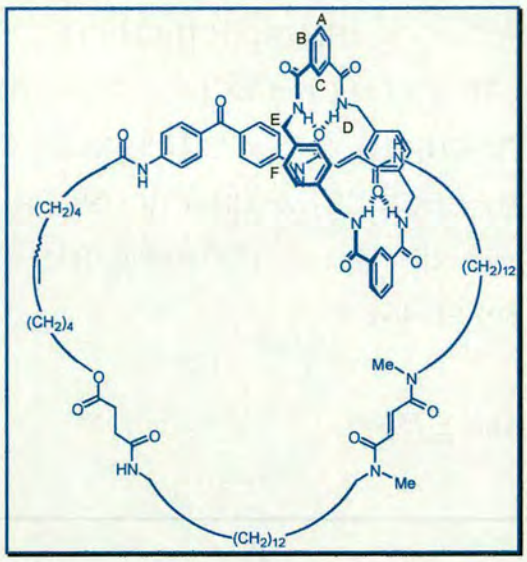

The three-station macrocycle, *E,E*-**4** (0.15 g, 0.14 mmol, 1 equiv.) and triethylamine (1.2 mL, 8.4 mmol, 60 equiv.) in 10 mL of $CHCl_3$ ($CHCl_3$ is stabilised with amylenes) was vigorously whilst solutions of *para*-xylylene diamine (0.23 g, 1.7 mmol, 12 equiv.) in 15 mL of $CHCl_3$ and isophthaloyl dichloride (0.33 g, 1.6 mmol, 11.5 equiv.) in 15 mL of $CHCl_3$ were simultaneously added over a period of 2 hours using motor-driven syringe pumps. The resulting suspension was filtered and concentrated under reduced pressure and subjected to column chromatography (silica gel, first column of 4:96 $CHCl_3$/MeOH followed by a second column of 3:97 MeOH/$CHCl_3$) to yield, in order of elution, the three-station macrocycle, *E,E*-**4**, [2]catenane, *E,E*-**1** and [3]catenane, *E,E*-**5**.

Selected data for the three-station [2]catenane, *E,E*-1: Yield 63 mg (50%); ^{1}H NMR (600 MHz, CD_2Cl_2): δ = 8.86–8.81 (brs, 2H, ArH_C), 8.31–8.25 (m, 4H, ArH_B), 7.87–7.68 (m, 12H, $N\underline{H}_D$ & ArH, benzophenone), 7.65 (brt, 2H, ArH_A), 7.38–7.16

(m, 2H, $NCH_3COC\underline{H}=C\underline{H}CONCH_3$), 7.07–7.04 (brs, 8H, ArH_F), 6.07–6.01 (m, 2H, $NHCOC\underline{H}=C\underline{H}CONH$), 5.42 (m, 2H, $CH_2C\underline{H}=C\underline{H}CH_2$), 5.20–5.10 (m, 4H, CH_E), 4.06 (m, 2H, CH_2CO_2), 3.95–3.80 (m, 4H, CH_E), 3.43–3.02 (m, 6H, 2 x $C\underline{H_2}NCH_3$ & $C\underline{H_2}NHCO$), 3.00–2.93 (s, 6H, NCH_3), 2.74 (m, 2H, $CH=CHCONHC\underline{H_2}$), 2.62 (m, 2H, $NHCOCH_2C\underline{H_2}CO_2$), 2.45 (m, 2H, $NHCOC\underline{H_2}CH_2CO_2$), 2.41 (t, J = 7.5 Hz, 2H, $C\underline{H_2}CONHAr$), 2.04 (m, 4H, 2 x $C\underline{H_2}CH=CHC\underline{H_2}$), 1.72 (m, 2H, $C\underline{H_2}CH_2CONHAr$), 1.56–0.64 (m, 46H, $CO_2CH_2C\underline{H_2}$ & 2 x $C\underline{H_2}CH_2NCH_3$ & $C\underline{H_2}CH_2NHCO$ & $CO_2CH_2CH_2C\underline{H_2}$ & $CH_2=CHCH_2C\underline{H_2}$ & $CH=CHCONHCH_2C\underline{H_2}$ & CH_2, alkyl); HRMS (FAB, NBA matrix): m/z = 1597.91870 $[(M+H)^+]$ (anal. calcd for $C_{94}H_{121}N_{10}O_{13}$: m/z = 1597.91146).

Three-station [3]catenane, *E,E*-5

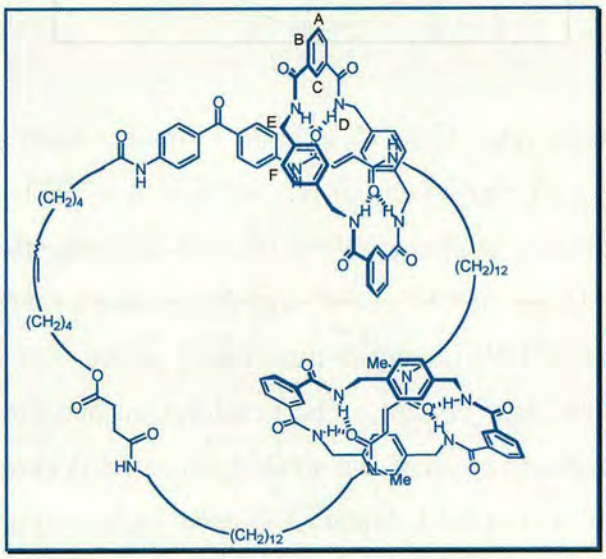

Selected data for the three-station [3]catenane *E,E*-5: Yield 63 mg (21%); ^1H NMR (600 MHz, CD_2Cl_2): δ = 8.78 (m, 2H, CONH), 8.36–8.04 (m, 12H, ArH_B & ArH_C), 7.86–7.51 (m, 20H, $N\underline{H}_D$ & ArH, benzophenone & ArH_A), 7.20–7.01 (brs, 16H, ArH_F), 6.19 (m, 2H, $NCH_3COC\underline{H}=C\underline{H}CONCH_3$), 6.00 (m, 2H, $NHCOC\underline{H}=C\underline{H}CONH$), 5.40 (m, 2H, $CH_2C\underline{H}=C\underline{H}CH_2$), 5.14–4.98 (m, 8H, CH_E),

4.03 (m, 2H, CH_2CO_2), 3.95–3.74 (m, 8H, CH_E), 3.40–3.00 (m, 6H, 2 x $C\underline{H_2}NCH_3$ & $C\underline{H_2}NHCO$), 2.97–2.68 (m, 8H, NCH_3, $CH{=}CHCONHC\underline{H_2}$), 2.61 (m, 2H, $NHCOCH_2C\underline{H_2}CO_2$), 2.39 (m, 4H, $NHCOC\underline{H_2}CH_2CO_2$ & $C\underline{H_2}CONHAr$), 2.02 (m, 4H, 2 x $C\underline{H_2}CH{=}CHC\underline{H_2}$), 1.69–0.63 (m, 48H, $C\underline{H_2}CH_2CONHAr$ & $CO_2CH_2C\underline{H_2}$ & 2 x $C\underline{H_2}CH_2NCH_3$ & $C\underline{H_2}CH_2NHCO$ & $CO_2CH_2CH_2C\underline{H_2}$ & $CH_2{=}CHCH_2C\underline{H_2}$ & $CH{=}CHCONHCH_2C\underline{H_2}$ & CH_2, alkyl); MS (FAB, NBA matrix): *m/z* = 2131 $[(M+H)^+]$.

Three-station [2]catenane, *Z,E*-1

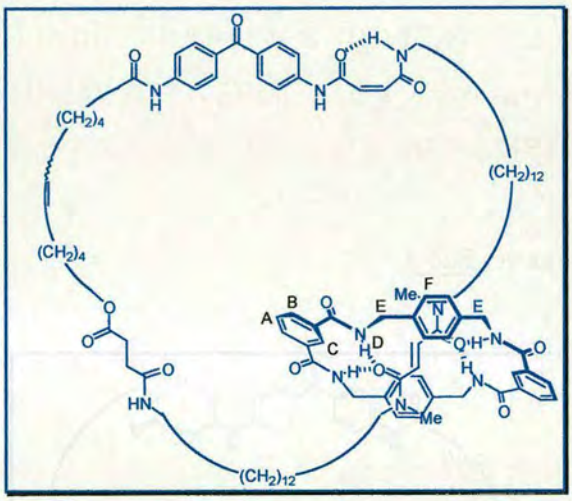

A 1 x 10^{-3} M solution of three-station catenane, *E,E*-**1** (7 mg) in CH_2Cl_2 (4.5 mL) was placed in a quartz vessel and directly irradiated at 350 nm using a multilamp photoreactor (model MLU18 manufactured by Photochemical Reactors Ltd, UK). The progress of the reaction was monitored by ^1H NMR spectroscopy and the photostationary state was reached after 10 minutes of irradiation. The reaction mixture (containing a mixture of *E,E*-**1** and *Z,E*-**1**) was concentrated under reduced pressure and subjected to column chromatography (silica gel, 3:97 MeOH/$CHCl_3$) to obtain the pure *Z,E*-isomer.

Selected data for the three-station [2]catenane *Z,E*-1: Yield 4.6 mg (66%); ^{1}H NMR (600 MHz, CD_2Cl_2/1% MeOD): δ = 8.82–8.74 (brs, 2H, ArH_C), 8.26–8.21 (m, 4H, ArH_B), 7.84–7.72 (m, 12H, $N\underline{H}_D$ & ArH, benzophenone), 7.65 (m, 2H, ArH_A), 7.04–7.01 (brs, 8H, ArH_F), 6.34–6.19 (m, 2H, $NCH_3COC\underline{H}$=$C\underline{H}CONCH_3$), 6.09–5.96 (m, 2H, $NHCOC\underline{H}$=$C\underline{H}CONH$), 5.41 (m, 2H, $CH_2C\underline{H}$=$C\underline{H}CH_2$), 5.12 (m, 4H, CH_E), 4.04 (m, 2H, CH_2CO_2), 3.78 (m, 4H, CH_E), 3.43–3.12 (m, 8H, 2 x $C\underline{H}_2NCH_3$ & $C\underline{H}_2NHCO$ & $CH{=}CHCONHC\underline{H}_2$), 2.98–2.92 & 2.72 & 2.68 (s, 6H, NCH_3), 2.60 (m, 2H, $NHCOCH_2C\underline{H}_2CO_2$), 2.41 (m, 4H, $NHCOC\underline{H}_2CH_2CO_2$ & $C\underline{H}_2CONHAr$), 2.04 (m, 4H, 2 x $C\underline{H}_2CH{=}CHC\underline{H}_2$), 1.71 (m, 2H, $C\underline{H}_2CH_2CONHAr$), 1.62–0.66 (m, 46H, $CO_2CH_2C\underline{H}_2$ & 2 x $C\underline{H}_2CH_2NCH_3$ & $C\underline{H}_2CH_2NHCO$ & $CO_2CH_2CH_2C\underline{H}_2$ & $CH_2{=}CHCH_2C\underline{H}_2$ & $CH{=}CHCONHCH_2C\underline{H}_2$ & CH_2, alkyl); HRMS (FAB, NBA matrix): *m/z* = 1597.91118 $[(M+H)^+]$ (anal. calcd for $C_{94}H_{121}N_{10}O_{13}$: *m/z* = 1597.91146).

Three-station [2]catenane, *Z,Z*-1

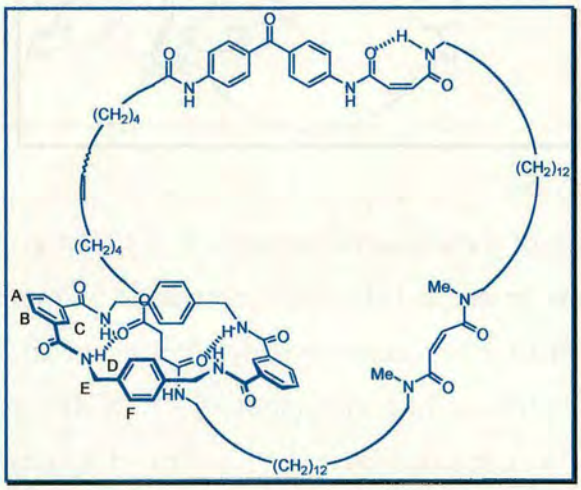

A 1 x 10^{-3} M solution of three-station catenane, *E,E*-**1** (16 mg) in CH_2Cl_2 (10 mL) was placed in a quartz vessel and directly irradiated at 350 nm using a multilamp photoreactor (model MLU18 manufactured by Photochemical Reactors Ltd, UK).

The progress of the reaction was monitored by ^{1}H NMR spectroscopy and the photostationary state was reached after 30 minutes of irradiation. The reaction mixture (containing a mixture of *E,E*-**1**, *Z,E*-**1**, *E,Z*-**1** and *Z,Z*-**1**) was concentrated under reduced pressure and subjected to column chromatography (silica gel, 3:97 MeOH/$CHCl_3$ to 4:96 MeOH/$CHCl_3$) to obtain pure *Z,Z*-**1**.

Selected data for the three-station [2]catenane *Z,Z*-1: Yield 5 mg (33%); ^{1}H NMR (600 MHz, CD_2Cl_2/1% MeOD): δ = 8.31 (brm, 2H, ArH_C), 8.12 (m, 4H, ArH_B), 7.78–7.69 (m, 12H, $N\underline{H}_D$ & ArH, benzophenone), 7.59 (m, 2H, ArH_A), 7.18 & 7.17 (brs, 8H, ArH_F), 6.33 (brs, 2H, $NCH_3COC\underline{H}=C\underline{H}CONCH_3$), 6.21 (m, 2H, $NHCOC\underline{H}=C\underline{H}CONH$), 5.29 (m, 2H, $CH_2C\underline{H}=C\underline{H}CH_2$), 4.50 (m, 8H, CH_E), 3.87 (m, 2H, CH_2CO_2), 3.31–3.22 (m, 6H, 2 x $C\underline{H}_2NCH_3$ & $C\underline{H}_2NHCO$), 2.95 & 2.94 & 2.88 & 2.87 & 2.86 (s, 8H, NCH_3 & $CH=CHCONHC\underline{H}_2$), 2.16 (m, 2H, $C\underline{H}_2CONHAr$), 1.93–1.85 (m, 4H, 2 x $C\underline{H}_2CH=CHC\underline{H}_2$), 1.77 (m, 2H, $NHCOCH_2C\underline{H}_2CO_2$), 1.52–1.23 (m, 50H, $NHCOC\underline{H}_2CH_2CO_2$ & $C\underline{H}_2CH_2CONHAr$ & $CO_2CH_2C\underline{H}_2$ & 2 x $C\underline{H}_2CH_2NCH_3$ & $C\underline{H}_2CH_2NHCO$ & $CO_2CH_2CH_2C\underline{H}_2$ & $CH_2=CHCH_2C\underline{H}_2$ & $CH=CHCONHCH_2C\underline{H}_2$ & CH_2, alkyl); HRMS (FAB, NBA matrix): *m/z* = 1597.92985 $[(M+H)^+]$ (anal. calcd for $C_{94}H_{121}N_{10}O_{13}$: *m/z* = 1597.91146).

Three-station macrocycle, *E,E*-4

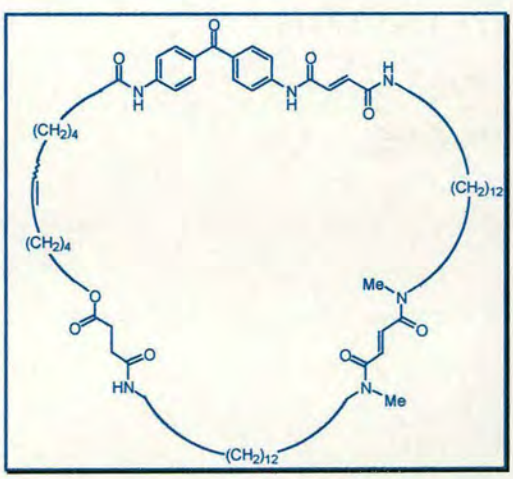

To a solution of 0.5 mM [12-({3-[(12-{3-[4-(4-hept-6-enoylamino-benzoyl)-phenylcarbamoyl]-acryloylamino}-dodecyl)-methyl-carbamoyl]-acryloyl}-methyl-amino)-dodecyl]-carbamic acid hex-5-enyl ester, **6** (0.50 g, 0.46 mmol, 1 equiv.) in 50 mL of anhydrous THF and 900 mL of anhydrous CH_2Cl_2 was added Grubbs' catalyst (0.19 g, 0.23 mmol, 0.5 equiv.) and stirred under a nitrogen atmosphere. The pink reaction mixture was stirred for 16 hours at room temperature. The resulting brown solution was concentrated under reduced pressure and subjected to column chromatography (silica gel, 3:97 MeOH/$CHCl_3$) to give the product as a grey solid.

Selected data for the three-station macrocycle *E,E*-4: Yield 0.29 g (59%); ^{1}H NMR (600 MHz, CD_2Cl_2/1% MeOD): δ = 10.32 (brs, 1H, ArNHCO), 9.11 (brs, 1H, ArNHCO), 7.82–7.70 (m, 10H, CH=CHCONH & $NHCOCH_2$ & ArH, benzophenone), 7.30 (m, 2H, NCH_3COCH=$CHCONCH_3$), 6.97 (m, 2H, NHCOCH=CHCONH), 6.55 (brm, 1H, NHCO), 5.41 (m, 2H, CH_2CH=$CHCH_2$), 4.04 (t, J = 6.6 Hz, 2H, CH_2CO_2), 3.44–3.28 (m, 4H, 2 x CH_2NCH_3 & CH_2NHCO), 3.13 (m, 2H, CH=CHCONHCH_2), 3.08 & 2.97 (s, 6H, NCH_3), 2.60 (m, 2H, $NHCOCH_2CH_2CO_2$), 2.42 (m, 2H, $NHCOCH_2CH_2CO_2$), 2.39 (t, J = 7.5 Hz, 2H, $CH_2CONHAr$), 2.04 (m, 4H, 2 x CH_2CH=$CHCH_2$), 1.70 (m, 2H, $CH_2CH_2CONHAr$), 1.55 (m, 8H, $CO_2CH_2CH_2$ & 2 x $CH_2CH_2NCH_3$ & CH_2CH_2NHCO), 1.43 (m, 6H, $CO_2CH_2CH_2CH_2$ & CH_2=$CHCH_2CH_2$ & CH=CHCONHCH_2CH_2), 1.34–1.21 (m, 32H, CH_2, alkyl); HRMS (FAB, NBA matrix): m/z = 1065.70618 [$(M+H)^+$] (anal. calcd for $C_{62}H_{93}N_6O_9$: m/z = 1065.70040).

Three-station macrocycle, *Z,E*-4

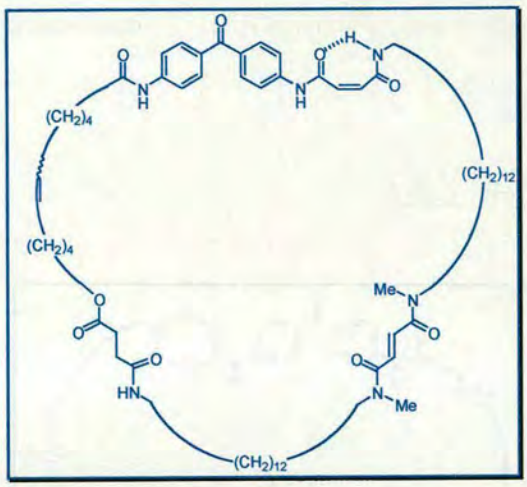

A 1 x 10^{-3} M solution of three-station macrocycle, *E,E*-**4** (10 mg) in CH_2Cl_2 (9 mL) was placed in a quartz vessel and directly irradiated at 350 nm using a multilamp photoreactor (model MLU18 manufactured by Photochemical Reactors Ltd, UK). The progress of the reaction was monitored by ^1H NMR spectroscopy and the photostationary state was reached after 10 minutes of irradiation. The reaction mixture (containing a mixture of *E,E*-**4** and *Z,E*-**4**) was concentrated under reduced pressure and subjected to column chromatography (silica gel, 3:97 MeOH/$CHCl_3$) to obtain the pure *Z,E*-isomer.

Selected data for the three-station macrocycle *Z,E*-4: Yield 6.7 mg (67%); ^1H NMR (600 MHz, CD_2Cl_2/1% MeOD): δ = 7.81–7.71 (m, 10H, CH=CHCONH & $NHCOCH_2$ & ArH, benzophenone), 7.30 (m, 2H, NCH_3COCH=$CHCONCH_3$), 6.23 (s, 2H, NHCOCH=CHCONH), 5.41 (m, 2H, CH_2CH=$CHCH_2$), 4.05 (t, J = 6.6 Hz, 2H, CH_2CO_2), 3.43–3.31 (s, 6H, 2 x CH_2NCH_3 & CH_2NHCO), 3.15 (m, CH=$CHCONHCH_2$), 3.08 & 2.96 (s, 6H, NCH_3), 2.60 (m, 2H, $NHCOCH_2CH_2CO_2$), 2.42 (m, 2H, $NHCOCH_2CH_2CO_2$), 2.38 (brt, 2H, $CH_2CONHAr$), 2.04 (m, 4H, 2 x CH_2CH=$CHCH_2$), 1.70 (m, 2H, $CH_2CH_2CONHAr$), 1.56 (m, 8H, $CO_2CH_2CH_2$ & 2 x $CH_2CH_2NCH_3$ & CH_2CH_2NHCO), 1.42 (m, 6H, $CO_2CH_2CH_2CH_2$ & CH_2=$CHCH_2CH_2$ & CH=$CHCONHCH_2CH_2$), 1.24 (m, 32H, CH_2, alkyl); HRMS

(FAB, NBA matrix): *m/z* = 1065.70091 [$(M+H)^+$] (anal. calcd for $C_{62}H_{93}N_6O_9$: *m/z* = 1065.70040).

Three-station macrocycle, *Z,Z*-4

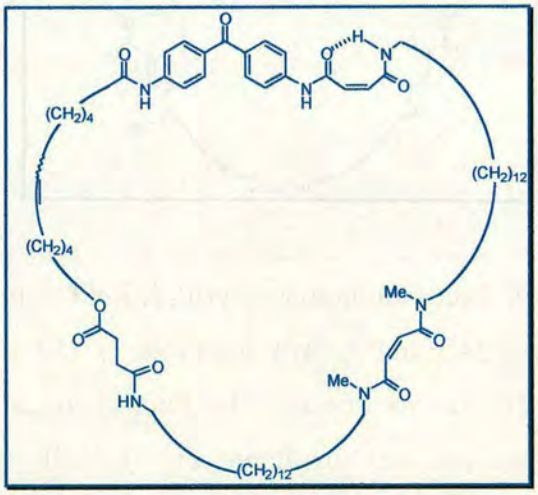

A 1 x 10^{-3} M solution of three-station macrocycle, *E,E*-**4** (10 mg) in CH_2Cl_2 (9 mL) was placed in a quartz vessel and directly irradiated at 350 nm using a multilamp photoreactor (model MLU18 manufactured by Photochemical Reactors Ltd, UK). The progress of the reaction was monitored by ^{1}H NMR spectroscopy and the photostationary state was reached after 10 minutes of irradiation. The reaction mixture (containing a mixture of *E,E*-**4**, *Z,E*-**4**, *E,Z*-**4** and *Z,Z*-**4**) was concentrated under reduced pressure and subjected to column chromatography (silica gel, 3:97 MeOH/$CHCl_3$) to obtain the pure *Z,Z*-isomer.

Selected data for the three-station macrocycle *Z,Z*-4: Yield 3.3 mg (33%); ^{1}H NMR (600 MHz, CD_2Cl_2/1% MeOD): δ = 7.81–7.71 (m, 8H, ArH, benzophenone), 6.35 (m, 2H, NCH_3COCH=CHCONCH_3), 6.24 (m, 2H, NHCOCH=CHCONH), 5.42 (m, 2H, CH_2CH=CHCH_2), 4.06 (m, 2H, CH_2CO_2), 3.33–3.15 (m, 8H, 2 x CH_2NCH_3 & CH_2NHCO & CH=CHCONHCH_2), 2.98–2.87 (s, 6H, NCH_3), 2.60 (m, 2H,

$NHCOCH_2C\underline{H_2}CO_2$), 2.43 (m, 2H, $NHCOC\underline{H_2}CH_2CO_2$), 2.39 (m, 2H, $C\underline{H_2}CONHAr$), 2.05 (m, 4H, 2 x $C\underline{H_2}CH{=}CHC\underline{H_2}$), 1.70 (m, 2H, $C\underline{H_2}CH_2CONHAr$), 1.56 (m, 8H, $CO_2CH_2C\underline{H_2}$ & 2 x $C\underline{H_2}CH_2NCH_3$ & $C\underline{H_2}CH_2NHCO$), 1.42 (m, 6H, $CO_2CH_2CH_2C\underline{H_2}$ & $CH_2{=}CHCH_2C\underline{H_2}$ & $CH{=}CHCONHCH_2C\underline{H_2}$), 1.36–1.22 (m, 32H, CH_2, alkyl); HRMS (FAB, NBA matrix): *m/z* = 1065.69974 [$(M+H)^+$] (anal. calcd for $C_{62}H_{93}N_6O_9$: *m/z* = 1065.70040).

([2](1,7,14,20-Tetraaza-2,6,15,19-tetraoxo-3,5,9,12,16,18,22,25-cetrabenzocyclohexacosane)-(But-2-enedioic acid [4-(4-diphenylacetylamino-benzoyl)-phenyl]-amide [12-({3-[2,2-diphenyl-ethyl)-methyl-carbamoyl]-acryloyl}-methyl-amino)-dodecyl]-amide)-rotaxane, 2

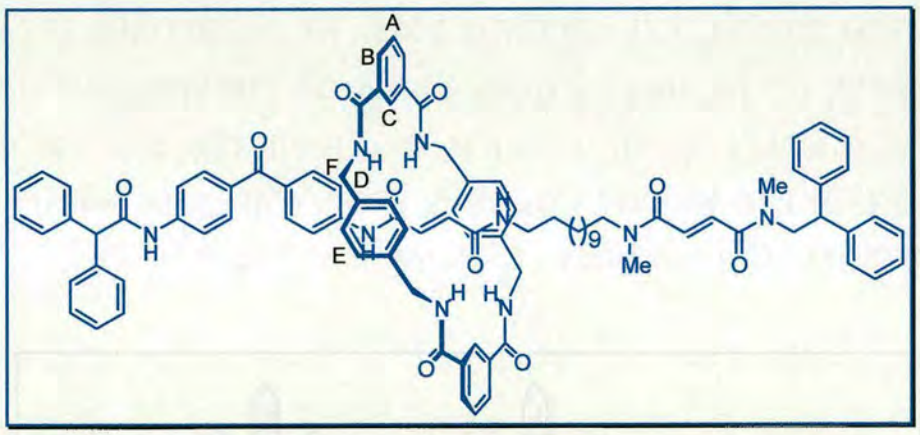

The thread, but-2-enedioic acid [4-(4-diphenylacetylamino-benzoyl)-phenyl]-amide [12-({3-[2,2-diphenyl-ethyl)-methyl-carbamoyl]-acryloyl}-methyl-amino)-dodecyl]-amide, **S27** (0.25 g, 0.25 mmol, 1 equiv.) and triethylamine (1.05 mL, 7.6 mmol, 30 equiv.) were dissolved in 10/90 mL MeCN/$CHCl_3$ ($CHCl_3$ is stabilised with amylenes) and stirred vigorously whilst solutions of *para*-xylylene diamine (0.41 g, 30 mmol, 12 equiv.) in 20 mL of $CHCl_3$ and isophthaloyl dichloride (0.59 g, 2.9 mmol, 11.5 equiv.) in 20 mL of $CHCl_3$ were simultaneously added over a period of 3 hours using motor-driven syringe pumps. The resulting suspension was filtered, concentrated under reduced pressure and subjected to column chromatography (silica

gel, 1:99 MeOH/$CHCl_3$, 2:98 MeOH/$CHCl_3$ and 3:97 MeOH/$CHCl_3$) to yield, in order of elution, the unconsumed thread, [2]rotaxane and [3]rotaxane.

[2]rotaxane:

Selected data for ([2](1,7,14,20-Tetraaza-2,6,15,19-tetraoxo-3,5,9,12,16,18,22,25-cetrabenzocyclohexacosane)-(But-2-enedioic acid [4-(4-diphenylacetylamino-benzoyl)-phenyl]-amide[12-({3-[2,2-diphenyl-ethyl)-methyl-carbamoyl]-acryloyl}-methyl-amino)-dodecyl]-amide)-rotaxane, 2: Yield 0.1 g (26%); m.p. 172 °C; ^{1}H NMR (400 MHz, $CDCl_3$): δ = 8.61–8.55 (brm, 2H, ArH_C), 8.22–8.10 (m, 4H, ArH_B), 7.87–7.59 (m, 14H, $N\underline{H}_D$ & ArH_A & ArH, benzophenone), 7.29–7.16 (m, 22H, ArH, phenyl & $NCH_3COC\underline{H}$=$C\underline{H}CONCH_3$), 6.96–6.87 (brs, 8H, ArH_F), 6.01–5.78 (m, 2H, NHCOC<u>H</u>=C<u>H</u>CONH), 5.06 (s, 1H, $Ph_2C\underline{H}CONH$), 4.95 & 4.36 (m, 4H, CH_E), 4.25 (m, 1H, $CH_2C\underline{H}Ph_2$), 4.00 (m, 2H, $C\underline{H}_2CHPh_2$), 3.91–3.67 (m, 4H, CH_E), 3.36–3.04 (m, 4H, CONHC<u>H</u>$_2$ & C<u>H</u>$_2$NCH_3CO), 2.90–2.65 (s, 6H, NCH_3), 1.43 & 1.18 (brs, 20H, CH_2, alkyl); HRMS (FAB, NBA matrix): *m/z* = 1524.74338 [$(M+H)^+$] (anal. calcd for $C_{95}H_{98}N_9O_{10}$: *m/z* = 1524.74367).

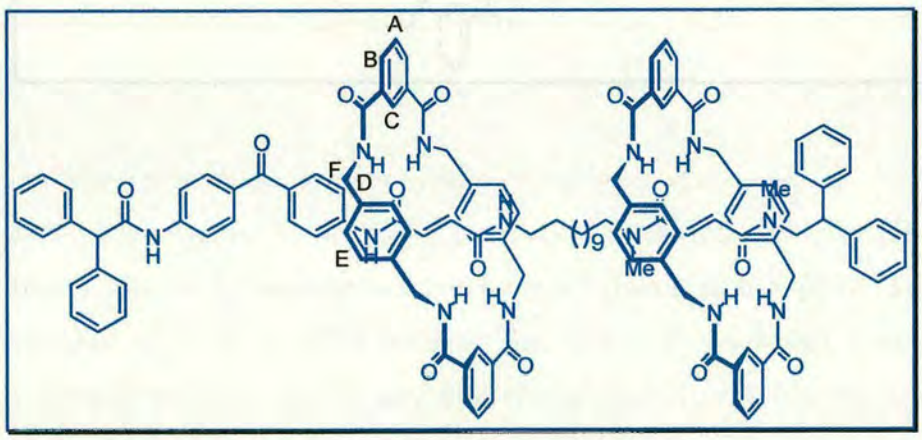

Selected data for [3]rotaxane, S1: Yield 0.1 g (19%); ^{1}H NMR (400 MHz, $CDCl_3$): δ = 8.59–8.54 (brm, 4H, ArH_C), 8.18–8.08 (m, 8H, ArH_B), 7.87–7.59 (m,

16H, $N\underline{H}_D$ & ArH, benzophenone), 7.29–7.12 (m, 24H, ArH_A & ArH, phenyl), 6.96–6.81 (brs, 16H, ArH_F), 6.00 (m, 2H, $NCH_3COC\underline{H}=C\underline{H}CONCH_3$), 5.83 (m, 2H, $NHCOC\underline{H}=C\underline{H}CONH$), 5.06 (s, 1H, $Ph_2C\underline{H}CONH$), 4.96 & 4.35 (m, 8H, CH_E), 4.22 (m, 1H, $CH_2C\underline{H}Ph_2$), 4.02 (m, 2H, $C\underline{H}_2CHPh_2$), 3.79 (m, 8H, CH_E), 3.35–3.05 (m, 4H, $CONHC\underline{H}_2$ & $C\underline{H}_2NCH_3CO$), 2.78–2.53 (s, 6H, NCH_3), 1.43–0.55 (brs, 20H, CH_2, alkyl); HRMS (FAB, NBA matrix): m/z = 2057.95846 $[(M+H)^+]$ (anal. calcd for $C_{127}H_{126}N_{13}O_{14}$: m/z = 2056.95472).

(12-Methylamino-dodecyl)-carbamic acid *tert*-butyl ester, 3

A sodium naphthalide solution [made from addition of sodium (1.30 g, 56.5 mmol, 5 equiv.) to a stirred solution of naphthalene (7.25 g, 56.5 mmol, 5 equiv.) in 300 mL of DME (freshly distilled over sodium and benzophenone) under a nitrogen atmosphere and stirred for 1 hour at room temperature after the solution had turned dark green] was added dropwise to a solution of {12-[methyl-(toluene-4-sulfonyl)-amino]-dodecyl}-carbamic acid *tert*-butyl ester, **S11** (5.30 g, 11.3 mmol, 1 equiv.) in 100 mL of anhydrous DME over 30 minutes under a nitrogen atmosphere at –35 °C. The resulting dark green solution was stirred for a further 10 minutes at –35 °C until TLC indicated no starting compound remained. The reaction was quenched with water (10 mL) and concentrated under reduced pressure to give a white solid. The white solid was dissolved in $CHCl_3$ and filtered through a silica plug using petroleum ether (60/80) to remove the excess naphthalene and **3** was removed using 20:80 $MeOH/CHCl_3$ washings, combined, concentrated and purified using column chromotography (silica gel, 2:98 $MeOH/CHCl_3$) to remove the impurities and (0.5:5:94.5 $NH_4OH/MeOH/CHCl_3$) to elute the product as a white solid.

Selected data for (12-methylamino-dodecyl)-carbamic acid *tert*-butyl ester, 3: Yield 3.02 g (85%); m.p. 53 °C; ^{1}H NMR (400 MHz, $CDCl_3$): δ = 4.54 (brs, 1H, OCONH), 3.09 (m, 2H, OCONHC<u>H</u>$_2$), 2.55 (t, *J* = 7.3 Hz, 2H, C<u>H</u>$_2$NHCH$_3$), 2.42 (s, 3H, NHC<u>H</u>$_3$), 1.44 (brs, 14H, OCONHCH$_2$C<u>H</u>$_2$ & C<u>H</u>$_2$CH$_2$NHCH$_3$ & N<u>H</u>CH$_3$ & CH$_3$, *t*-butyl), 1.25 (m, 16H, CH$_2$, alkyl); ^{13}C NMR (100 MHz, $CDCl_3$): δ = 157.64, 78.94, 52.23, 40.62, 36.55, 30.05, 29.93, 29.56, 29.54, 29.53, 29.27, 28.42, 27.34, 26.79; HRMS (FAB, THIOG): *m/z* = 315.30068 [$(M+H)^+$] (anal. Calcd for $C_{18}H_{39}N_2O_2$: *m/z* = 315.30115). Anal. calcd for $C_{18}H_{38}N_2O_2$: C 68.74, H 12.18, N 8.91. Found C 68.75, H 12.17, N 8.80.

[12-({3-[(12-{3-[4-(4-Hept-6-enoylamino-benzoyl)-phenylcarbamoyl]-acryloylamino}-dodecyl)-methyl-carbamoyl]-acryloyl}-methyl-amino)-dodecyl]-carbamic acid hex-5-enyl ester, <u>6</u>

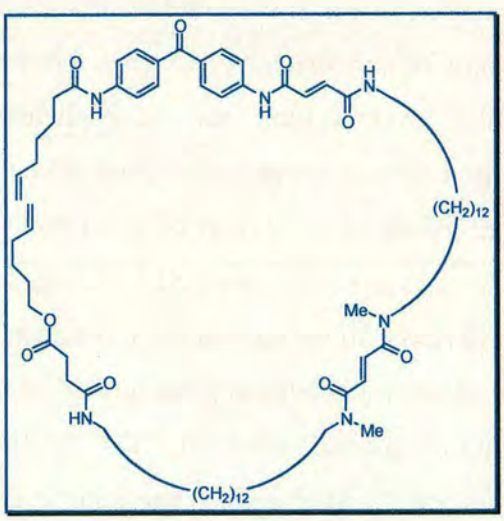

To a stirred suspension of [12-({3-[(12-{3-[4-(4-hept-6-enoylamino-benzoyl)-phenylcarbamoyl]-acryloylamino}-dodecyl)-methyl-carbamoyl]-acryloyl}-methyl-amino)-dodecyl]-carbamic acid *tert*-butyl ester-trifluoro-acetate salt, **S17** (1.35 g, 1.43 mmol, 1 equiv.) in 25 mL of THF was added succinic acid monohex-5-enyl

ester, **S18** (0.37 g, 1.86 mmol, 1.3 equiv) in 25 mL of $CHCl_3$, followed by 0.5 mL of triethylamine until pH 14. This was followed by addition of BOP (0.95 g, 2.15 mmol, 1.5 equiv) and a further 0.5 mL of triethylamine to maintain a basic mixture. After 10 minutes a pale yellow solution was obtained and the reaction mixture was stirred at room temperature for a further 2 hours. Concentration under reduced pressure gave a yellow oil which was subjected to column chromatography (silica gel, 3:97 MeOH/$CHCl_3$). Excess HMPA remained in the yellow oil, which was washed with Et_2O to give the product as a pale white solid.

Selected data for [12-({3-[(12-{3-[4-(4-Hept-6-enoylamino-benzoyl)-phenylcarbamoyl]-acryloylamino}-dodecyl)-methyl-carbamoyl]-acryloyl}-methyl-amino)-dodecyl]-carbamic acid hex-5-enyl ester, 6: Yield 1.22 g (86%); ^{1}H NMR (400 MHz, $CDCl_3$/1% MeOD): δ = 10.26 (brs, 1H, ArNHCO), 8.65 (brs, 1H, ArNHCO), 7.76–7.64 (m, 10H, CH=CHCONH & $NHCOCH_2$ & ArH, benzophenone), 7.32 (m, 2H, NCH_3COCH=$CHNCH_3$), 6.98 & 6.91 (d, J = 15.2 Hz, 2H, NHCOCH=CHCONH), 5.77 (m, 2H, CH_2=CH), 4.94 (m, 4H, CH_2=CH), 4.04 (t, J = 6.6 Hz, CO_2CH_2), 3.39 (m, 4H, CH_2NCH_3), 3.29 (m, 2H, CH_2NHCO), 3.16 (m, CH=CHCONHCH_2), 3.08 & 2.98 (s, 6H, NCH_3), 2.62 (t, J = 6.8 Hz, $NHCOCH_2CH_2CO_2$), 2.42 (t, J = 6.8 Hz, $NHCOCH_2CH_2CO_2$), 2.37 (t, J = 7.3 Hz, 2H, $CH_2CONHAr$), 2.05 (m, 4H, CH_2=CHCH_2), 1.72 (quint, J = 7.6 Hz, 2H, $CH_2CH_2CONHAr$), 1.57 (m, 8H, $CO_2CH_2CH_2$ & 2 x $CH_2CH_2NCH_3$ & CH_2CH_2NHCO), 1.44 (m, 6H, $CO_2CH_2CH_2CH_2$ & CH_2=$CHCH_2CH_2$ & CH=CHCONHCH$_2$CH_2), 1.23 (brs, 32H, CH_2, alkyl); ^{13}C NMR (100 MHz, $CDCl_3$/1% MeOD): δ = 195.05, 191.35, 173.49, 172.45, 171.79, 165.41, 164.78, 163.56, 142.36, 142.03, 138.38, 138.25, 134.02, 133.44, 132.78, 132.64, 131.37, 131.32, 131.00, 119.26, 119.18, 118.67, 114.81, 114.71, 64.79, 50.39, 49.98, 49.76, 49.55, 49.34, 49.12, 48.91, 48.70, 48.41, 39.91, 39.68, 39.54, 37.26, 35.57, 34.26, 33.42, 33.20, 30.85, 29.62, 29.46, 29.41, 29.36, 29.28, 29.24, 29.19, 29.04, 28.42,

27.89, 27.01, 26.85, 26.55, 25.06, 24.93; HRMS (FAB, THIOG matrix): *m/z* = 1093.73126 [$(M+H)^+$] (anal. calcd for $C_{64}H_{97}N_6O_9$: *m/z* = 1093.73170).

Hept-6-enoyl chloride, S2

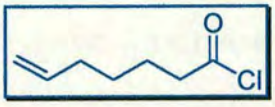

To a stirred solution of 6-heptenoic acid (4.60 mL, 33.8 mmol, 1 equiv.) in 90 mL of CH_2Cl_2 was added thionyl chloride (19.7 mL, 270 mmol, 8 equiv.), one drop of DMF (cat.) and stirred at 65 °C for 2 hours. Distillation of thionyl chloride and CH_2Cl_2 yielded the acid chloride as a yellow oil.

Selected data for hept-6-enoyl chloride, S2: Yield 4.98 g (quantitative); ^{1}H NMR (400 MHz, $CDCl_3$): δ = 5.78 (m, 1H, CH_2=C<u>H</u>), 5.01 (m, 2H, C<u>H$_2$</u>=CH), 2.90 (m, 2H, CH_2COCl), 2.08 (m, 2H, CH_2=CHC<u>H$_2$</u>), 1.74 (m, 2H, C<u>H$_2$</u>CH_2COCl), 1.47 (m, 2H, CH_2=$CHCH_2$C<u>H$_2$</u>); ^{13}C NMR (100 MHz, $CDCl_3$): δ = 174.14, 138.20, 115.60, 47.32, 33.50, 27.95, 24.85.

Hept-6-enoic acid {4-[1-(4-amino-phenyl)-2-oxo-vinyl]-phenyl}-amide, S3

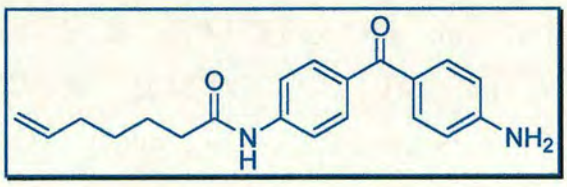

To a stirred solution of 4,4'-diaminobenzophenone (10.00 g, 47.1 mmol, 1 equiv.) and triethylamine (9.9 mL, 70.7 mmol, 1.5 equiv.) in 700 mL of THF was added hept-6-enoyl chloride, **S2** (3.30 g, 22.6 mmol, 0.48 equiv.) in 100 mL of THF at 0 °C over 10 minutes. The reaction mixture was stirred at room temperature for 2 hours. The volume of THF was reduced to 50 mL and 500 mL of $CHCl_3$ was added. The

organic phase was washed with 1 M aqueous HCl (3 x 350 mL), saturated aqueous $NaHCO_3$ (3 x 350 mL), brine (350 mL), dried over anhydrous $MgSO_4$ and concentrated under reduced pressure to give a mixture of monosubstituted and disubstituted benzophenone as a yellow oil. The yellow oil was subjected to column chromatography (silica gel, 40:60 $CHCl_3$/cyclohexane) to elute the disubstituted benzophenone and $CHCl_3$ to elute the desired monosubstituted product.

Monosubstituted:

Selected data for hept-6-enoic acid {4-[1-(4-amino-phenyl)-2-oxo-vinyl]-phenyl}-amide, S3: Yield 7.23 g (96%); m.p. 136 °C; ^{1}H NMR (400 MHz, DMSO-d_6): δ = 10.12 (brs, 1H, CONH), 7.73 (d, J = 8.6 Hz, 2H, ArH, benzophenone), 7.61 (d, J = 8.6 Hz, 2H, ArH, benzophenone), 7.53 (d, J = 8.6 Hz, 2H, ArH, benzophenone), 6.62 (d, J = 8.6 Hz, 2H, ArH, benzophenone), 6.11 (brs, 2H, NH_2), 5.83 (m, 1H, CH_2=C<u>H</u>), 5.02 (m, 2H, C<u>H$_2$</u>=CH), 2.38 (t, J = 7.6 Hz, 2H, C<u>H$_2$</u>CONH), 2.06 (q, J = 7.6 Hz, 2H, CH_2=CHC<u>H$_2$</u>), 1.62 (quintet, J = 7.6 Hz, 2H, C<u>H$_2$</u>CH_2CONH), 1.41 (quintet, J = 7.6 Hz, 2H, CH_2=$CHCH_2$C<u>H$_2$</u>); ^{13}C NMR (100 MHz, DMSO-d_6): δ = 192.41, 171.60, 153.36, 142.05, 138.52, 133.13, 132.32, 130.14, ,124.18, ,118.02, 114.81, 112.48, 36.26, 32.90, 27.82, 24.50; HRMS (FAB, THIOG matrix): m/z = 323.17639 [$(M+H)^+$] (anal. calcd for $C_{20}H_{23}N_2O_2$: m/z = 323.17595).

Disubstituted:

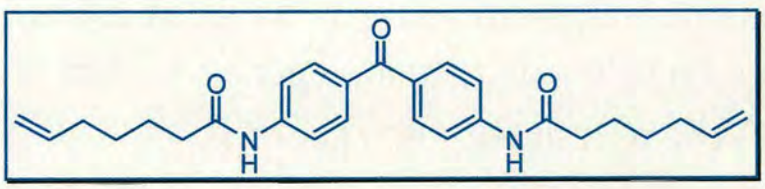

Selected data for hept-6-enoic acid {4-[1-(4-hept-6-enoylamino-phenyl)-2-oxo-vinyl]-phenyl}-amide, S4: Yield 0.88 g (4%); m.p. 179 °C; ^{1}H NMR (400 MHz,

DMSO-d_6): δ = 10.27 (brs, 2H, CONH), 7.78 (d, J = 8.8 Hz, 4H, ArH, benzophenone), 7.71 (d, J = 8.8 Hz, 4H, ArH, benzophenone), 5.83 (m, 2H, CH_2=C<u>H</u>), 5.01 (m, 4H, C<u>H_2</u>=CH), 2.39 (t, J = 7.3 Hz, 4H, C<u>H_2</u>CONH), 2.07 (q, J = 7.3 Hz, 4H, CH_2=CHC<u>H_2</u>), 1.63 (m, 4H, C<u>H_2</u>CH_2CONH), 1.42 (m, 4H, CH_2=CHCH_2C<u>H_2</u>); ^{13}C NMR (100 MHz, DMSO-d_6): δ = 193.31, 171.75, 143.04, 134.51, 131.64, 130.82, 118.13, 114.81, 36.28, 32.89, 27.81, 24.46; HRMS (FAB, THIOG matrix): m/z = 433.25903 [$(M+H)^+$] (anal. calcd for $C_{27}H_{33}N_2O_3$: m/z = 433.24912).

3-Chlorocarbonyl-acrylic acid ethyl ester, <u>S5</u>

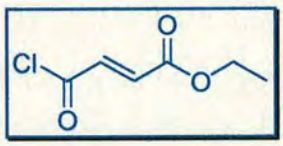

To a suspension of fumaric acid monoethyl ester (4.00 g, 47 mmol, 1 equiv.) in 30 mL of CH_2Cl_2 was added one drop of DMF (cat.) and thionyl chloride (16 mL, 222 mmol, 8 equiv.) and heated to 40 °C for 30 minutes until complete dissolution. Distillation of thionyl chloride and CH_2Cl_2 yielded the acid chloride as a pale yellow oil.

Selected data for 3-chlorocarbonyl-acrylic acid ethyl ester, S5: Yield 4.51 g (quantitative); ^{1}H NMR (400 MHz, $CDCl_3$): δ = 7.01 (d, J = 15.3 Hz, 1H, C<u>H</u>=CH), 6.96 (d, J = 15.3 Hz, 1H, CH=C<u>H</u>), 4.30 (q, J = 7.0 Hz, 2H, C<u>H_2</u>CH_3), 1.34 (t, J = 7.0 Hz, 3H, CH_2C<u>H_3</u>); ^{13}C NMR (100 MHz, $CDCl_3$): δ = 165.80, 164.15, 138.30, 137.12, 62.46, 14.44; MS (ESI): m/z = 197.7 [$(M+Cl)^-$].

3-[4-(4-Hept-6-enoylamino-benzoyl)-phenylcarbamoyl]-acrylic acid ethyl ester, S6

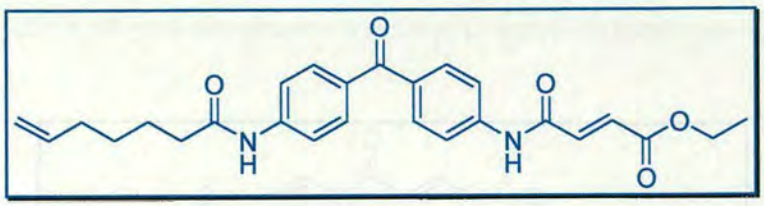

To a stirred solution of hept-6-enoic acid {4-[1-(4-amino-phenyl)-2-oxo-vinyl]-phenyl}-amide, **S3** (6.00 g, 17.9 mmol, 1 equiv.) and triethylamine (5 mL, 70.9 mmol, 2 equiv.) in 80 mL of THF was added 3-chlorocarbonyl-acrylic acid ethyl ester, **S5** (4.40 g, 26.9 mmol, 1.5 equiv.) in 20 mL of THF at 0 °C over 10 minutes. The reaction mixture was stirred at room temperature for 2 hours. The volume of THF was reduced to 20 mL and 50 mL of $CHCl_3$ was added. The organic phase was washed with 1 M aqueous HCl (3 x 50 mL), saturated aqueous $NaHCO_3$ (3 x 50 mL), brine (50 mL), dried over anhydrous $MgSO_4$ and concentrated under reduced pressure to give the product as a yellow solid.

Selected data for 3-[4-(4-hept-6-enoylamino-benzoyl)-phenylcarbamoyl]-acrylic acid ethyl ester, S6: Yield 7.24 g (90%); m.p. 225 °C; ^{1}H NMR (400 MHz, DMSO-d_6): δ = 10.91 (brs, 1H, CONH), 10.27 (brs, 1H, CONH), 7.86, (d, J = 8.8 Hz, 2H, ArH, benzophenone), 7.78 (d, J = 8.8 Hz, 2H, ArH, benzophenone), 7.76 (d, J = 9.0 Hz, 2H, ArH, benzophenone), 7.73 (d, J = 9.0 Hz, 2H, ArH, benzophenone), 7.26 (d, J = 15.3 Hz, 1H, C$\underline{H}$=CH), 6.77 (d, J = 15.3 Hz, 1H, CH=C$\underline{H}$), 5.83 (m, 1H, CH_2=C$\underline{H}$), 5.01 (m, 2H, C$\underline{H_2}$=CH), 4.24 (q, J = 7.0 Hz, 2H, C$\underline{H_2}CH_3$), 2.39 (t, J = 7.3 Hz, 2H, C$\underline{H_2}$CONH), 2.08 (q, J = 7.3 Hz, 2H, CH_2=CHC$\underline{H_2}$), 1.64 (q, J = 7.3 Hz, 2H, C$\underline{H_2}CH_2$CONH), 1.42 (quintet, J = 7.3 Hz, 2H, CH_2=CHCH$_2$C$\underline{H_2}$), 1.29 (t, J = 7.3 Hz, 3H, $CH_2C\underline{H_3}$); ^{13}C NMR (100 MHz, DMSO-d_6): δ = 193.31, 171.79, 164.78, 161.76, 143.19, 142.11, 138.51, 137.23, 132.74, 131.43, 130.90, 130.86, 129.99, 118.75, 118.16, 114.82, 60.85, 36.28, 32.89, 27.81, 24.45, 13.98; HRMS (FAB,

THIOG matrix): *m/z* = 449.20833 $[(M+H)^+]$ (anal. calcd for $C_{26}H_{29}N_2O_5$: *m/z* = 449.20765).

3-[4-(4-Hept-6-enoylamino-benzoyl)-phenylcarbamoyl]-acrylic acid, S7

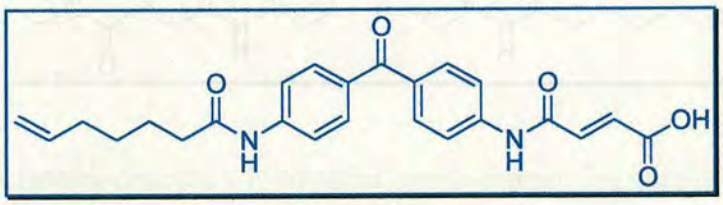

To a stirred solution of 3-[4-(4-hept-6-enoylamino-benzoyl)-phenylcarbamoyl]-acrylic acid ethyl ester, **S6** (2.00 g, 4.5 mmol, 1 equiv.) in 20 mL of THF was added 1 M aqueous NaOH (0.20 g in 5 mL H_2O, 4.9 mmol, 1.1 equiv.). The yellow solution was stirred at room temperature for 16 hours after which TLC indicated some unreacted ester remained. Additional 1 M aqueous NaOH (0.04 g in 1 mL H_2O, 0.98 mmol, 0.2 equiv.) was added and stirred for a further 6 hours. Water was added to the reaction mixture, followed by dropwise addition of concentrated HCl until pH 1. The reaction mixture extracted with 1:5 THF/$CHCl_3$ (3 x 50 mL), dried with anhydrous $MgSO_4$ and concentrated under reduced pressure to give the acid as a yellow solid.

Selected data for 3-[4-(4-hept-6-enoylamino-benzoyl)-phenylcarbamoyl]-acrylic acid, S7: Yield 1.64 g (83%); m.p. 263 °C; ^{1}H NMR (400 MHz, DMSO-d_6): δ = 10.92 (brs, 1H, CONH), 10.32 (brs, 1H, CONH), 7.92–7.77 (m, 8H, ArH, benzophenone), 7.25 (d, *J* = 15.3 Hz, 1H, C<u>H</u>=CH), 6.77 (d, *J* = 15.3 Hz, 1H, CH=C<u>H</u>), 5.88 (m, 1H, CH_2=C<u>H</u>), 5.07 (m, 2H, C<u>H_2</u>=CH), 2.44 (t, *J* = 7.3 Hz, 2H, C<u>H_2</u>CONH), 2.12 (q, *J* = 7.3 Hz, 2H, CH_2=CHC<u>H_2</u>), 1.68 (m, 2H, C<u>H_2</u>CH_2CONH), 1.47 (quintet, *J* = 7.3 Hz, 2H, CH_2=$CHCH_2$C<u>H_2</u>); ^{13}C NMR (100 MHz, DMSO-d_6): δ = 193.31, 171.79, 166.17, 162.05, 143.17, 142.16, 138.51, 136.73, 132.66, 131.42, 131.28, 130.93, 130.89, 118.73, 118.13, 114.84, 36.28, 32.91, 27.80, 24.42; HRMS

(FAB, THIOG matrix): *m/z* = 421.17715 [$(M+H)^+$] (anal. calcd for $C_{24}H_{25}N_2O_5$: *m/z* = 421.17635).

(12-Amino-dodecyl)-carbamic acid *tert*-butyl ester, S8

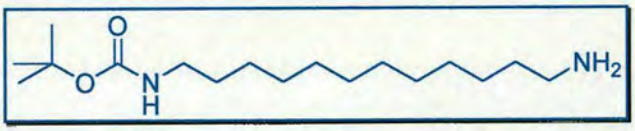

To a solution of 1,12-diaminododecane (20 g, 100 mmol, 1 equiv.) in 600 mL of $CHCl_3$ (slight suspension) was added a solution of di-*tert*-butyl dicarbonate (10.90 g, 50 mmol, 0.5 equiv.) in 200 mL of $CHCl_3$. Immediate precipitation occurred on addition and the resulting suspension was stirred for 16 hours at room temperature. The precipitate was filtered and the filtrate concentrated under reduced pressure to give a white solid (a mixture of diamine, monoprotected and diprotected amine). The white solid was subjected to column chromatography (silica gel, 5:95 MeOH/$CHCl_3$ and 1:10:89 NH_4OH/MeOH/$CHCl_3$) to yield in order of elution the diprotected amine and monoprotected amine.

Selected data for (12-amino-dodecyl)-carbamic acid *tert*-butyl ester, S8: Yield 8.53 g (57%); m.p. 96 °C; ^1H NMR (400 MHz, $CDCl_3$): δ = 4.54 (brs, 1H, OCONH), 3.09 (m, 2H, OCONHC$\underline{H}_2$), 2.67 (t, *J* = 6.8 Hz, 2H, C$\underline{H}_2NH_2$), 1.43 (brs, 13H, CH_3, *t*-butyl & CH_2, alkyl), 1.38 (brs, 2H, NH_2), 1.25 (brs, 16H, CH_2, alkyl); ^{13}C NMR (100 MHz, $CDCl_3$): δ = 157.64, 79.69, 42.24, 40.63, 33.86, 30.06, 29.60, 29.55, 29.53, 29.48, 29.28, 28.42, 26.88, 26.80; HRMS (FAB, THIOG matrix): *m/z* = 301.28491 [$(M+H)^+$] (anal. calcd for $C_{17}H_{37}N_2O_2$: *m/z* = 301.28550).

Diprotected:

Selected data for (12-*tert*-butoxycarbonylamino-dodecyl)-carbamic acid *tert*-butyl ester, S9: Yield 3.7 g (43%); m.p. 115 °C; ^{1}H NMR (400 MHz, $CDCl_3$): δ = 4.51 (brs, 2H, OCONH), 3.10 (m, 4H, OCONHC<u>H</u>$_2$), 1.45 (brs, 13H, CH_3, *t*-butyl & CH_2, alkyl), 1.27 (m, 16H, CH_2, alkyl); ^{13}C NMR (100 MHz, $CDCl_3$): δ = 157.62, 79.69, 40.63, 30.06, 29.51, 29.27, 28.43, 26.79, 20.60; HRMS (FAB, THIOG matrix): *m/z* = 401.33864 [$(M+H)^+$] (anal. calcd for $C_{22}H_{45}N_2O_4$: *m/z* = 401.33793).

[12-(Toluene-4-sulfonylamino)-dodecyl]-carbamic acid *tert*-butyl ester, <u>S10</u>

To a stirred solution of (12-amino-dodecyl)-carbamic acid *tert*-butyl ester, **S8** (3.80 g, 12.6 mmol, 1 equiv.) and triethylamine (2.1 mL, 15.2 mmol, 1.2 equiv.) in 10 mL of $CHCl_3$ was added *p*-toluenesulfonyl chloride (2.70 g, 13.9 mmol, 1.1 equiv.) in 15 mL of THF over ten minutes. The reaction mixture was stirred for 16 hours after which, 50 mL of $CHCl_3$ was added. The organic phase was washed with 1 M aqueous HCl (3 x 50 mL), saturated aqueous $NaHCO_3$ (3 x 50 mL), brine (50 mL), dried over anhydrous $MgSO_4$ and concentrated under reduced pressure to give a white solid. The white solid was found to contain both the product and unreacted *p*-toluenesulfonyl chloride, which was removed by washing with warm hexane (3 x 50 mL).

Selected data for [12-(toluene-4-sulfonylamino)-dodecyl]-carbamic acid *tert*-butyl ester, S10: Yield 5 g (88%); m.p. 98 °C; ^{1}H NMR (400 MHz, $CDCl_3$): δ = 7.75 (d, *J* = 8.1 Hz, 2H, ArH, phenyl), 7.30 (d, *J* = 8.1 Hz, 2H, ArH, phenyl), 4.57 (brs, 1H, $NHSO_2$), 4.52 (brs, 1H, OCONH), 3.10 (m, 2H, $OCONHC\underline{H}_2$), 2.92 (q, *J* = 6.8 Hz, 2H, $C\underline{H}_2NHSO_2$), 2.43 (s, 3H, $ArCH_3$), 1.44 (brs, 13H, $OCONHCH_2C\underline{H}_2$ & $C\underline{H}_2CH_2NHSO_2$ & CH_3, *t*-butyl), 1.28–1.20 (m, 16H, CH_2, alkyl); ^{13}C NMR (100 MHz, $CDCl_3$): δ = 156.40, 143.60, 137.49, 130.03, 127.50, 79.69, 43.61, 41.02, 30.44, 29.91, 29.88, 29.86, 29.82, 29.78, 29.65, 29.43, 28.83, 27.17, 26.89, 21.90; HRMS (FAB, THIOG matrix): *m/z* = 455.29346 $[(M+H)^+]$ (anal. calcd for $C_{24}H_{43}N_2O_4S$: *m/z* = 455.29436). Anal. calcd for $C_{24}H_{42}N_2O_4S$: C 63.40, H 9.31, N 6.16. Found C 63.25, H 9.44, N 5.85.

{12-[Methyl-(toluene-4-sulfonyl)-amino]-dodecyl}-carbamic acid *tert*-butyl ester, S11

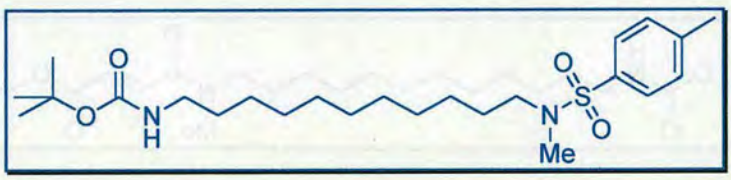

To a solution of [12-(toluene-4-sulfonylamino)-dodecyl]-carbamic acid *tert*-butyl ester, **S10** (6.60 g, 14.5 mmol, 1 equiv.) in 85 mL of acetone was added methyl iodide (27 mL, 435 mmol, 30 equiv.) followed by addition of vacuum dried K_2CO_3 (21.1 g, 145 mmol, 10 equiv.). The resulting suspension was heated at 40 °C for 16 hours; TLC showed some unreacted **S10** remained. Additional methyl iodide (10.8 mL, 174 mmol, 12 equiv.) was added and stirred at 40 °C for a further 16 hours until completion. The suspension was filtered and concentrated under reduced pressure to give a viscous oil. This was dissolved in 100 mL of $CHCl_3$ and washed with water (50 mL), brine (2 x 50mL), dried over anhydrous $MgSO_4$ and concentrated under reduced pressure to give a white solid.

Selected data for {12-[methyl-(toluene-4-sulfonyl)-amino]-dodecyl}-carbamic acid *tert*-butyl ester, S11: Yield 6.63 g (98%); m.p. 51 °C; ^{1}H NMR (400 MHz, $CDCl_3$): δ = 7.66 (d, *J* = 8.1 Hz, 2H, ArH, phenyl), 7.31 (d, *J* = 8.1 Hz, 2H, ArH, phenyl), 4.52 (brs, 1H, OCONH), 3.10 (m, 2H, OCONHC<u>H</u>$_2$), 2.96 (t, *J* = 7.1 Hz, 2H, C<u>H</u>$_2$NCH$_3$SO$_2$) 2.70 (s, 3H, ArCH$_3$), 2.48 (s, 3H, NCH$_3$), 1.52–1.44 (m, 13H, OCONHCH$_2$C<u>H</u>$_2$ & C<u>H</u>$_2$CH$_2$NCH$_3$SO$_2$ & CH$_3$, *t*-butyl), 1.28–1.25 (m, 16H, CH$_2$, alkyl); ^{13}C NMR (100 MHz, $CDCl_3$): δ = 155.99, 143.14, 134.55, 129.60, 127.41, 78.99, 50.11, 40.63, 34.55, 30.06, 29.71, 29.53, 29.51, 29.29, 29.22, 28.43, 27.59, 26.81, 26.51, 21.51; HRMS (FAB, THIOG matrix): *m/z* = 469.30959 [(M+H)$^+$] (anal. calcd for $C_{25}H_{45}N_2O_4S$: *m/z* = 469.31001). Anal. calcd for $C_{25}H_{44}N_2O_4S$: C 64.04, H 9.46, N 5.98. Found C 64.18, H 9.44, N 5.85.

3-[(12-*tert*-Butoxycarbonylamino-dodecyl)-methyl-carbamoyl]-acrylic acid ethyl ester, <u>S12</u>

A solution of fumaric acid monoethyl ester (1.46 g, 10.1 mmol, 1 equiv.), (12-methylamino-dodecyl)-carbamic acid *tert*-butyl ester, **3** (3.50 g, 11.1 mmol, 1.1 equiv.) and DMAP (1.24 g, 10.1 mmol, 1 equiv.) in 250 mL of $CH_2Cl_2$was stirred at 0 °C for 10 minutes followed by addition of EDCI.HCl (1.94 g, 10.1 mmol, 1 equiv.). The reaction mixture was stirred for 16 hours at room temperature. The organic layer was washed with 1 M aqueous HCl (3 x 150 mL), saturated aqueous $NaHCO_3$ (3 x 150 mL), brine (150 mL), dried over anhydrous $MgSO_4$ and concentrated under reduced pressure to give a yellow oil. The yellow oil was subjected to column chromatography (silica gel, 40:60 hexane/EtOAc) to yield the product as a colourless oil.

Selected data for 3-[(12-*tert*-butoxycarbonylamino-dodecyl)-methyl-carbamoyl]-acrylic acid ethyl ester, S12: Yield 3.97 g (89%); ^{1}H NMR (400 MHz, $CDCl_3$): δ = 7.39 (d, *J* = 15.4 Hz) & 7.38 (d, *J* = 15.2 Hz)[(1H, C<u>H</u>=CH)], 6.80 (d, *J* = 15.2 Hz) & 6.78 (d, *J* = 15.4 Hz) [(2H, C<u>H</u>=C<u>H</u>)], 4.51 (brs, 1H, OCONH), 4.26 (q, *J* = 7.1 Hz, 2H, $C\underline{H}_2CH_3$), 3.44 & 3.37 (m, 2H, $C\underline{H}_2NCH_3$), 3.11–3.02 (m, 5H, $OCONHC\underline{H}_2$ & $NC\underline{H}_3$), 1.55 (m, 2H, CH_2, alkyl), 1.45 (brs, 13H, $OCONHCH_2C\underline{H}_2$ & $C\underline{H}_2CH_2NCH_3$ & CH_3, *t*-butyl), 1.34–1.26 (m, 16H, $CH_2C\underline{H}_3$, CH_2, alkyl); ^{13}C NMR (100 MHz, $CDCl_3$): δ = 165.85, 164.59, 164.33, 155.98, 134.15, 133.84, 131.03, 130.98, 78.95, 61.06, 60.37, 50.27, 48.17, 40.61, 35.57, 33.98, 30.04, 29.49, 29.34, 29.25, 28.94, 28.41, 27.02, 26.89, 26.82, 26.78, 26.53, 21.03, 14.15; HRMS (FAB, THIOG matrix): *m/z* = 441.33215 [$(M+H)^+$] (anal. calcd for $C_{24}H_{45}N_2O_5$: *m/z* = 441.33285).

12-[(3-ethoxycarbonyl-acryloyl)-methyl-amino]-dodecyl-trifluoro-acetate salt, <u>S13</u>

To a stirred solution of 3-[(12-*tert*-butoxycarbonylamino-dodecyl)-methyl-carbamoyl]-acrylic acid ethyl ester, **S12** (1.70 g, 3.86 mmol, 1 equiv.) in 10 mL of $CHCl_3$ was added trifluoroacetic acid (20 mL, 38.6 mmol, 10 equiv.) and stirred at room temperature for 30 minutes until completion. The reaction mixture was concentrated under reduced pressure to give the product as a pale yellow oil.

Selected data for 12-[(3-ethoxycarbonyl-acryolyl)-methyl-amino]-dodecyl-trifluoro-acetate salt, S13: Yield 1.55 g (quantitative); ^{1}H NMR (400 MHz, $CDCl_3$): δ = 8.82 (brt, 3H, $CF_3CO_2^{-}\,{}^{+}NH_3$), 7.36 (2d, *J* = 15.4 Hz, 1H, C<u>H</u>=CH), 6.74 (2d, *J* = 15.4 Hz, 1H, CH=C<u>H</u>), 4.26 (q, *J* = 7.1 Hz, 2H, $C\underline{H}_2CH_3$), 3.43 (m, 2H, $C\underline{H}_2NCH_3$),

3.13–3.05 (m, 5H, OCONHC<u>H</u>$_2$ & NC<u>H</u>$_3$), 1.68–1.57 (m, 4H, CH_2, alkyl), 1.32 (t, J = 7.1, 3H, $CH_2C\underline{H}_3$), 1.26 (brs, 16H, CH_2, alkyl); ^{13}C NMR (100 MHz, $CDCl_3$): δ = 166.28, 166.17, 165.93, 160.35 (q, CF_3), 133.21, 132.80, 132.24, 132.08, 61.91, 61.39, 50.97, 49.03, 40.88, 36.12, 34.69 ,29.11, 29.07, 29.04, 29.02, 28.93, 28.81, 28.62, 28.54, 28.48, 27.56, 27.26, 27.23, 26.64, 26.47, 26.25, 25.89, 25.82, 13.91.

3-[(12-{3-[4-(4-Hept-6-enoylamino-benzoyl)-phenylcarbamoyl]-acryloylamino}-dodecyl)-methyl-carbamoyl]-acrylic acid ethyl ester, <u>S14</u>

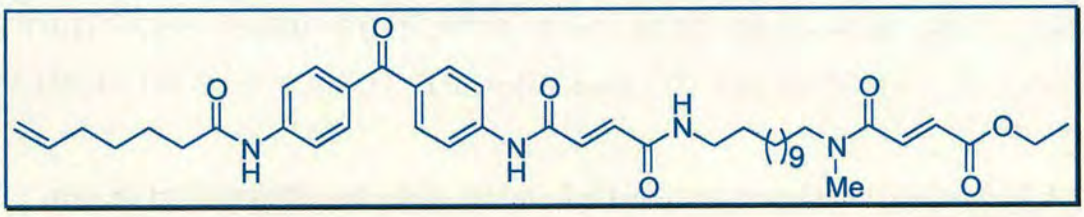

To a stirred solution of 12-[(3-ethoxycarbonyl-acryloyl)-methyl-amino]-dodecyl-trifluoro-acetate salt, **S13** (2.63 g, 5.80 mmol, 1.3 equiv) in 35 mL of $CHCl_3$ was added an excess of triethylamine (4 mL) until pH 10. This was followed by addition of a slight suspension of 3-[4-(4-hept-6-enoylamino-benzoyl)-phenylcarbamoyl]-acrylic acid, **S7** (2.00 g, 4.46 mmol, 1 equiv.) in 25 mL of THF to obtain a dark brown solution; a further 0.5 mL of triethylamine was added to maintain a basic pH. To the resulting reaction mixture was added BOP (2.96 g, 6.69 mmol, 1.5 equiv) and stirred at room temperature for 1 hour. Concentration under reduced pressure gave a brown oil which was subjected to column chromatography (silica gel, 2:98 MeOH/$CHCl_3$) to give the product as a yellow solid.

Selected data for 3-[(12-{3-[4-(4-hept-6-enoylamino-benzoyl)-phenylcarbamoyl]-acryloylamino}-dodecyl)-methyl-carbamoyl]-acrylic acid ethyl ester, S14: Yield 2.46 g (69%); m.p. 234 °C; ^{1}H NMR (600 MHz, DMSO-d_6): δ = 10.79 (brs, 1H, ArNHCO), 10.27 (brs, 1H, ArNHCO), 8.50 (brt, 1H, CONH), 7.87–7.71 (m, 8H,

ArH, benzophenone), 7.41 (d, J = 15.4 Hz, 1H, $NCH_3COC\underline{H}=CHCO_2$), 7.10 & 7.03 (d, J = 15.1 Hz, 2H, $NHCOC\underline{H}=C\underline{H}CONH$), 6.55 (2d, J = 15.4 Hz, 1H, $NCH_3COCH=C\underline{H}CO_2$), 5.83 (m, 1H, $CH_2=C\underline{H}$), 5.01 (m, 2H, $C\underline{H_2}=CH$), 4.20 (q, J = 7.10 Hz, 2H, $C\underline{H_2}CH_3$), 3.18 (m, 2H, $CH=CHCONHC\underline{H_2}$), 3.05 & 2.90 (s, 3H, NCH_3), 2.39 (t, J = 7.4 Hz, 2H, $C\underline{H_2}CONHAr$), 2.08 (q, J = 7.2 Hz, $CH_2=CHC\underline{H_2}$), 1.64 (m, 2H, $C\underline{H_2}CH_2CONHAr$), 1.46 (m, 6H, $CH_2=CHCH_2C\underline{H_2}$ & $C\underline{H_2}NCH_3$ & CH_2, alkyl), 1.25 (m, 19H, $CH_2C\underline{H_3}$, CH_2, alkyl); ^{13}C NMR (100 MHz, DMSO-d_6): δ = 193.33, 171.82, 165.06, 163.82, 163.54, 163.16, 162.76, 143.13, 142.43, 138.51, 135.13, 134.74, 134.63, 132.51, 132.41, 132.22, 132.06, 131.53, 130.89, 129.50, 129.43, 118.60, 118.13, 114.86, 60.66, 49.06, 47.08, 36.27, 35.01, 33.36, 32.90, 28.92, 28.80, 28.70, 28.65, 28.52, 28.18, 27.79, 26.36, 26.16, 25.76, 24.45, 13.98; HRMS (FAB, THIOG matrix): m/z = 743.44061 $[(M+H)^+]$ (anal. calcd for $C_{43}H_{59}N_4O_7$: m/z = 743.43838). Anal. calcd for $C_{43}H_{58}N_4O_7$: C 69.52, H 7.87, N 7.54. Found C 69.14, H 7.80, N 7.33.

3-[(12-{3-[4-(4-Hept-6-enoylamino-benzoyl)-phenylcarbamoyl]-acryloylamino}-dodecyl)-methyl-carbamoyl]-acrylic acid, S15

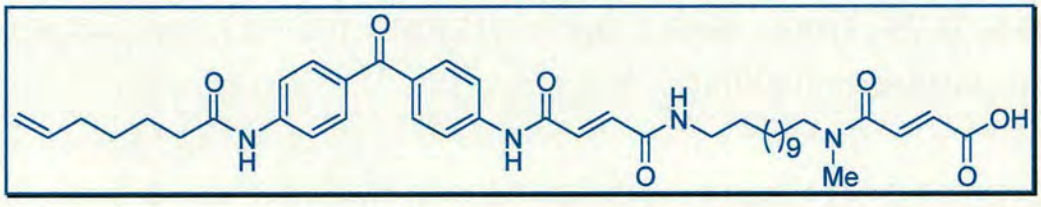

To 3-[(12-{3-[4-(4-hept-6-enoylamino-benzoyl)-phenylcarbamoyl]-acryloylamino}-dodecyl)-methyl-carbamoyl]-acrylic acid ethyl ester, **S14** (1.50 g, 2.02 mmol, 1 equiv.) was added 60 mL of THF and 10 mL MeOH, which resulted in the formation of a yellow viscous solution. This was followed by addition of 1 M aqueous NaOH (0.10 g in 2.5 mL H_2O, 2.42 mmol, 1.2 equiv.), after 5 minutes, a brown solution was obtained that was left to stir at room temperature for 16 hours. Water was added to the reaction mixture followed by dropwise addition of concentrated HCl until pH 1.

The reaction mixture extracted with 1:5 THF/$CHCl_3$ (3 x 80 mL), combined, dried over anhydrous $MgSO_4$ and concentrated under reduced pressure to give the acid as a yellow solid.

Selected data for 3-[(12-{3-[4-(4-hept-6-enoylamino-benzoyl)-phenylcarbamoyl]-acryloylamino}-dodecyl)-methyl-carbamoyl]-acrylic acid, S15: Yield 1.44 g (quantitative); m.p. 242 °C; ^{1}H NMR (400 MHz, DMSO-d_6): δ = 10.80 (brs, 1H, ArNHCO), 10.28 (brs, 1H, ArNHCO), 8.51 (brt, 1H, CONH), 7.87–7.72 (m, 8H, ArH, benzophenone), 7.35 (d, J = 15.4 Hz, 1H, $NCH_3COC\underline{H}=CHCO_2$), 7.10 & 7.03 (d, J = 15.2 Hz, 2H, $NHCOC\underline{H}=C\underline{H}CONH$), 6.50 (2d, J = 15.4 Hz, 1H, $NCH_3COCH=C\underline{H}CO_2$), 5.83 (m, 1H, $CH_2=C\underline{H}$), 5.02 (m, 2H, $C\underline{H_2}=CH$), 3.18 (q, J = 6.8 Hz, 2H, $CH=CHCONHC\underline{H_2}$), 3.05 & 2.90 (s, 3H, NCH_3), 2.39 (t, J = 7.6 Hz, 2H, $C\underline{H_2}CONHAr$), 2.08 (q, J = 7.1 Hz, $CH_2=CHC\underline{H_2}$), 1.63 (m, 2H, $C\underline{H_2}CH_2CONHAr$), 1.46 (m, 6H, $CH_2=CHCH_2C\underline{H_2}$ & $C\underline{H_2}NCH_3$ & CH_2, alkyl), 1.26 (m, 19H, $CH_2C\underline{H_3}$, CH_2, alkyl); ^{13}C NMR (100 MHz, DMSO-d_6): δ = 193.31, 171.79, 166.45, 163.59, 163.14, 162.76, 143.15, 142.43, 138.52, 134.63, 134.48, 134.05, 132.41, 132.22, 131.45, 130.94, 130.90, 130.80, 130.70, 118.59, 118.12, 114.86, 49.10, 47.08, 36.27, 34.99, 33.40, 32.91, 28.94, 28.81, 28.67, 28.29, 27.80, 26.38, 26.20, 25.84, 24.45; HRMS (FAB, THIOG matrix): m/z = 715.40873 [$(M+H)^+$] (anal. calcd for $C_{41}H_{55}N_4O_7$: m/z = 715.40708).

[12-({3-[(12-{3-[4-(4-Hept-6-enoylamino-benzoyl)-phenylcarbamoyl]-acryloylamino}-dodecyl)-methyl-carbamoyl]-acryloyl}-methyl-amino)-dodecyl]-carbamic acid *tert*-butyl ester, S16

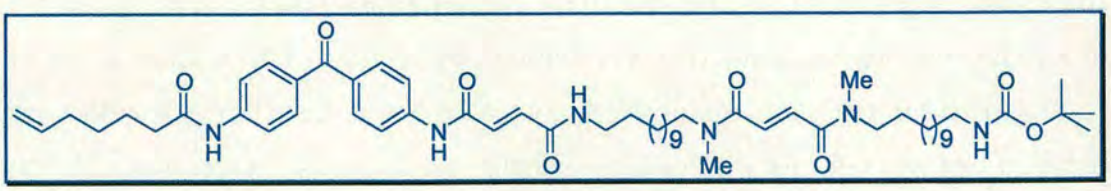

To a stirred solution of (12-methylamino-dodecyl)-carbamic acid *tert*-butyl ester, **3** (0.85 g, 2.69 mmol, 1.3 equiv) in 30 mL of $CHCl_3$ was added a slight suspension of 3-[(12-{3-[4-(4-hept-6-enoylamino-benzoyl)-phenylcarbamoyl]-acryloylamino}-dodecyl)-methyl-carbamoyl]-acrylic acid **S15** (1.48 g, 2.07 mmol, 1 equiv.) in 35 mL of THF to give a orange suspension. Triethylamine (1 mL) was added until pH 10 followed by BOP (1.37 g, 3.11 mmol, 1.5 equiv). The resulting suspension was stirred at room temperature for 10 minutes, after which, an orange solution was obtained which was stirred for a further 90 minutes. Concentration under reduced pressure gave a yellow oil which was subjected to column chromatography (silica gel, 3:97 MeOH/$CHCl_3$) to give the product as a pale yellow solid.

Selected data for [12-({3-[(12-{3-[4-(4-hept-6-enoylamino-benzoyl)-phenylcarbamoyl]-acryloylamino}-dodecyl)-methyl-carbamoyl]-acryloyl}-methyl-amino)-dodecyl]-carbamic acid *tert*-butyl ester, S16: Yield 1.54 g (74%); m.p. 204 °C; ^{1}H NMR (400 MHz, DMSO-d_6): δ = 10.78 (brs, 1H, ArNHCO), 10.26 (brs, 1H, CONHAr), 8.49 (brt, 1H, CH=CHCONH), 7.87–7.71 (m, 8H, ArH, benzophenone), 7.20 (m, 2H, NCH_3COCH=$CHCONCH_3$), 7.10 & 7.03 (d, J = 15.1 Hz, 2H, NHCOCH=CHCONH), 6.74 (brt, 1H, $NHCO_2$), 5.83 (m, 1H, CH_2=CH), 5.01 (m, 2H, CH_2=CH), 3.38 (m, 2H, CH_2, alkyl), 3.19 (m, 2H, CH=CHCONHCH_2), 3.04 (brs, 2H, NCH_3), 2.90 (m, 6H, NCH_3 & CH_2NHCO_2), 2.39 (t, J = 7.3 Hz, 2H, CH_2CONHAr), 2.08 (q, J = 7.1 Hz, CH_2=CHCH_2), 1.64 (m, 2H, CH_2CH_2CONHAr), 1.46 (m, 8H, CH_2=$CHCH_2CH_2$ & CH_2NCH_3 & CH_2, alkyl), 1.38 (s, 9H, $NHCO_2C(CH_3)_3$), 1.24 (m, 38H, CH_2, alkyl); ^{13}C NMR (100 MHz, DMSO-d_6): δ = 193.29, 171.77, 164.42, 164.14, 163.16, 162.77, 157.69, 143.15, 142.44, 138.51, 134.64, 132.43, 132.21, 131.48, 131.09, 131.04, 130.90, 130.86, 130.74, 130.70, 118.59, 118.13, 114.03, 77.19, 49.12, 47.05, 36.28, 34.99, 33.37, 32.90, 29.42, 28.93, 28.82, 28.74, 28.67, 28.38, 28.21, 27.81, 26.51, 26.38, 26.21, 25.91, 24.45; HRMS (FAB, THIOG matrix): *m/z*=1011.69013 [$(M+H)^+$] (anal. calcd for $C_{59}H_{91}N_6O_8$: *m/z* = 1011.68984).

[12-({3-[(12-{3-[4-(4-hept-6-enoylamino-benzoyl)-phenylcarbamoyl]-acryloylamino}-dodecyl)-methyl-carbamoyl]-acryloyl}-methyl-amino)-dodecyl]-carbamic acid *tert*-butyl ester-trifluoro-acetate salt, S17

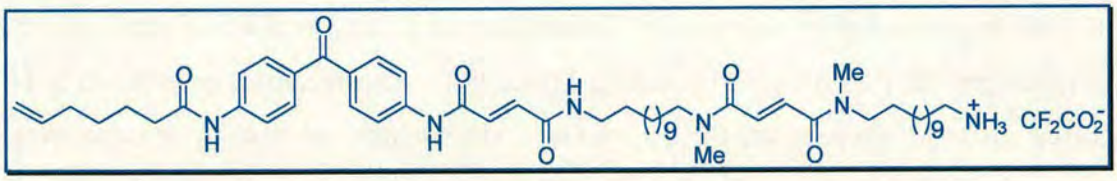

To a stirred suspension of [12-({3-[(12-{3-[4-(4-hept-6-enoylamino-benzoyl)-phenylcarbamoyl]-acryloylamino}-dodecyl)-methyl-carbamoyl]-acryloyl}-methyl-amino)-dodecyl]-carbamic acid *tert*-butyl ester, **S16** (1.45 g, 1.43 mmol, 1 equiv.) in 10 mL of $CHCl_3$ was added trifluoroacetic acid (5 mL, excess) and the resulting yellow solution was stirred at room temperature for 30 minutes until completion. The reaction mixture was concentrated under reduced pressure and precipitated using Et_2O to give a pale yellow solid.

Selected data for [12-({3-[(12-{3-[4-(4-hept-6-enoylamino-benzoyl)-phenylcarbamoyl]-acryloylamino}-dodecyl)-methyl-carbamoyl]-acryloyl}-methyl-amino)-dodecyl]-carbamic acid *tert*-butyl ester, S17: Yield 1.4 g (95%); m.p. 195 °C; ^{1}H NMR (400 MHz, $CDCl_3$): δ = 10.81 (brs, 1H, ArNHCO), 10.30 (brs, 1H, ArNHCO), 8.52 (brt, *J* = 5.6 Hz, 1H, CONH), 7.87–7.71 (m, 8H, ArH, benzophenone), 7.68 (brs, 3H, $C\underline{H}_2NH_3$), 7.20 (m, 2H, $NCH_3COC\underline{H}=C\underline{H}NCH_3$), 7.10 & 7.03 (d, *J* = 15.6 Hz, 2H, $NHCOC\underline{H}=C\underline{H}CONH$), 5.83 (m, 1H, $CH_2=C\underline{H}$), 5.01 (m, 2H, $C\underline{H}_2=CH$), 3.36 (m, 2H, $C\underline{H}_2$, alkyl), 3.18 (m, 2H, $CONHC\underline{H}_2$), 3.05 & 2.90 (s, 6H, NCH_3), 2.77 (m, 2H, $C\underline{H}_2NH_3$), 2.39 (t, *J* = 7.3 Hz, 2H, $C\underline{H}_2CONHAr$), 2.07 (q, *J* = 7.1 Hz, $CH_2=CHC\underline{H}_2$), 1.63 (m, 2H, $C\underline{H}_2CH_2CONHAr$), 1.46 (m, 10H, $CH_2=CHCH_2C\underline{H}_2$ & $C\underline{H}_2CH_2NCH_3$ & $CONHCH_2C\underline{H}_2$, & CH_2, alkyl), 1.25 (m, 34H, $CH_2C\underline{H}_3$, CH_2, alkyl); ^{13}C NMR (100 MHz, $CDCl_3$): δ = 193.30, 171.80, 164.36, 164.13, 163.15, 162.76, 143.16, 142.44, 138.51, 134.63, 132.41, 132.22, 131.44,

131.09, 131.03, 130.93, 130.89, 130.74, 130.68, 118.58, 118.12, 114.85, 49.11, 47.06, 36.27, 34.97, 33.41, 32.91, 28.94, 28.87, 28.81, 28.67, 28.48, 28.39, 27.80, 26.94, 26.51, 26.37, 26.22, 25.91, 25.72, 24.45; HRMS (FAB, THIOG matrix): *m/z* = 1046.60148 [$(M+Na)^+$] (anal. calcd for $C_{56}H_{82}F_3N_6O_8Na$: *m/z* = 1046.60442).

Succinic acid monohex-5-enyl ester, S18

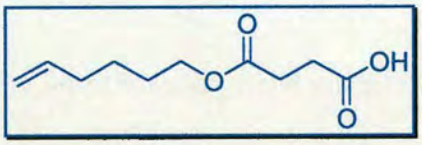

To a solution of succinic anhydride (2.00 g, 20.0 mmol, 1 equiv.) in 90 mL of CH_2Cl_2 was added triethylamine (4.2 mL, 30.0 mmol, 1.5 equiv.) followed by 5-hexen-1-ol (2.4 mL, 20.0 mmol, 1 equiv.) and stirred at room temperature for 16 hours. The resulting solution mixture was washed with 1 M aqueous HCl (3 x 50 mL), brine (50 mL), dried with anhydrous $MgSO_4$ and concentrated under reduced pressure to give the product as a colourless oil.

Selected data for succinic acid monohex-5-enyl ester, S18: Yield 3.92 g (98%); ^{1}H NMR (400 MHz, $CDCl_3$): δ = 5.80 (m, 1H, CH_2=C<u>H</u>), 5.00 (m, 2H, C<u>H_2</u>=CH), 4.12 (t, *J* = 6.6 Hz, 2H, C<u>H_2</u>OCO), 2.69 (t, *J* = 6.6 Hz, 2H, OCOC<u>H_2</u> or C<u>H_2</u>CO_2H), 2.64 (t, *J* = 6.6 Hz, 2H, OCOC<u>H_2</u> or C<u>H_2</u>CO_2H), 2.09 (m, 2H, CH_2=CHC<u>H_2</u>), 1.66 (m, 2H, C<u>H_2</u>CH_2OCO), 1.46 (m, 2H, CH_2=$CHCH_2$C<u>H_2</u>); ^{13}C NMR (100 MHz, $CDCl_3$): δ = 177.13, 172.15, 138.29, 114.83, 64.80, 33.22, 28.90, 28.80, 27.98, 25.12; HRMS (FAB, NBA matrix): *m/z* = 201.11250 [$(M+H)^+$] (anal. calcd for $C_{10}H_{17}O_4$: *m/z* = 201.11268).

_N_-[4-(4-Amino-benzoyl)-phenyl]-2,2-diphenyl-acetamide, S19

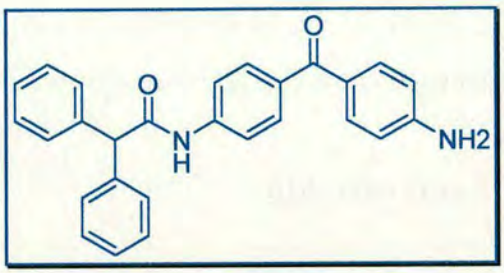

To a stirred solution of 4,4'-diaminobenzophenone (3.00 g, 14.1 mmol, 1 equiv.) and triethylamine (1.97 mL, 14.1 mmol, 1 equiv.) in 210 mL of THF was added diphenyl acetyl chloride (1.57 g, 6.78 mmol, 0.48 equiv.) in 50 mL of THF at 0 °C over 10 minutes. The reaction mixture was allowed to warm to room temperature and stirred for a further 2 hours. The volume of THF was reduced to 20 mL and 50mL of $CHCl_3$ was added. The combined organic phase was washed with 1 M aqueous HCl (3 x 50 mL), saturated aqueous $NaHCO_3$ (3 x 50 mL), brine (50 mL), dried over anhydrous $MgSO_4$, filtered and concentrated under reduced pressure to give the product as a yellow solid.

Selected data for _N_-[4-(4-amino-benzoyl)-phenyl]-2,2-diphenyl-acetamide, S19: Yield 2.5 g (90%); m.p. 266 °C; ^{1}H NMR (400 MHz, DMSO-d_6): δ = 10.73 (brs, 1H, CONH), 7.78 (d, J = 8.8 Hz, 2H, ArH, benzophenone), 7.63 (d, J = 8.6 Hz, 2H, ArH, benzophenone), 7.53 (d, J = 8.6 Hz, 2H, ArH, benzophenone), 7.41–7.26 (m, 10H, ArH, phenyl), 6.62 (d, J = 8.8 Hz, 2H, ArH, benzophenone), 6.13 (brs, 2H, NH_2), 5.25 (s, 1H, $Ph_2C\underline{H}$); ^{13}C NMR (100 MHz, DMSO-d_6): δ = 192.38, 170.28, 153.44, 141.70, 139.69, 133.68, 132.35, 130.16, 128.51, 128.38, 126.88, 124.08, 118.34, 112.47, 57.39; HRMS (FAB, THIOG martix): m/z = 407.17588 [$(M+H)^+$] (anal. calcd for $C_{27}H_{23}N_2O_2$: m/z = 407.17595).

3-[4-(4-Diphenylacetylamino-benzoyl)-phenylcarbamoyl]-acrylic acid ethyl ester, S20

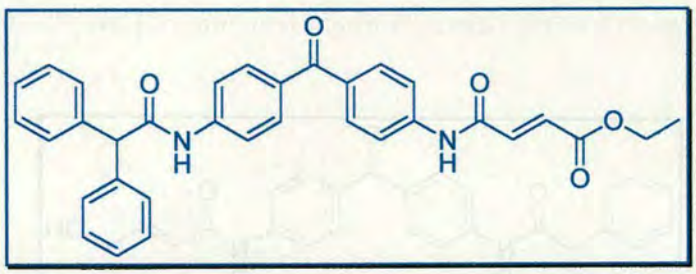

To a stirred solution of *N*-[4-(4-amino-benzoyl)-phenyl]-2,2-diphenyl-acetamide, **S19** (1.50 g, 3.69 mmol, 1 equiv.) and triethylamine (0.77 mL, 5.53 mmol, 1.5 equiv.) in 100 mL of THF was added 3-chlorocarbonyl-acrylic acid ethyl ester, **S5** (0.90 g, 5.53 mmol, 1.5 equiv.) in 10 mL of THF at 0 °C over 10 minutes. The reaction mixture was allowed to warm to room temperature and stirred for a further 2 hours. The volume of THF was reduced to 10 mL and 50 mL of $CHCl_3$ was added. The combined organic phase was washed with 1 M aqueous HCl (3 x 50 mL), saturated aqueous $NaHCO_3$ (3 x 50 mL), brine (50 mL), dried over anhydrous $MgSO_4$, filtered and concentrated under reduced pressure to give the product as a yellow solid.

Selected data for 3-[4-(4-diphenylacetylamino-benzoyl)-phenylcarbamoyl]-acrylic acid ethyl ester, S20: Yield 1.52 g (77%); m.p. >283 °C (decompose); ^{1}H NMR (400 MHz, DMSO-d_6): δ = 10.94 (brs, 1H, CONH), 10.84 (brs, 1H, CONH), 7.88–7.73 (m, 8H, ArH, benzophenone), 7.40–7.25 (m, 11H, ArH, phenyl & C<u>H</u>=CH), 6.77 (d, J = 15.41 Hz, 1H, CH=C<u>H</u>), 5.27 (s, 1H, $Ph_2C\underline{H}$), 4.24, (q, J = 7.07 Hz, 2H, $C\underline{H}_2CH_3$), 1.29 (t, J = 7.07 Hz, 3H, $CH_2C\underline{H}_3$); ^{13}C NMR (100 MHz, DMSO-d_6): δ = 193.34, 170.45, 166.18, 162.07, 142.84, 142.22, 139.58, 137.21, 136.72, 132.56, 131.93, 131.31, 130.96, 130.02, 128.51, 126.92, 118.73, 118.45,

60.88, 57.39, 13.98; HRMS (FAB, THIOG matrix): *m/z* = 533.20830 $[(M+H)^+]$ (anal. calcd for $C_{33}H_{29}N_2O_5$: *m/z* = 533.20765).

3-[4-(4-Diphenylacetylamino-benzoyl)-phenylcarbamoyl]-acrylic acid, S21

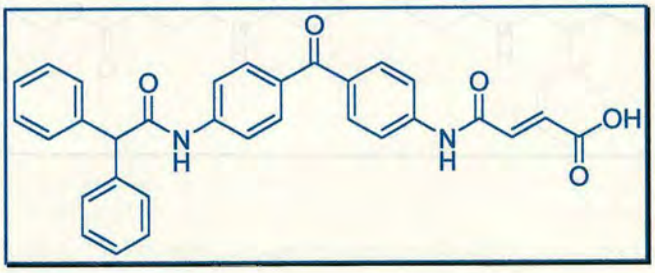

To a stirred solution of 3-[4-(4-diphenylacetylamino-benzoyl)-phenylcarbamoyl]-acrylic acid ethyl ester, **S20** (1.00 g, 1.9 mmol, 1 equiv.) in 20 mL of THF was added 1 M aqueous NaOH (0.08 g in 2.1 mL H_2O, 2.1 mmol, 1.1 equiv.). The yellow solution was stirred at room temperature for 16 hours after which TLC indicated some unreacted ester remained. Additional 1 M aqueous NaOH (16 mg in 0.42 mL H_2O, 0.42 mmol, 0.2 equiv.) was added and the reaction mixture was stirred for an extra 6 hours. The volume of THF was reduced to 5 mL and poured into water, followed by acidifying *via* dropwise addition of concentrated HCl until the formation of the acid as a precipitate, which was filtered and washed with diethyl ether to give an orange solid.

Selected data for 3-[4-(4-diphenylacetylamino-benzoyl)-phenylcarbamoyl]-acrylic acid, S21: Yield 0.92 g (98%); m.p. 228 °C; ^{1}H NMR (400 MHz, DMSO-d_6): δ = 13.03 (brs, 1H, COOH), 10.86 (brs, 1H, CONH), 10.79 (brs, 1H, CONH), 7.87–7.71 (m, 8H, ArH, benzophenone), 7.40–7.27 (m, 10H, ArH, phenyl), 7.19 (d, *J* = 15.3 Hz, 1H, C<u>H</u>=CH), 6.73 (d, *J* = 15.3 Hz, 1H, CH=C<u>H</u>), 5.25 (s, $Ph_2C\underline{H}$); HRMS (FAB, THIOG matrix): *m/z* = 505.17610 $[(M+H)^+]$ (anal. calcd for $C_{31}H_{25}N_2O_5$: *m/z* = 505.17635).

3-(2,2-Diphenyl-ethylcarbamoyl)-acrylic acid ethyl ester, S22

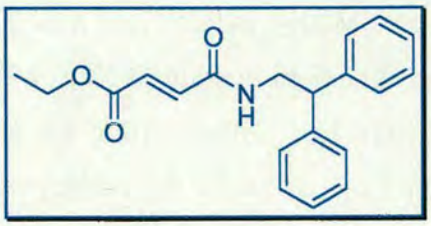

To a solution of 2,2-diphenylamine (5.00 g, 25 mmol, 1.1 equiv.) in 150 mL of CH_2Cl_2 was added fumaric acid monoethyl ester (3.32 g, 23 mmol, 1 equiv.), followed by addition of DMAP (2.81 g, 23 mmol, 1 equiv.). The resulting mixture was cooled to 0 °C and EDCI.HCl (4.42 g, 23 mmol, 1 equiv.) was added and stirred at room temperature for 16 hours. The reaction mixture was washed successively with 1 M aqueous HCl (50 mL), saturated $NaHCO_3$ (2 x 50 mL), brine (50 mL), dried over anhydrous $MgSO_4$ and concentrated under reduced pressure to give the product as a white solid.

Selected data for 3-(2,2-diphenyl-ethylcarbamoyl)-acrylic acid ethyl ester, S22: Yield 7.48 g, (91%); ^{1}H NMR (400 MHz, $CDCl_3$): δ = 7.67–7.10 (m, 10H, ArH, phenyl), 6.78 (2d, J = 15.3 Hz, 2H, CH=CH), 6.03 (brt, 1H, NHCO), 4.30–4.10 (m, 3H, Ph_2CH & CH_2CH_3), 4.01 (2d, J = 7.9 Hz, 2H, Ph_2CHCH_2), 1.32 (t, J = 7.2 Hz, 3H, CH_2CH_3); ^{13}C NMR (100 MHz, $CDCl_3$): δ = 165.0, 164.0, 141.92, 136.5, 130.9, 129.2, 128.4, 127.4, 61.57, 50.8, 44.55, 14.51; HRMS (FAB, NBA matrix): m/z = 324.15982 [$(M+H)^+$] (anal. calcd for $C_{20}H_{22}NO_3$: m/z = 324.15997).

3-(2,2-Diphenyl-ethyl)-methyl-carbamoyl)-acrylic acid ethyl ester, S23

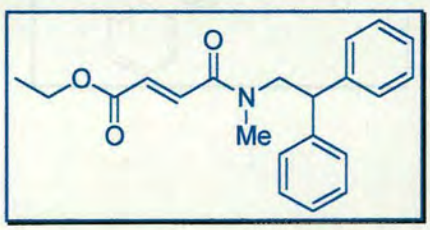

A solution of 3-(2,2-diphenyl-ethylcarbamoyl)-acrylic acid ethyl ester, **S22** (1.50 g, 4.64 mmol, 1 equiv.), in 30 mL of anhydrous DMF was stirred at room temperature, under a nitrogen atmosphere. Methyl iodide (1.44 mL, 23.2 mmol, 5 equiv.) was added followed by addition of sodium hydride (0.22 g, 9.28 mmol, 1.2 equiv., 60% dispersion in oil) over 10 minutes. After stirring for a further 20 minutes, the reaction was quenched with 5 mL of EtOH, the solvent was reduced and 50 mL of EtOAc was added followed by washing of the organic phase with water (3 x 20 mL), dried over anhydrous $MgSO_4$, filtered and concentrated under reduced pressure to give a brown oil. Column chromotography (silica gel, 2:98 MeOH/$CHCl_3$) yielded the product as a yellow oil.

Selected data for 3-(2,2-diphenyl-ethyl)-methyl-carbamoyl)-acrylic acid ethyl ester, S23: Yield 1.2 g (76%); ^{1}H NMR (400 MHz, $CDCl_3$): δ = 7.31–7.17 (m, 10H, ArH, phenyl), 6.90 & 6.70 & 6.40 (d, J = 15.4 Hz, 2H, C<u>H</u>=C<u>H</u>), 4.44 (t, J = 8.1 Hz) & 4.20[(m, 1H, C<u>H</u>Ph_2)], 4.20 (m, 2H, $CH_3C\underline{H_2}$), 4.09 & 4.01 (d, J = 8.1 Hz, 2H, $C\underline{H_2}CHPh_2$), 2.95 & 2.77 (s, 3H, NCH_3), 1.29 (m, 3H, $C\underline{H_3}CH_2$); ^{13}C NMR (100 MHz, $CDCl_3$): δ = 165.74, 165.59, 165.20, 164.84, 157.64, 141.77, 141.05, 134.08, 133.07, 130.97, 130.02, 128.82, 128.60, 128.16, 128.14, 127.22, 126.80, 61.11, 60.88, 55.61, 53.49, 49.88, 48.80, 36.73, 34.61, 14.19, 14.16; HRMS (FAB, THIOG matrix): m/z = 338.17526 [$(M+H)^+$] (anal. calcd for $C_{21}H_{24}N_2O_2$: m/z = 338.17562).

3-(2,2-Diphenyl-ethyl)-methyl-carbamoyl)-acrylic acid, <u>S24</u>

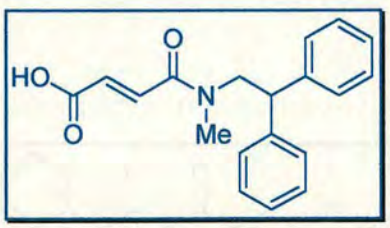

To a solution of 3-(2,2-diphenyl-ethyl)-methyl-carbamoyl)-acrylic acid ethyl ester, **S23** (1.00 g, 3 mmol, 1 equiv.) in 20 mL of EtOH was added 1 M aqueous NaOH (0.59 g in 14.8 mL H_2O, 14.8 mmol, 5 equiv.) and stirred at room temperature for 30 minutes. The volume of EtOH was reduced to 5 mL and poured into water followed by acidifying *via* dropwise addition of concentrated HCl until a precipitate resulted. The precipitate was filtered to give the acid as a colourless solid.

Selected data for 3-(2,2-diphenyl-ethyl)-methyl-carbamoyl)-acrylic acid (mixture of two rotamers), S24: Yield 0.77 g (84%); m.p. 97 °C; ^{1}H NMR (400 MHz, $CDCl_3$): δ = 7.30–7.17 (m, 11H, ArH, phenyl & C<u>H</u>=C<u>H</u>), 6.93 & 6.68 & 6.38 (d, J = 15.2 Hz, 1.5 H, C<u>H</u>=C<u>H</u>), 4.44 (t, J = 8.1 Hz) & 4.18 (t, J = 7.6 Hz)[(2H, C<u>H</u>Ph_2)], 4.08 (d, J = 8.1 Hz) & 4.01 (d, J = 7.6 Hz)[(2H, C<u>H$_2$</u>CHPh_2)], 2.99 & 2.77 (s, 3H, NCH_3); ^{13}C NMR (100 MHz, $CDCl_3$): δ = 169.47, 169.36, 165.13, 164.82, 157.64, 141.65, 140.90, 135.75, 134.61, 130.25, 129.11, 128.87, 128.63, 128.14, 127.32, 126.86, 55.72, 53.58, 49.67, 48.76, 36.79, 34.71; HRMS (FAB, NBA matrix): m/z = 310.14494 [$(M+H)^+$] (anal. calcd for $C_{19}H_{20}NO_3$: m/z = 310.14432).

[12-({3-[2,2-Diphenyl-ethyl)-methyl-carbamoyl]-acryloyl-methyl-amino)-dodecyl]-carbamic acid tert-butyl ester, <u>S25</u>

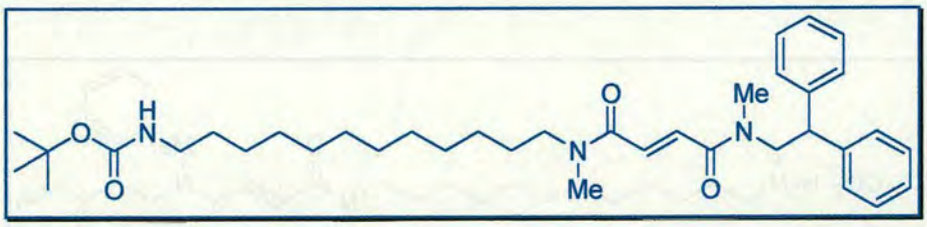

To a stirred solution of (12-methylamino-dodecyl)-carbamic acid *tert*-butyl ester, **3** (0.60 g, 1.9 mmol, 1.2 equiv.) in 10 mL of $CHCl_3$ was added excess triethylamine until pH 14. This was followed by addition of 3-(2,2-diphenyl-ethyl)-methyl-carbamoyl)-acrylic acid, **S24** (0.49 g, 1.6 mmol, 1 equiv.) in 5mL of THF and BOP

(1.05 g, 2.4 mmol, 1.5 equiv.) in 5 mL of $CHCl_3$. Triethylamine was added until pH 14 and the reaction mixture was stirred at room temperature for 16 hours. Concentration under reduced pressure gave a yellow oil which was subjected to column chromatography (silica gel, 2:98 MeOH/$CHCl_3$) to give the product as a yellow solid.

Selected data for [12-({3-[2,2-diphenyl-ethyl)-methyl-carbamoyl]-acryloyl-methyl-amino)-dodecyl]-carbamic acid tert-butyl ester, S25: Yield 0.9 g (94%); ^{1}H NMR (400 MHz, $CDCl_3$): δ = 7.16–6.81 (m, 12H, CH=CH & ArH, phenyl), 4.25 & 4.02 (m, 2H, NHCO, C<u>H</u>Ph), 3.87 (m, 2H, C<u>H</u>$_2$CHPh), 3.24–3.10 (m, 2H, C<u>H</u>$_2$N), 2.90 (brm, C<u>H</u>$_2$N), 2.80 & 2.71 & 2.68 & 2.59 (s, 6H, NCH_3), 1.36 (m, 2H, C<u>H</u>$_2$-CH_2N), 1.25 (brs, 11H CH_3, *t*-butyl, CH_2, alkyl), 1.05 (brs, 16H, CH_2, alkyl); ^{13}C NMR (100 MHz, $CDCl_3$): δ = 160.87, 160.48, 157.78, 141.47, 131.63, 131.37, 130.96, 130.70, 129.90, 128.78, 128.20, 127.17, 126.94, 55.55, 54.13, 50.64, 48.73, 40.29, 36.94, 36.90, 36.56, 35.79, 35.12, 34.62, 29.08, 28.08, 28.91, 28.65, 27.31, 26.37, 26.02; HRMS (FAB, THIOG matrix): *m/z* = 606.42744 [$(M+H)^+$] (anal. calcd for $C_{37}H_{56}N_3O_4$: *m/z* = 606.42708).

12-({3-[(2,2-diphenyl-ethyl)-methyl-carbamoyl]-acryloyl}-methyl-amino)-dodecyl-trifluoro-acetate salt, <u>S26</u>

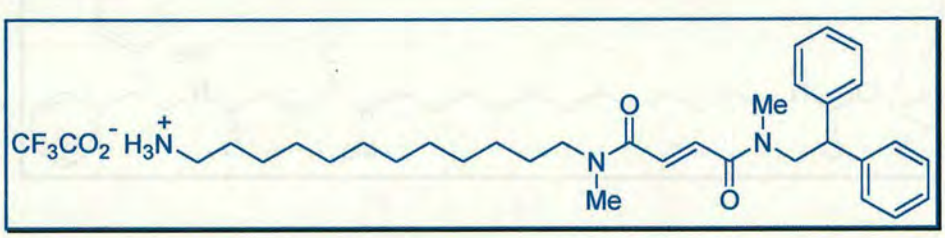

To a stirred solution of [12-({3-[2,2-diphenyl-ethyl)-methyl-carbamoyl]-acryloyl-methyl-amino)-dodecyl]-carbamic acid tert-butyl ester, **S25** (0.88 g, 1.45 mmol, 1 equiv.) in 10 mL of $CHCl_3$ was added trifluoroacetic acid (0.6 mL, 7.3 mmol,

1 equiv.) and stirred at room temperature for 30 minutes until completion. The reaction mixture was concentrated under reduced pressure to afford a yellow oil.

Selected data for 12-({3-[(2,2-diphenyl-ethyl)-methyl-carbamoyl]-acryloyl}-methyl-amino)-dodecyl-trifluoro-acetate salt, S26: Yield 0.9 g (quantitative); ^{1}H NMR (400 MHz, $CDCl_3$): δ = 8.18 (brs, 3H, NH_3), 7.19–6.72 (m, 12H, CH=CH, ArH, phenyl), 4.29 & 4.07 (m, 1H, CHPh), 3.97 (m, 2H, $C\underline{H}_2$CHPh), 3.32–3.15 (m, CH_2N), 2.98–2.51 (m, 8H, CH_2, alkyl & CH=CH), 1.56–1.40 (m, 4H, CH_2, alkyl), 1.13 (brs, 16H, CH_2, alkyl).

But-2-enedioic acid [4-(4-diphenylacetylamino-benzoyl)-phenyl]-amide [12-({3-[2,2-diphenyl-ethyl)-methyl-carbamoyl]-acryloyl}-methyl-amino)-dodecyl]-amide, S27

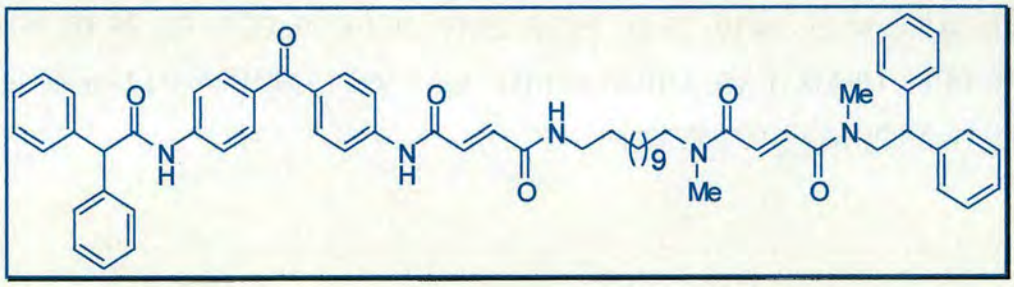

To a stirred solution of 12-({3-[(2,2-diphenyl-ethyl)-methyl-carbamoyl]-acryloyl}-methyl-amino)-dodecyl-trifluoro-acetate salt, **S26** (0.90 g, 1.45 mmol, 1.2 equiv.) in 20 mL of $CHCl_3$ was added excess triethylamine until pH 14. This was followed by addition of 3-[4-(4-diphenylacetylamino-benzoyl)-phenylcarbamoyl]-acrylic acid, **S21** (0.61 g, 1.21 mmol, 1 equiv.) in 5 mL of DMF and BOP (0.80 g, 1.82 mmol, 1.5 equiv.) in 5 mL of $CHCl_3$. Additional triethylamine was added until pH 14 and the reaction mixture was stirred at room temperature for 16 hours. Concentration under reduced pressure gave an yellow oil which was subjected to column chromatography (silica gel, 2:98 MeOH/$CHCl_3$) to give a pale yellow solid.

Selected data for But-2-enedioic acid [4-(4-diphenylacetylamino-benzoyl)-phenyl]-amide[12-({3-[2,2-diphenyl-ethyl)-methyl-carbamoyl]-acryloyl}-methyl-amino)-dodecyl]-amide, S27: Yield 0.35 g (24%); ^{1}H NMR (400 MHz, $CDCl_3$/1% MeOD): δ = 7.70–7.56 (m, 8H, ArH, benzophenone), 7.31–7.13 (m, 22H, ArH, phenyl & $NCH_3COC\underline{H}=C\underline{H}CONCH_3$), 7.02 & 6.92 (d, *J* = 15.2 Hz, 2H, $NHCOC\underline{H}=C\underline{H}CONH$), 5.05 (s, 1H, $Ph_2C\underline{H}CONH$), 4.36 & 4.13 (m, 1H, $CH_2C\underline{H}Ph_2$), 4.00 (m, 2H, $C\underline{H}_2CHPh_2$), 3.35–3.14 (m, 4H, $CONHC\underline{H}_2$ & $C\underline{H}_2NCH_3CO$), 3.02–2.71 (s, 6H, NCH_3), 1.47 & 1.17 (brs, 20H, CH_2, alkyl); ^{13}C NMR (100 MHz, $CDCl_3$): δ = 194.78, 170.86, 165.94, 165.59, 165.25, 164.70, 163.48, 142.02, 141.95, 141.74, 141.04, 140.99, 138.92, 134.08, 133.42, 133.09, 132.94, 131.29, 131.28, 130.97 ,130.68, 130.56, 130.27, 128.87, 128.78, 128.70, 128.56, 128.17, 128.12, 128.09, 127.43, 127.05, 126.99, 126.77, 119.33, 119.25, 118.80, 65.86, 59.45, 55.31, 55.26, 53.82, 53.76, 50.35, 50.20, 49.98, 49.84, 49.63, 49.41, 49.20, 48.99, 48.83, 48.40, 48.29, 40.08, 39.94, 36.75, 36.70, 35.55, 35.47, 34.82, 34.75, 34.25, 34.19, 29.41, 29.28, 29.17, 29.10, 29.03, 26.99, 26.87, 26.78, 26.55, 15.11; HRMS (FAB, THIOG matrix): *m/z* = 992.53390 $[(M+H)^+]$ (anal. calcd for $C_{63}H_{70}N_5O_6$: *m/z* = 992.53261).

6.5 References

1. Boyer, P. D. Energy, Life, and ATP (Nobel Lecture). *Angew. Chem. Int. Ed.* **37**, 2296–2307 (1998).
2. Walker, J. E. ATP Synthesis by Rotary Catalysis (Nobel lecture). *Angew. Chem. Int. Ed.* **37**, 2308–2319 (1998).
3. Kelly, T. R., De Silva, H. & Silva, R. A. *Nature* **401**, 150–152 (1999).
4. Kelly, T. R., Silva, R. A., De Silva, H., Jasmin, S. & Zhao, Y. *J. Am. Chem. Soc.* **122**, 6935–6949 (2000).
5. Koumura, N., Zijlstra, R. W. J., van Delden, R. A., Harada, N. & Feringa, B. L. Light-driven monodirectional molecular rotor. *Nature* **401**, 152–155 (1999).
6. Feringa, B. L., Koumura, N., van Delden, R. A. & ter Wiel, M. K. J. Light-driven molecular switches and motors. *Appl. Phys. A* **75**, 301–308 (2002).
7. Koumura, N. L., Geertsema, E. M., van Gelder, M. B., Meetsma, A. & Feringa, B. L. Second generation light-driven molecular motors. Unidirectional rotation controlled by a single stereogenic center with near-perfect photoequilibria and acceleration of the speed of rotation by structural modification. *J. Am. Chem. Soc.* **124**, 5037–5051 (2002).
8. van Delden, R. A., Koumura, N., Harada, N. & Feringa, B. L. *Proc. Natl. Acad. Sci. USA* **99**, 4945–4949 (2002).
9. Johnston, A. G., Leigh, D. A., Murphy, A., Smart, J. P. & Deegan, M. D. The synthesis and solubilisation of amide macrocycles via rotaxane formation. *J. Am. Chem. Soc.* **118**, 10662–10663 (1996).
10. Lane, A. S., Leigh, D. A. & Murphy, A. Peptide-based molecular shuttles. *J. Am. Chem. Soc.* **119**, 11092–11093 (1997).
11. Leigh, D. A., Murphy, A., Smart, J. P. & Slawin, A. M. Z. Glycylglycine rotaxanes – The hydrogen bond directed assembly of synthetic peptide rotaxanes. *Angew. Chem. Int. Ed. Engl.* **36**, 728–732 (1997).

12. Clegg, W. et al. "Smart" rotaxanes: Shape memory and control in tertiary amide peptido [2]rotaxanes. *J. Am. Chem. Soc.* **121**, 4124–4129 (1999).

13. Gatti, F. G. et al. Stiff, and sticky in the right places: The dramatic influence of preorganizing guest binding sites on the hydrogen bond-directed assembly of rotaxanes. *J. Am. Chem. Soc.* **123**, 5983–5989 (2001).

14. Wurpel, G. W. H., Brouwer, A. M., van Stokkum, I. H. M., Farran, A. & Leigh, D. A. Enhanced hydrogen bonding induced by optical excitation: Unexpected subnanosecond photoinduced dynamics in a peptide-based [2]rotaxane. *J. Am. Chem. Soc.* **123**, 11327–11328 (2001).

15. Asakawa, M. et al. Switching "on" and "off" the expression of chirality in peptide rotaxanes. *J. Am. Chem. Soc.* **124**, 2939–2950 (2002).

16. Biscarini, F. et al. The effect of mechanical interlocking on crystal packing: Predictions and testing. *J. Am. Chem. Soc.* **124**, 225–233 (2002).

17. Brancato, G. et al. From reactants to products via simple hydrogen-bonding networks: Information transmission in chemical reactions. *Proc. Natl. Acad. Sci. USA* **99**, 4967–4971 (2002).

CHAPTER SEVEN

Conclusions

Hydrogen bonding has been shown to be an extraordinarily effective tool for directing organic synthesis. With careful preorganisation of the distance, orientation and choice of hydrogen bond donating ability in a template, near-quantitative yields in hydrogen bond-directed rotaxane forming reactions can be achieved. Without such predetermined organisation, hydrogen bonding is *still* such a powerful influence that it 'finds a way' to direct the formation of rotaxanes in alkyl *bis*amides of virtually any length.

It has also been demonstrated that hydrogen bonding is a powerful tool for controlling large amplitude motions in mechanically interlocked systems: the rate of macrocycle pirouetting in a rotaxane can be varied, the position of the macrocycle on the thread of a molecular shuttle controlled, and even the direction of rotation of a macrocycle in a catenane governed, all solely through the use of light and thermal stimuli.

Can these types of molecules be used to realise Feynman's vision? Who knows! What I'm sure of, however, is that if 'molecular machines' are to become a practical reality it will require collaborations between combinations of synthetic chemists, physical chemists, materials scientists, physicists and engineers to make it happen. I hope the studies in this Thesis have contributed something towards this second industrial revolution.

"Do not go where the path may lead, instead go where there is no path and leave a trail."

Ralf Waldo Emerson

Other publications arising from my PhD Studies

(1999-2002)

Benzylic Imine Catenates: Readily Accessible Octahedral Analogues of the Sauvage Catenates

David A Leigh, Paul J Lusby, Simon J Teat, Andrew J Wilson, and Jenny K Y Wong

Angew. Chem. Int. Ed. ***2001***, 40, *1538–1543*

Benzylic Imine Catenates: Readily Accessible Octahedral Analogues of the Sauvage Catenates**

David A. Leigh,* Paul J. Lusby, Simon J. Teat, Andrew J. Wilson, and Jenny K. Y. Wong

Historically, one of the triumphs of coordination chemistry has been its application to the synthesis of mechanically interlocked molecular architectures, that is catenanes, rotaxanes, and knots.[1–10] In 1984 Sauvage et al. used the preferred tetrahedral geometry of Cu^{I} to organize appropriately derivatized phenanthroline ligands into a fixed mutually orthogonal orientation, whereupon a double macrocyclization reaction gave the [2]catenate in 27% yield (Scheme 1a).[2]

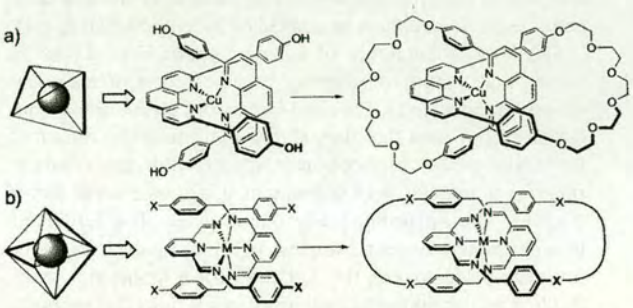

Scheme 1. Synthesis of catenates by orthogonalization of coordinated ligands about metal templates with a) tetrahedral and b) octahedral coordination preference. M in (b): Mn^{2+}, Fe^{2+}, Co^{2+}, Ni^{2+}, Cu^{2+}, Zn^{2+}, Cd^{2+}, Hg^{2+}.

[*] Prof. D. A. Leigh, Dr. P. J. Lusby, A. J. Wilson, J. K. Y. Wong
Centre for Supramolecular and Macromolecular Chemistry
Department of Chemistry, University of Warwick
Coventry CV47AL (UK)
Fax: (+44) 24-7652-3258
E-mail: David.Leigh@Warwick.ac.uk

Dr. S. J. Teat
CCLRC Daresbury Laboratory
Warrington (UK)

[**] This work was supported by the EPSRC. D.A.L. is an EPSRC Advanced Research Fellow (AF/982324). We thank Dr. B. P. Murphy (Manchester Metropolitan University) for useful discussions and Drs. T. J. Kidd, S. M. Lacy (University of Warwick), G. Di Orazio and R. Nasreen (University of Manchester, Institute of Science and Technology) for early ligand design.

Supporting information for this article is available on the WWW under http://www.angewandte.com or from the author.

  1433-7851/01/4008-1538 $ 17.50+.50/0

Subsequent studies on the system boosted yields to near quantitative levels (by ring closing metathesis, RCM)[3] and extended the interlocked architectures available to [*n*]catenates ($n = 2-8$),[4] catenands (the demetalated, but still interlocked ligands),[5] rotaxanes,[6] pseudo-rotaxanes,[7] and knots.[8] Interlocked ligands can have remarkable properties; catenates are amongst the most stable complexes of Cu^{I} that exist with a neutral ligand,[5] and catenands also stabilize[9] the ordinarily disfavored tetrahedral geometries of Ni^{I} and Cu^{0}. However, although other metals have been introduced[9] and alternative trigonal-bipyrimidal "stations" employed in redox-switchable systems,[10] the basic catenate assembly system based on a low oxidation state, tetrahedrally coordinated metal template and phenanthroline ligands has remained largely unchanged. Expanding this elegant strategy to include catenates with higher oxidation state, octahedrally coordinated metal centers is of obvious appeal (Scheme 1b),[11] and pioneering work in this regard has been carried out by Schröder et al.,[12] Busch et al.,[13] and others,[14, 14] yet only two octahedral catenates[1d, 14] (and two knots[15, 16]) have been described to date. Catenanes assembled by hydrogen bonds can exhibit a continuous range of (tunable) dynamic properties,[17, 18] but the strong coordination bonds present in catenates lock the macrocyclic components in fixed positions whereas, in the absence of the metal, these rings rotate with virtually complete (but uncontrolled) freedom. The difference in the type of dynamics available to each system led us to seek a route to catenates of a size and shape that would be both compatible and interchangeable in molecular devices with benzylic amide catenanes assembled by hydrogen bonds (e.g. **I**).

The basic architecture of benzylic amide macrocycles is rather well suited to adapting to other sorts of assembly processes (Scheme 2). The rigid framework positions multiple donor groups such that they converge towards the center of the cavity, while the isophthalic spacer holds the aromatic rings in a parallel arrangement at a distance ideal for π stacking with an orthogonally bound guest. The 1,3-linked benzylic motif ensures a complete 180° turn for each fragment (in comparison to, say, the 120° turn for a diphenylphenanthroline unit) holding the endgroups in positions that promote intracomponent rather than intercomponent cyclizations.[19] Thus, the only changes necessary to obtain a system based on metal ion chelation (i.e. arriving at complexes with the benzylic bis(2,6-diiminopyridine)catenand ligand **1**) was to replace the amide groups with imine groups and, for stability reasons, the phenolic esters with ethers (Scheme 2).

The zinc(II) perchlorate complex $[Zn\mathbf{2}_2](ClO_4)_2$ was isolated as a precipitate in 83% yield from simple addition of a solution of the Schiff base ligand **2**[20] in dichloromethane to a methanolic solution of $Zn(ClO_4)_2 \cdot 6H_2O$. Imines are one of the few classes of substrates not normally compatible with olefin metathesis (indeed, the free Schiff-base ligand **2** cannot be converted into the macrocycle by RCM). However, precoordination ties up the imine groups and the tetraolefin complex $[Zn\mathbf{2}_2](ClO_4)_2$ smoothly underwent double macrocyclization by RCM with Grubbs' catalyst ($[Ru(=CHPh)(PCy_3)_2Cl_2]$, CH_2Cl_2, Ar, RT, 4 h) to give the zinc(II) catenate $[Zn\mathbf{1}](ClO_4)_2$ in 73% yield as a mixture of *E*,*E*, *E*,*Z*, and *Z*,*Z* diastereomers (Scheme 2a). Exposure of the reaction mixture to the metathesis catalyst for four days equilibrated the products to give almost exclusively the *E*,*E* isomer.

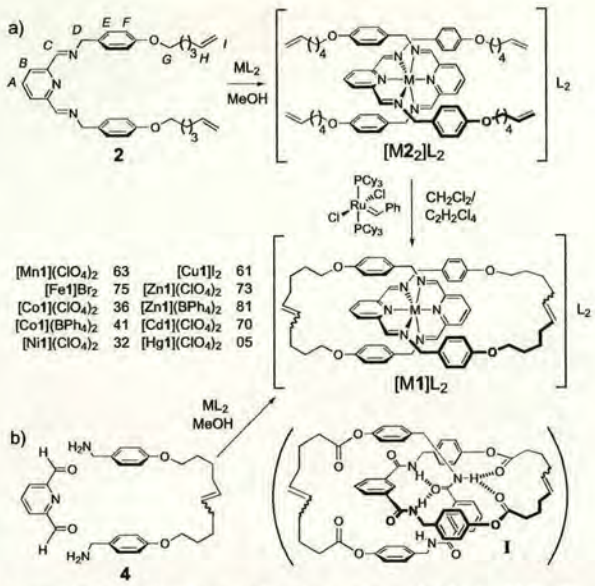

Scheme 2. Synthesis of benzylic imine catenates $[M\mathbf{1}]L_2$ by a) double macrocyclization of a preformed octahedral complex $[M\mathbf{2}_2]L_2$, b) spontaneous metal-promoted assembly of nonchelated precursors. The yields (in %) refer to route (a); the yields from route b are not yet optimized, but are uniformally higher. The ligand design is based on that of benzylic amide catenanes, e.g. **I**.[17b]

In contrast to the situation with the classic tetrahedral phenanthroline system, the same catenate $[Zn\mathbf{1}](ClO_4)_2$ could also be prepared by assembling the coordinating sites in situ (Scheme 2b). Treatment of the bis-amine **4**[21] with 2,6-pyridinedicarbaldehyde and $Zn(ClO_4)_2 \cdot 6H_2O$ in methanol resulted in the precipitation of the (*E*,*E*)-catenate after one hour in 53% yield. In this case, the metal center orders the construction of the catenate about itself, through the reversible formation of four imine bonds from five components, as the lowest energy means by which it can satisfy its desired octahedral coordination geometry.

The ^1H NMR spectra of free ligand **2**, zinc(II) precursor complex $[Zn\mathbf{2}_2](ClO_4)_2$, and zinc(II) catenate $[Zn\{(E,E)\text{-}\mathbf{1}\}](ClO_4)_2$ are shown in Figure 1a–c. Shielding of the benzylic aromatic rings (H_E, H_F) in both the precursor complex (Figure 1b) and the catenate (Figure 1c) with respect to the free ligand (Figure 1a) is indicative of the entwined (in the case of $[Zn\mathbf{2}_2]L_2$) or interlocked (in the case of $[Zn\{(E,E)\text{-}\mathbf{1}\}]L_2$) architectures. Interestingly, subtle but significant differences take place in the shifts of all the non-alkyl chain resonances between $[Zn\{(E,E)\text{-}\mathbf{1}\}]L_2$ and $[Zn\mathbf{2}_2]L_2$, indicating that a certain amount of reorganization of the ligands needs to occur during catenate formation.

Single crystals suitable for investigation by X-ray crystallography using a synchrotron source were obtained from slow vapor diffusion of diethyl ether into a solution of $[Zn\{(E,E)\text{-}\mathbf{1}\}](ClO_4)_2$ in acetonitrile.[22] The crystal structure (Figure 2) confirms the interlocked molecular architecture, the octahedral geometry around the coordinated zinc and the *E* configuration of the olefinic bonds in both rings. The benzylic

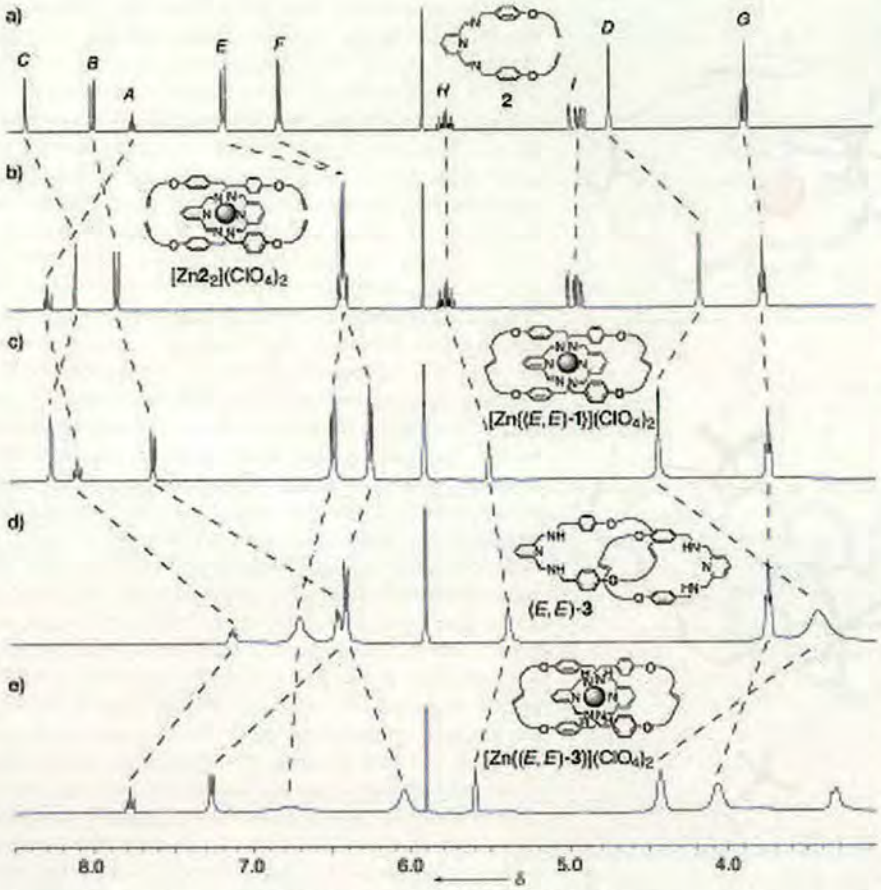

Figure 1. ^{1}H NMR spectra (400 MHz, $C_2D_2Cl_4$, 298 K) of a) free Schiff-base ligand **2**, b) acyclic tetraolefin precursor complex [Zn**2**$_2$](ClO$_4$)$_2$, c) benzylic imine catenate [Zn{(*E*,*E*)-**1**}](ClO$_4$)$_2$, d) free benzylic amine catenand (*E*,*E*)-**3**, and e) benzylic amine catenate [Zn{(*E*,*E*)-**3**}](ClO$_4$)$_2$. The assignments correspond to the lettering shown in Scheme 2 for compound **2**.

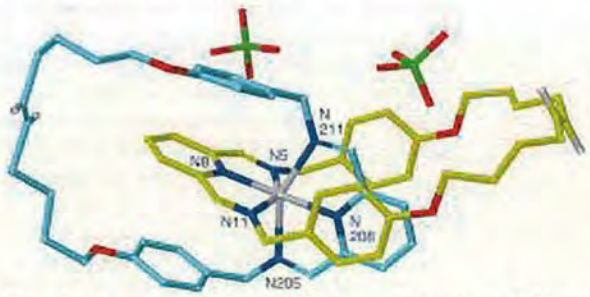

Figure 2. Structure of [Zn{(*E*,*E*)-**1**}](ClO$_4$)$_2$ as determined by X-ray crystallography.[22] Carbon atoms of one macrocycle are shown in light blue and those of the other in yellow; oxygen atoms are red, nitrogen dark blue, chlorine green, hydrogen white, and zinc silver. Non-olefinic hydrogen atoms and a molecule of acetonitrile are omitted for clarity. Selected bond lengths [Å]: Zn-N5 2.289, Zn-N8 2.048, Zn-N11 2.211, Zn-N205 2.264, Zn-N208 2.045, Zn-N211 2.276; other selected interatomic distances [Å]: N5-N11 4.348, N8-N208 4.081, N205-N211 4.388; ligand bite angles [°]: N5-Zn-N11 150.14, N205-Zn-N211 150.34.

groups of each macrocycle π-stack with the 2,6-diiminopyridine groups of the other interlocked ring, an interaction which is also clearly present in the precursor complex [Zn**2**$_2$]L$_2$ in halogenated solvents (see NMR data in Figure 1) and doubtless contributes to intracomponent rather than intercomponent cyclization occurring during RCM. Metal coordination necessarily buries the polar imine groups at the center of the molecular structure with the alkyl chains to the outside; a similar overall co-conformation to that observed in the solid state for amphiphilic benzylic amide catenanes.[17a]

The bite angle of the ligand in [Zn{(*E*,*E*)-**1**}](ClO$_4$)$_2$ is slightly smaller (150°) than in nonmacrocyclic bis(2,6-diiminopyridine) complexes with Zn^{II}[13] (151°) and Ni^{II}[12, 13] (151–156°), indicating that the ligand is able to adapt to the demands of its environment. Encouraged, we investigated the tolerance of the octahedral catenate assembly system by extending the RCM approach to metals both across and down the periodic table with respect to zinc (i.e. Mn ← Zn and Zn → Hg). The results (see Scheme 2) were uniformally satisfying with the precursor complexes and catenates obtained in each case, often in good yields despite the mixture of diastereomers complicating the purification process.[23] Preliminary studies show that the same catenates are also readily produced by the direct imine bond formation route (Scheme 2b). The crystal structures of two of these new catenates, [Cu{(*E*,*E*)-**1**}](ClO$_4$)$_2$ and [Co{(*E*,*E*)-**1**}]I$_2$, were obtained by using a synchrotron radiation source (Figure 3). The bite angles in these catenates proved larger than in the zinc system (152.1 and 152.7° (Cu), 152.9 and 154.5° (Co)) in line with observed trends with acyclic ligands, confirming the geometrical flexibility of the benzylic bis(2,6-diiminopyridine)catenand ligand system. Interestingly, all the catenates are much more thermally stable than the corresponding precursor complexes. Whilst the acyclic coordination compounds [M**2**$_2$]L$_2$ typically possess sharp melting points in the range 221–252 °C, the analogous [M**1**]L$_2$ catenates tend to gradually lose color and decompose at temperatures in excess of 350 °C.

The properties of the zinc(II) catenate [Zn{(*E*,*E*)-**1**}](ClO$_4$)$_2$ were investigated in more detail (Scheme 3). By single-phase or biphasic extraction of [Zn{(*E*,*E*)-**1**}](ClO$_4$)$_2$ in various organic solvents (DMF, $CHCl_3/H_2O$, etc.) with up to 100 equivalents of EDTA, disodium salt, no signs of demetalating the catenate were obtained, suggesting that the

  1433-7851/01/4008-1540 $ 17.50+.50/0

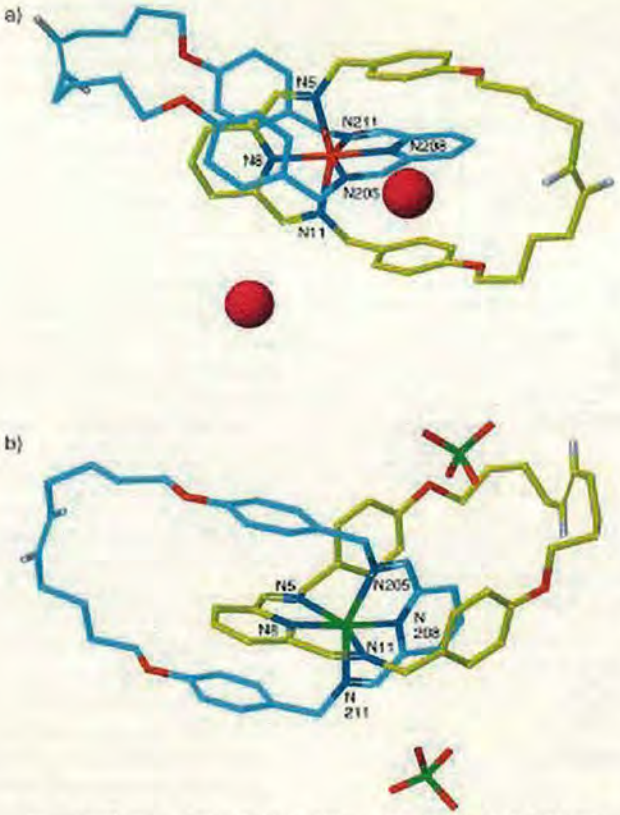

Figure 3. Structures of a) $[Co\{(E,E)\text{-}\mathbf{1}\}]I_2$ and b) $[Cu\{(E,E)\text{-}\mathbf{1}\}](ClO_4)_2$ as determined by X-ray crystallography.[22] Color code as in Figure 2, cobalt red, copper green, iodide purple. Non-olefinic hydrogen atoms are omitted for clarity. Ligand bite angles [°]: N5-Co-N11 152.9, N205-Co-N211 154.5; N5-Cu-N11 152.1, N205-Cu-N211 152.7.

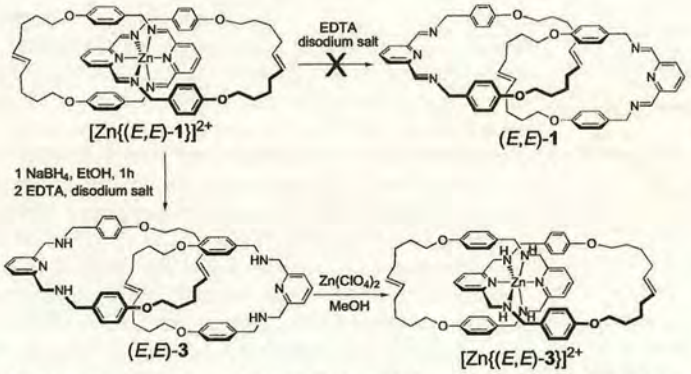

Scheme 3. The chemistry of the octahedral metal catenate $[Zn\{(E,E)\text{-}\mathbf{1}\}](ClO_4)_2$. Direct demetalation is unsuccessful, but reduction of the imine groups allows extraction of the zinc to yield the free benzylic amine catenand (E,E)-**3** (78%). Remetalation affords the benzylic amine catenate $[Zn\{(E,E)\text{-}\mathbf{3}\}](ClO_4)_2$ (ca. 100%).

combination of the directional, planar diiminopyridyl coordinating motif and the tight, encapsulated architecture provides exceptional kinetic stability. However, reduction of the imine groups followed by washing with aqueous EDTA, disodium salt, resulted in the free benzylic amine catenand (E,E)-**3**. Remetallation proceeded smoothly to give the corresponding, clearly more labile, benzylic amine catenate $[Zn\{(E,E)\text{-}\mathbf{3}\}](ClO_4)_2$. The ^1H NMR spectra of (E,E)-**3** and $[Zn\{(E,E)\text{-}\mathbf{3}\}](ClO_4)_2$ are shown in Figure 1d and e, respectively. The compact nature of the free ligand (E,E)-**3** is convincingly demonstrated by the shielding of several resonances compared to the acyclic ligand **2**. Protons H_E and H_F, for example, which intrinsically should be relatively unaffected by imine reduction, are shifted in (E,E)-**3** by a similar magnitude to those in the $[Zn(\{E,E)\text{-}\mathbf{1}\}](ClO_4)_2$ catenate and the $[Zn\mathbf{2}_2](ClO_4)_2$ precursor complex despite no directed intercomponent interactions being present between the macrocycles in the catenand. The broad appearance of several resonances in the spectrum of the catenand is probably due to co-conformational exchange processes that are not fast on the NMR time scale at room temperature. The broadened peaks in the spectrum of the amine catenate $[Zn\{(E,E)\text{-}\mathbf{3}\}]L_2$, however, may be a result of multiple asymmetric centers being produced by coordination of the four nitrogen atoms which are prochiral in the free ligand **3**.

In conclusion, a simple, versatile and effective route exists to octahedrally coordinated analogues of the Sauvage catenates. This route should be extendable to the synthesis of other metal-based interlocked architectures (such as rotaxanes, shuttles, and knots), and the octahedrally coordinated catenates should be interchangeable in possible molecular devices with catenanes assembled by hydrogen bonds. Catenates are not only a means of stabilizing unusual oxidation states and normally disfavored geometries, but could also find uses in areas where complexes with particularly high kinetic stabilities are required, such as radiotherapy[24] and magnetic resonance imaging,[25] because of the wide range of metals that can adopt octahedral coordination patterns. Finally, we are well aware that metal complexes of 2,6-diiminopyridine ligands also form an important new generation of non-metallocene olefin polymerization catalysts[26] and that intertwined versions of such structures exhibit novel forms of columnar liquid crystalline behavior.[27] The possible application of translationally switchable mechanically interlocked architectures (containing unsaturated metal centers in the case of potential polymerization catalysts) to these areas should be fascinating.

Experimental Section

Route (a) of Scheme 2 (RCM): Grubbs' metathesis catalyst $[Ru(=CHPh)(PCy_3)_2Cl_2]$ (0.02 g, 0.0243 mmol, 20 mol%) was placed in a sealed, argon-purged, flame-dried Schlenk tube, and subjected to a constant stream of argon for ten minutes. A degassed and argon-purged solution of the $[M\mathbf{2}_2]L_2$ complex (0.122 mmol) in anhydrous dichloromethane (500 mL) was transferred to the Schlenk tube by injection over ten minutes. Reaction was allowed to continue until all the starting material was consumed as evidenced by TLC (typically 4 h), or, in order to maximize the amount of *E,E* diastereomer, for 4 days. The resulting solution was evaporated to dryness and purified by repeated chromatography (silica gel, 1–5% MeOH in CH_2Cl_2 as eluent) to give the catenates $[M\mathbf{1}]L_2$ as variously colored solids. Selected data for $[Zn\{(E,E)\text{-}\mathbf{1}\}](ClO_4)_2$: yield: 112 mg, 73%; m.p. 350°C (decomp); ^1H NMR (400 MHz, $[D_6]$DMSO): $\delta = 1.58$ (m, 8H, CH_2), 1.74 (m, 8H, CH_2), 2.12 (m, 8H, $CH_2CH{=}CH$), 3.85 (t, 8H, $J =$

6.5 Hz, H_G), 4.49 (brs, 8H, H_D), 5.61 (t, 4H, J = 3.0 Hz, H_H), 6.36 (AA'BB' system, 8H, J = 8.0 Hz, H_E), 6.53 (AA'BB' system, 8H, J = 8.0 Hz, H_F), 7.70 (d, 4H, J = 8.0 Hz, H_B), 8.42 (t, 2H, J = 8.0 Hz, H_A), 8.50 (s, 4H, H_C); ^{13}C NMR (100 MHz, [D$_6$]DMSO): δ = 25.89, 28.05, 31.50, 60.76, 67.17, 113.91, 127.02, 129.34, 129.97, 130.62, 144.37, 145.25, 158.24, 160.27, FAB-MS (*m*BNA matrix): *m/z*: 1126 $[M-ClO_4^-]^+$; anal. calcd for: $C_{62}H_{70}O_{12}N_6Cl_2Zn$ (1225): C 60.73, H 5.71, N 6.86%, found: C 60.46, H 5.97, N 6.67%.

Route (b) of Scheme 2: A solution of 2,6-pyridinedicarbaldehyde (0.97 g, 7.2 mmol) in methanol (10 mL) was added dropwise over 30 min to a solution of bis-amine **4** (7.2 mmol) and metal salt (ML_2, 3.6 mmol) in methanol (10 mL). The reaction mixture was stirred at room temperature for 1 h after which time the [**M1**]L_2 catenate could either be isolated as a precipitate by filtration, or the solvent removed under reduced pressure and the resulting solid purified as for the RCM procedure.

Received: August 14, 2000
Revised: February 5, 2001 [Z15632]

[1] a) *Molecular Catenanes, Rotaxanes and Knots* (Eds.: J.-P. Sauvage, C. Dietrich-Buchecker), Wiley-VCH, Weinheim, **1999**; for catenanes based on coordination bonds other than the Sauvage catenates see: b) G.-J. M. Gruter, F. J. J. de Kanter, P. R. Markies, T. Nomoto, O. S. Akkerman, F. Bicklehaupt, *J. Am. Chem. Soc.* **1993**, *115*, 12179–12180; c) M. Fujita, F. Ibukuro, H. Hagihara, K. Ogura, *Nature* **1994**, *367*, 720–723; d) C. Piguet, G. Bernardinelli, A. F. Williams, B. Bocquet, *Angew. Chem.* **1995**, *107*, 618–621; *Angew. Chem. Int. Ed. Engl.* **1995**, *34*, 582–584; e) D. M. P. Mingos, J. Yau, S. Menzer, D. J. Williams, *Angew. Chem.* **1995**, *107*, 2045–2047; *Angew. Chem. Int. Ed. Engl.* **1995**, *34*, 1894–1895; f) A. C. Try, M. M. Harding, D. G. Hamilton, J. K. M. Sanders, *Chem. Commun.* **1998**, 723–724; g) D. Whang, K.-M. Park, J. Heo, P. Ashton, K. Kim, *J. Am. Chem. Soc.* **1998**, *120*, 4899–4900; h) C. P. McArdle, M. J. Irwin, M. C. Jennings, R. J. Puddephatt, *Angew. Chem.* **1999**, *111*, 3571–3573; *Angew. Chem. Int. Ed.* **1999**, *38*, 3376–3378; i) M. Fujita, *Acc. Chem. Res.* **1999**, *32*, 53–61; j) H. W. Gibson, S.-H. Lee, *Can. J. Chem.* **2000**, *78*, 347–355; for catenane-like coordination interpenetrating networks see: k) S. R. Batten, R. Robson, *Angew. Chem.* **1998**, *110*, 1558–1595; *Angew. Chem. Int. Ed.* **1998**, *37*, 1460–1494; l) A. J. Blake, N. R. Champness, H. Hubberstey, W.-S. Li, M. A. Withersby, M. Schröder, *Coord. Chem. Rev.* **1999**, *183*, 117–138.

[2] C. O. Dietrich-Buchecker, J.-P. Sauvage, J.-M. Kern, *J. Am. Chem. Soc.* **1984**, *106*, 3043–3045; for the earliest Cu^{I} catenate synthesis, involving a threaded intermediate complex, see: C. O. Dietrich-Buchecker, J.-P. Sauvage, J.-P. Kintzinger, *Tetrahedron Lett.* **1983**, *24*, 5095–5098.

[3] a) B. Mohr, M. Weck, J.-P. Sauvage, R. H. Grubbs, *Angew. Chem.* **1997**, *109*, 1365–1367; *Angew. Chem. Int. Ed. Engl.* **1997**, *36*, 1308–1310; b) M. Weck, B. Mohr, J.-P. Sauvage, R. H. Grubbs, *J. Org. Chem.* **1999**, *64*, 5463–5471.

[4] F. Bitsch, C. O. Dietrich-Buchecker, A.-K. Khémiss, J.-P. Sauvage, A. V. Dosselaer, *J. Am. Chem. Soc.* **1991**, *113*, 4023–4025.

[5] C. O. Dietrich-Buchecker, J.-P. Sauvage, J.-M. Kern, *J. Am. Chem. Soc.* **1989**, *111*, 7791–7800.

[6] a) C. Wu, P. R. Lecavalier, Y. X. Shen, H. W. Gibson, *Chem. Mater.* **1991**, *3*, 569–572; b) J.-C. Chambron, V. Heitz, J.-P. Sauvage, *J. Chem. Soc. Chem. Commun.* **1992**, 1131–1133.

[7] J.-P. Collin, P. Gavinã, J.-P. Sauvage, *J. Chem. Soc. Chem. Commun.* **1996**, 2005–2006.

[8] C. O. Dietrich-Buchecker, J. P. Sauvage, *Angew. Chem.* **1989**, *101*, 192–195; *Angew. Chem. Int. Ed. Engl.* **1989**, *28*, 189–192.

[9] N. Armaroli, L. De Cola, V. Balzani, J.-P. Sauvage, C. O. Dietrich-Buchecker, J.-M. Kern, A. Bailal, *J. Chem. Soc. Dalton Trans.* **1993**, 3241–3247.

[10] D. J. Cárdenas, A. Livoreil, J.-P. Sauvage, *J. Am. Chem. Soc.* **1996**, *118*, 11980–11981.

[11] The idea of using octahedral ligand geometries in catenate formation was actually proposed a decade *before* the Sauvage tetrahedral system was introduced (V. I. Sokolov, *Russ. Chem. Rev.* **1973**, *42*, 452–463). For more recent discussions of possible strategies to catenates based on metal templates with octahedral coordination preference, see: D. H. Busch, *J. Incl. Phenom.* **1992**, *12*, 389–395; N. V. Gerbeleu, V. B. Arion, J. Burgess, *Template Synthesis of Macrocyclic Compounds*, Wiley-VCH, Weinheim, **1999**.

[12] A. J. Blake, A. J. Lavery, T. I. Hyde, M. J. Schröder, *J. Chem. Soc. Dalton Trans.* **1989**, 965–970.

[13] A. L. Vance, N. W. Alcock, J. A. Heppert, D. H. Busch, *Inorg. Chem.* **1998**, *37*, 6912–6920.

[14] J.-P. Sauvage, M. Ward, *Inorg. Chem.* **1991**, *30*, 3869–3874.

[15] G. Rapenne, C. Dietrich-Buchecker, J.-P. Sauvage, *J. Am. Chem. Soc.* **1999**, *121*, 994–1001.

[16] C. A. Hunter, *Chem. Br.* **1998**, *34*(5), 17.

[17] a) D. A. Leigh, K. Moody, J. P. Smart, K. J. Watson, A. M. Z. Slawin, *Angew. Chem.* **1996**, *108*, 326–321; *Angew. Chem. Int. Ed. Engl.* **1996**, *35*, 306–310; b) T. J. Kidd, D. A. Leigh, A. J. Wilson, *J. Am. Chem. Soc.* **1999**, *121*, 1599–1600.

[18] D. A. Leigh, A. Murphy, J. P. Smart, M. S. Deleuze, F. Zerbetto, *J. Am. Chem. Soc.* **1998**, *120*, 6458–6467.

[19] The importance of these structural features for promoting catenate formation was exemplified by a very recent study which showed that it is not possible to produce octahedral catenates from terpy ligands which were not well preorganized for intracomponent cyclization (N. Belfrekh, C. Dietrich-Buchecker, J.-P. Sauvage, *Inorg. Chem.* **2000**, *39*, 5169–5172).

[20] Compound **2** was conveniently prepared in three steps from 4-hydroxybenzonitrile: 1) $HO(CH_2)_4CH{=}CH_2$, Ph_3P, DEAD, THF, 0°C, 59%; 2) $LiAlH_4$, THF, −78°C → reflux, 94%; 3) 2,6-pyridinedicarbaldehyde, MeOH, 92%.

[21] Compound **4** was conveniently prepared in three steps from 5-hexenyloxybenzylamine: 1) tBoc$_2$O, NEt_3, MeOH, 87%; 2) [Ru(=CHPh)$(PCy_3)_2Cl_2$], CH_2Cl_2, Ar, RT, 24 h, 78%; 3) CF_3CO_2H, then NEt_3, CH_2Cl_2, 93%.

[22] [Zn[(*E*,*E*)-**1**]]$(ClO_4)_2$: $C_{62}H_{70}Cl_2N_6O_{12}Zn \cdot 0.5(C_2H_3N)$, M_r = 1248.04, crystal size 0.14 × 0.08 × 0.06 mm, monoclinic $P2_1/c$, a = 10.6258(5), b = 17.4158(9), c = 33.4757(18) Å, β = 97.232(2)°, V = 6145.6(5) Å^3, Z = 4, ρ_{calcd} = 1.349 Mg m^{-3}; synchrotron radiation (CCLRC Daresbury Laboratory Station 9.8, silicon monochromator, λ = 0.69280 Å), μ = 0.553 mm^{-1}, T = 150(2) K. 22797 data (7081 unique, R_{int} = 0.0489, 1.65 < θ < 21.00°) were collected on a Siemens SMART CCD diffractometer using narrow frames (0.2° in ω), and were corrected semiempirically for absorption and incident beam decay (transmission 0.83–1.00). The structure was solved by direct methods and refined by full-matrix least-squares methods on F^2 values of all data (G. M. Sheldrick, SHELXTL Manual, Version 5, Siemens Analytical X-ray Instruments, Madison, WI, **1994**) to give $wR = \{\Sigma[w(F_o^2 - F_c^2)^2]/\Sigma[w(F_o^2)^2]\}^{1/2}$ = 0.2984, conventional R = 0.1087 for F values of 7081 reflections with $F_o^2 > 2\sigma(F_o^2)$, S = 1.066 for 761 parameters. Residual electron density extremes were 0.974 and −0.563 e Å^{-3}. The alkyl chains were modeled by using both geometrical and displacement parameter restraints. Hydrogen atoms were added in calculated positions and constrained to a riding model. Data for the copper catenate [Cu[(*E*,*E*)-**1**]]$(ClO_4)_2$ was collected and solved as above except: $C_{62}H_{71}CuN_6O_{12}$, M_r = 1226.69, crystal size 0.14 × 0.10 × 0.01 mm, monoclinic $P2_1/c$, a = 10.2948(6), b = 17.4273(10), c = 33.1511(18) Å, β = 96.120(2)°, V = 5913.8(6) Å^3, Z = 4, ρ_{calcd} = 1.378 Mg m^{-3}; synchrotron radiation (CCLRC Daresbury Laboratory Station 9.8, silicon monochromator, λ = 0.68950 Å), μ = 0.528 mm^{-1}, T = 150(2) K. 10342 data (3460 unique, R_{int} = 0.0784, 1.93 < θ < 16.50°), correction for absorption and incident beam decay (transmission 0.9298–0.9947) $wR = [\Sigma[w(F_o^2 - F_c^2)^2]/\Sigma[w(F_o^2)^2]]^{1/2}$ = 0.3840, conventional R = 0.1556 for F values of 3460 reflections with $F_o^2 > 2\sigma(F_o^2)$, S = 2.349 for 339 parameters. Residual electron density extremes were 0.795 and −0.785 e Å^{-3}. Data for the cobalt catenate [Co[(*E*,*E*)-**1**]]I_2 was collected and solved as the others except: $C_{63}H_{70}CoI_2N_{6.5}O_4$, M_r = 1294.99, crystal size 0.14 × 0.10 × 0.01 mm, monoclinic $P2_1/c$, a = 10.2948(6), b = 17.4273(10), c = 33.1511(18) Å, β = 96.120(2)°. V = 5913.8(6) Å^3, Z = 4, ρ_{calcd} = 1.454 Mg m^{-3}; synchrotron radiation (CCLRC Daresbury Laboratory Station 9.8, silicon monochromator, λ = 0.68950 Å), μ = 1.386 mm^{-1}, T = 150(2) K. 28253 data (5997 unique, R_{int} = 0.1119, 1.93 < θ < 20.00°), correction for absorption and incident beam decay (transmission 0.8296–0.9863), $wR = [\Sigma[w(F_o^2 - F_c^2)^2]/\Sigma[w(F_o^2)^2]]^{1/2}$ = 0.2662, conventional R = 0.1246

  1433-7851/01/4008-1542 $ 17.50+.50/0

for F values of 5997 reflections with $F_o^2 > 2\sigma(F_o^2)$, $S = 1.215$ for 689 parameters. Residual electron density extremes were 0.955 and -1.662 e Å^{-3}. Crystallographic data (excluding structure factors) for the structures reported in this paper have been deposited with the Cambridge Crystallographic Data Centre as supplementary publication no. CCDC-147870 ([Zn{(*E*,*E*)-**1**}](ClO$_4$)$_2$), CCDC-152441 ([Cu{(*E*,*E*)-**1**}](ClO$_4$)$_2$), and CCDC-152442 ([Co{(*E*,*E*)-**1**}]I$_2$). Copies of the data can be obtained free of charge on application to CCDC, 12 Union Road, Cambridge CB2 1EZ, UK (fax: (+44) 1223-336-033; e-mail: deposit@ccdc.cam.ac.uk).

[23] The yields listed in Scheme 2 are yields after chromatography or recrystallization. Sometimes the mixture of olefin diastereomers complicates purification and, in particular, is a factor in the modest yields of [Co**1**]L$_2$ and [Ni**1**]L$_2$. The very low yield of [Hg**1**]L$_2$ by route (a) is caused by the lability of the ligands in the precursor complex [Hg**2**$_2$]L$_2$, which liberates free amine or imine in the reaction and prevents RCM occurring. All compounds gave satisfactory mass spectra, elemental analysis, IR, UV/Vis, and, with the exception of the paramagnetic catenates, ^{13}C and ^{1}H NMR data.

[24] S. Jurisson, D. Berning, W. Jia, D. Ma, *Chem. Rev.* **1993**, *93*, 1137–1156.

[25] D. Parker, *Chem. Br.* **1994**, 818–822.

[26] G. J. P. Britovsek, V. C. Gibson, D. F. Wass, *Angew. Chem.* **1999**, *111*, 448–468; *Angew. Chem. Int. Ed.* **1999**, *38*, 428–447.

[27] L. Douce, A. El-Ghayoury, A. Skoulios, R. Ziessel, *Chem. Commun.* **1999**, 2033–2034.

  1433-7851/01/4008-1543 $ 17.50+.50/0

The Effect of Mechanical Interlocking on Crystal Packing:

Predictions and Testing

Fabio Biscarini, Massimiliano Cavallini, David A Leigh, Salvador León,

Simon J Teat, Jenny K Y Wong and Francesco Zerbetto

J. Am. Chem. Soc. ***2002***, 124, *255–233*

JACS
ARTICLES
Published on Web 12/13/2001

The Effect of Mechanical Interlocking on Crystal Packing: Predictions and Testing

Fabio Biscarini,[†] Massimiliano Cavallini,[†] David A. Leigh,*[,‡] Salvador León,[§] Simon J. Teat,[||] Jenny K. Y. Wong,[‡] and Francesco Zerbetto*[,§]

Contribution from the Consiglio Nazionale delle Ricerche, Istituto di Spettroscopia Molecolare, Via P. Gobetti 101, 40129, Bologna, Italy, Centre for Supramolecular and Macromolecular Chemistry, Department of Chemistry, University of Warwick, Coventry CV4 7AL, U.K., Dipartimento di Chimica "G. Ciamician", Università degli Studi di Bologna, V. F. Selmi 2, I-40126, Bologna, Italy, and CLRC Daresbury Laboratory, Warrington, Cheshire, WA4 4AD, U.K.

Received April 3, 2001. Revised Manuscript Received September 18, 2001

Abstract: The first statistical analyses of the X-ray crystal structures of mechanically interlocked molecular architectures, the first molecular mechanics-based solid-state calculations on such structures and atomic force microscopy (AFM) experiments are used in combination to predict and test which types of benzylic amide macrocycle-containing rotaxanes possess mobile components in the crystalline phase and thus could form the basis of solid-state devices that function through mechanical motion at the molecular level. The statistical studies and calculations show that crystals formed by rotaxanes possess similarities and unanticipated differences with respect to the crystal packing of noninterlocked molecules. Trends in the rotaxane series correlate quantities related to crystal packing, molecular size, stoichiometry, and H-bonding. In accordance with the findings of Gavezzotti et al. for conventional molecular architectures, a principal component analysis (PCA) showed that three vectors related to the size, packing parameters, and stoichiometry are sufficient to describe the crystal properties of benzylic amide macrocycle-containing rotaxanes. When hydrogen bond-related quantities are included in a second PCA, they combine with the size and the stoichiometry vectors but not with packing-related parameters, indicating that the intramolecular "saturation" of the H-bonds (between the interlocked components) takes precedence over crystal assembly (i.e., intermolecular packing) in these systems. However, cluster analyses also suggest a major role for the energy of interaction between the macrocycle and its crystal environment. The identification of such a "privileged" interaction is of fundamental importance to the development of rotaxanes with in-crystal mobility of one or more of their interlocked components, a prerequisite for the exploitation of molecular level mechanical motion in the solid state. The set of trends found, together with the calculated energies, was used to propose guidelines for which benzylic amide macrocycle-containing rotaxanes are best suited to become building blocks for systems with mobile submolecular units in the crystalline phase. An experimental test of the predictive power of such guidelines was carried out using AFM on a rotaxane and its thread, identified by the study as a promising candidate for solid-state mobility. Intuitively, the rotaxane should be less mobile in the solid state since it has multiple sets of both hydrogen bond donors and acceptors that can form strong inter- and intramolecular H-bonds. Conversely, the thread has no hydrogen bond donors and cannot form such bonds. The AFM experiments, however, confirm the statistical analysis prediction that the rotaxane is considerably more mobile in the solid than the thread.

Introduction

Molecules crystallize as the result of relatively weak interactions between the crystallizing components; noncovalent binding during the crystal assembly process ultimately yields a lower total energy than the individual components have with a solvent or at infinite distances. When considering molecules with mechanically interlocked molecular architectures, catenanes (interlocked rings) and rotaxanes (where a macrocycle is locked onto a linear thread by two bulky "stoppers"),[1] the picture is somewhat altered because the separation of the interlocked components is intrinsically restricted. The presence of a mechanical bond often enables the interlocked components to interact together in a very efficient manner, altering the mode of binding they could have on external species, in general, and

* To whom correspondence should be addressed. D.A.L.: E-mail, David.Leigh@ed.ac.uk. F.Z.: E-mail, gatto@ciam.unibo.it.
[†] Istituto di Spettroscopia Molecolare.
[‡] University of Warwick. Present address: Department of Chemistry, University of Edinburgh, The King's Buildings, West Mains Road, Edinburgh EH9 3JJ, U.K.
[§] Università degli Studi di Bologna.
[||] CLRC Daresbury Laboratory.

(1) (a) Amabilino, D. B.; Stoddart, J. F. *Chem. Rev.* **1995**, *95*, 2725−2828. (b) Sauvage, J.-P., Dietrich-Buchecker, C., Eds.; *Molecular Catenanes, Rotaxanes, and Knots*; Wiley-VCH: Weinheim, 1999.

10.1021/ja0159362 CCC: $22.00

within a crystal, in particular. The interlocking also generates special degrees of freedom where one submolecular unit may undergo large amplitude dynamics with respect to the other. The presence and the effects of these motions (including "shuttling" in the case of rotaxanes and "circumrotation" in the case of catenanes) are well-established in solution,[2] but only recently has it been seen in the solid,[3] the phase in which practical applications of such molecular architectures are likely to first find application. In fact, large amplitude intercomponent motions in catenane and rotaxane in the crystalline state are usually "locked" by intermolecular crystal packing interactions, and for such dynamics to exist on a reasonably fast, that is, millisecond-to-second time scale, the packing forces must necessarily be minimized. The forces bringing a molecular crystal together and the forces governing the ring dynamics are thus strongly connected, and their investigation can be carried out concomitantly. In the past, for molecules with conventional architectures, crystal structure analysis combined with molecular mechanics calculations proved that the cohesive, i.e., packing energy is interwoven with several molecular and crystal parameters (ranging from the number of valence electrons, to some packing indexes, to the molecular surface).[4] The approach pioneered by Gavezzotti was also able to ascertain that, out of a very large number of parameters one could consider, only the combination of size, packing, and stoichiometry parameters is necessary to describe the structural properties of a large number of organic crystals.[4] Here we apply this method to crystals of rotaxanes. The large family of rotaxanes based on a thread containing a hydrogen bonding template for the benzylic isophthalamide macrocycle, **1**,[5] offers a unique opportunity for investigating systematically the effect of intramolecular threading in the structures of crystals. It was the aim of this study to perform molecular mechanics calculations and structural analyses of the X-ray structures of benzylic amide rotaxanes to ascertain whether similarities or differences with other small organic molecules exist and to uncover a hierarchy of interactions and rules governing their crystal structures. The results provide a unique insight into which types of rotaxanes are more likely to show motion of the macrocycle in the solid state. The predictions were tested by carrying out atomic force microscopy (AFM) on a rotaxane and its corresponding thread, identified by the statistical analysis as a promising candidate for possessing mobility in the solid phase. Although the AFM tip does not probe directly the motion of submolecular units, an AFM experiment can provide indirect information on the packing interactions in the crystal. The AFM was used as a tool for scratching the crystal with a controlled load force. The load force, acting onto the surface of the (anisotropic) molecular crystal, modifies the material, as the shearing force exerted by the tip exceeds the adhesion forces within the crystal. The minimum load force required for scratching a comparable amount of material from a crystal is qualitatively related to the adhesion force, which depends on the packing interactions. Comparison of the miminum load forces for the rotaxane and its thread provides insight on the packing interactions in the solid state.

Computational Background

Recently, both the short time scale (subpicosecond), harmonic, and the long time scale (up to microsecond), large-amplitude, dynamics of benzylic amide macrocycle-containing catenanes and rotaxanes have been studied[6] using the MM3 model.[7] This force field was developed by fitting both heats of formation and structural results in the gas phase and in crystals of simple organics. MM3 is specifically parametrized to describe H-bonds in terms of dipole interactions and includes specific interatomic nonbonded potential energy functions that allow a quantitative treatment of the van der Waals and the electrostatic interactions which play an essential role in hydrogen bonding and in the $\pi-\pi$ interactions between aromatic rings. Despite the molecular complexities involved, the method successfully reproduces experimentally determined rotational barriers and steric energies in these types of catenane and rotaxane systems. All the calculations reported were performed using the TINKER package.[8] Ewald summation was used for the electrostatic interaction thereby including all the possible terms. The crystal structures of the rotaxanes were optimized starting from the structures determined by X-ray diffraction data. The reoptimization was necessary because the degree of disorder was not the same in all of the structures and was necessary to avoid

(2) See, for example: (a) Ballardini, R.; Balzani, V.; Credi, A.; Brown, C. L.; Gillard, R. E.; Montali, M.; Philp, D.; Stoddart, J. F.; Venturi, M.; White, A. J. P.; Williams, B. J.; Williams, D. J. *J. Am. Chem. Soc.* **1997**, *119*, 12503-12513. (b) Anelli, P.-L.; Spencer, N.; Stoddart, J. F. *J. Am. Chem. Soc.* **1991**, *113*, 5131−5133. (c) Ashton, P. R.; Bissell, R. A.; Spencer, N.; Stoddart, J. F.; Tolley, M. S. *Synlett* **1992**, 914−918. (d) Ashton, P. R.; Bissell, R. A.; Górski, R.; Philp, D.; Spencer, N.; Stoddart, J. F.; Tolley, M. S. *Synlett* **1992**, 919−922. (e) Ashton, P. R.; Bissell, R. A.; Spencer, N.; Stoddart, J. F.; Tolley, M. S. *Synlett* **1992**, 923−926. (f) Bissell, R. A.; Córdova, E.; Kaifer, A. E.; Stoddart, J. F. *Nature* **1994**, *369*, 133−137. (g) Benniston, A. C.; Harriman, A.; Lynch, V. M. *J. Am. Chem. Soc.* **1995**, *117*, 5275−5291. (h) Benniston, A. C. *Chem. Soc. Rev.* **1996**, *25*, 427−435. (i) Collin, J.-P.; Gavina, P.; Sauvage, J.-P. *Chem. Commun.* **1996**, 2005−2006. (j) Ashton, P. R.; Ballardini, R.; Balzani, V.; Boyd, S. E.; Credi, A.; Gandolfi, M. T.; Gómez-López, M.; Iqbal, S.; Philp, D.; Preece, J. A.; Prodi, L.; Ricketts, H. G.; Stoddart, J. F.; Tolley, M. S.; Venturi, M.; White, A. J. P.; Williams, D. J. *Chem.-Eur. J.* **1997**, *3*, 152−170. (k) Anelli, P.-L.; Asakawa, M.; Ashton, P. R.; Bissell, R. A.; Clavier, G.; Górski, R.; Kaifer, A. E.; Langford, S. J.; Mattersteig, G.; Menzer, S.; Philp, D.; Slawin, A. M. Z.; Spencer, N.; Stoddart, J. F.; Tolley, M. S.; Williams, D. J. *Chem.-Eur. J.* **1997**, *3*, 1113−1135. (l) Lane, A. S.; Leigh, D. A.; Murphy, A. *J. Am. Chem. Soc.* **1997**, *119*, 11092−11093. (m) Murakami, H.; Kawabuchi, A.; Kotoo, K.; Kunitake, M.; Nakashima, N. *J. Am. Chem. Soc.* **1997**, *119*, 7605−7606. (n) Gong, C.; Glass, T. E.; Gibson, H. W. *Macromolecules* **1998**, *31*, 308−313. (o) Leigh, D. A.; Troisi, A.; Zerbetto, F. *Angew. Chem., Int. Ed.* **2000**, *39*, 350−353. (p) Brouwer, A. M.; Frochot, C.; Gatti, F. G.; Leigh, D. A.; Mottier, L.; Paolucci, F.; Roffia, S.; Wurpel, G. W. H. *Science* **2001**, *291*, 2124−2128.

(3) (a) Cavallini, M.; Lazzaroni, R.; Zamboni, R.; Biscarini, F.; Timpel, D.; Zerbetto, F.; Clarkson, G. J.; Leigh, D. A. *J. Phys. Chem. B* **2001**, *105*, 10826−10830. (b) Gase, T.; Grando, D.; Chollet, P.-A.; Kajzar, F.; Murphy, A.; Leigh, D. A. *Adv. Mater.* **1999**, *11*, 1303−1306. (c) Collier, C. P.; Mattersteig, G.; Wong, E. W.; Beverly, K.; Sampaio, J.; Raymo, F. M.; Stoddart, J. F.; Heath, J. R. *Science* **2000**, *289*, 1172−1175.

(4) (a) Gavezzotti, A.; Desiraju, G. R. *Acta Crystallogr.* **1988**, *B44*, 427−434. (b) Gavezzotti, A. *J. Chem. Soc., Perkin Trans. 2* **1995**, 1399−1404. (c) Sorescu, D. C.; Rice, B. M.; Thompson, D. L. *J. Phys. Chem. A* **1999**, *103*, 989−998. (d) Gavezzotti, A. *J. Am. Chem. Soc.* **1989**, *111*, 1835−1843. (e) Gavezzotti, A. *J. Phys. Chem.* **1991**, *95*, 8948−8955. (f) Gavezzotti, A.; Filippini, G. *Acta Crystallogr.* **1992**, *B48*, 537−545. (g) Dunitz, J. D.; Gavezzotti, A. *Acc. Chem. Res.* **1999**, *32*, 677−684.

(5) (a) Johnston, A. G.; Leigh, D. A.; Murphy, A.; Smart, J. P.; Deegan, M. D. *J. Am. Chem. Soc.* **1996**, *118*, 10662−10663. (b) Leigh, D. A.; Murphy, A.; Smart, J. P.; Slawin, A. M. Z. *Angew. Chem., Int. Ed. Engl.* **1997**, *36*, 728−732. (c) Clegg, W.; Gimenez-Saiz, C.; Leigh, D. A.; Murphy, A.; Slawin, A. M. Z.; Teat, S. J. *J. Am. Chem. Soc.* **1999**, *121*, 4124−4129.

(6) (a) Leigh, D. A.; Murphy, A.; Smart, J. P.; Deleuze, M. S.; Zerbetto, F. *J. Am. Chem. Soc.* **1998**, *120*, 6458−6467. (b) Deleuze, M. S.; Leigh, D. A.; Zerbetto, F. *J. Am. Chem. Soc.* **1999**, *121*, 2364−2379. (c) Bermudez, V.; Capron, N.; Gase, T.; Gatti, F. G.; Kajzar, F.; Leigh, D. A.; Zerbetto, F.; Zhang, S. W. *Nature* **2000**, *406*, 608−611. (d) Fustin, C.-A.; Leigh, D. A.; Rudolf, P.; Timpel, D.; Zerbetto, F. *ChemPhysChem* **2000**, *1*, 97−100.

(7) (a) Allinger, N. L.; Yuh, Y. H.; Lii, J.-H. *J. Am. Chem. Soc.* **1989**, *23*, 8551−8566. (b) Lii, J.-H.; Allinger, N. L. *J. Am. Chem. Soc.* **1989**, *23*, 8566−8575. (c) Lii, J.-H.; Allinger, N. L. *J. Am. Chem. Soc.* **1989**, *23*, 8576−8582.

(8) (a) Ponder, J. W.; Richards, F. *J. Comput. Chem.* **1987**, *8*, 1016−1024. (b) Kundrot, C.; Ponder, J. W.; Richards, F. *J. Comput. Chem.* **1991**, *12*, 402−409. (c) Dudek, M. J.; Ponder, J. W. *J. Comput. Chem.* **1995**, *16*, 791−816.

Table 1. Comparison of the Packing Energies, Absolute Value in kcal mol^{-1}, of Selected Cases

system	CSD ref code	PE (lit)	PE (this work)
anthracene	ANTCEN	19.06[a]	20.01
ovalene	OVALEN01	38.47[a]	38.12
o-aminobenzoic acid	AMBACO03	24.19[b]	21.61
p-aminobenzoic acid	AMBNAC	25.67[b]	19.83
2,3-dimethyl-2,3-dinitrobutane	BECJEY	25.33[c]	22.21
2,2′,4,4′,6,6′-hexanitrostilbene	GIMBOT	51.67[c]	46.45
n-octane	OCTANE	14−17[d]	11.34
n-hexadecane		20−22[d]	19.35
tetrahydrofuran-3,4-dione	HYFURN	10−12[e]	8.43
(2*S*,3*S*)-tetrahydro-3-acetoxy-5-oxo-2,3-furan-dicarboxylic anhydride	CORZAK	14−18[e]	12.40
fumaronitrile	BISJIW	9−10[f]	10.94
phenanthridine	PHENAT	14−16[f]	17.48

[a] See ref 4a. [b] See ref 4b. [c] See ref 4c. [d] See ref 4d. [e] See ref 4e. [f] See ref 4f.

ambiguities caused by the definition of the position of the hydrogens (which are absent in X-ray structures). Comparison of the optimized structures with the X-ray structures showed only minor changes in the position of the heavy atoms.

For each of the minimized structures, the packing energy, PE, was calculated together with the molecular van der Waals surface, S_m, volume, V_m, and Kitaigorodski packing coefficient, C_k, that is, the ratio of the occupied to total volume of the cell. The atomic radii used to evaluate S_m, V_m, and C_k were taken from the work of Gavezzotti and co-workers on various organic systems.[4] To provide a firm comparison with previous work, a number of noninterlocked systems were treated with the same procedure. These examples were selected for their similarity with fragments of the rotaxanes studied here and can be described as fused ring aromatic hydrocarbons, disubstituted benzenes, nitro derivatives, hydrocarbons, oxohydrocarbons, and azahydrocarbons. On average, the discrepancy between previously reported values and the present ones is less than 10%, see Table 1.

Computational Results

Overall 28 crystal structures (**1**−**26**, Figure 1) were considered in the work, all of which are available in the Cambridge Crystallographic Database (the CCDC numbers are given in Table 2). The large majority of the molecules (25) were rotaxanes. Three extra cases were included to make the comparison more complete; the first was macrocycle **1** itself, the second was its interlocked dimer, the [2]catenane **2**, and the third was an example of a crystal structure of an uninterlocked thread **3**.

As a first step, we examined the solid-state structures to determine the correlation and interconnections that exist between various physical quantities. In this we mainly follow, with some additions, the well-established approach of Gavezzotti and co-workers.[4] The data also offered the opportunity to evaluate which rotaxanes may show "crystal plasticity" (i.e., retaining the order induced through intermolecular packing, but distorting the original structure through mechanical perturbations) and/or mobility of the macrocycle in the solid phase. Both these properties can appear if some of the noncovalent bonding interactions in the crystal are energetically low. In the first case, plasticity can arise as a result of low packing energies; in the second case, ring mobility may be caused if the ring−thread and the ring−external environment interactions are both low. In both cases, a low density of the solid would assist the phenomena. These two properties are of particular interest because applications of rotaxanes and catenanes in materials science applications and/or molecular level devices are both likely to depend on inducing movements in the interlocked components in the solid state. For example, a rotaxane displaying a high degree of plasticity could be used for surface patterning with an AFM tip, while the ring mobility (e.g., shuttling) could be exploited to create solid-state devices based on the variation of other properties (e.g., fluorescence) triggered by purely mechanical motion.

Initially, the simplest approach is to focus on the energy trends, some of which emerge clearly. Table 2 shows a summary of the molecular mechanics energies. The packing energies, PE, range from 51.1 to 93.0 kcal mol^{-1}. Each PE contains three contributions, that is, H-bonding, $\pi-\pi$ stacking, and other van der Waals interactions. In quantitative terms, each one plays a similar role, with the $\pi-\pi$ stacking interactions usually giving the largest contribution. No direct correlation was found between PE and H-bonding and $\pi-\pi$ stacking energies, while a fair correlation, $r = 0.67$, was obtained by fitting PE versus the energy of other van der Waals interactions. Somewhat surprisingly, the lack of a direct correlation between H-bond energy or $\pi-\pi$ stack energy and PE indicates that there is no common mode of interaction which dominates the way these rotaxanes interact within their crystals. In other words, the visual inspection of the data shows that the stoppers, which can usually create $\pi-\pi$ stacking interactions, and the isophthalamide macrocycle, which can create both H-bonding and $\pi-\pi$ stacking interactions, contribute to hold together the crystals using noncorrelated amounts of the three different kinds of noncovalent forces.

Attention was then given to the interactions of one of the two mechanically connected units, the macrocycle, either with the thread or within the crystal lattice. A good correlation, $r = 0.87$, was obtained by fitting the PE versus the interaction energy of the macrocycle with its crystal environment. The proportionality is important because it reduces the complexity of the considerations one has to make to understand the forces that exist in the rotaxane solid-state structures. Interestingly, the proportionality holds for each of the three energy components mentioned above when the rotaxane−crystal and the macrocycle−environment energies are considered. The correlation coefficients were (i) for the hydrogen bond energy, $r = 0.95$, (ii) for the $\pi-\pi$ stacking energy, $r = 0.82$, and (iii) for the other van der Waals energy contributions, $r = 0.92$. Other fittings of the various types of energy were attempted without success. *The analysis of the molecular mechanics calculations shows that each component of the packing energy tends to scale with the same component of the energy of interaction between the macrocycle and its crystal environment.*

To establish the effects of mechanical interlocking, the calculated energies must also be compared with those of other types of molecules (Figure 2). Figure 2a shows that this class of rotaxanes, for low packing coefficients, tends to pack with a packing energy intermediate between those of low molecular weight organic compounds and proteins.[9] Qualitatively, it is the presence of multiple hydrogen bonds that makes loose packing

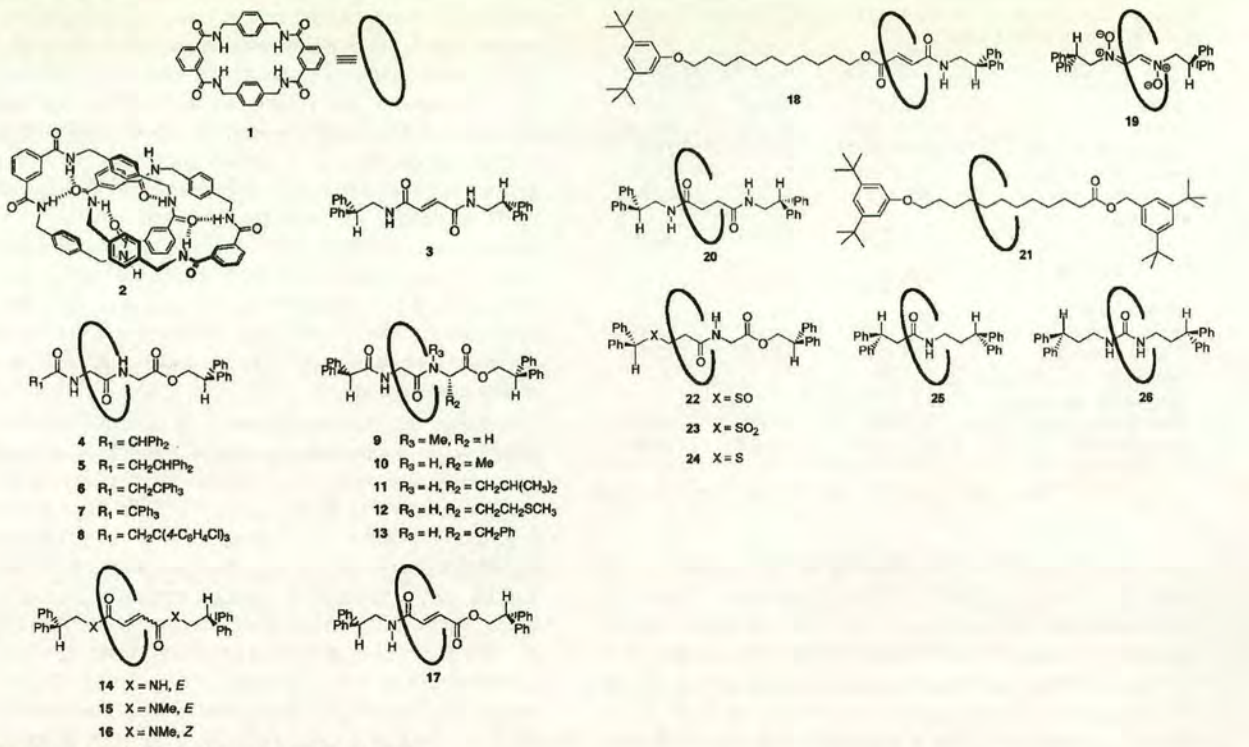

Figure 1. Molecules **1**–**26** investigated in this work.

Table 2. Noncovalent Inter- and Intramolecular Energy Contributions, Absolute Value in kcal mol^{-1}, for the Crystal Structures[a]

	molecule–crystal				macrocycle–thread[b]				macrocycle–crystal				
system	HB	$\pi\pi$	vdW	PE	HB	$\pi\pi$	vdW	tot	HB	$\pi\pi$	vdW	tot	CCCD
1	29.7	8.5	12.5	50.7									157 384
2	19.9	13.5	20.5	53.9	25.4	8.1	19.3	52.8	9.9	6.8	10.3	27.0	160 504
3	16.0	10.6	22.0	48.6									160 651
4	11.6	33.4	18.8	63.8	14.7	7.7	12.6	35.0	9.0	17.7	7.4	34.1	101 367
5	20.5	39.6	14.8	74.9	14.6	6.9	10.6	32.2	14.4	18.5	8.4	41.3	161 350
6	1.9	37.6	25.6	65.1	17.8	10.6	16.9	45.3	1.2	17.4	15.4	34.0	161 351
7	12.1	35.7	13.6	61.4	14.4	9.8	12.7	36.9	10.1	16.4	6.7	33.2	161 352
8	19.0	41.9	31.3	92.2	15.2	8.8	12.5	36.5	14.6	18.0	10.2	42.8	160 505
9	5.8	35.8	16.8	58.3	13.6	11.0	15.5	40.1	5.8	19.1	8.1	33.0	179–101 321
10	3.1	33.2	19.5	55.8	18.8	8.1	16.5	43.4	1.5	17.3	11.0	29.8	147 201
11	0.0	34.5	26.0	60.5	18.9	9.6	19.1	47.6	0.0	18.4	14.5	32.9	101 368
12	16.1	31.5	31.3	77.0	13.9	10.0	13.6	37.6	9.4	16.5	12.4	38.3	101 369
13	11.5	34.1	47.4	93.0	18.7	10.8	17.0	46.5	3.7	17.8	29.1	50.6	101 370
14a[c]	*0.0*	*30.6*	*25.7*	*56.3*	*23.5*	*8.3*	*21.7*	*53.5*	*0.0*	*18.1*	*19.4*	*37.5*	157 383
(DMSO)	7.1	30.6	32.9	70.6	16.4	8.3	12.8	37.5	0.0	18.1	22.6	40.7	
14b[c]	*0.0*	*43.7*	*19.4*	*63.1*	*27.4*	*7.4*	*31.6*	*66.4*	*0.0*	*23.2*	*6.2*	*29.4*	140 045
(DMF)	4.7	43.7	43.0	91.4	18.1	7.4	12.3	37.8	0.0	23.2	12.6	*35.8*	
14c	24.0	36.2	43.0	79.0	9.2	7.9	9.4	26.4	17.0	16.7	14.0	47.7	160 650
(acetonitrile)													
15	0.0	32.7	22.3	55.0	19.1	10.8	18.0	47.9	0.0	14.1	15.5	29.6	149 673
16	8.7	36.7	13.4	58.8	9.8	11.0	19.8	40.6	8.7	17.2	5.7	31.6	149 672
17	19.5	28.8	21.8	70.1	9.6	8.0	9.0	26.6	16.9	15.3	7.8	40.0	140 046
18	6.1	33.7	29.2	69.0	10.7	8.5	11.7	30.9	4.5	21.2	18.5	44.2	160 506
19	11.1	36.4	4.5	51.1	4.8	9.1	15.3	29.1	11.1	16.5	3.4	31.0	146 020
20	29.1	22.6	20.2	71.8	7.5	6.7	9.7	23.9	22.6	11.5	9.3	43.4	157 381
21	7.8	12.7	58.0	78.4	9.7	5.1	15.8	30.6	7.8	9.6	33.6	51.0	127 612
22	8.0	29.6	18.3	55.8	24.4	9.5	12.0	46.0	5.0	14.8	10.7	30.5	161 353
23	7.8	26.7	39.5	74.0	21.7	11.5	15.9	49.2	7.8	13.5	19.8	41.1	160 507
24	6.5	32.8	17.5	56.8	15.1	7.2	16.7	39.0	6.5	17.7	8.1	32.3	160 649
25	12.4	33.0	12.8	58.1	8.9	9.1	21.5	39.5	12.4	14.3	8.5	35.2	160 648
26	28.7	27.4	34.3	90.4	9.4	9.4	17.0	35.8	17.5	11.8	19.3	48.6	157 380

[a] HB indicates the energy of hydrogen-bonding; $\pi\pi$ indicates the energy of the π-electron stacks; vdW indicates the energy of the remaining van der Waals contributions; PE is the packing energy. [b] For isophthalamide catenane **2**, these terms correspond to the macrocycle–macrocycle intramolecular interactions. [c] For these rotaxanes, the first row (in *italics*) gives the values for the "complex" formed by one rotaxane molecule and its nearest solvent molecules, while the values in the second row refer to the rotaxane molecule alone. Both were included in the Supporting Information.

energetically very efficient. Significantly, the macrocycle, **1**, its interlocked dimer, **2**, and the thread, **3**, fall inside the bracket typical of low molecular weight organic compounds. The apparent difference between rotaxanes and the other small

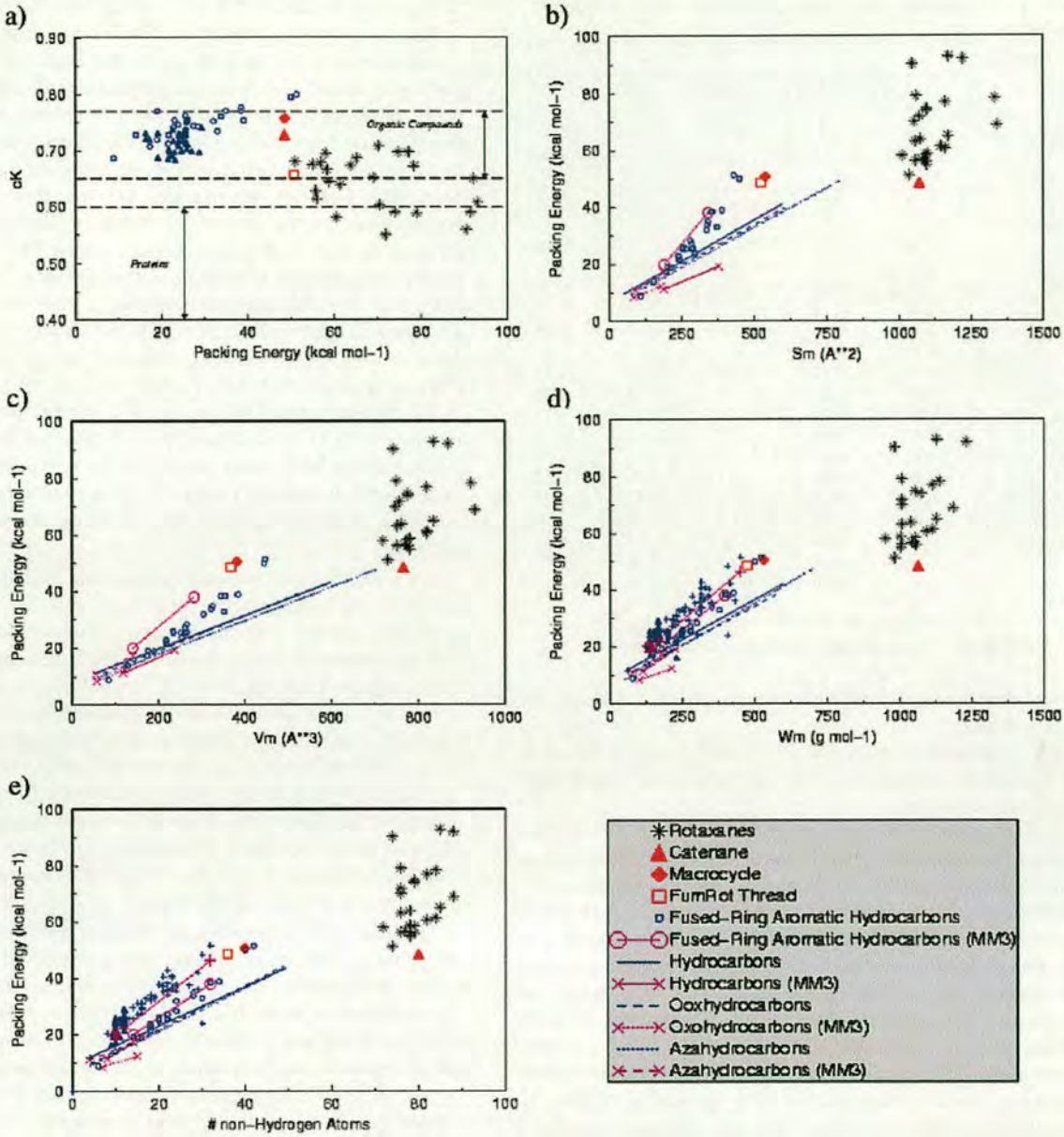

Figure 2. (a) Comparison of packing coefficients versus packing energies; (b) packing energies versus molecular surfaces; (c) packing energies versus molecular volumes; (d) packing energies versus molecular weights; (e) packing energies versus the number of nonhydrogen atoms.

organic molecules of Figure 2a ceases to exist when one considers Figure 2b–e, where packing energies are plotted versus molecular surfaces, volumes, weights, and the number of nonhydrogen atoms. Extrapolation of the data for organic molecules smaller than the rotaxanes shows that their data are located within the ideal bracket area generated by typical organic molecules. *Comparison with other small organic molecules therefore emphasizes a prominent role in the packing of intermolecular hydrogen bonding, but proves that many properties of benzylic amide macrocycle-containing rotaxanes tend to have similar trends to those of noninterlocked molecules.*

More quantitative correlations between the molecular mechanics results and the molecular parameters can be attempted following previous work[4] with the principal component analysis (PCA). As in the case of the extensive work carried out by Gavezzotti and co-workers,[4] the properties were divided into (i) size parameters, (ii) stoichiometry parameters, and (iii) packing parameters. The size parameters were W_m, the molecular weight, Z_v, the number of valence electrons, S_m, the molecular surface, V_m, the molecular volume, PE, the packing energy, and N_{nonH}, the number of nonhydrogen atoms.

The stoichiometry parameters were N_{nonH}/N_H, the ratio of the number of nonhydrogen atoms over the number of hydrogen atoms, S_{nonH}/S_H, the ratio of the surface of the nonhydrogen

(9) For organic compounds the Kitaigorodski index range is 0.65–0.77, see: (a) Kitaigorodski, A. I. *Molecular Crystals and Molecules*; Academic Press: New York, 1973; p 167. For proteins the Kitaigorodski index range is 0.40–0.60, see: (b) Crick, F. H. C.; Kendrew, J. C. *J. Mol. Biol.* **1968**, *33*, 491–497. (c) Andersson, K. M.; Hormöller, S. *Acta Crystallogr.* **2000**, *D56*, 789–790.

Table 3. Composition of the Factors in the Principal Component Analysis[a]

Eigenvalues	1	2	3	4	5
value	6.312	5.927	3.307	2.427	0.805
% of variability	32	30	17	12	4
cumulative %	32	61	78	90	94
Vectors	**1**	**2**	**3**	**4**	**5**
PE	0.15	0.27	−0.16	0.29	−0.25
E_{mac-th}	−0.24	−0.21	−0.27		
E_{mac-xt}	0.16	0.31	−0.12		−0.38
E_{hb}	0.27		−0.23	0.31	
$E_{hb(intra)}$	−0.23	−0.16	−0.30	0.21	
$E_{hb(inter)}$	0.36	0.14		0.11	
$E_{hb(mac)}$	0.36	0.11	0.10		0.14
$r_{hb(1)}$	0.35	0.16			
$r_{hb(2)}$	0.35	0.15	0.10		0.11
W_m	−0.19	0.29		0.31	0.10
Z_v	−0.23	0.32		0.12	
S_m	−0.21	0.35			
V_m	−0.21	0.35			
N_{nonH}	−0.22	0.29		0.27	0.10
N_{nonH}/N_H	0.10	−0.24		0.43	0.32
S_{nonH}/S_H		−0.22	−0.12	0.47	
V_m/S_m		0.23		−0.11	0.77
D_c		−0.10	0.45	0.32	
D_{el}		−0.10	0.49	0.17	
C_k			0.51	0.11	

[a] Coefficients <0.1 in absolute values have been omitted.

atoms over the surface of the hydrogen atoms, and V_m/S_m, the exposure ratio.

The packing parameters were D_c, the density, D_{el}, the number of electrons per unit volume in the cell, and C_k, the Kitaigorodski packing coefficient.

Only the bulk modulus at zero pressure and 60% of the melting temperature was not included in the analysis since these values are not available for these molecules. As in the case of hydrocarbons,[4g] the multidimensional space is reduced by PCA to a three-dimensional space. The first component is dominated by the size parameters, while the other two are best described as in-phase and out-of-phase combinations of packing and stoichiometry parameters. This further indicates that, in many senses, the crystal properties of interlocked systems do not differ from those of the standard systems. The presence of threading, however, creates a large number of hydrogen bonds that can be taken as its mark. A second PCA was then carried out with eight new parameters: E_{mac-th}, the interaction energy macrocycle−thread, E_{mac-xt}, the interaction energy of the macrocycle with the rest of its environment, E_{hb}, the total hydrogen bonding energy, $E_{hb(intra)}$, the hydrogen bonding energy for the interaction between the macrocycle and the thread, $E_{hb(inter)}$, the intermolecular hydrogen bonding energy, $E_{hb(mac)}$, the intermolecular hydrogen bonding energy of the macrocycle, $r_{hb(1)} = N_{hb(inter)}/N_{hb(intra)}$, the ratio of the inter- and intramolecular hydrogen bonds, and $r_{hb(2)} = N_{hb(mac)}/N_{hb(intra)}$, the ratio of the inter- and intramolecular hydrogen bonds of the macrocycle.

The various types of energy strongly correlate with each other as all the hydrogen-bond-related quantities do. The nearly block matrix of the hydrocarbons[4] for the size, stoichiometry, and packing components is preserved. Table 3 shows the composition of the PCA matrix eigenvectors. The 20-dimensional space of the parameters reduces to a 5-dimensional space with only 6% loss of information. This is similar to that found by Dunitz and Gavezzotti for hydrocarbons.[4g] The 20 quantities are so strongly interdependent that only a combination of five of them suffices to describe all the others. The first two descriptors, that is, eigenvectors, are the plus and minus combinations of the previously found size-related eigenvector with the hydrogen bond parameters. *The description of size and H-bonds is therefore intrinsically entangled.* The third eigenvector is similar to the packing terms dominated vector found for the hydrocarbons. The last two eigenvectors are the plus and minus combinations of the previously found stoichiometry-related eigenvector with hydrogen bond parameters. *The description of stoichiometry and H-bonding is therefore also intrinsically entangled.* The entanglement arises on a statistical basis and may have different individual origins; for instance, in the series from 4 to 13 the structural variations do not modify the H-bonding groups but change either a stopper or a side chain of the thread. Increasing the size of a stopper decreases the intermolecular H-bond capability (and therefore increases the intramolecular one), while increasing the size of a side chain in the thread disrupts the possibility of intramolecular hydrogen bonds (and therefore increases the possibility of intermolecular bonding).

The preferential mixing of hydrogen bond quantities with the size and the stoichiometry parameters and the lack of an equivalent mixing with the packing parameters suggest that packing properties are not determined by H-bonding. This is a surprising result in view of the low crystal density of this class of rotaxanes which is readily ascribed to the presence of multiple hydrogen bonds. *The straightforward interpretation one can offer is that intramolecular "saturation" of the H-bonds takes precedence over their use in the crystal assembly. In terms of a hypothetical hierarchy of phenomena, the establishment of H-bonds intramolecularly is physically of higher importance than the actual crystal density*, a feature that one might attempt to exploit for crystal engineering.

The principal component analysis gives a picture similar to that obtained for other organic systems with the additional inference offered for the different roles of intra- and intermolecular H-bonds. While it is highly satisfactory that only a few components suffice to describe the packing of these materials, the strong interconnection shown by the various parameters fails in providing a simple understanding of the "rules of the game" for the crystal structures of these compounds. Accordingly, cluster analysis (CA) was then used to determine the existence of partial correlation between subsets of rotaxanes, where the PE scales with one or more of the quantities were used in the PCA. The clusters were formed for five different properties, Table 4: (i) the intermolecular hydrogen bond strength, which, pursuing the analogy with proteins, is responsible for the low crystal density; (2) the strength of interaction between the macrocycle and the thread, from which partly depends the possibility of motion of the macrocycle; (3) the strength of interaction between the macrocycle and the environment, which is the second energy component from which depends the possibility of motion of the macrocycle; (4) the crystal density, whose low value would provide an environment for motion of the macrocycle; and (5) the Kitaigorodski packing coefficient, which also has to be low for motion of the macrocycle to exist.

The exact ranges of values that bracket the clusters are shown for each of the five properties listed above in column 4 of Table 4. In many cases, it was possible to obtain a further correlation

Table 4. Cluster Analysis: The Rotaxanes Are Divided into Five Sets of Several Clusters of Differing Ranges of One of the Parameters Studied[a]

$E_{hb(inter)}$	cluster	rotaxanes	property	slope	intercept	r
0−3.1	1	6, 10, 11, 14a, 14b, 15				
5.8−16.1	2	4, 7, 9, 12, 13, 16, 18, 19, 21, 22, 23, 24, 25	E_{mac-xt}	0.55	1.35	0.90
19−29.1	3	5, 8, 14c, 17, 20, 26	E_{mac-th}	1.52	33.78	0.86
			$E_{\pi-\pi(intra)}$	7.39	20.98	0.82
E_{mac-th}						
23.9−32.2	1	5, 14c, 17, 18, 19, 20, 21	E_{mac-xt}	0.62	−0.77	0.91
35.0−40.1	2	4, 7, 8, 9, 12, 24, 25, 26	E_{mac-xt}	2.28	−18.42	0.94
43.4−66.4	3	6, 10, 11, 13, 14a, 14b, 15, 16, 22, 23	E_{mac-xt}	1.59	8.46	0.91
E_{mac-xt}						
29.4−35.2	1	4, 6, 7, 9, 10, 11, 14b, 15, 16, 19, 22, 24, 25				
37.5−44.2	2	5, 8, 12, 14a, 17, 18, 20, 24				
47.7−51.0	3	13, 14c, 21, 26	E_{mac-th}	1.03	−52.62	0.90
D_c						
1.06−1.14	1	10, 13, 14a−c, 16, 18, 21, 22, 23	E_{mac-xt}	1.28	17.90	0.89
1.17−1.30	2	4, 5, 6, 7, 8, 9, 12, 15, 17, 19, 25, 26	E_{mac-xt}	2.50	−23.04	0.91
			W_m	0.11	−55.99	0.76
C_k						
0.58−0.61	1	11, 13, 14a−c, 22, 23	E_{mac-xt}	1.47	11.99	0.89
0.63−0.65	2	7, 8, 10, 16, 18	E_{mac-xt}	1.74	4.12	0.81
			$r_{hb(1)}$	22.53	33.25	0.84
			W_m	0.15	−96.95	0.89
			N_{nonH}	2.59	−148.99	0.81
0.67−0.71	3	4, 5, 6, 9, 12, 15, 17, 19, 21, 24, 25	E_{mac-xt}	1.34	15.77	0.86

[a] The nature and ranges for the parameter are given in column 1. In column 4, the property that correlates with the packing energy is given, and, in column 7, the results of the linear regression are given.

within the cluster between the packing energy and the properties shown in column 4. For instance, in the first set of entries in the table, the rotaxanes divide into three clusters of increasing intermolecular hydrogen bonding strength. For medium H-bond strengths (5.8−16.1 kcal mol^{-1}), the packing energy scales with the energy of interaction between the macrocycle and its crystal environment. This correlation had already been observed for the whole series; however, in this cluster, the value of r increases from 0.87 to 0.90. For large H-bond strengths, the packing energy correlates both with the energy of interaction of the macrocycle with the thread and with the $\pi-\pi$ stacking energy. Where strong H-bonds can be formed, it is the interactions of the macrocycle that govern the packing energy.

In the second set of entries of Table 4, three clusters form with respect to the energy of interaction between the macrocycle and the thread. Within each cluster there is a further correlation between the packing energy of the rotaxane and the energy of interaction of the macrocycle and its external environment. This indicates that these types of energies (E_{mac-th} and E_{mac-xt}) are strongly related as one would, perhaps, expect.

In the third entry, clusters are also formed as a function of the interaction between the macrocycle and its external environment. Only when such an interaction is large, the packing energy correlates with the strength of the macrocycle−thread interaction.

The density and the Kitaigorodski packing coefficient (last two entries) also form clusters where there is further correlation between the packing energy and a number of other parameters. The already fair general correlation obtained for packing energy versus the macrocycle−crystal environment interactions, $r = 0.87$, tends to improve within each cluster.

The cluster analysis shows that, regardless of the parameter considered, a prominent role is played in the packing energy by the interactions between the macrocycle and its crystal environment.

The existence of general trends within this large family of rotaxanes is rewarding. The question, however, arises whether one can make predictions on a specific rotaxane using the knowledge of these data. The unusual degree of freedom that exists in these systems offers the opportunity of *ad hoc* investigations. To create mobility of the ring in the solid or on a surface, one requires weak inter- and intramolecular interactions and the possibility of "maneuvering" which, in general, is provided by shape compatibility. Since all the molecules studied here have rather similar shapes, other parameters such as density must be considered. The ring mobility can be instrumental for crystal plasticity which can be obtained partly through the rings motion. It can also be used *per se* to give switchable polymorphic phases. Figure 3 shows 3-D plots of (a) density versus packing energy versus the sum of the interaction energy of the macrocycle−thread and macrocycle−crystal environment and (b) density versus interaction energy of the macrocycle−thread versus the interaction energy of the macrocycle−crystal environment. A "compromise" for a low value of the three quantities exists; rotaxanes **14** (crystallized from DMSO and DMF), **15**, **16**, **18**, **20**, and **22** are the best suited. Their threads are based on fumaramide, succinamide, and various sulfur-based motifs. The fumaramide-based rotaxanes **14** and **15** are particularly interesting in this respect, since they can be prepared in high yields[6c] and are now being explored by AFM techniques to verify their potential.

Testing the Prediction

The analysis of the calculations has focused on a few types of rotaxanes that should be characterized by high solid-state mobility. We checked the existence of such high mobility by AFM for a candidate rotaxane **15**, which appeared promising from the statistical studies, and compared it to its thread. In fact, *a priori* this system intuitively appears unlikely to possess increased mobility in the rotaxane because the thread has no hydrogen bond donors and thus cannot form strong intermolecular hydrogen bonds in the solid state by itself, whereas the rotaxane has multiple sets of both hydrogen bond donors and

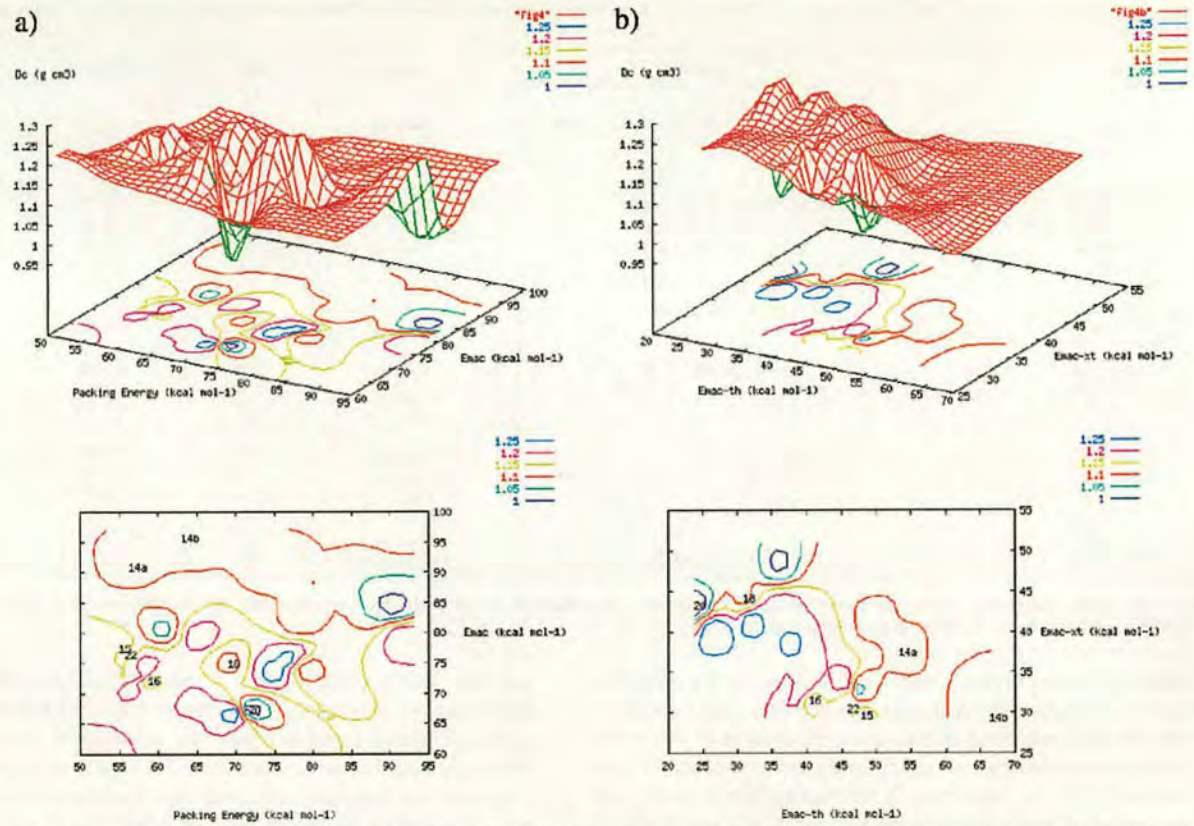

Figure 3. (a) Density versus packing energy versus the sum of the interaction energy of the macrocycle−thread and macrocycle−crystal environment; (b) density versus interaction energy of the macrocycle−thread versus the interaction energy of the macrocycle−crystal environment.

acceptors which can form both strong and directional inter- and intramolecular H-bonds.

Figure 4 shows the morphology of a crystal of rotaxane **15** with terraces and well-defined angles (90°) which indicates growth oriented on the *ab* plane of the monoclinic crystal. The line profile (see Figure 4b) shows terrace steps which are integer multiples of 1.0 ± 0.1 nm. This distance matches the lattice distance along the *c* axis. The typical force used for imaging the crystals in contact mode ranged between 0.5 and 0.8 nN. Figure 4c and d shows the result of scanning a 500 nm by 500 nm area of the crystal surface by increasing the load force from 0.5 to 2 nN. The higher force modifies the top two layers within the scanned area. Friction force microscopy reveals a strong contrast of the modified area with respect to the rest of the crystal. The root-mean-square roughness of the surface increases from 0.704 nm outside to 1.32 nm inside the scratched area.

We repeated the experiment using the same cantilever on the crystal of the thread of **15** and adopting the same experimental conditions (i.e., scan rate, duration of the maximum load force). The unchanged quality of the tip was checked by acquiring topography of the thread crystal. To obtain the same result, an increase in the load force from 0.5 to 14 nN is required. This is nearly one order of magnitude higher than in the rotaxane.

This result confirms the theoretical prediction that interlocking with the macrocycle leads to higher mobility of **15** in the solid state. Although this mobility may be associated with either intra- or intermolecular movement, the statistical treatment of rotaxane crystal structures can clearly be used to predict which type of rotaxane building blocks may show mechanical movement in the solid state.

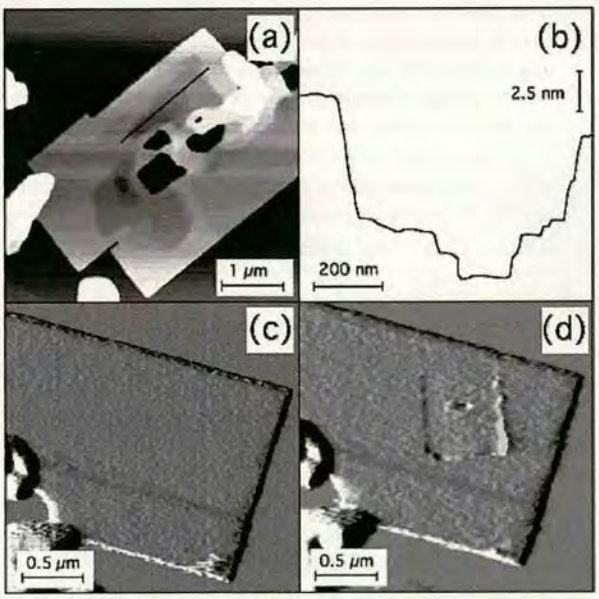

Figure 4. (a) AFM topographical image (height range $z = 0-45$ nm) of rotaxane **15** microcrystals obtained by deposition from an acetone solution followed by annealing for 7 min in air at 420 K. Set point load force is 0.5 N. (b) Profile along the solid line shown in (a); the terraces have a step height ~1.0 ± 0.1 nm. (c) AFM image (error signal) before and after (d) surface patterning with a 2 nN load force.

Some Rules and Conclusions

This paper is ultimately about the comparative ability of macrocycle **1** to bind to other molecules inside and outside its cavity. The conclusions one can gather, which are ultimately important for the future design of benzylic amide macrocycle-containing rotaxanes that can shuttle and/or spin in the solid state, can be put in the form of some simple rules of thumb: (1) Comparison of the rotaxane crystal structures with other small organic molecules and proteins shows a prominent role of the hydrogen bond in rotaxane packing. (2) Analysis of molecular mechanics calculations shows that each of the three energy components of the packing energy (H-bond, $\pi-\pi$ stack, and other van der Waals) of the rotaxanes tends to scale with the same component of the energy of interaction between the macrocycle and its crystal environment. (3) The PCA showed that many properties of the crystal structures of benzylic amide macrocycle-containing rotaxanes tend to have trends similar to those of noninterlocked small organic molecules. (4) The PCA showed that the description of molecular size and H-bonds is strongly interrelated. (5) The PCA showed that the description of stoichiometry and H-bonds is strongly interrelated. (6) Formation of intramolecular hydrogen bonds in these carefully designed rotaxane systems often takes precedence over their use in the crystal assembly. Therefore, establishing intramolecular interactions is of higher importance than the crystal density. (7) The cluster analysis shows that, regardless of the parameter considered, a very prominent role is played in the packing energy by the interactions between the macrocycle and its crystal environment.

Apart from this set of simple rules, the present work further shows that the key properties of low crystal packing density and weak macrocycle interactions can co-exist and that by using the computational protocol partly developed here it is possible to select a rotaxane where the presence of the macrocycle induces a higher mobility in the solid. AFM experiments corroborated the predictions made for one of the rotaxanes, showing that this system presents higher in-crystal mobility than its thread. Such results are important for the selection of rotaxane building blocks that could act as components for molecular shuttles and machines which would function as part of a solid-state device.

Atomic Force Microscopy Experimental Procedure

Films of both a promising candidate rotaxane (**15**) and its corresponding thread were grown by drop-casting from acetone (Aldrich, chromatography grade) solutions (0.4 mg/mL) onto highly oriented phyrolitic graphite (HOPG) which was cleaved prior to drop casting. To obtain molecular crystals, both rotaxane and thread films were annealed for 7 min in air at 100−120 °C. Both compounds form tiny crystals with the shape of the rotaxane crystals being better defined. An atomic force microscope operated in contact mode was used both for imaging and for performing lithography with silicon oxide tips (Ultralevers, Thermomicroscope, USA) with 10 nm nominal radius of curvature and cantilevers with a force constant equal to 0.24 N/m (min 0.10−max 0.47 N/m).

Acknowledgment. We would like to thank the referees for encouraging us to experimentally check the prediction of higher solid-state mobility for the fumaramide rotaxanes and Ricardo García for useful discussions. This work was partly supported by the TMR initiative of the European Union through contracts FMRX-CT96-0059 and FMRX-CT97-0097. F.Z. also acknowledges partial support from MURST project "Dispositivi Supramolecolari" and the University of Bologna "Funds for selected research topics" initiative. D.A.L. is an EPSRC Advanced Research Fellow (AF/982324).

Supporting Information Available: A table with the PCA correlations matrix, plots of the correlation between some noncovalent interactions (PDF). This material is available free of charge via the Internet at http://pubs.acs.org.

JA0159362

From Reactants to Products via *Simple Hydrogen Bonding Networks: Information Transmission in Chemical Reactions*

Giuseppe Brancato, Frédéric Coutrot, David A Leigh, Aden Murphy, Jenny K Y Wong and Francesco Zerbetto

Proc. Natl. Acad. Sci. USA **2002**, 99, *4967–4971*

From reactants to products via simple hydrogen-bonding networks: Information transmission in chemical reactions

Giuseppe Brancato*, Frédéric Coutrot†, David A. Leigh†‡, Aden Murphy§, Jenny K. Y. Wong†, and Francesco Zerbetto*‡

*Dipartimento di Chimica "G. Ciamician," Università degli Studi di Bologna, via F. Selmi n.2, 40126, Bologna, Italy; †Department of Chemistry, University of Edinburgh, The King's Buildings, West Mains Road, Edinburgh EH9 3JJ, United Kingdom; and §Nanoarchitectonics Research Center, National Institute of Advanced Industrial Science and Technology, Tsukuba Central 5, 1-1-1 Higashi, Tsukuba, Ibaraki 305-8565, Japan

Edited by Jack Halpern, University of Chicago, Chicago, IL, and approved February 5, 2002 (received for review December 22, 2001)

The transmission of information is ubiquitous in nature and often occurs through supramolecular hydrogen bonding processes. Here we report that there is a remarkable correlation during synthesis between the efficiency of the hydrogen-bond-directed assembly of peptide-based [2]rotaxanes and the symmetry distortion of the macrocycle in the structure of the final product. It transpires that the ability of the flexible macrocycle-precursor to wrap around an unsymmetrical hydrogen bonding template affects both the reaction yield and a quantifiable measure of the symmetry distortion of the macrocycle in the product. When the yields of peptide rotaxane-forming reactions are high, so is the symmetry distortion in the macrocycle; when the yields are low, indicating a poor fit between the components, the macrocycle symmetry is relatively unaffected by the thread. Thus during a synthetic sequence, as in complex biological assembly processes, hydrogen bonding can code and transmit "information"—in this case a distortion from symmetry—between chemical entities by means of a supramolecularly driven multicomponent assembly process. If this phenomenon is general, it could have far reaching consequences for the use of supramolecular-directed reactions in organic chemistry.

continuous symmetry measure | hydrogen bonds | molecular recognition | rotaxanes | symmetry distortion

Hydrogen bonding routinely codes and transmits information during the course of biological activity, most celebratedly with nucleic acids, but also in the selective signaling and interactions of proteins, carbohydrates, hormones, and numerous other functional biomolecules (1). Here we show that information contained in hydrogen bonding motifs can be stored over the course of a multistep reaction pathway that starts from simple building blocks and ends in a set of unconventional molecular architectures, namely peptide-based rotaxanes (molecular systems in which a macrocyclic ring is locked onto a linear "thread" by two bulky "stoppers") (2, 3). Subsequently, the information (symmetry) can be quantitatively extracted (in the form of its distortion) from the solid-state structures of the mechanically interlocked products and related to the yields of the chemical reactions that formed them.

The synthesis and properties of rotaxanes and molecular shuttles based on various dipeptide threads and benzylic amide macrocycles have been described (4–8). In fact, the structural tolerance of the assembly process allows the preparation of rotaxanes derived from oligopeptide sequences of at least 2–5 amino acid residues as long as they contain at least one non-N-terminal glycine residue (9). The five-component "clipping" reactions (Fig. 1) produce rotaxanes because cooperative multipoint hydrogen bonding between the open chain precursor **1** (which, in the absence of a suitable template, preferentially adopts a linear *syn–anti* conformation) and the thread **2** promotes a conformational change that brings the reactive end groups in close proximity leading to rapid cyclization of **1**. During the crucial phase of the reaction, the forming macrocycle

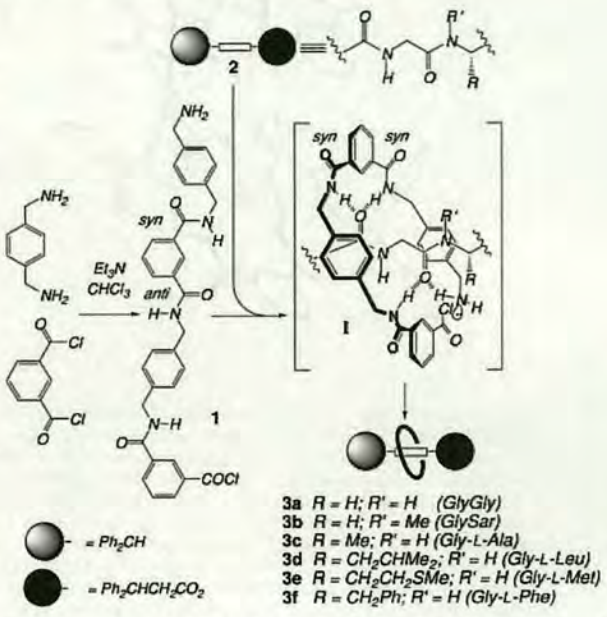

Fig. 1. Rotaxane formation by means of peptide-based hydrogen bond templates. Sar, sarcosine.

establishes a complicated pattern of weaker secondary interactions (including π–π, CH–π, dipole–dipole, van der Waals, etc.) with the template that depend overwhelmingly on the ability of the two amide groups of the thread to coordinate the incoming molecule by means of hydrogen bonding, as shown in supramolecular complex **I**. In general, the better the fit—both electrostatically and sterically—that the interacting surfaces of "host" and "guest" can adopt as the flexible macrocycle-precursor wraps around the thread in **I**, the higher the yield of the reaction will be.

Apart from being implicated in directing the covalent-bond-forming reactions, multipoint hydrogen bonding between the unsymmetrical thread and the macrocycle in the rotaxane necessarily also distorts the ring from its original isolated symmetry

This paper was submitted directly (Track II) to the PNAS office.

Abbreviation: CSM, continuous symmetry measurement.

Data deposition: Crystallographic data for **3a–f** (excluding structure factors) are available from the Cambridge Crystallographic Data Centre as supplementary publication numbers CCDC-141367 (**3a**), CCDC-179-101321 (**3b**), CCDC-147201 (**3c**), and CCDC-141368 to CCDC-141370 (**3d–f**). Copies of the data can be obtained free of charge on application to CCDC, Cambridge CB2 1EZ, United Kingdom (e-mail: teched@chemcrys.cam.ac.uk).

‡To whom reprint requests may be addressed. E-mail: david.leigh@ed.ac.uk or gatto@ciam.unibo.it.

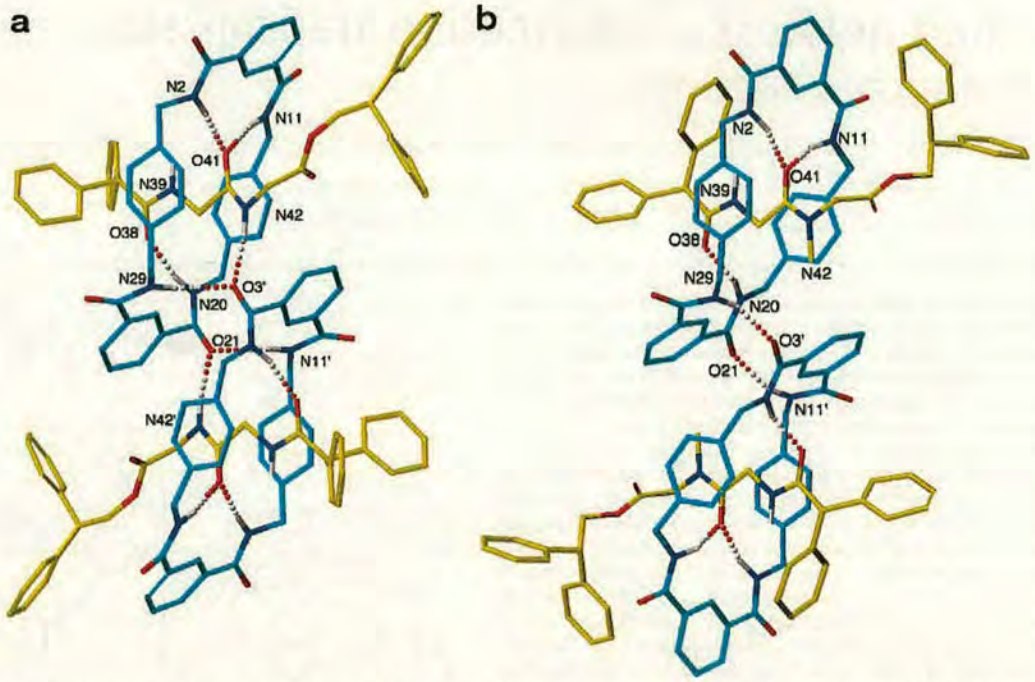

Fig. 2. The solid-state structures of peptido[2]rotaxanes **3a–f** as determined by x-ray crystallography. Carbon atoms of the macrocyclic ring are shown in light blue, and the carbon atoms of the peptide threads are shown in yellow; oxygen atoms are depicted red, nitrogen atoms are depicted in dark blue, and sulfur, green. Non-amide hydrogen atoms have been removed for clarity; those indicated were placed in chemically reasonable positions. (*a*) Gly-Gly rotaxane **3a**, intramolecular hydrogen bond distances: O41–N2 = 3.01 Å; O41–N11 = 3.19 Å; O38–N20 = 2.87 Å; intermolecular hydrogen bond distances: O21–N11′ = O3′–N29 = 3.06 Å; O3′–N42 = O21–N42′ = 2.88 Å; hydrogen bond angles: O41–H–N2 = 174.0°; O41–H–N11 = 170.1°; O38–H–N20 = 165.3°; O21–H–N11′ = O3′–H–N29 = 149.5°; O3′–H–N42 = O21–H–N42′ = 169.1°. (*b*) Gly-Sar rotaxane **3b**, intramolecular hydrogen bond distances: O41–N2 = 3.01 Å; O41–N11 = 3.09 Å; O38–N20 = 2.75 Å; intermolecular hydrogen bond distances: O3′–N29 = O21–N11′ = 2.93 Å; hydrogen bond angles: O41–]H–N2 = 163.5°; O41–H–N11 = 157.5°; O38–H–N20 = 142.7°; O3′–H–N29 = O21–H–N11′ = 147.4°. (*Figure continues on the opposite page.*) (*c*) Gly-L-Ala rotaxane **3c**, intramolecular hydrogen bond distances: O38–N29 = 3.30 Å; O38–N20 = 2.93 Å; O41–N11 = 2.99 Å; O41–N2 = 3.01 Å; hydrogen bond angles: O38–H–N29 = 174.1°; O38–H–N20 = 162.7°; O41–H–N11 = 170.9°; O41–H–N2 = 167.5°. (*d*) Gly-L-Leu rotaxane **3d**, intramolecular hydrogen bond distances: O38–N29 = 2.98 Å; O38–N20 = 3.26 Å; O41–N11 = 3.05 Å; O41–N2 = 3.13 Å; hydrogen bond angles: O38–H–N29 = 156.8°; O38–H–N20 = 153.6°; O41–H–N11 = 172.5°; O41–H–N2 = 162.0°; selected dihedral angles: C7–C8–C10–O10 = 158.0°; C5–C4–C3–O3 = 158.7°; C25–C26–C28–O28 = 155.4°; C23–C22–C21–O21 = 140.2°. (*e*) Gly-L-Met rotaxane **3e**, intramolecular hydrogen bond distances: O38–N29 = 3.18 Å; O38–N20 = 2.90 Å; O41–N11 = 3.10 Å; O41–N2 = 2.97 Å; hydrogen bond angles: O38–H–N29 = 157.5°; O38–H–N20 = 162.3°; O41–H–N11 = 165.4°; O41–H–N2 = 171.7°; selected dihedral angles: C7–C8–C10–O10 = 154.2°; C5–C4–C3–O3 = 150.9°; C25–C26–C28–O28 = 149.6°; C23–C22–C21–O21 = 141.1°. (*f*) Gly-L-Phe rotaxane **3f**, intramolecular hydrogen bond distances: O38–N29 = 3.02 Å; O38–N20 = 3.15 Å; O41–N11 = 2.98 Å; O41–N2 = 3.17 Å; hydrogen bond angles: O38–H–N29 = 160.3°; O38–H–N20 = 149.4°; O41–H–N11 = 169.3°; O41–H–N2 = 164.8°; selected dihedral angles: C7–C8–C10–O10 = 156.0°; C5–C4–C3–O3 = 155.7°; C25–C26–C28–O28 = 143.6°; C23–C22–C21–O21 = 150.7°. Crystallographic data for **3a–f** (excluding structure factors) are available from the Cambridge Crystallographic Data Centre as supplementary publication numbers CCDC-141367 (**3a**), CCDC-179-101321 (**3b**), CCDC-147201 (**3c**), and CCDC-141368 to CCDC-141370 (**3d–f**). Copies of the data can be obtained free of charge on application to CCDC, Cambridge CB2 1EZ, United Kingdom (e-mail: teched@chemcrys.cam.ac.uk).

(for example, hydrogen bonds simultaneously present between the macrocycle and the different amide groups of the thread cannot be of identical energies, and thus the symmetry of the macrocycle is intrinsically broken). Loosely speaking, the stronger the hydrogen bonding between the components, the larger the deformation of the symmetry caused by the thread can be. Synthetic yields and symmetry distortion in the product are therefore influenced by the same phenomenon. A direct relationship between the two, however nontrivial, would imply that the reactions that form the rotaxanes conserve and transmit information from reactants to products. An interesting corollary to this relationship would be that an increase in the hydrogen bonding ability of certain sections of an unsymmetrical template may not necessarily increase a reactions yield; it could be that only the part resulting in symmetry distortion of the final product carries information related to the efficiency of the assembly process. Importantly, such a distortion is amenable to prediction by molecular modeling calculations.

The x-ray crystal structures of six dipeptide rotaxanes (**3a–f**), each containing the same benzylic amide macrocycle, show varying conformations and co-conformations (ref. 9; "co-conformation" refers to the relative positions and orientations of the mechanically interlocked components with respect to each other; ref. 10) of the interlocked components as illustrated in Fig. 2. Despite cyclization of the open-chain precursor **1** occurring about a near-identical template in each case (the variations in the structure of the threads all occur at the periphery of the template region shown in **I**), the yields of the reactions vary from 32% to 62%.

To quantify various aspects of symmetry measures, several approaches have been proposed (11–23). One is the continuous symmetry measure (CSM; refs. 17–23), which has proved suc-

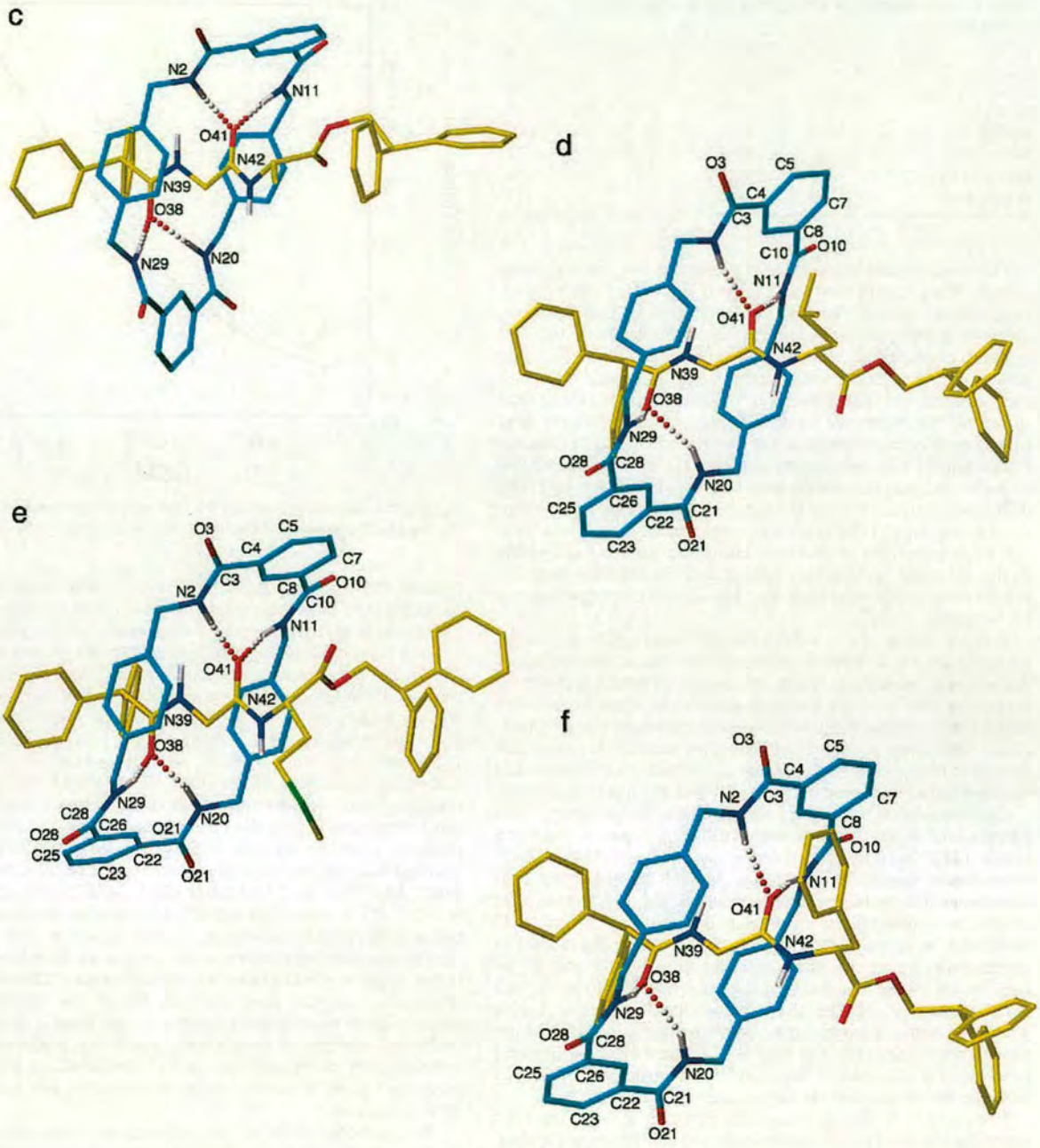

Fig. 2. (*Continued.*)

cessful in a number of cases (17–23). In this approach, Avnir and collaborators calculate CSM or the symmetry deviation, S, as the norm of the vector defined by the difference between the optimal idealized structure—obtained by numerical techniques—and the actual structure. A simple equation connects S to the Cartesian coordinates of the atoms:

$$S = \frac{100}{nA^2} \sum_{i=1}^{n} (p_i - \hat{p}_i)^2, \qquad [1]$$

where n is the number of equivalent points (i.e., atoms) in the symmetry of interest, A is a normalization factor given by the distance between the center of mass of the molecule and its own farthest atom, p_i is the coordinates of the atoms, and $\hat{p}_i$ is the coordinates of the atoms of the optimal structure that are determined by numerical optimization techniques (one for each structure). In this way, in agreement with the approach proposed by Avnir (17–23), S does not measure the distance to a predetermined general structure but to the closest symmetry sought. $S = 0$ coincides with perfect symmetry, i.e., no symmetry lowering, and $S = 100$ collapses the system to a single point.

Table 1. CSM, *S*, and reaction yields, *Y*, for dipeptide [2]rotaxanes 3a–f

	S	*Y*, %
3a Gly-Gly	0.17	62
3b Gly-Sar	0.18	60
3c Gly-L-Ala	0.13	45
3d Gly-L-Leu	0.02	37
3e Gly-L-Met	0.03	36
3f Gly-L-Phe	0.02	32

The benzylic amide macrocycle present in the peptide rotaxanes **3a–f** can exist in boat (C_{2v}), chair (C_{2h}), or half-chair/twist-boat conformations (see Fig. 2). Evaluation of the symmetry measure in different point groups, i.e., with respect to different symmetry operations, was thought likely to give quantities that would not be directly comparable. For example, the chair conformation has an inversion center, which is absent in the boat structure. Forcing its use would have made *S* unrealistically large for the boat conformation. It was therefore decided to limit the calculation of *S* to the twofold axes that (*i*) are roughly parallel to the thread, and (*ii*) pass through the *p*-xylylene fragments. The difference between the two is the preference for the ring to adopt (*i*) the boat or (*ii*) the chair-like conformation. As seen from the x-ray structures, both these conformations are accessible in the rotaxane architecture but have different consequences for the intercomponent hydrogen bonding geometries that can be adopted.

Table 1 shows the *S* values for the macrocycle in the six rotaxane crystal structures. In three cases, **3a–c**, the symmetry distortion is substantial. Since the thread possesses only trivial symmetry, the values are a consequence of the effectiveness with which the macrocycle wraps around the hydrogen-bonding template. The three rotaxane systems with smaller *S* values can therefore be considered to contain threads that are intrinsically less well suited to interacting positively with the macrocyclic ring.

Examination of the six crystal structures helps explain this pattern and shows the presence of different types of hydrogen bonds (24), "standard" two-center systems and "bifurcated" three-center bonds. In two cases, **3a** and **3b**, there are also intermolecular hydrogen bonds seen in the solid state that cannot be involved in the mechanism of formation of "isolated" molecules in solution (see below). Importantly, the rotaxane architecture forces the intramolecular bifurcated bonds to be orthogonal to the lone pairs of the acceptor, resulting in their being somewhat weaker than conventional hydrogen bonds where the acidic hydrogen atoms on nitrogen point directly at the oxygen lone pairs (i.e., the region of highest electron density) (this motif is also seen in the x-ray crystal structures of various benzylic amide macrocycle-based catenanes; see ref. 25).

In more detail: (*i*) The Gly-Gly site (rotaxane **3a**) is the least sterically hindered for the macrocycle and also the most flexible, allowing it to adopt the most favorable hydrogen bonding geometries in solution or the solid state. The macrocycle adopts a chair conformation, and the crystal structure shows one standard and one pair of bifurcated hydrogen bonds (plus the intermolecular one), all in the range of 2.87–3.19 Å and 165.3–174.0°, typical geometries for strong amide–amide hydrogen bonds (26); (*ii*) the Gly-Sar (**3b**) system displays a similar hydrogen bonding pattern to Gly-Gly, but the extra methyl group distorts the macrocycle into a less favorable half chair/twist boat-like structure; (*iii*) the Gly-L-Ala rotaxane (**3c**) has two pairs of intercomponent bifurcated (i.e., weaker) hydrogen bonds, and the macrocycle adopts a boat conformation to form medium length (2.93–3.30 Å) but reasonably linear NH···O hydrogen bonds in the range 162.7–174.1°; (*iv*) the last three

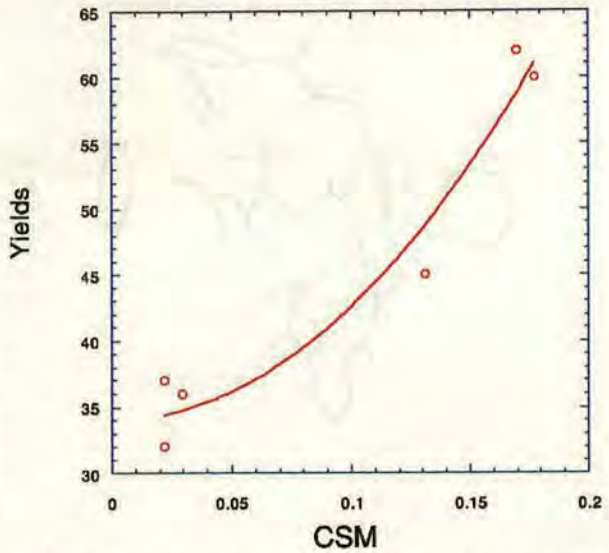

Fig. 3. The relationship between the CSM from the solid-state structure of the peptido[2]rotaxanes and the five-component reaction yield.

systems (**3d–f**) also possess two pairs of bifurcated hydrogen bonds, but the larger steric bulk at their chiral centers prevents the macrocycle from adopting a boat conformation from which it could form the same type of hydrogen bond geometries as **3c**. Thus, although the macrocycle adopts a relatively unstrained chair conformation, this geometry means that several of the NH···O hydrogen bonds have to be longer than normal and distorted from linearity (e.g., N20···O38 = 3.26 Å, N20H···O38 = 153.6° **3d**; N29···O38 = 3.18 Å, N29H···O38 = 157.5° **3e**; N20···O38 = 3.15 Å, N20H···O38 = 149.4° **3f**) and therefore relatively weak. Moreover, to form these hydrogen bonds at all, some of the amide groups of the macrocycle have to twist out of planarity with the benzene rings of the isophthaloyl unit, decreasing the π-electron conjugation (e.g., C23–C22–C21–O21 = 140.2° **3d**, C23–C22–C21–O21 = 141.1° **3e**, C25–C26–C28–O28 = 143.6° **3f**). Comparison of the hydrogen bonding patterns with the symmetry-lowering values, *S*, thus confirms that stronger intercomponent interactions in the solid state do correspond to larger symmetry distortions in the macrocycle. This finding is consistent with the idea that the better the ability of the macrocycle to wrap around the thread and form a close fitting, reciprocal pattern of interactions, the more effective it is at following the electronic and steric "contours" of the thread, adopting a complementary shape to its partner and a distortion in its symmetry.

The synthetic yields of the rotaxane-forming reactions are shown in Table 1.[¶] Given the many factors that can contribute to both reaction yields (e.g., solubility of products and intermediates, and different degrees of intramolecular hydrogen bonding in the threads) and crystal structure geometries (solvent, temperature, and concentration at which the crystals were grown), the correlation between the CSM of the solid-state structures and the yields is remarkable and, in particular, implies a close similarity between the structures of the final products and the intermediate supramolecular complex **I**, which leads to the transition state for ring closure.

[¶]The rotaxane-forming reactions were carried out under identical conditions (6, 9) and repeated at least three times. The yields of individual experiments were remarkably reproducible, all falling within a 2% range.

The yields are probably dependent on the relative strengths of the three amide–amide hydrogen bonds between the open-chain precursor **1** and the thread, shown in **I** (the fourth hydrogen bond, between an amine and an amide, will be much weaker because the hydrogen bond acidity, α_2^H, of amines is in the range 0.00–0.26, compared with the typical α_2^H of a secondary amide of 0.38) (27). The two rotaxanes formed in highest yield (**3a** and **3b**, 62% and 60%), thus each have one standard intercomponent hydrogen bond (strong), two bifurcated intercomponent hydrogen bonds (less strong), and a symmetry-lowering S of 0.17 and 0.18, respectively. The Gly-L-Ala rotaxane, **3c**, formed in a lower yield (45%), has only bifurcated hydrogen bonds (weak, but linear because it can adopt a boat conformation) and a CSM value of 0.13. The three rotaxanes formed in the most modest yields (32–37%), **3d–f**, each have two pairs of relatively weak bifurcated hydrogen bonds and a CSM value less than 0.04. Ironically, the three threads that have the bulkiest amino acid side chains (i.e., the most pronounced asymmetric centers) give the smallest symmetry distortions in the macrocycle; the reason behind this, the poor fit between the macrocycle and thread, also accounts for their modest yields.

Fig. 3 further illustrates the relationship between CSM and the reaction yields. Although the two-parameter parabola (without the linear term) has a high r^2 value (>0.95), its presence is mainly to assist the eye. [Nonlinear trends of S versus physical quantities have been observed (15, 16). It is, however, intriguing to notice that molecular distortions along either a vibrational motion or a bond tend to increase the energy quadratically. For discussion of this point see ref. 28.] CSM, in the special form of continuous chirality measure (21), has been correlated to other dynamic and energy-related quantities such as the binding activity of trypsin/arylammonium inhibitors, D_2-dopamine receptor/dopamine derivative agonists, trypsin/organophosphates inhibitors, acetylcholinesterase/organophosphate and butyrylcholinesterase/organophosphates (21), and has been used to establish relationships between chirality content and stereoinduction (22). In the latter case, three-term parabolas were used to fit computed chirality contents versus enantiomeric excesses, and the r^2 values found there, 0.63–0.92, are comparable to that obtained above.

The fundamental picture that emerges from this study is of a system in which the ability of a flexible macrocycle precursor to wrap around an unsymmetrical hydrogen bonding template determines, and thus relates, both reaction yield and the symmetry distortion in the product. When the yields of peptide rotaxane-forming reactions are high, so is the symmetry distortion in the macrocycle; when the yields are low, indicating a poor fit between the components, the macrocycle symmetry is relatively unaffected by the thread. Thus in synthetic chemistry, as in complex biological systems, hydrogen bonding can code and transmit information between chemical entities by a supramolecularly driven multicomponent assembly process. The case reported here is, however, unique both in terms of its simplicity and the way the information, i.e., symmetry, is stored and subsequently extracted. If this result proves to be a general phenomenon, it could have far-reaching consequences for the use of supramolecular-directed covalent bond-forming reactions in organic synthesis.

1. Jeffrey, G. A. & Saenger, W. (1991) *Hydrogen Bonding in Biological Structures* (Springer, New York).
2. Amabilino, D. B. & Stoddart, J. F. (1995) *Chem. Rev.* **95,** 2725–2828.
3. Sauvage, J.-P. & Dietrich-Buchecker, C., eds. (1999) *Molecular Catenanes, Rotaxanes and Knots* (Wiley/VCH, Weinheim, Germany).
4. Leigh, D. A., Murphy, A., Smart, J. P. & Slawin, A. M. Z. (1997) *Angew. Chem. Int. Ed. Engl.* **36,** 728–732.
5. Lane, A. S., Leigh, D. A. & Murphy A. (1997) *J. Am. Chem. Soc.* **119,** 11092–11093.
6. Clegg, W., Gimenez-Saiz, C., Leigh, D. A., Murphy, A., Slawin, A. M. Z. & Teat, S. J. (1999) *J. Am. Chem. Soc.* **121,** 4124–4129.
7. Leigh, D. A., Troisi, A. & Zerbetto, F. (2000) *Angew. Chem. Int. Ed.* **39,** 350–353.
8. Wurpel, G. W. H., Brouwer, A. M., van Stokkum, I. H. M., Farran, A. & Leigh D. A. (2001) *J. Am. Chem. Soc.* **123,** 11327–11328.
9. Asakawa, M., Brancato, G., Fanti, M., Leigh, D. A., Shimizu, T., Slawin, A. M. Z., Wong, J. K. Y., Zerbetto, F. & Zhang S. (2002) *J. Am. Chem. Soc.*, in press. (Published on the Web ASAP contents March 1, 2002.)
10. Fyfe, M. C. T., Glink, P. T., Menzer, S., Stoddart, J. F., White, A. J. P. & Williams, D. J. (1997) *Angew. Chem. Int. Ed. Engl.* **36,** 2068–2069.
11. Murray-Rust, P., Rüsti, H. B. & Dunitz, J. (1978) *Acta Crystallogr. B* **34,** 1787–1793.
12. Gilat, G. (1985) *Chem. Phys. Lett.* **121,** 9–12.
13. Rassat, A. (1984) *C. R. Acad. Sci. Paris II* **299,** 53–55.
14. Maruani, J. & Mezey, P. G. (1990) *Mol. Phys.* **69,** 97–113.
15. Ruch, E. (1972) *Acc. Chem. Res.* **5,** 49–56.
16. Buda, A. B. & Mislow, K. (1992) *J. Am. Chem. Soc.* **114,** 6006–6012.
17. Zabrodsky Hel-Or, H., Peleg, S. & Avnir, D. (1992) *J. Am. Chem. Soc.* **114,** 7843–7851.
18. Zabrodsky Hel-Or, H., Peleg, S. & Avnir, D. (1993) *J. Am. Chem. Soc.* **115,** 8278–8289.
19. Zabrodsky Hel-Or, H., Peleg, S. & Avnir, D. (1993) *J. Am. Chem. Soc.* **115,** 11656–11656.
20. Zabrodsky Hel-Or, H., Peleg, S. & Avnir, D. (1995) *J. Am. Chem. Soc.* **117,** 462–473.
21. Krinan, S. & Avnir, D. (1998) *J. Am. Chem. Soc.* **120,** 6152–6159.
22. Gao, D., Schefzick, S. & Lipkowitz, K. B. (1999) *J. Am. Chem. Soc.* **121,** 9481–9482.
23. Lipkowitz, K. B., Schefzick, S. & Avnir, D. (2001) *J. Am. Chem. Soc.* **123,** 6710–6711.
24. Jeffrey, G. A. (1997) *An Introduction to Hydrogen Bonding* (Oxford Univ. Press, Oxford).
25. Johnston, A. G., Leigh, D. A., Pritchard, R. J. & Deegan, M. D. (1995) *Angew. Chem. Int. Ed. Engl.* **34,** 1209–1212.
26. Taylor, R. & Kennard, O. (1984) *Acc. Chem. Res.* **17,** 320–326.
27. Abraham, M. H. (1993) *Chem. Soc. Rev.* **22,** 73–83.
28. Brancato, G. & Zerbetto, F. (2001) *J. Phys. Chem. A* **104,** 11439–11442.

Switching "On" and "Off" the Expression of Chirality

in Peptide Rotaxanes

Masumi Asakawa, Giuseppe Brancato, Marianna Fanti, David A leigh

Toshimi Shimizu, Alexandra M Z Slawin, Jenny K Y Wong,

Francesco Zerbetto and Songwei Zhang

J. Am. Chem. Soc. ***2002***, 124, *2939–2950*

JACS
ARTICLES
Published on Web 03/01/2002

Switching "On" and "Off" the Expression of Chirality in Peptide Rotaxanes

Masumi Asakawa,[†] Giuseppe Brancato,[‡] Marianna Fanti,[‡] David A. Leigh,*[,‖,⊥,▽] Toshimi Shimizu,[†] Alexandra M. Z. Slawin,[#] Jenny K. Y. Wong,[‖,▽] Francesco Zerbetto,*[,‡,§] and Songwei Zhang[‖]

Contribution from the Nanoarchitectonics Research Center, National Institute of Advanced Industrial Science and Technology, Tsukuba Central 5, 1-1-1 Higashi, Tsukuba, Ibaraki 305-8565, Japan, Dipartimento di Chimica "G. Ciamician", Università degli Studi di Bologna, V. F. Selmi 2, 40126, Bologna, Italy, Centre for Supramolecular and Macromolecular Chemistry, Department of Chemistry, University of Warwick, Coventry CV4 7AL, U.K., and School of Chemistry, University of St Andrews, North Haugh, St. Andrews, Fife KY16 9ST, U.K.

Received April 11, 2001. Revised Manuscript Received December 15, 2001

Abstract: The hydrogen-bond-directed synthesis, X-ray crystal structures, and optical properties of the first chiral peptide rotaxanes are reported. Collectively these systems provide the first examples of single molecular species where the expression of chirality in the form of a circular dichroism (CD) response can selectively be switched "on" or "off", and its magnitude altered, through controlling the interactions between mechanically interlocked submolecular components. The switching is achievable both thermally and through changes in the nature of the environment. Peptido[2]rotaxanes consisting of an intrinsically achiral benzylic amide macrocycle locked onto various chiral dipeptide (Gly-L-Ala, Gly-L-Leu, Gly-L-Met, Gly-L-Phe, and Gly-L-Pro) threads exhibit strong (10−20k deg cm^2 dmol^{-1}) negative induced CD (θ) values in nonpolar solvents (e.g. $CHCl_3$), where the intramolecular hydrogen bonding between thread and macrocycle is maximized. In polar solvents (e.g., MeOH), where the intercomponent hydrogen bonding is weakened, or switched off completely, the elliptical polarization falls close to zero in some cases and can even be switched to large positive values in others. Importantly, the mechanism of generating the switchable CD response in the chiral peptide rotaxanes is also determined: a combination of semiempirical calculations and geometrical modeling using the continuous chirality measure (CCM) shows that the chirality is transmitted from the amino acid asymmetric center on the thread via the macrocycle to the C-terminal stopper of the rotaxane. This understanding could have important implications for other areas where chiral transmission from one chemical entity to another underpins a physical or chemical response, such as the seeding of supertwisted nematic liquid crystalline phases or asymmetric synthesis.

Introduction

The absence of certain symmetry elements is the de facto requirement for chirality. Structures that possess only axes of symmetry or no symmetry at all—in fact the great majority of molecular shapes—are chiral, whereas those with a plane of symmetry (i.e., S_1), inversion center (S_2), or higher axes of rotoreflection (S_{3+}), are not. However, molecular level flexibility often permits the interconversion of low-symmetry enantiomeric shapes on short time scales such that many molecules are never effectively chiral despite principally adopting chiral conformations. While the presence of chirality is easily identifiable for any particular molecular structure, the *expression* of that chirality—i.e., the magnitude of the effects that the asymmetry has on the chemical and physical properties of the system—is much more elusive to quantify, understand, and, ultimately, control.[1] Sometimes the influence of a chiral center can be negligible; for example, a single asymmetric carbon atom at one end of a long alkyl chain generally has little effect on the properties of a prochiral center at the other end. Alternatively, the effects of molecular asymmetry can be greatly amplified; some chiral seed molecules need only be present in tiny amounts in order to induce and sustain the supertwist nematic phases exploited in liquid crystal displays. Control over the magnitude of the expression of chiral shape and associated phenomena is thus of great interest, particularly if it produces effects that can be triggered—or switched—through external stimuli.

Rotaxanes,[2] molecules consisting of a macrocyclic ring locked onto a linear "thread" by bulky "stoppers", are a class of compounds well-suited for exploring switchable phenomena.

* To whom correspondence should be addressed.
† Nanoarchitectonics Research Center.
‡ Dipartimento di Chimica "G. Ciamician".
‖ Centre for Supramolecular and Macromolecular Chemistry.
⊥ E-mail: David.Leigh@ed.ac.uk.
▽ Current address: Department of Chemistry, University of Edinburgh, The King's Buildings, West Mains Road, Edinburgh EH9 3JJ, U.K.
School of Chemistry.
§ E-mail: gatto@ciam.unibo.it.

(1) For a recent comprehensive review on chiroptic molecular switches, see: Feringa, B. L.; van Delden, R. A.; Koumura, N.; Geertsema, E. M. *Chem. Rev.* **2000**, *100*, 1789−1816.

10.1021/ja015995f CCC: $22.00

Several systems have been developed where the position of the macrocyclic ring can be switched from site to another—so-called "molecular shuttles"—in response to a range of stimuli, including light, electrons, pH, and the nature of the environment.[3] One of the major issues still to be properly explored with such architectures, however, is the nature of the physical and chemical effects that can be influenced utilizing mechanical bonding. Here we describe how a chiral optical response, circular dichroism, for hydrogen bond-assembled peptide rotaxanes[3d,4] with the general structure GlyX, where X is a chiral amino acid, can be controlled in terms of both magnitude and sign through the use of external stimuli which affect the intercomponent interactions between macrocycle and thread. The phenomenon is closely related to the ability of chiral species to induce an asymmetric response in the optical absorption bands of achiral partners (induced circular dichroism, ICD) through host–guest complexation[5] and represents the first examples of single molecular species where ICD can be selectively switched "on" or "off" through controlling the interactions between mechanically interlocked submolecular components. As a direct consequence of the tight fitting interlocked molecular architecture, switchable chiral transmission in peptide rotaxanes can be expressed over remarkably long distances.

Synthesis

The hydrogen bond-mediated synthesis of benzylic amide macrocycle-containing rotaxanes derived from achiral glycyl- and sarcosyl-(*N*-methyl glycine) dipeptide threads has previously been described.[3d,4a,b] Our mechanistic understanding of the five-component assembly process suggested that the route should allow the synthesis of rotaxanes based on any short oligopeptide sequence containing at least one non-N-terminus glycine residue.[6] Since all the coded α-amino acids besides glycine (and many uncoded and unnatural ones) possess asymmetric carbon atoms, this provides access to a virtually limitless range of main chain chiral rotaxanes where an asymmetric center is locked in close proximity to an intrinsically achiral macrocycle. Accordingly, a series of dipeptide threads **1**–**5** (Gly-L-Ala (**1**), Gly-L-Leu (**2**), Gly-L-Met (**3**), Gly-L-Phe (**4**), and Gly-L-Pro (**5**)) were prepared and converted into the corresponding chiral peptido[2]rotaxanes (**6**–**10**) in yields of 32–45%, for **6**–**9**, and 6%, for **10** (Scheme 1). The poor yield of the proline derivative is probably due to several factors including (i) the greater steric crowding of the hydrogen bonding sites of the thread by this bulky amino acid and (ii) the tertiary amide group stabilizing conformations of the thread which are unfavorable for rotaxane formation.

UV–Vis Spectroscopy and Circular Dichroism Experiments

To investigate the effect of the mechanical interlocking on the chiral environments of these systems, UV–vis absorption spectra (Figure 1 and Table 1) and circular dichroism measurements (Figures 2–4 and Table 2) in the wavelength region of aromatic ring excitation (230–320 nm) were carried out on dilute (0.1 mM) solutions of each thread and rotaxane in $CHCl_3$, MeCN, and MeOH. The solvents were chosen as being (i) relatively nonpolar ($CHCl_3$; the rotaxanes were insufficiently soluble in less polar solvents such as cyclohexane), (ii) polar, but uncompetitive for disrupting amide–amide hydrogen bonds (MeCN), and (iii) polar and competitive at solvent concentrations for disrupting amide-amide hydrogen bonds (MeOH; dimethyl sulfoxide, which we have previously used for breaking hydrogen bonds in amide rotaxane systems,[3d,4a,b] absorbs strongly in the UV–vis region of interest for this study). Note that the strong absorbance of all three solvents below 250 nm precludes accurate UV–vis measurements below this wavelength (which would have been desirable given that the trough of most of the CD responses of the peptide rotaxanes are in this region). The modest solubilities of the rotaxanes meant that higher concentrations of the substrates could not be used and, therefore, there may be a higher than usual error limit (~10%) in the quantitative values of these experiments. Fortunately, however, the use of a 0.1 cm path length permitted the reproducible measurement of CD spectra in the range 230–

(2) (a) Schill, G. *Catenanes, Rotaxanes and Knots*, Academic Press: New York, 1971. (b) Chambron, J.-C.; Dietrich-Buchecker, C. O.; Sauvage, J.-P. *Top. Curr. Chem.* **1993**, *165*, 131–162. (c) Gibson, H. W.; Bheda, M. C.; Engen, P. T. *Prog. Polym. Sci.* **1994**, *19*, 843–945. (d) Amabilino, D. B.; Stoddart, J. F. *Chem. Rev.* **1995**, *95*, 2725–2828. (e) Leigh, D. A.; Murphy, A. *Chem., Ind.* **1999**, 178–183. (f) Sauvage, J.-P., Dietrich-Buchecker, C., Eds. *Molecular Catenanes, Rotaxanes and Knots*; Wiley-VCH: Weiheim, 1999. For chiral rotaxanes, see: (g) Archut, A.; Müller, W. M.; Baumann, S.; Habel, M.; Vögtle, F. *Liebigs Ann.* **1997**, 495–499. (h) Ashton, P. R.; Everitt, S. R. L.; Gómez-López, M.; Jayamaran, N.; Stoddart, J. F. *Tetrahedron Lett.* **1997**, *38*, 5691–5694. (i) Yamamoto, C.; Okamoto, T.; Schmidt, T.; Jäger, R.; Vögtle, F. *J. Am. Chem. Soc.* **1997**, *119*, 10547–10548. (j) Schimdt, T.; Schmieder, R.; Müller, W. M.; Kiupel, B.; Vögtle, F. *Eur. J. Org. Chem.* **1998**, 2003–2007. (k) Ashton, P. R.; Bravo, J. A.; Raymo, F. M.; Stoddart, J. F.; White, A. J. P.; Williams, *Eur. J. Org. Chem.* **1999**, *899*, 9–908. (l) Schmieder, R.; Hübner, G.; Seel, C.; Vögtle, F. *Angew. Chem. Int. Ed.* **1999**, *38*, 3528–3530.

(3) For examples of molecular shuttles and other stimuli-responsive rotaxanes, see: (a) Bissell, R. A.; Córdova, E.; Kaifer, A. E.; Stoddart, J. F. *Nature* **1994**, *369*, 133–137. (b) Ashton, P. R.; Ballardini, R.; Balzani, V.; Boyd, S. E.; Credi, A.; Gandolfi, M. T.; Gómez-López, M.; Iqbal, S.; Philp, D.; Preece, J. A.; Prodi, L.; Ricketts, H. G.; Stoddart, J. F.; Tolley, M. S.; Venturi, M.; White, A. J. P.; Williams, D. J. *Chem. Eur. J.* **1997**, *3*, 152–170. (c) Anelli, P.-L.; Asakawa, M.; Ashton, P. R.; Bissell, R. A.; Clavier, G.; Górski, R.; Kaifer, A. E.; Langford, S. J.; Mattersteig, G.; Menzer, S.; Philp, D.; Slawin, A. M. Z.; Spencer, N.; Stoddart, J. F.; Tolley, M. S.; Williams, D. J. *Chem. Eur. J.* **1997**, *3*, 1113–1135. (d) Lane, A. S.; Leigh, D. A.; Murphy, A. *J. Am. Chem. Soc.* **1997**, *119*, 11092–11093. (e) Murakami, H.; Kawabuchi, A.; Kotoo, K.; Kunitake, M.; Nakashima, N. *J. Am. Chem. Soc.* **1997**, *119*, 7605–7606. (f) Gong, C.; Glass, T. E.; Gibson H. W. *Macromolecules* **1998**, *31*, 308–313. (g) Armaroli, N.; Balzani, V.; Collin, J. P.; Gaviña, P.; Sauvage, J.-P.; Ventura, B. *J. Am. Chem. Soc.* **1999**, *121*, 4397–4408. (h) Shigekawa, H.; Miyake, K.; Sumaoka, J.; Harada, A.; Komiyama, M. *J. Am. Chem. Soc.* **122**, 5411 2000. (i) Ballardini, R.; Balzani, V.; Dehaen, W.; Dell'Erba, A. E.; Raymo, F. M.; Stoddart, J. F.; Venturi, M. *Eur. J. Org. Chem.* **2000**, 591–602. (j) Consuelo Jiménez, M.; Dietrich-Buchecker, C.; Sauvage, J.-P. *Angew. Chem. Int. Ed.* **2000**, *39*, 3284–3287. (k) Kawaguchi, Y.; Harada, A. *Org. Lett.* **2000**, *2*, 1353. (l) Bermudez, V.; Capron, N.; Gase, T.; Gatti, F. G.; Kajzar, F.; Leigh, D. A.; Zerbetto, F.; Zhang, S. *Nature* **2000**, *406*, 608–611. (m) Ashton, P. R.; Ballardini, R.; Balzani, V.; Credi, A.; Dress, K. R.; Ishow, E.; Kleverlaan, C. J.; Kocian, O.; Preece, J. A.; Spencer, N.; Stoddart, J. F.; Venturi, M.; Wenger, S. *Chem. Eur. J.* **2000**, *6*, 3558–3574. (n) Brouwer, A. M.; Frochot, C.; Gatti, F. G.; Leigh, D. A.; Mottier, L.; Paolucci, F.; Roffia, S.; Wurpel, G. W. H. *Science* **2001**, *291*, 2124–2128.

(4) (a) Leigh, D. A.; Murphy, A.; Smart, J. P.; Slawin, A. M. Z. *Angew. Chem., Int. Ed. Engl.* **1997**, *36*, 728–731. (b) Clegg, W.; Gimenez-Saiz, C.; Leigh, D. A.; Murphy, A.; Slawin, A. M. Z.; Teat, S. J. *J. Am. Chem. Soc.* **1999**, *121*, 4124–4129. (c) Leigh, D. A.; Troisi, A.; Zerbetto, F. *Angew. Chem. Int. Ed.* **2000**, *39*, 350–353.

(5) For ICD in host–guest complexes, see, for example: (a) Kodaka, M. *J. Am. Chem. Soc.* **1993**, *115*, 3702–3705. (b) Forman, J. E.; Barrans, R. E.; Dougherty, D. A. *J. Am. Chem. Soc.* **1995**, *117*, 9213–9228. (c) Yashima, E.; Matsushima, T.; Okamoto, Y. *J. Am. Chem. Soc.* **1997**, *119*, 6345–6359. (d) Asakawa, M.; Ashton, P. R.; Hayes, W.; Janssen, H. M.; Meijer, E. W.; Menzer, S.; Pasini, D.; Stoddart, J. F.; White, A. J. P.; Williams, D. J. *J. Am. Chem. Soc.* **1998**, *120*, 920–931. (e) Meillon, J.-C.; Voyer, N.; Biron, E.; Sanschagrin, F.; Stoddart, J. F. *Angew. Chem. Int. Ed.* **2000**, *39*, 143–145. For the use of hydrogen bonding to assemble remarkable chiral supramolecular arrays, see, for example: (f) Suárez, M.; Branda, N.; Lehn, J.-M.; Decian, A.; Fischer, J. *Helv. Chim. Acta* **1998**, *81*, 1–13. (g) Prins, L. J.; Huskens, J.; de Jong, F.; Timmerman, P.; Reinhoudt, D. N. *Nature* **1999**, *398*, 498–502. (h) Hirschberg, J. H. K. K.; Brunsveld, L.; Ramzi, A.; Vekemans, J. A. J. M.; Sijbesma, R. P.; Meijer, E. W. *Nature* **2000**, *407*, 167–170. (i) Prins, L. J.; de Jong, F.; Timmerman, P.; Reinhoudt, D. N. *Nature* **2000**, *408*, 181–184.

(6) Certain amino acids require chemical protection of sensitive functionality in order to be incorporated into rotaxanes by this synthetic strategy.

Scheme 1 The Syntheses of Peptide Rotaxanes **6**–**10** and **12**

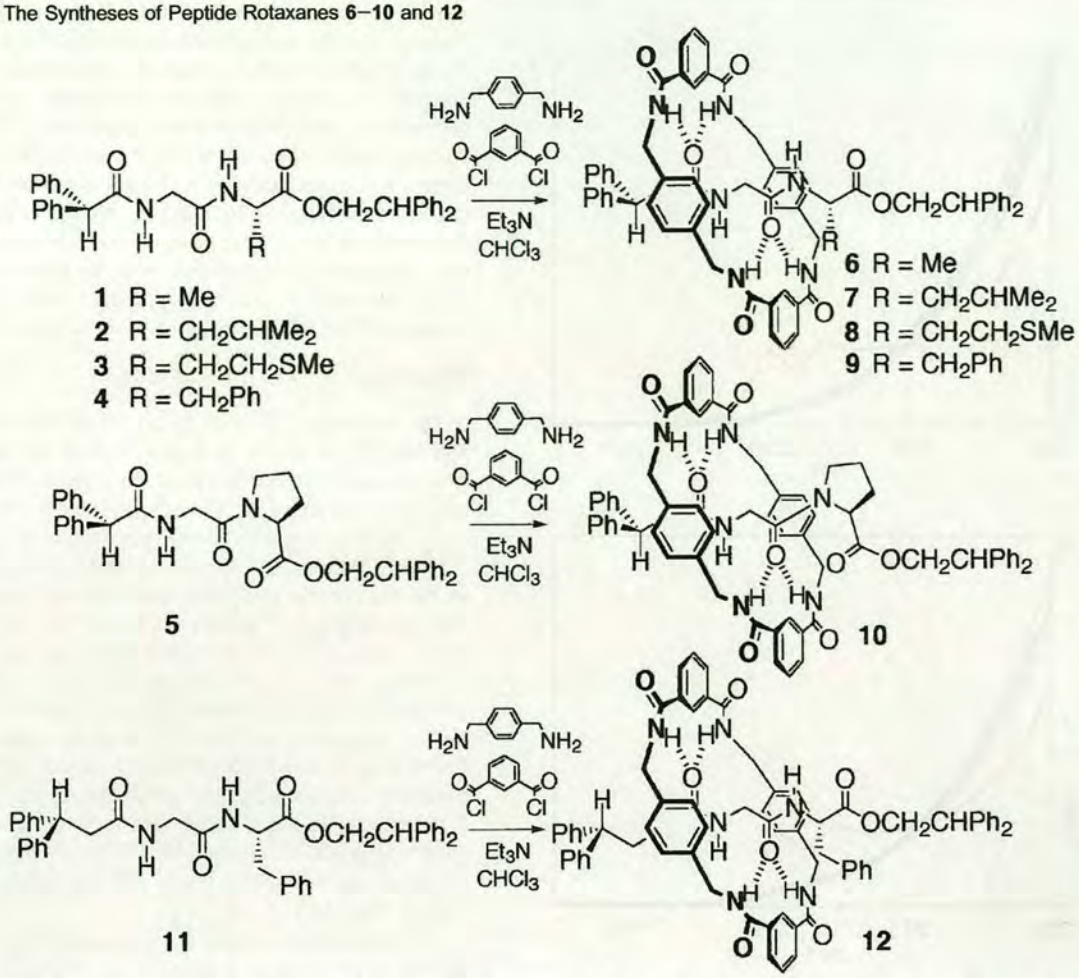

250 nm, even in $CHCl_3$, despite the strong absorbance of the solvent at these wavelengths. As a further control, identical CD measurements were also obtained using a different spectopolarimeter and experimental set up. *In all cases, the threads exhibited a zero CD response in each solvent system*, illustrating the lack of influence of the amino acid chiral centers on the four (five in the case of **4**) phenyl rings of the threads. In contrast, all five chiral peptide rotaxanes exhibited large molar ellipticities, the strength and sign of which varied with the nature of the solvent.

Figure 2 shows the room temperature CD spectra of the peptide rotaxanes in each solvent system. A number of general features are immediately apparent:

1. For each peptide rotaxane a strong negative ICD is observed in $CHCl_3$, the environment in which the intercomponent hydrogen bonding between macrocycle and thread is strongest. Since the CD response is absent in the spectra of each of the uninterlocked components, the ICD can be unambiguously attributed to the mechanically interlocked architecture of the system.

2. For each rotaxane in MeOH, the solvent in which the intercomponent hydrogen bonding is weakest, the magnitude of the ICD response is greatly reduced with respect to that in $CHCl_3$ and the *sign* of the response actually reversed in the case of the Gly-L-Ala, Gly-L-Met, and Gly-L-Phe rotaxanes **6**, **8**, and **9**.

3. The Gly-L-Leu and Gly-L-Phe rotaxanes (**7** and **9**) give comparable CD responses in MeCN and $CHCl_3$ suggesting that the co-conformations[7] adopted by the rotaxane components in these solvents are similar, the inference being that the intercomponent hydrogen bonding in these two rotaxanes is less easy to disrupt than in the other three systems.

4. For the various rotaxanes, the molar ellipticity in $CHCl_3$ varies between 5 and 20 000 deg cm^2 dmol^{-1} yet the active chromophore (be it on the stoppers or the macrocycle) is the same in each case! *Thus the size and shape of the amino acid substituent plays a crucial role in the efficient transmission of chiral information from the asymmetric center to the chromophore.*

The CD response of the Gly-L-Met rotaxane **8** is particularly noteworthy and Figures 3 and 4 show its dependence as a function of (a) the nature of the environment and (b) temperature. It has the largest magnitude room-temperature response of the dipeptide rotaxanes investigated here (-19900 deg cm^2 dmol^{-1} at a λ_{max} of 246 nm in $CHCl_3$) and the sign of the CD signal switches from negative to positive in MeOH ($+3390$ deg cm^2 dmol^{-1}) at a very similar wavelength (242 nm): a net change of >23000 deg cm^2 dmol^{-1} within a 4 nm range! The

(7) "Co-conformation" refers to the relative positions and orientations of the mechanically interlocked components with respect to each other [Fyfe, M. C. T.; Glink, P. T.; Menzer, S.; Stoddart, J. F.; White, A. J. P.; Williams, D. J. *Angew. Chem., Int. Ed. Engl.* **1997**, *36*, 2068–2069].

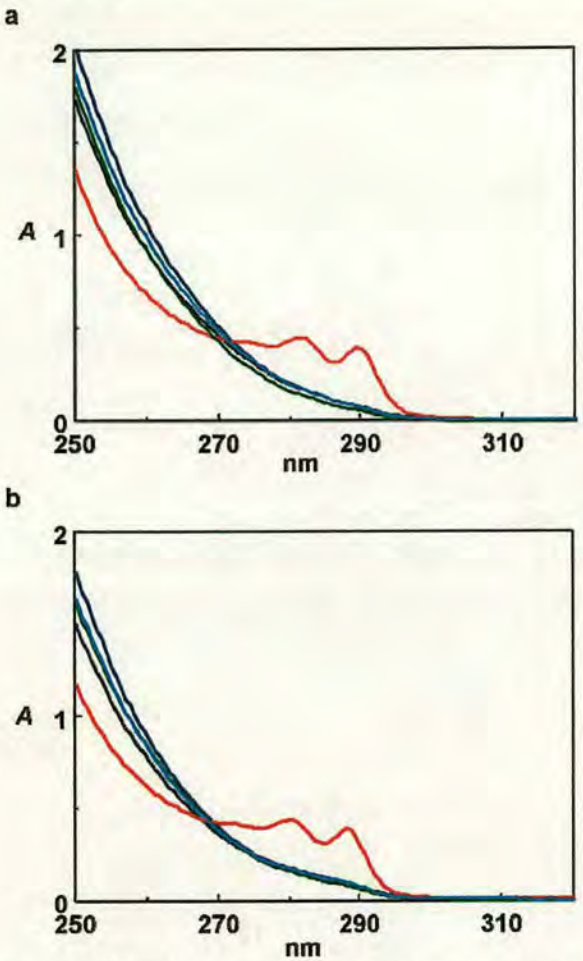

Figure 1. UV-visible spectra (0.1 mM) of peptide rotaxanes **6** (Gly-L-Ala, cyan), **7** (Gly-L-Leu, black), **8** (Gly-L-Met, blue), **9** (Gly-L-Phe, red), and **10** (Gly-L-Pro, green) in (a) MeOH, (b) $CHCl_3$. A = absorbance.

change in sign means that conditions exist (in this case 1:10 $CHCl_3$/MeOH at 298K, blue curve in Figure 3) where the chirality of **8** does *not* give rise to a CD response, but where it can be effectively switched "on"—to generate either a positive or negative value—by very small changes in the nature of the environment.

The sensitivity of the CD response that operates in these peptide rotaxanes and its dependence on the subtle nature of the intercomponent hydrogen bond strength between macrocycle and thread is well illustrated by the series of CD spectra shown in Figure 3. It is remarkable to note that adding an equal volume of MeOH to **8** in neat $CHCl_3$ (green and cyan curves, Figure 3) leads to only a 15% drop in signal intensity, yet going from 83% MeOH in $CHCl_3$ to neat MeOH (black and red curves, Figure 3), solutions of virtually identical polarity and dielectric constants, results in a switch in the CD response at 242 nm from −5590 to +3390 deg cm^2 $dmol^{-1}$!

The variation in the range of the CD response controllable by modulating the intercomponent hydrogen bonding by external factors is further demonstrated by the variable temperature CD spectra of **8** shown in Figure 4. In $CHCl_3$, where the intercomponent hydrogen bonding is strong, the CD response of **8** is unchanged over the range 263−333 K. However, in MeOH the signal is highly temperature dependent. At 263 K the CD response is large and *negative* suggesting that at low temperatures MeOH is unable to break the intercomponent hydrogen bonding, i.e., the co-conformation adopted by the rotaxane components is reminiscent of that adopted in $CHCl_3$. Increasing the temperature—i.e., increasing the ability of the solvent to disrupt the intercomponent hydrogen bonding—incrementally decreases the negative ICD signal, passing through zero, and ultimately leads to a large *positive* CD response at 333 K. The use of temperature to moderate both the size and handedness of the expression of a chiral response provides a further useful feature of these mechanically interlocked systems.

What Gives Rise to the ICD Signal?

The electronic (UV−vis) spectra of the rotaxanes in $CHCl_3$ and MeOH are shown in Figure 1. The spectra are largely structure and solvent invariant throughout the series, with absorption starting at wavelengths just below 300 nm (~35000 cm^{-1}) in agreement with that observed for other isophthalamide systems.[8] The electronically excited states of the phenyl groups of the macrocycle are conjugated with the π systems of the two adjacent carbonyl groups and have lower gaps than isolated phenyl rings. The lowest excited states of these systems are therefore a mixture of $n_o\pi^*$ and L_b (B_{2u} in D_{6h} symmetry) benzenic transitions. At about 250 nm (40000 cm^{-1}), the more intense benzenic L_a (B_{1u} in D_{6h} symmetry) states appear. The contribution of the macrocyclic ring to these transitions becomes evident if one compares the extinction coefficients of thread and rotaxane (Table 1). Significantly, the threads all have electronic transitions around 240−250 nm; in the corresponding rotaxanes, the states of the thread and macrocycle can be mixed through their degeneracy.

The molar ellipticities for the rotaxanes are given in Table 2 and the corresponding spectra shown in Figure 2. The main band is in the 240−250 nm region. In the hydrogen bond-disrupting solvent, MeOH, the bands are consistently smaller than in the non-hydrogen bond disrupting solvents, MeCN and $CHCl_3$. In MeOH the chiral peptide moiety can hydrogen bond to the solvent weakening or displacing the intramolecular hydrogen bonds that exist in a non-hydrogen bond disrupting solvent.

The ICD signal is clearly intrinsic to the mechanically interlocked molecular architecture of the peptide rotaxanes, since the resonances are absent for solutions of the uninterlocked, but otherwise chemically identical, components. While it is tempting to assume that the asymmetric center of the peptide simply forces the macrocycle chromophores (the aromatic rings) into a chiral environment giving rise to a CD response, this is not the only possible origin of the signal. The diphenylmethine stoppers also provide benzenic states which could elicit a CD response in the near UV, but like the aromatic rings of the macrocycle, they do not intrinsically carry any rotatory power and are too remote from the chiral center to be directly influenced by it (remember that none of the threads **1**−**5** exhibit a CD response in any of the solvents employed). Thus, the observed CD spectra must be caused by (long range) interactions between the chiral center and *either* the stoppers *or* the

(8) Brouwer, A. M.; Buma, W. J.; Caudano, R.; Fanti, M.; Fustin, C.-A.; Leigh, D. A.; Murphy, A.; Rudolf, P.; Zerbetto, F.; Zwier, J. M. *Chem. Phys.* **1998**, *238*, 421−428.

Table 1. Extinction Coefficients, ϵ, mol^{-1}, at Selected Wavelengths, Λ, nm, of Threads **1**–**5** and Rotaxanes **6**–**10** in $CHCl_3$

Threads					
nm	Gly-L-Ala (**1**)	Gly-L-Leu (**2**)	Gly-L-Met (**3**)	Gly-L-Phe (**4**)	Gly-L-Pro (**5**)
290	19	110	79	74	117
280	145	133	96	84	142
270	617	649	658	691	692
260	958	1020	1149	1198	1088
250	684	755	893	871	807
Rotaxanes					
nm	Gly-L-Ala (**6**)	Gly-L-Leu (**7**)	Gly-L-Met (**8**)	Gly-L-Phe (**9**)	Gly-L-Pro (**10**)
290	763	795	749	538	585
280	2088	1954	2004	1672	1621
270	4891	4610	5071	4307	4296
260	10133	9151	10553	9236	9165
250	18405	17413	20247	17148	18058

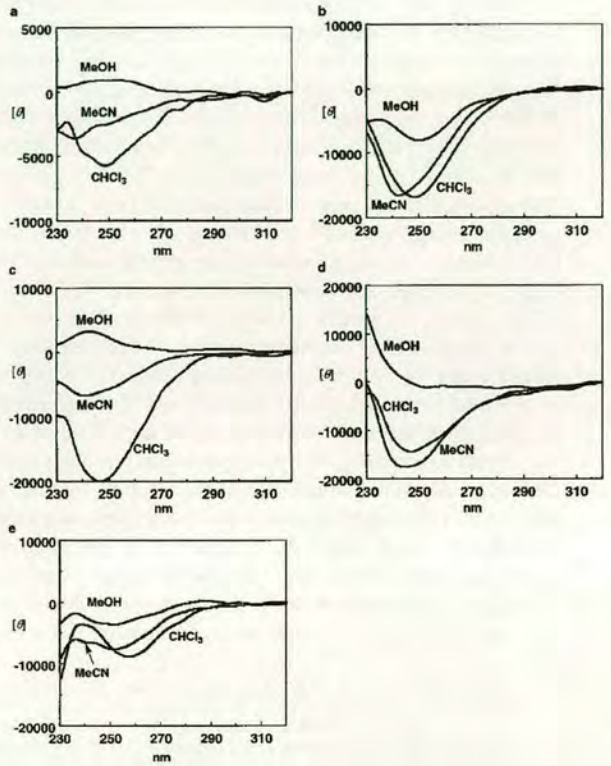

Figure 2. CD Spectra (0.1 mM) of (a) Gly-L-Ala rotaxane **6**, (b) Gly-L-Leu rotaxane **7**, (c) Gly-L-Met rotaxane **8**, (d) Gly-L-Phe rotaxane **9**, and (e) Gly-L-Pro rotaxane **10** in $CHCl_3$, MeCN, and MeOH at 298 K.

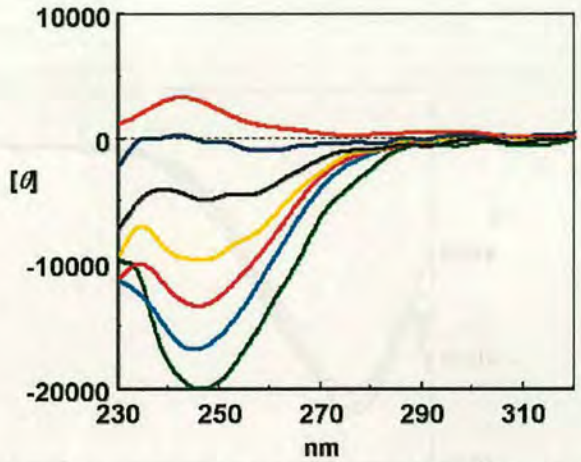

Figure 3. Environment-dependent CD spectra (0.1 mM) of Gly-L-Met rotaxane **8** in (a) 100% $CHCl_3$ (green), (b) 1:1 $CHCl_3$/MeOH (cyan), (c) 2:3 $CHCl_3$/MeOH (magenta), (d) 1:2 $CHCl_3$/MeOH (yellow), (e) 1:5 $CHCl_3$/MeOH (black), (f) 1:10 $CHCl_3$/MeOH (blue), and (g) 100% MeOH (red).

macrocycle aromatic chromophores, but it is not clear which. Evidence to distinguish between the two possibilities was provided by a combination of computer simulations and *X*-ray crystallography.

X-ray Crystallography

Four (**6**–**9**) of the five peptide rotaxanes studied provided single crystals suitable for structure determination by X-ray crystallography (Figure 5a–d). While care has to be taken when extrapolating from the solid-state to the situation in solution, these structures could be used to provide insights into the probable intercomponent interactions present and shape of the rotaxanes in nonpolar solvents. In particular, the crystal structures gave a starting point for understanding how the intercomponent hydrogen bonding interactions can effectively render either the macrocycle or stoppers chiral.

In principle, either the macrocycle or either of the N-terminus and C-terminus stoppers could be influenced by the chiral environment provided by the asymmetric center. When considered in isolation, the macrocycle in a boat conformation (close to that seen in the Gly-L-Ala crystal structure, Figure 5a) belongs to the C_{2v}, achiral, point group and in a chair conformation (close to that seen in the other three *X*-ray structures) to the achiral C_{2h} point group. Although rotation of a single amide group to point a carbonyl toward the cavity center effectively makes the macrocycle chiral (the faces of the ring are held in different environments, anyway: one points toward the N-terminus of the peptide, the other the C-terminus) there seems to be no reason for the macrocycle to do this and the absence of such conformations in any of the four crystal structures suggests against this possibility. The same considerations apply to the two phenyl groups of either stopper which could also assume chiral conformations but then would require suitable stabilization mechanisms to hold them in place. The large negative CD response is recorded for each of these four rotaxanes in $CHCl_3$, a situation where the conformations and co-conformations adopted by the rotaxane components is likely to be similar to those found in the solid-state X-ray crystal structures. The double

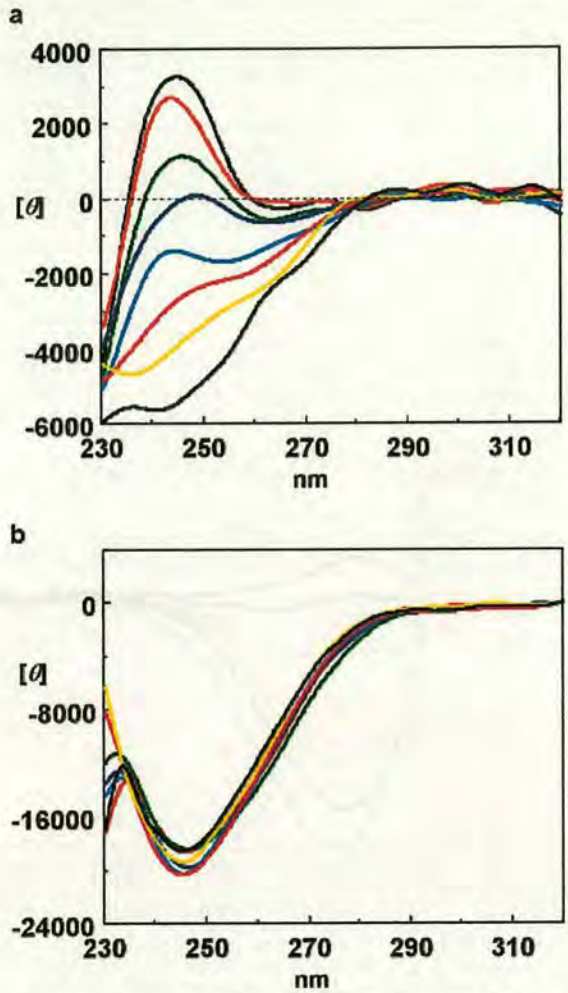

Figure 4. Temperature-dependent (263−333K) CD spectra (0.1 mM) of Gly-L-Met rotaxane **8** in (a) MeOH, (b) $CHCl_3$: 263 K (black), 273 K (red), 283 K (green), 293 K (blue), 303 K (cyan), 313 K (magenta), 323 K (yellow), and 333 K (black).

Table 2. Molar Ellipticities, θ, deg cm^2 dmol^{-1}, at Selected Wavelengths, λ, nm, of Chiral Peptide Rotaxanes **6**−**10**

rotaxane	solvent	λ	θ
Gly-L-Ala (**6**)	MeCN	237	−3530
	$CHCl_3$	248	−5670
	MeOH	252	+972
Gly-L-Leu (**7**)	MeCN	242	−16500
	$CHCl_3$	248	−16700
	MeOH	250	−7880
Gly-L-Met (**8**)	MeCN	241	−6580
	$CHCl_3$	246	−19900
	MeOH	242	+3390
Gly-L-Phe (**9**)	MeCN	242	−17300
	$CHCl_3$	247	−14500
	MeOH	251	−30
Gly-L-Pro (**10**)	MeCN	251	−7490
	$CHCl_3$	257	−8700
	MeOH	251	−3470

bifurcated hydrogen bond motif seen in each of the four X-ray structures effectively locks the macrocycle in place close to the chiral center. The stereochemistry of the amino acid dictates how one isophthaloyl unit of the macrocycle is situated below the hydrogen atom, rather than the more bulky alkyl substituent, of the chiral center. As well as providing a chiral environment for the macrocycle, this effectively locks the isophthaloyl ring extremely close to the C-terminus stopper whether the macrocycle adopts a boat (as with the Gly-L-Ala rotaxane, **6**) or a chair conformation (the other three cases).

The availability of the X-ray crystal structures of **6**−**9** also allowed us to undertake molecular modeling studies to pinpoint the origin of the CD signal using a combination of semiempirical calculations and geometrical modeling. The X-ray structures provide reliable geometries in all probability similar to those responsible for the ICD responses in $CHCl_3$.

Modeling the Spectroscopic Signatures

Modeling of the rotaxane CD spectra was performed with the intent of understanding the origin of the signal rather than quantitative analysis of the spectral patterns (see Experimental Section). First, the four rotaxanes (**6**−**9**) were considered in their entirety. For each rotaxane, the CD spectra were simulated[9] using the semiempirical procedure INDO/S (intermediate neglect of differential overlap/spectroscopic parametrization),[10] employing the *X*-ray crystal structures as starting geometries optimized with the MM3[11] model implemented in the TINKER[12] program. The approach is the same as that used previously to study the potential energy surface[13] and dynamics[14] of benzylic amide [2]catenanes in non-hydrogen-bonding solvents and their vibrations[15] in the solid state. Considering the size and the complexity of the system, the results are very satisfactory with the shape of the experimental curves accurately reproduced by the simulations (Figure 6). To understand which of the three sets of aromatic chromophores (C-terminus and N-terminus diphenylmethine stoppers and the macrocycle) were actually giving rise to the CD response, each was removed in turn (and replaced with hydrogen atoms in the case of the stoppers to maintain a chemically reasonable structure) and the spectra recalculated. Remarkably, when either the macrocycle or the N-terminus diphenylmethine stopper were removed from each rotaxane, the CD signal calculated was nearly the same as that found for the full system. However, in all cases the calculated CD response

(9) (a) Kaito, A.; Hatano, M. *Bull. Chem. Soc. Jpn.* **1980**, *53*, 3064−3068. (b) Oblink, J. H.; Hezemans, A. M. F. *Theor. Chim. Acta (Berlin)* **1976**, *43*, 75−87. (c) Michl, J. *Tetrahedron* **1984**, *40*, 3845−3934 and references therein; (d) West, R.; Downing, J. W.; Inagaki, S.; Michl, J. *J. Am. Chem. Soc.* **1981**, *103*, 5073−5078. (e) Orlandi, G.; Poggi, G.; Zerbetto, F. *Chem. Phys. Lett.* **1994**, *224*, 113−117. (f) Fanti, M.; Orlandi, G.; Poggi, G.; Zerbetto, F. *Chem. Phys.* **1997**, *223*, 159−168.

(10) (a) Del Bene, J.; Jaffé, H. H. *J. Chem. Phys.* **1968**, *48*, 1807−1813. (b) Nishimoto, K.; Mataga, N. *Z. Phys. Chem.* **1957**, *13*, 140−157. (c) Ellis R. L., Jaffé, H. H., Segal, G. A., Ed. In *Modern Theoretical Chemistry*; Plenum: New York, 1977; Vol. 4, p 49. (d) Pople, J. A.; Santry, D. P.; Segal, J. A. *J. Chem. Phys.* **1965**, *43*, S129−S135. (e) Ridley, J. E.; Zerner, M. C. *Theor. Chim. Acta* **1973**, *32*, 111−134. (f) Ridley, J. E.; Zerner, M. C. *Theor. Chim. Acta* **1976**, *42*, 223−236. (g) Zerner, M. C.; Loew, G. H.; Kirchner, R. F.; Mueller-Westerhoff, U. T. *J. Am. Chem. Soc.* **1980**, *102*, 589−599. (h) Edwards, W. D.; Zerner, M. C. *Theor. Chim. Acta* **1987**, *72*, 347−361. (i) Bendale, R. D.; Baker, J. D.; Zerner, M. C. *Int. J. Quantum Chem. Symp.* **1991**, *25*, 557−568.

(11) (a) Allinger, N. L.; Yuh, Y. H.; Lii, J.-H. *J. Am. Chem. Soc.* **1989**, *111*, 8551−8566. (b) Lii, J.-H.; Allinger, N. L.; *J. Am. Chem. Soc.* **1989**, *111*, 8566−8575. (c) Lii, J.-H.; Allinger, N. L.; *J. Am. Chem. Soc.* **1989**, *111*, 8576−8582.

(12) (a) Ponder, J.; Richards, F.; *J. Comput. Chem.* **1987**, *8*, 1016−1024. (b) Kundrot, C.; Ponder, J.; Richards, F. *J. Comput. Chem.* **1991**, *12*, 402−409. (c) Dudek, M. J.; Ponder, *J. Comput. Chem.* **1995**, *16*, 791−8169.

(13) Leigh, D. A.; Murphy, A.; Smart, J. P.; Deleuze M. S.; Zerbetto, F. *J. Am. Chem. Soc.* **1998**, *120*, 6458−6467.

(14) Deleuze M. S.; Leigh, D. A.; Zerbetto, F. *J. Am. Chem. Soc.* **1999**, *121*, 2364−2379.

(15) Caciuffo, R.; Degli Esposti, A.; Deleuze, M. S.; Leigh, D. A.; Murphy, A.; Paci, B.; Parker, S. F.; Zerbetto, F. *J. Chem. Phys.* **1998**, *109*, 11094−11100.

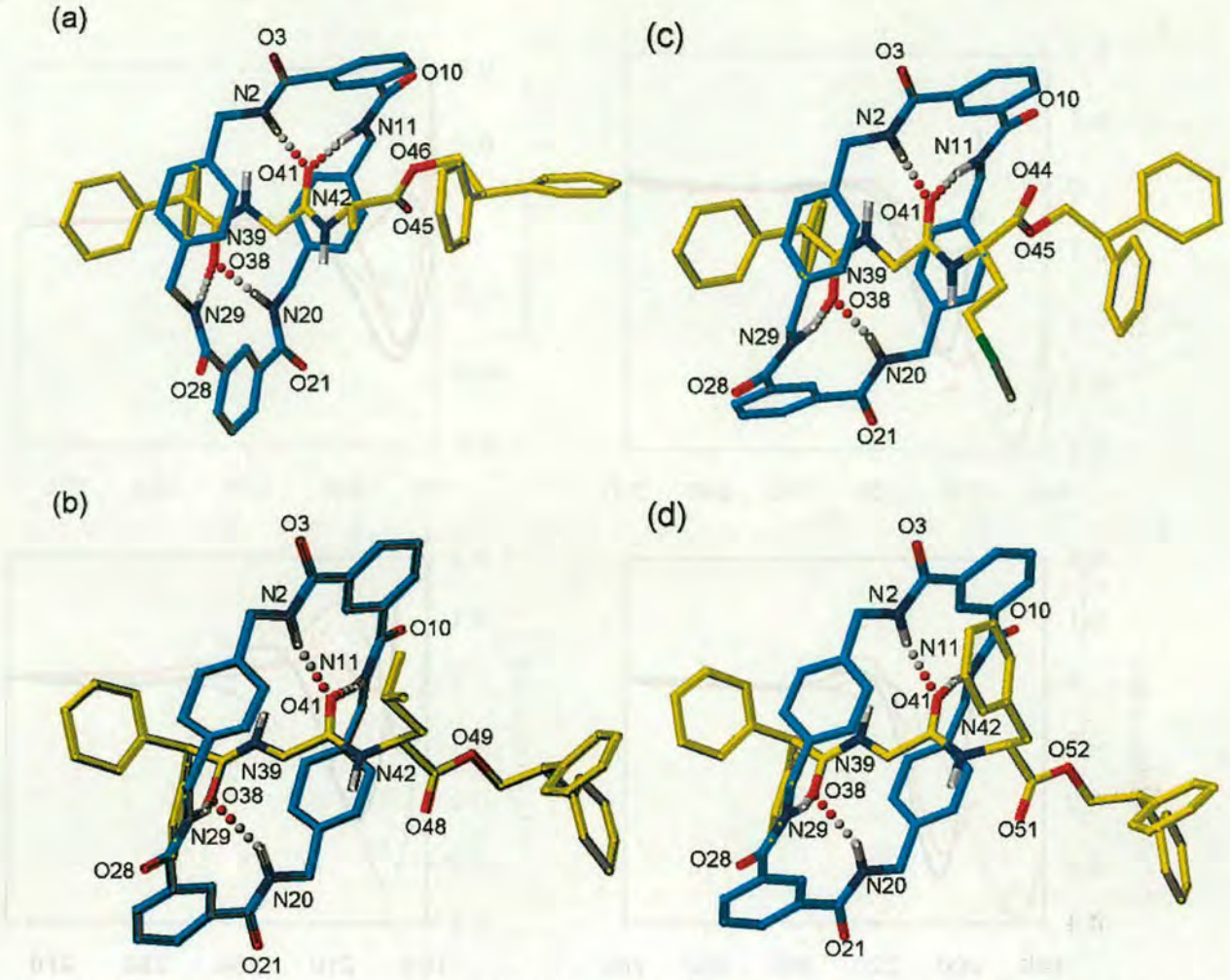

Figure 5. The solid-state structures of peptido[2]rotaxanes **6**–**9** as determined by X-ray crystallography. Carbon atoms of the macrocyclic ring are show in light blue and the carbon atoms of the peptide threads in yellow; oxygen atoms are depicted red, nitrogen atoms dark blue, and sulfur green. Nonamide hydrogen atoms have been removed for clarity; those indicated were placed in chemically reasonable positions: (a) Gly-L-Ala rotaxane **6**, intramolecular hydrogen bond distances (Å): O38−HN29 = 2.23, O38−HN20 = 1.89, O41−HN11 = 1.93, O41−HN2 = 1.95. Hydrogen bond angles (deg): O38−H−N29 = 174.1, O38−H−N20 = 162.7, O41−H−N11 = 170.9, O41−H−N2 = 167.5. (b) Gly-L-Leu rotaxane **7**, intramolecular hydrogen bond distances (Å): O38−HN29 = 1.97, O38−HN20 = 2.26, O41−HN11 = 1.98, O41−HN2 = 2.09. Hydrogen bond angles (deg): O38−H−N29 = 156.8, O38−H−N20 = 153.6, O41−H−N11 = 172.5, O41−H−N2 = 162.0. Selected dihedral angles (deg): C5−C4−C10−O10 = 158.0, C7−C8−C10−O10 = 158.7, C23−C22−C21−O21 = 155.4, C25−C26−C28−O28 = 140.2. (c) Gly-L-Met rotaxane **8**, intramolecular hydrogen bond distances (Å): O38−HN29 = 2.16, O38−HN20 = 1.87, O41−HN11 = 2.05, O41−HN2 = 1.90. Hydrogen bond angles (deg): O38−H−N29 = 157.5, O38−H−N20 = 162.3, O41−H−N11 = 165.4, O41−H−N2 = 171.7. Selected dihedral angles (deg): C5−C4−C3−O3 = 150.9, C7−C8−C10−O10 = 154.2, C25−C26−C28−O28 = 149.6, C23−C22−C21−O21 = 141.1. (d) Gly-L-Phe rotaxane **9**, intramolecular hydrogen bond distances (Å): O38−HN29 = 1.99, O38−HN20 = 2.18, O41−HN11 = 1.93, O41−HN2 = 2.13. Hydrogen bond angles (deg): O38−H−N29 = 160.3, O38−H−N20 = 149.4, O41−H−N11 = 169.3, O41−H−N2 = 164.8. Selected dihedral angles (deg): C7−C8−C10−O10 = 156.0, C5−C4−C3−O3 = 155.7, C25−C26−C28−O28 = 143.6, C23−C22−C21−O21 = 150.7.

was dramatically decreased by removal of the C-terminus diphenylmethine group. Details of the simulations are shown in Figure 6.

The Origin of the CD Response in Chiral Peptido[2]-rotaxanes

The nature of the well expressed chirality of the peptide rotaxanes in $CHCl_3$ can now be understood. The co-conformation seen in all the chiral peptide rotaxane X-ray crystal structures which places one of the isophthaloyl groups of the macrocycle under the hydrogen atom of the chiral center of the thread is locked in place in nonpolar solvents by the four intercomponent hydrogen bonds. In this position, the isophthaloyl group both restricts the rotation of the C-terminus diphenylmethine unit and destabilizes one or more of the three rotamers of the stopper, creating a well expressed chiral environment for the phenyl rings of the stopper which, in fact, are the chromophores responsible for the CD signal. Chiral information is thus transmitted from the asymmetric center on the thread to the macrocycle and on to the stopper of the thread. *Effectively, the tight fitting mechanically interlocked rotaxane architecture promotes a long distance chiral interaction.* Furthermore, with this mechanism of chiral transmission the ability of the different rotaxanes to modulate the magnitude of the CD signal can be attributed to the small angle variations

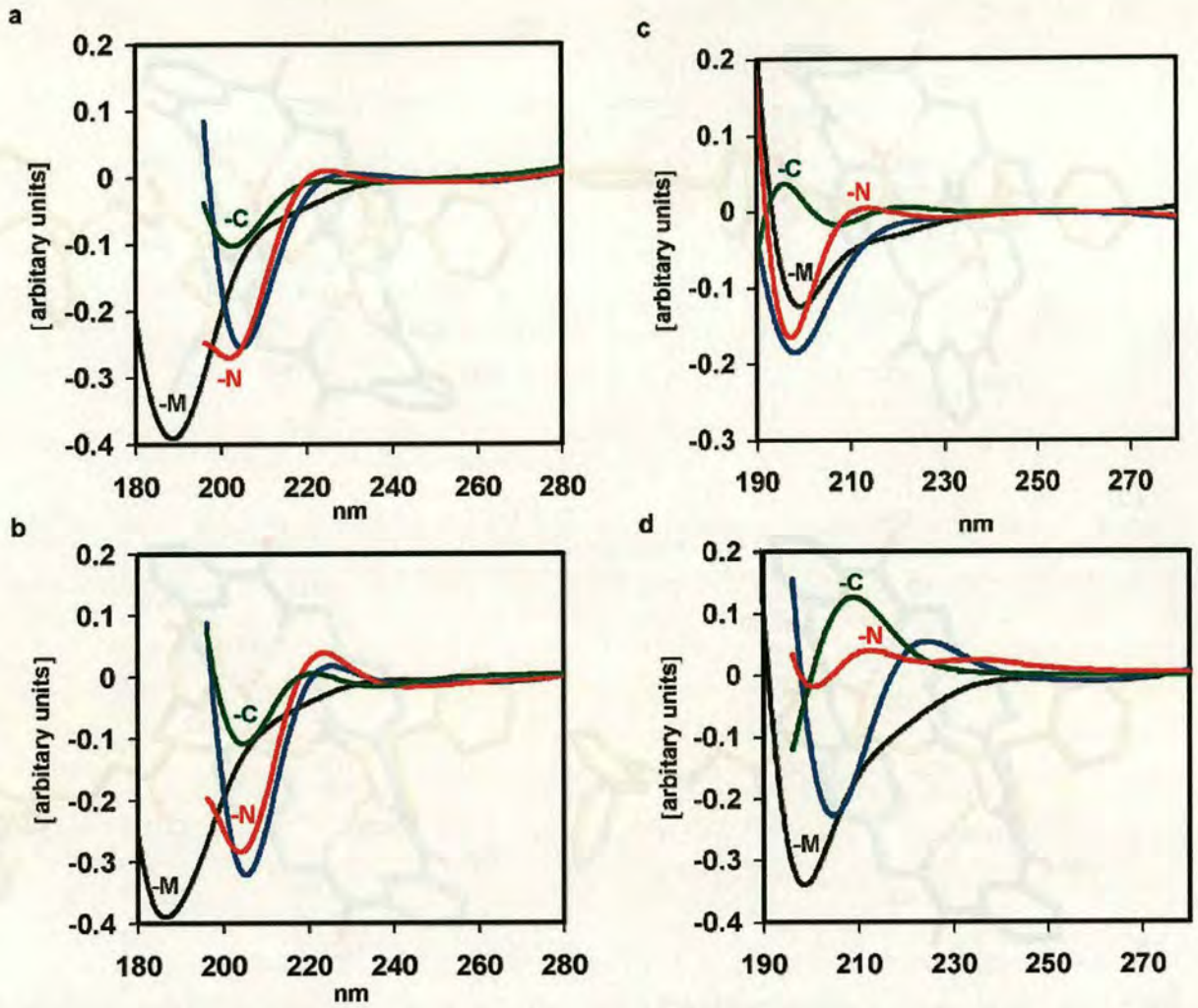

Figure 6. Simulated CD spectra of (a) Gly-L-Ala rotaxane **6**, (b) Gly-L-Leu rotaxane **7**, (c) Gly-L-Met rotaxane **8**, and (d) Gly-L-Phe rotaxane **9**, calculated as complete structures (blue curves, no label) and with each type of chromophore unit selectively removed: i.e., rotaxane-minus-N-terminus-stopper (red curves), rotaxane-minus-C-terminus-stopper (green curves), and rotaxane-minus-macrocycle (black curves).

that the two phenyl groups at the C-terminus can adopt in the different rotaxanes, a feature obviously determined by the size and shape of the alkyl substituents of the different amino acids in the rotaxanes.

It is also interesting to note that removal of the chromophore-bearing fragments shifts the spectral transitions to higher energy. In particular, removal of the macrocycle increases the energy of the main band by about 3000−5000 cm^{-1}, which, in turn, shows that, energetically, the ring takes part in the process although it does not, in the end, contribute to the CD signal itself. Its role is therefore to contribute to the electronic wave function and to the electric part of the transition dipole moment.

Testing the Hypothesis

To check that the C-terminus stopper is really the major contributor to the CD response of chiral peptide rotaxanes in nonpolar solvents, a further dipeptide rotaxane (**12**) was synthesized from a Gly-L-Phe thread (**11**) possessing a single additional methylene group between the ester unit and the C-terminus diphenylmethine stopper. This small structural change is well away from the hydrogen bonding motif used to template rotaxane formation (indeed, the yields of **9** and **12** are identical) and so should not affect the co-conformation adopted by the macrocycle and peptidic portion of the thread. However, the extra flexibility and small increase in distance provided by the extra methylene spacer should allow more facile rotation of the C-terminus diphenylmethine group and presumably place the phenyl rings in an environment where the chirality is less well expressed. Indeed, this is exactly what is found. The CD response of **12** in $CHCl_3$ is identical in shape and λ_{max} to that of **9**, but with an intensity reduced by 25% at all wavelengths. Similarly, replacing the C-terminus diphenylmethine stopper of **9** with a dicyclohexylmethine unit switches off the CD signal completely.

Quantifying the Expression of Chirality

While the modeling of the spectra with the removal of the chromophore-bearing fragments and their corroboration by experiment gives convincing results, the question arises as to whether one can quantify the amount of chirality the individual

Table 3. Continuous Chirality Measure of the Diphenylmethine Stoppers and the Macrocycle of Rotaxanes **6**–**9**

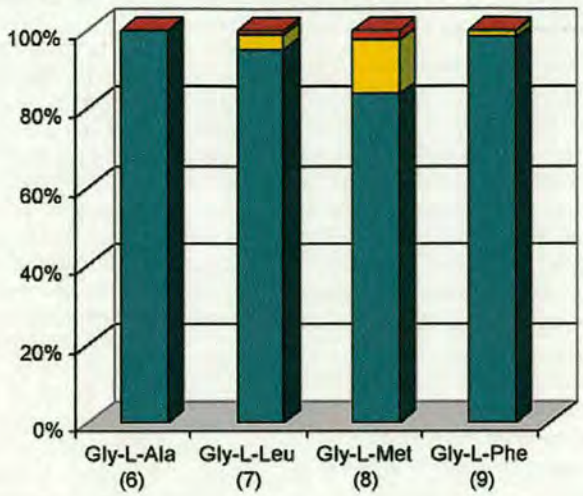

	Gly-L-Ala (**6**)	Gly-L-Leu (**7**)	Gly-L-Met (**8**)	Gly-L-Phe (**9**)
C-terminus stopper	1.122	1.569	0.031	1.659
macrocycle	0.001	0.064	0.005	0.032
N-terminus stopper	0.000	0.021	0.001	0.008

Table 4. Calculated Rotary Power of the First Four Transitions of Diphenylmethane for the Torsion of a Single Phenyl Group[a]

	0°[0.000]	15°[0.138]	30°[0.540]	45°[1.169]	60°[0.800]	75°[0.205]	90°[0.000]
S_1	0.00(270)	3.22(270)	5.08(270)	1.22(270)	−1.37(271)	−2.07(271)	0.00(271)
S_2	0.00(268)	−1.02(268)	−1.64(268)	1.63(268)	2.24(266)	1.53(265)	0.00(265)
S_3	0.00(234)	−18.30(233)	−30.20(230)	−31.89(227)	−25.01(222)	−15.94(218)	0.00(217)
S_4	0.00(209)	7.79(210)	16.20(211)	19.24(212)	12.64(213)	2.23(212)	0.00(209)

[a] In square brackets, the continuous chirality measure. (Notice that the torsion of a phenyl group changes the atoms that are reflected through the plane of symmetry.) In round brackets, the calculated excitation wavelength.

fragments contain and whether it relates to the calculated spectra. Quantitative techniques to measure the chirality have been proposed before. Here the continuous chirality measure,[16] CCM, was selected because it makes no assumption on a reference structure. CCM has already been found to rationalize a number of phenomena including the binding activities of trypsin/arylammonium inhibitors, D_2-dopamine receptor/dopamine derivative agonists, trypsin/organophosphates inhibitors, acetylcholinesterase/organophosphate and butyrylcholinesterase/organophosphates, carbon rearrangements in fullerenes, and the classification of enantiomerization pathways.[17] In the present context, the intent is to estimate the amount of chirality in the three chromophore-bearing fragments of the rotaxanes. Table 3 shows the chirality measures of the two stoppers and the macrocycle for each of the four peptide rotaxanes, **6**–**9**. In keeping with it being the major contributor to the CD response, the C-terminus diphenylmethine group has the largest chirality measure in all the rotaxanes, followed by the macrocycle. The N-terminus stopper is practically achiral in all cases, despite the X-ray structures suggesting that it is in more intimate contact with the macrocycle than the C-terminus unit. The simulation of the CD spectrum and the calculation of the CCM for a simple model system containing two phenyl groups supports the same conclusion. In Table 4, the rotatory power and the CCM are given for the torsion about a C−C bond of a phenyl group of diphenylmethane. Relatively small CCM suffice to give a large CD rotatory power similar to that seen for the Gly-L-Met rotaxane, **8**. The implication is that the CD spectrum is a highly nonlinear function of CCM.

Conclusions

The mechanically interlocked architectures of readily accessible, main-chain chiral peptido[2]rotaxanes enable them to exhibit a remarkable form of physical behavior, namely the variation in *size* and, in some cases, even the *sign* of their chiral response (observed through circular dichroism) as a result of changes in the nature of their local environment or thermal stimuli. In the absence of strong intercomponent interactions (e.g., in polar solvents at ambient and higher temperatures), the macrocycle is able to move relatively freely with respect to the thread and the chiral center is not effective in inducing a chiral environment for chromophores present on the macrocycle or stoppers. Under appropriate conditions (e.g., at low temperatures or in nonpolar solvents), however, when the intercomponent interactions are strong and highly directional, the steric requirements of the chiral center at the periphery of the hydrogen bonding template forces the macrocycle to adopt a very specific coconformation with the thread. Consequently, the conforma-

(16) (a) Zabrodsky, H.; Avnir, D. *J. Am. Chem. Soc.* **1995**, *117*, 462–473. (b) Avnir, D.; Katzenelson, O.; Helor, H. Z. *Chem. Eur. J.* **1996**, *2*, 744–746. (c) Katzenelson, O.; Helor, H. Z.; Avnir, D. *Chem Eur. J.* **1996**, *2*, 174–181.

(17) (a) Krinan, S.; Avnir, D. *J. Am. Chem. Soc.* **1998**, *120*, 6152–6159. (b) Pinto, Y.; Fowler, P. W.; Mitchell, D.; Avnir, D. *J. Phys. Chem. B* **1998**, *102*, 5776–5784. (c) Pinto, Y.; Salomon, Y.; Avnir, D. *J. Math. Chem.* **1998**, *23*, 13–29.

tionally fixed macrocycle locks the diphenylmethine group of the C-terminus stopper into a chiral environment, generating a CD response.

In light of the mechanism of CD signal generation, the success of the spectral simulations and the sizes of the CCM's, the expression of chirality is shown to be a nonlinear effect that can effectively be transmitted over long distances via bridges of low asymmetry. The generality and wide applicability of the CCM means that the induction of chirality into the C-terminus stopper may manifest itself beyond a simple ICD response. *Thus the switching "on" and "off" of the expression of chirality in peptide rotaxanes by controlling intercomponent interactions, i.e., through the "mechanical bond", may be a general phenomenon, not limited to a simple optical response.* This understanding could have important implications for other areas where chiral transmission from one chemical entity to another underpins a physical or chemical response, such as the seeding of supertwisted nematic liquid crystalline phases or asymmetric synthesis.

Experimental Procedures

General Method for the Preparation of Benzylic Amide Macrocycle-Containing Chiral Peptido[2]rotaxanes. The enantiopure[18] L-configuration amino acid dipeptide threads (**1**−**5**, **11**, 0.96 mmol) and triethylamine (1.55 g, 15.4 mmol) were dissolved in anhydrous chloroform (200 mL) and stirred vigorously, while solutions of xylylene diamine (7.68 mmol) in anhydrous chloroform (40 mL) and isophthaloyl chloride (7.68 mmol) in anhydrous chloroform (40 mL) were simultaneously added over a period of 4 h using motor-driven syringe pumps. The resulting suspension was filtered and concentrated under reduced pressure to afford the crude product which was then washed with ethyl acetate to leave only the unconsumed thread and [2]rotaxane in solution. This mixture was subjected to column chromatography (silica gel, CH_2Cl_2/MeOH as eluent) to yield, in order of elution, the unconsumed thread and the corresponding peptido[2]rotaxane (**6**−**10**, **12**). Selected data for [2]-(1,7,14,20-tetraaza-2,6,15,19-tetraoxo-3,5,9,12,16,18,22,25-tetrabenzocyclohexacosane)-(diphenylacetylglycylalaninate 2,2-diphenylethyl ester)-rotaxane (**6**): yield 45%; mp 238−239 °C; ^{1}H NMR (400 MHz, $CDCl_3$) δ 8.32 (s, 2H, isophthaloyl 2-*H*), 8.31 (d, 1H, CON*H*CH), 8.16 (d, 2H, J = 7.6 Hz, isophthaloyl 5-*H*), 8.14 (d, 2H, J = 7.6 Hz, isophthaloyl 4-*H* and 6-*H*), 7.58 (t, 4H, broad, macrocyclic N*H*CH_2), 7.3−7.0 (m, 20H, Ar*H*), 6.89, 6.79 (d, 8H, J = 7.7 Hz, *p*-xylylenediamine Ar-*H*), 5.60 (t, 1H, J = 3.5 Hz, CON*H*CH_2), 4.65 (d, 1H, J = 5.0 Hz, OC*H*H′CH), 4.61 (d, 1H, J = 5.0 Hz, OCH*H*′CH), 4.5−4.0 (m, 8H, macrocyclic NHCH_2), 4.31 (s, 1H, Ph_2C*H*CO), 4.10 (t, 1H, J = 5.0 Hz, CH_2C*H*Ph_2), 3.78 (m, 1H, NHC*H*CO), 2.64 (dd, 1H, J = 3.5 Hz, NHC*H*H′CO) 2.45 (dd, 1H, J = 3.5 Hz, NHCH*H*′CO), 0.98 (d, 3H, J = 4.6 Hz, CHCH_3); ^{13}C NMR (100 MHz, 10% CD_3OD in $CDCl_3$) δ 178.60, 172.45, 171.55, 166.78, 165.55, 140.50, 138.88, 137.68, 134.19, 131.95, 129.70, 129.46, 129.06, 128.99, 128.81, 128.75, 128.38, 128.32, 128.09, 127.43, 127.36, 124.56, 67.43, 58.18, 51.22, 48.81, 43.98, 41.80, 29.62, 16.33; FAB-MS (*m*NBA matrix) *m*/*z* 1053 [(rotaxane+H)$^+$]. Anal. Calcd for $C_{65}H_{60}N_6O_8$: C 74.1, H 5.7, N 8.0. Found: C 74.4, H 5.9, N 7.6. Selected data for [2]-(1,7,14,20-tetraaza-2,6,15,19-tetraoxo-3,5,9,12,16,18,22,25-tetrabenzocyclohexacosane)-(diphenylacetylglycylleucine 2,2-diphenylethyl ester)-rotaxane (**7**): yield 37%; mp 278−280 °C; ^{1}H NMR (400 MHz, $CDCl_3$) δ 8.18 (t, 4H, J = 7.7 Hz, isophthaloyl 4-H 6-H), 8.15 (s, 2H, isophthaloyl 2-H), 7.77 (d, 1H, broad, Leu N*H*CHCO), 7.62 (t, 2H, J = 7.7 Hz, isophthaloyl 5-H), 7.06−7.30 (m, 20H, thread Ar-*H*), 6.99 (d, 4H, AA′BB′ system, J = 8.0 Hz, *p*-xylylenediamine Ar-H_a), 6.90 (d, 4H, AA′BB′ system, J = 8.0 Hz, *p*-xylylenediamine Ar-H_b), 5.52 (t, 1H, J = 3.5 Hz, Gly CON*H*CHH′), 4.73 (m, 1H, Leu NHC*H*CO), 4.45 (m, 2H, COOCH_2-CHPh_2), 4.40 (m, 8H, macrocyclic CH_2NH), 4.26 (s, 1H, thread Ph_2C*H*CO), 3.96 (m, 1H, COOCH$_2$C*H*Ph_2), 2.75 (d, 2H, J = 3.6 Hz, Gly NHCH_2CO), 1.25 (m, 3H, CH_2C*H*$(CH_3)_2$ and CH_2CH$(CH_3)_2$); 0.72 (d, 3H, J = 6.0 Hz, CH_2CHCH_3CH′$_3$), 0.66 (d, 3H, J = 6.0 Hz, CH_2-CHCH_3C*H*′$_3$); ^{13}C NMR (100 MHz, $CDCl_3$) δ = 172.29, 172.12, 169.08, 167.15, 166.85, 140.31, 138.71, 137.12, 136.84, 133.81, 131.46, 129.24, 128.81, 128.69, 128.61, 128.31, 127.92, 127.82, 127.50, 126.91, 124.52, 67.30, 57.82, 51.19, 43.83, 40.30, 29.56, 24.36, 21.90; FAB-MS (*m*NBA matrix) *m*/*z* 1095 [(rotaxane+H)$^+$]. Anal. Calcd for $C_{68}H_{66}N_6O_8$: C 74.6, H 6.0, N 7.7. Found: C 75.0, H 6.2, N 7.5. Selected data for [2]-(1,7,14,20-tetraaza-2,6,15,19-tetraoxo-3,5,9,12,-16,18,22,25-tetrabenzocyclohexacosane)−(diphenylacetylglycylmethionine 2,2-diphenylethyl ester rotaxane (**8**): yield 36%; mp 261−262 °C; ^{1}H NMR (400 MHz, $CDCl_3$): δ 8.36 (s, 2H, isophthaloyl 2-H), 8.23 (d, 2H, J = 8.0 Hz, isophthaloyl 4-H), 8.18 (d, 2H, J = 8.0, isophthaloyl 6-H), 7.62 (t, 2H, J = 8.0 Hz, isophthaloyl 5-H), 7.47, (m, 4H, broad, macrocyclic N*H*), 7.07−7.23 (m, 20H, thread stoppers Ar-*H*), 6.92 (d, 4H, J = 7.8 Hz, *p*-xylylenediamine Ar-H_a), 6.84 (d, 4H, J = 7.8 Hz, *p*-xylylene Ar-H_b), 5.57 (m, 1H, broad, Gly CON*H*CH_2), 4.74 (m, 1H, Met NHC*H*CO), 4.48 (m, 3H, COOCH_2-CHPh_2 and COOCH2CHPh_2), 4.35 (m, 8H, macrocyclic NHCH_2), 4.26 (s, 1H, thread Ph_2CHCO), 2.62 (m, 2H, broad, Gly NHCH_2CO), 2.13 and 2.08 (m, 4H, Met CHCH_2CH_2SCH_3), 1.80 (s, 3H, Met CHCH_2-CH_2SCH_3); ^{13}C NMR (100 MHz, $CDCl_3$): δ 171.98, 171.29, 168.76, 167.34, 167.01, 140.18, 140.04, 138.91, 136.71, 136.69, 133.75, 130.70, 130.54, 128.68, 128.53, 128.26, 128.14, 127.62, 126.92, 126.60, 125.37, 67.81, 57.32, 50.86, 50.79, 43.81, 43.70, 30.10, 29.04, 14.00; FAB-MS (*m*NBA matrix) *m*/*z* 1113 [(rotaxane+H)$^+$]. Anal. Calcd. for $C_{67}H_{64}N_6O_8S$: C 72.3, H 5.7, N 7.5, S 2.9. Found: C 72.8, H 5.8, N 7.8, S 2.7. Selected data for [2]-(1,7,14,20-tetraaza-2,6,15,19-tetraoxo-3,5,9,12,16,18,22,25-tetrabenzocyclohexacosane)-(diphenylacetylglycylphenylalanine 2,2-diphenylethyl ester)-rotaxane (**9**): yield 32%; mp 227−229 °C; ^{1}H NMR (400 MHz, $CDCl_3$) δ 8.35 (s, 2H, isophthaloyl 2-*H*), 8.22 (t, 4H, J = 7.7 Hz, isophthaloyl 4-*H*, 6-*H*), 7.65 (t, 2H, J = 7.7 Hz, isophthaloyl 5-H), 7.39 (t, 4H, broad macrocyclic CON*H*CHH′), 7.08−7.26 (m, 25H, Ar-*H* of thread); 6.97 (d, 1H, J = 6.8 Hz, Phe N*H*CHCO), 6.74 (d, 4H, AA′BB′ system J = 7.8 Hz, *p*-xylylenediamine Ar-H_a), 6.50 (d, 4H, AA′BB′ system J = 7.8 Hz, *p*-xylylenediamine Ar-H_b), 5.38 (t, 1H, broad, Gly N*H*CH_2CO), 4.70 (m, 1H, Phe NHC*H*CO), 4.40 (m, 2H, COOCH_2CHPh_2), 4.24 (m, 1H, COOCH$_2$-C*H*Ph_2), 4.14 (s, 1H, Ph_2C*H*CO), 4.08 (m, 8H, macrocyclic CH_2NH), 2.58 (m, 2H, Gly CONHCH_2), 2.52 (m, 2H, Phe C*HH*′Ph); ^{13}C NMR (100 MHz, $CDCl_3$) δ 171.58, 170.78, 169.31, 167.58, 166.73, 139.74, 138.48, 136.57, 136.22, 133.57, 133.51, 130.85, 130.75, 128.79, 128.60, 128.54, 128.46, 128.35, 128.18, 128.02, 127.56, 127.49, 127.01, 126.37, 124.60, 67.40, 56.64, 50.34, 53.55, 49.87, 43.45, 43.03, 36.56; FAB-MS (*m*NBA matrix) *m*/*z* 1129 [(rotaxane+H)$^+$]. Anal. Calcd for $C_{71}H_{64}N_6O_8$: C 75.5, H 5.7, N 7.5. Found: C 74.5, H 5.5, N 7.3. Selected data for [2]-(1,7,14,20-tetraaza-2,6,15,19-tetraoxo-3,5,9,12,16,-18,22,25-tetrabenzocyclohexacosane)-(diphenylacetylglycylproline 2,2-diphenylethyl ester)-rotaxane (**10**): yield 6%; ^{1}H NMR (400 MHz, $CDCl_3$) δ 8.50 (s, 2H, isophthaloyl 2-H), 8.39 (d, 2H, J = 8.0 Hz, isophthaloyl 4-H or 6-H), 8.30 (d, 2H, J = 8.0 Hz, isophthaloyl 4-H or 6-H), 7.69 (t, 2H, J = 8.0 Hz, isophthaloyl 5-H), 7.6−6.9 (m, 20H, Ar-*H*), 6.94 (d, 4H, J = 8.0 Hz, xylylene-H_a), 6.78 (d, 4H, J = 8.0 Hz, xylylene-H_b), 5.66 (broad, 1H, CON*H*CH_2), 4.74 (dd, 1H, J = 15.0 Hz, 8 Hz, OC*H*H′CHPh$_2$), 4.60 (broad, 4H, macrocyclic NHC*H*H′), 4.40 (s, 1H, Ph_2CHCO), 4.30 (broad, 4H, macrocyclic NHCH*H*′), 4.08 (m, 1H, OCH*H*′CHPh$_2$), 3.82 (dd, 1H, J = 8.0 Hz, 5 Hz, OC*H*H′CH), 2.85 (d, 1H, J = 6.0 Hz, NHCH*H*′CO), 2.80 (m, 1H, Pro NC*H*H′CH_2), 2.60 (m, 1H, Pro NCH*H*′CH_2), 2.52 (d, 1H, J = 5.0 Hz, Gly NHCH*H*′CO), 2.45 (d, 1H, J = 5.0 Hz, Gly NHC*H*H′CO), 1.9−1.3 (m, 4H, Pro NCH_2CH_2CH_2CH); ^{13}C NMR (100 MHz, $CDCl_3$) δ 172.45, 171.01 167.80, 165.78, 141.55, 138.23, 137.56, 136.26, 133.75, 131.45, 129.34, 128.84, 128.28, 128.78 128.43, 127.42, 127.14, 127.00, 126.89,

(18) Racemic Gly-DL-Phe rotaxane (**4**) was prepared as a control and, as expected, did not give a CD response in any solvent.

124.52, 72.54, 68.37, 56.72, 52.10, 43.80, 41.39, 30.78, 25.56, 20.38 19.55; FAB-MS (*m*NBA matrix) *m/z* 1079 [(rotaxane+H)$^+$]. Anal. Calcd for $C_{67}H_{62}N_6O_8$: C 74.6, H 5.8, N 7.8. Found: C 74.0, H 5.9, N 7.7. Selected data for [2]-(1,7,14,20-tetraaza-2,6,15,19-tetraoxo-3,5,9,-12,16,18,22,25-tetrabenzocyclohexacosane)-(diphenylacetylglycylphenylalanine 3,3-diphenyl-1-propyl ester)-rotaxane (**12**): yield 42%; mp 260−262 °C; ^{1}H NMR (400 MHz, $CDCl_3$) δ 8.19 (t, 4H, J = 8.3 Hz, isophthaloyl 4-*H* and 6-*H*), 8.18 (s, 2H, isophthaloyl 5-*H*), 7.61 (t, 2H, J = 8.3 Hz, isophthaloyl 2-*H*), 7.37 (t, 2H, J = 5.3 Hz, macrocyclic N*H*), 7.36−7.10 (m, 25H, thread Ar-*H*), 7.04 (t, 2H, J = 5.4 Hz, macrocyclic N*H*), 6.89 (d, 4H, AA′BB′ system J = 8.0 Hz, *p*-xylylene Ar-H_a), 6.76 (d, 4H, AA′BB′ system J = 8.0 Hz, *p*-xylylene Ar-H_b), 5.47 (t, 1H, broad, Gly N*H*CH_2CO), 4.44 (dd, 4H, J = 4.5 Hz, 13.9 Hz, macrocyclic C*H*H′NH), 4.31 (dd, 4H, J = 4.5 Hz, 13.9 Hz, macrocyclic CH*H*′NH), 4.19 (s, 1H, Ph_2CHCO), 3.98 (m, 1H, $COOCH_2$-$CH_2CH$$Ph_2$), 3.82 (m, 2H, $COOCH_2CH_2CHPh_2$), 3.81 (m, 1H, Phe NHC*H*CO), 3.11 (dd, 1H, J = 5.0 Hz, 14.1 Hz, Phe C*H*H′Ph), 2.88 (dd, 1H, J = 9.5 Hz, 13.9 Hz, Phe CH*H*′Ph), 2.76 (m, 2H, broad, Gly CONHCH_2); 2.14 (m, 2H, $COOCH_2CH_2CHPh_2$); ^{13}C NMR (100 MHz, $CDCl_3$) δ 172.49, 171.23, 170.15, 166.89, 166.73, 143.94, 138.78, 138.70, 137.66, 137.22, 136.19, 134.27, 134.17, 132.15, 131.89, 129.71, 129.21, 129.15, 128.78, 128.28, 128.18, 128.07, 127.99, 126.94, 124.14, 64.89 (COOCHH′CHH′CHPh$_2$), 58.68 (Ph_2CHCO), 55.46 (Phe NH-C*H*CO), 48.05, (COOCHH′CHH′CHPh$_2$), 44.61, 44.44, (macrocyclic $NHCH_2$), 42.66 (Gly CONHCHH′), 37.93 (Phe CHCHH′Ph), 34.21 (COOCHH′CHH′CHPh$_2$); FAB-MS (*m*NBA matrix) *m/z* 1143 [(rotaxane+H)$^+$]. Anal. Calcd for $C_{72}H_{66}N_6O_8$: C 75.6, H 5.8, N 7.4. Found: C 75.5, H 5.9, N 7.3.

X-ray Crystallographic Structure Determinations. 6: $C_{66}H_{65}N_6O_{10}$-Cl_3 M = 1208.59, crystal size 0.25 × 0.10 × 0.10 mm^3, monoclinic $P2_1/n$, a = 20.367(2), b = 11.124(1), c = 27.591(2) Å, β = 101.83-(1)°, V = 6118.3(9) Å^3, Z = 4, ρ_{calcd} = 1.312 mg m^{-3}; (graphite monochromated Mo Kα radiation, λ = 0.71073 Å), μ = 0.214 mm^{-1}, T = 150(2) K. 19043 data (8463 unique, R_{int} = 0.3107, 2.00 < θ < 25.00°), were collected on the EPSRC National Service Enraf Nonius Kappa CCD diffractometer with area detector using ϕ and ω scans and were corrected semiempirically for absorption and sample decay (transmission 0.95−0.98). The structure was solved by direct methods and refined by full-matrix least-squares on F^2 values of all data (G. M.Sheldrick, SHELXTL manual, Siemens Analytical *X*-ray Instruments, Madison WI, 1994, version 5) to give $wR = \{\Sigma[w(F_o^2 - F_c^2)^2]/\Sigma[w(F_o^2)^2]\}^{1/2}$ = 0.132, conventional R = 0.054 for F values of 1338 reflections with $F_o^2 > 2\sigma(F_o^2)$, S = 0.465 for 768 parameters. Residual electron density extremes were 0.247 and −0.210 Å^{-3}. All non-hydrogen atoms were refined anisotropically. Hydrogen atoms were constrained to chemically reasonable positions.

7: $C_{70}H_{72}Cl_6N_6O_{10}$, M = 1370.09, crystal size 0.30 × 0.30 × 0.10 mm^3, monoclinic $P2_1$, a = 10.964(3), b = 32.032(7), c = 11.285(7) Å, β = 117.72(4), V = 3508(3) Å^3, Z = 2, ρ_{calcd} = 1.297 mg m^{-3}; Cu Kα radiation (λ = 1.5418 Å), μ = 2.729 mm^{-1}, T = 293(2)K. 5649 data (5342 unique, R_{int} = 0.105, 2.76 < θ < 60.12°), were collected on a Siemens SMART CCD diffractometer using narrow frames (0.3° in ω) and were corrected semiempirically for absorption and incident beam decay (transmission 0.62−1.00). The structure was solved by direct methods and refined by full-matrix least-squares on F^2 values of all data (Bruker SMART and Bruker SHELXTL) to give $wR = \{\Sigma[w(F_o^2 - F_c^2)^2]/\Sigma[w(F_o^2)^2]\}^{1/2}$ = 0.087, conventional R = 0.058 for F values of 1575 reflections with $F_o^2 > 2\sigma(F_o^2)$, S = 3.28 for 449 parameters. Residual electron density extremes were 0.25 and −0.24 Å^{-3}. Amide hydrogen atoms were refined isotropically subject to a distance constraint N−H = 0.98 Å, with the remainder constrained. Due to the low number of observed data, anisotropic displacement parameters were used only for oxygen and nitrogen atoms with all remainder atoms isotropic.

Experimental details for **8** and **9** were the same as for **7** except for the following. **8**: $C_{67}H_{68}N_6O_{10}S$, M = 1149.33, crystal size 0.002 × 0.080 × 0.100 mm^3, triclinic P1, a = 10.839(10), b = 11.151(10), c = 14.639(2) Å, α = 69.56, β = 83.67, γ = 62.14°, V = 1462.66(3) Å^3, Z = 1, ρ_{calcd} = 1.305 mg m^{-3}; synchrotron radiation (CCLRC Daresbury Laboratory Station 9.8, silicon monochromator, λ = 0.6875 Å), μ = 0.122 mm^{-1}, T = 160(2) K. 9754 data (8170 unique, R_{int}=0.0299, 1.44 < θ < 28.68°), were collected on a Siemens SMART CCD diffractometer using narrow frames (0.3° in ω), and were corrected semiempirically for absorption and incident beam decay (transmission 0.32−1.00). The structure was solved and refined as described above for **7** to give $wR = \{\Sigma[w(F_o^2 - F_c^2)^2]/\Sigma[w(F_o^2)^2]\}^{1/2}$ = 0.1651, conventional R = 0.0589 for F values of 7528 reflections with $F_o^2 > 2\sigma(F_o^2)$, S = 1.082 for 799 parameters. Residual electron density extremes were 0.444 and −0.341 Å^{-3}. Amide hydrogen atoms were refined isotropically subject to a distance constraint N−H = 0.98 Å, with the remainder constrained; anisotropic displacement parameters were used for all non-hydrogen atoms. **9**: $C_{73}H_{70}Cl_6N_6O_{10}$, M = 1404.05, crystal size 0.004 × 0.030 × 0.070 mm^3, monoclinic $P2_1$, a=10.993, b = 31.217, c = 11.255(10) Å, β = 118.71, V = 3387.62(3) Å^3, Z = 2, ρ_{calcd} = 1.376 mgmg m^{-3}; synchrotron radiation (CCLRC Daresbury Laboratory Station 9.8, silicon monochromator, λ = 0.68750 Å), μ = 0.318 mm^{-1}, T = 160(2) K. 22328 data (14814 unique, R_{int} = 0.0306, 1.26 < θ < 28.56°) were collected on a Siemens SMART CCD diffractometer using narrow frames (0.3° in ω), and were corrected semiempirically for absorption and incident beam decay (transmission 0.38−1.00). The structure was solved and refined as described above for **7** to give $wR = \{\Sigma[w(F_o^2 - F_c^2)^2]/\Sigma[w(F_o^2)^2]\}^{1/2}$ = 0.1843, conventional R = 0.0641 for F values of 10279 reflections with $F_o^2 > 2\sigma(F_o^2)$, S = 0.972 for 897 parameters. Residual electron density extremes were 0.561 and −0.521 Å^{-3}. Amide hydrogen atoms were refined isotropically subject to a distance constraint N−H = 0.98 Å, with the remainder constrained; anisotropic displacement parameters were used for all non-hydrogen atoms.

Crystallographic data for **6**−**9** (excluding structure factors) have been deposited with the Cambridge Crystallographic Data Centre as supplementary publication numbers CCDC-147201 (**6**), CCDC-141368 (**7**), CCDC-141369 (**8**), and CCDC-141370 (**9**).[21]21

UV−Vis and CD Spectroscopy. The electronic absorption spectra were recorded on a Hewlett-Packard 8453 diode array spectrometer at 0.1 mM substrate concentrations using commercially available spectrograde solvents. Circular dichroism measurements were recorded in the range 230−320 nm on a JASCO J-720WI-L spectropolarimeter at 0.1 mM substrate concentrations with a path length of 0.1 cm. The path length allowed the reproducible measurement of CD spectra even in $CHCl_3$ in the range 230−250 nm, despite the strong absorbance of the solvent at these wavelengths. As a control, identical CD measurements were also obtained using a JASCO J630 spectopolarimeter.

Computational Experimental Details. In unoriented samples, in general, and in solution, in particular, the circular dichroism response of a system is proportional to the product of the electronic transition dipole moment, M, and the magnetic transition moment, $\mathcal{M}$.[19] If we label the ground state as 0 and the final state as f, the product $M_i(0f)$-$\mathcal{M}_i(0f)$, with $i = x$, y, or z, can be nonzero for molecules that belong to point groups in which rotations and translations transform as the same irreducible representation. Following previous work,[9] the spectra were simulated using the semiempirical procedure INDO/S (intermediate neglect of differential overlap/spectroscopic parametrization).[10] The configuration interaction was limited to single excited configurations in the molecular orbital space given by the sum of the π and n orbitals. As a consequence of the large line broadening present in the circular dichroism spectra, to compare experiment and theory it was necessary to convolute the calculated stick spectrum (electronic energies and intensities) with a line shape. Since the experimental data were obtained in solution, the line shape should be described by a Gaussian function.

(19) (a) Rosenfeld, R. Z. *Physik* **1928**, *52*, 161. (b) Michl, J.; Thulstrup, E. W. *Spectroscopy with Polarized Light*; VCH: New York, 1986.

Each line calculated quantum chemically was then broadened by multiplying it by a function $G(\nu) = (e^{-(\nu-\nu_0)^2/a^2}/a\pi^{0.5})$ where ν is the excitation wavenumber, in cm^{-1}, ν_0 is the wavenumber of the electronic state, in cm^{-1}, and "a" the broadening constant, 3000 cm^{-1}.

The rotaxane structures **6**−**9** were optimized using the MM3[11] model implemented in the TINKER[12] program starting from the geometries provided by *X*-ray crystallography.

To investigate the asymmetric nature of the ICD response, chirality was treated as a continuous geometric quantity that can vary between 0 and 100. This approach follows the model known as the continuous chirality measure (CCM), developed by Avnir and collaborators.[16] In dipeptide rotaxanes, chirality arises from the deviation from a symmetry plane. In this scheme, the plane is not determined a priori and must be found numerically by optimization techniques.[20] The chirality value, *S*, is then calculated as

$$S = \frac{100}{D^2}\sum_i (p_i - \hat{p}_i)^2 \qquad (1)$$

where D is a normalization factor given by the distance between the geometrical center of the molecule and the most distant atom, p_i are the atomic coordinates, and $\hat{p}_i$ are the coordinates of the atoms of the nearest structure that contains a symmetry plane. $S = 0$ coincides with ideal symmetry (in this case achirality); $S = 100$ collapses the system to a single point.

Two features of the simulations should be commented upon: The first is the energy location that is over estimated by a few thousand cm^{-1}; the second is the relative ordering of the experimental CD intensities—Gly-L-Ala (**6**) < Gly-L-Phe (**9**) < Gly-L-Met (**8**) < Gly-L-Leu (**7**)—for the main band around 240−250 nm that was not well reproduced by the simulations. This band is due to transitions to electronic states that are a combination of the L_a benzenic states of the two isophthaloyl groups with the L_b benzenic states of the *p*-xylylene fragments and the diphenylmethine stoppers. In previous work on the [2]catenane, i.e., the interlocked dimer of the macrocycle, similar semiempirical calculations yielded 5.6 eV (221 nm) for the energy of the L_a states.[8] The present result of ~210 nm is consistent with those calculations. Because of the eight phenyl groups present in the molecules, the level of degeneration of the spectroscopic states is high and the differences can be ascribed to a not perfectly balanced description of the interactions between the levels. This did not affect the qualitative use of the simulations in uncovering the actual origin of the CD signal in peptide rotaxanes.

Acknowledgment. This work was supported by the TMR initiative of the European Union through contracts FMRX-CT96-0059 and FMRX-CT97-0097 and a British Council UK-Japan Cooperative Research Travel award. F.Z. acknowledges partial support from the MURST project "Dispositivi Supramolecolari". D.A.L. is an EPSRC Advanced Research Fellow (AF/982324).

Supporting Information Available: Tables of crystal data, structure solution and refinement, atomic coordinates, bond lengths and angles, and anisotropic thermal parameters for the X-ray crystal structures of **6**−**9**. This material is available free of charge via the Internet at http://pubs.acs.org.

JA015995F

(20) Press, W. H.; Teukolsky, S. A.; Vetterling, W. T.; Flannery, B. P. *Numerical Recipes, The Art of Scientific Computing*, 2nd ed.; Cambridge University Press: Cambridge, 1992.

(21) Copies of the data can be obtained free of charge on application to The Director, CCDC, 12 Union Road, Cambridge CB2 1EZ, U.K. (Fax: international code + (1223)336−033. E-mail: teched@chemcrys.cam.ac.uk.)